DEVELOPMENT OF PARAFFIN-NANOFIBER NANOCOMPOSITE FOR THERMAL HYSTERESIS ENHANCEMENT OF PARAFFIN ACTUATORS

Ahmet Kutlu

T.C.
BURSA ULUDAĞ UNIVERSITY
GRADUATE SCHOOL OF NATURAL AND APPLIED SCIENCES

DEVELOPMENT OF PARAFFIN-NANOFIBER NANOCOMPOSITE FOR THERMAL HYSTERESIS ENHANCEMENT OF PARAFFIN ACTUATORS

Ahmet KUTLU
0000-0002-9389-0281

Prof. Dr. Yakup AYKUT
(Supervisor)

Prof. Dr. Recep EREN
(Second Supervisor)

PhD THESIS
DEPARTMENT OF TEXTILE ENGINEERING

BURSA – 2022

THESIS APPROVAL

This thesis titled "DEVELOPMENT OF PARAFFIN-NANOFIBER NANOCOMPOSITE FOR THERMAL HYSTERESIS ENHANCEMENT OF PARAFFIN ACTUATORS" and prepared by Ahmet KUTLU has been accepted as a **PhD THESIS** in Bursa Uludağ University Graduate School of Natural and Applied Sciences, Department of Textile Engineering following a unanimous vote of the jury below.

Supervisor : Prof. Dr. Yakup AYKUT

Head :	Prof. Dr. Hakan Aydın 0000-0001-7364-6281 Bursa Uludağ University, Faculty of Engineering, Department of Mechanical Engineering	Signature
Member:	Prof. Dr. Yakup Aykut 0000-0002-5263-1985 Bursa Uludağ University, Faculty of Engineering, Department of Textile Engineering	Signature
Member:	Assoc. Prof. Dr. Fatih Süvari 0000-0001-5708-7993 Bursa Uludağ University, Faculty of Engineering, Department of Textile Engineering	Signature
Member:	Assoc. Prof. Dr. Mahmut Ali Ermeydan 0000-0001-6389-2649 Bursa Technical University, Faculty of Forestry , Department of Forest Industry Engineering	Signature
Member:	Dr. Cihan Kaboğlu 0000-0002-6249-0565 Bursa Technical University, Faculty of Engineering and Natural Sciences, Department of Metalurgical and Materials Engineering	Signature

I approve the above result
Prof. Dr. Hüseyin Aksel EREN
Institute Director
... / … / …

I declare that this thesis has been written in accordance with the following thesis writing rules of the U.U Graduate School of Natural and Applied Sciences;

- All the information and documents in the thesis are based on academic rules,
- audio, visual and written information and results are in accordance with scientific code of ethics,
- in the case that the works of others are used, I have provided attribution in accordance with the scientific norms,
- I have included all attributed sources as references,
- I have not tampered with the data used,
- and that I do not present any part of this thesis as another thesis work at this university or any other university.

…/ … / …

Ahmet KUTLU

ÖZET

Doktora Tezi

PARAFİN AKTİVATÖRLERİN ISIL HİSTEREZİS ÖZELLİKLERİNİN İYİLEŞTİRİLMESİ İÇİN PARAFİN-NANOLİF NANOKOMPOZİT GELİŞTİRİLMESİ

Ahmet KUTLU

Bursa Uludağ Üniversitesi
Fen Bilimleri Enstitüsü
Tekstil Mühendisliği Anabilim Dalı

Danışman: Prof. Dr. Yakup AYKUT

Otomotivden, elektronik ve dayanıklı ev aletlerine kadar çok geniş alanda kullanıma sahip olan parafin aktivatörlerin en büyük sorunu parafin malzemesinin ısı iletkenliğinin düşük olması ve dolayısıyla ısıl histerezis değerlerinin kötü olmasıdır. Bu çalışmanın amacı nanoliflerin takviyesinin parafin aktivatörlerin ısıl histerezis özelliklerine etkisinin incelenmesidir. Öncelikle nanolif yüzeyi ve farklı karbon atom sayısına sahip sıvı parafinin etkileşimi elektroçekim yöntemiyle üretilmiş nanolif ile deneysel olarak değerlendirilmiştir. Tek iğneli uniaksiyel elektroçekim ile tek adımda hızlı ve kolay bir parafin/poliakrilonitril hibrid nanolif üretimi üzerine çalışmalar yapılmıştır. Üretilen hibrid parafin/poliakrilonitril yapısı parafin aktivatörün histerezis değerinin iyileştirilmesi için kullanılmıştır. Dört farklı erime noktasına sahip parafin çeşidi ile ağırlıkça %2.5, 5, 7.5 ve 10 oranlarında parafin/poliakrilonitril karışımı kullanılarak parafin aktivatör üretilmiş ve ısıl histerezis değerinde %15.3 oranına kadar iyileşme sağlanmıştır. Isıl histerezisde nanolif takviyesi ile elde edilen iyileşme, metal oksit nanoparçacık takviyesi ile kıyaslanmıştır. CuO, Fe_3O_4, ZnO, Al_2O_3 nanoparçacıkları ve poliakrilonitril nanolif takviyesi üretilen parafin aktivatör numuneleri, sırasıyla %24.6, 26.2, 20.0, 29.2 ve 30.8 oranlarında ısıl histerezis iyileştirmesi gözlenmiştir. Dispersiyon ısıl stabilitesinin, parafin aktivatörün histerezis performansına etkisini ölçmek için bu numuneler yüksek ısıda yaşlandırma testine tabi tutulmuştur. Nanolif kullanımında histerezis değerinde en yüksek iyileşme görülürken, yüksek sıcaklıkta yaşlandırma tetsi sonunda yine nanolif katkılı numune en düşük performans kaybına uğramıştır.

Anahtar Kelimeler: Nanolif, parafin aktivatör, histerezis, elektroçekim, poliakrilonitril

2022, xi + 133 pages.

ABSTRACT

PhD Thesis

DEVELOPMENT OF PARAFFIN-NANOFIBER NANOCOMPOSITE FOR THERMAL HYSTERESIS ENHANCEMENT OF PARAFFIN ACTUATORS

Ahmet KUTLU

Bursa Uludağ University
Graduate School of Natural and Applied Sciences
Department of Textile Engineering

Supervisor: Prof. Dr. Yakup AYKUT

The most important problem of paraffin actuators, which are used in a wide range of technical areas from automotive engine cooling systems to electronics and household appliances, is the low thermal conductivity of the paraffin material and its poor thermal hysteresis. This study determines the effect of nanofiber addition on the thermal hysteresis behavior of paraffin actuators. Interactions of electrospun nanofibers mat with the liquid paraffins with different amount of carbon were also investigated. Preparation of paraffin/polyacrylonitrile hybrid nanofibers via single needle (uniaxial) electrospinning system was studied. As-spun paraffin/polyacrylonitrile nanofibers were used for thermal hysteresis enhancement. Paraffin actuators are prepared with paraffins of four different melting points consisting paraffin/polyacrylonitrile nanofiber with the wt.% of 2.5, 5, 7.5 and 10. The hysteresis value was enhanced up to 15.3%. CuO, Fe_3O_4, ZnO, Al_2O_3 metal oxide nanoparticles addition and polyacrylonitrile nanofiber addition are used for thermal hysteresis enhancement comparison and an improvement as 24.6, 26.2, 20.0, 29.2 and 30.8 % sequentially for the samples compared with pure paraffin. Dispersion thermal stability effect on hysteresis performance of those paraffin actuators are also compared and nanofiber added paraffin actuator showed at least hysteresis performance loss at high temparature storage test.

Key words: Nanofiber, Paraffin Actuator, Thermal Hysteresis, Electrospinning, Polyacrylonitrile

2022, xi + 133 pages.

PREFACE AND/OR ACKNOWLEGDEMENT

My passion for developing a paraffin actuator with enhanced thermal behavior especially for vehicle engine cooling systems is relaying on the demand of innovation for the since long decades constant remained paraffin compound which is still suffering for thermally deaf and untouched micro-scaled structure. An innovative and affordable nanostructured solution will not only improve the engine performance of vehicles, but also protect the environment in terms of exhaust emission releases.

This thesis would not have been possible without the excellent guidance and support of my supervisor Prof. Dr. Yakup Aykut. I am very thankful to him for keeping me on track towards this demanding journey. I would also like to acknowledge the support of my co-supervisor Prof. Dr. Recep Eren during the recovery of my scientific study to research articles. It has been a pleasure working with them on this research and I look forward to future collaborations together.

I would like to express my thanks and appreciation to all my colleagues at Research and Development Center of Kirpart AS, and especially Management Board of Kirpart AS who made possible my PhD Study during my employment.

Special thanks and appreciation is to my wife Buket for her patience and prayers during my unceasingly endeavor.

Ahmet KUTLU
28/02/2022

CONTENTS

Page

SYMBOLS and ABBREVIATIONS

Symbol	Definition
◦C	Celcius
cps/eV	counts per second per electron-volt
H	Enthalpy
keV	kilo electronic volts
kJ/L	kilojoule/liter
kJ/kg	kilojoule/kilogram : latent heat
λ	Thermal Conductivity (W/mK)
λ_{solid}	Thermal Conductivity at solid phase
$\lambda_{sol/liq}$	Thermal Conductivity at solid-liquid phase transition
λ_{liquid}	Thermal Conductivity at liquid phase
n	number of carbon atoms
μL/min	microliter/minute
Mv	Molecular weight
ρ	density
S(mm)	Stroke in millimeters
T(°C)	Temparature in Celcius
t(s)	Time in seconds
wt.%	Weight percent
w/v %	Weight /Volume percent

Abbreviation	Definition
2D	two dimensional
CT	Computer Tomography
DMF	N-N Dimetylformamide
DSC	Differential scanning chromatography
DTA	Differential thermal analysis
DTST	Dispersion thermal stability test
EDS	Energy-dispersive X-Ray spectroscopy
FTIR	Fourier transformation infrared spectroscopy
H	Enthalpy
NP	Nanoparticle
NF	Nanofiber
P/PAN	Paraffin/Polyacrylonitrile
PAN	Polyacrylonitrile
PCM	Phase Change Material
PVA	Polyvinylalchol
SEM	Scanning electron microscopy
SP/PAN	Solid paraffin/Polyacrylonitrile
TEM	Transmission electron microscopy
TGA	Thermo gravimetric analysis
TH	Thermal Hysteresis

FIGURES

Page

TABLES

Pages

1. INTRODUCTION

Emerging nanofiber production methods enable nanocomposite material production technologies which are exclusively compatible with their application areas for desired specific property enhancement. Methods of polymer nanofiber production with electrospining will be emphasized in the next chapter. Method based nanofiber SEM images are inclosed under related topic, for more visualisation and recognation of the contributed utility provided by that technology.

Paraffin is widely used as thermal regulating material because of its exclusive properties including diverse melting temperatures, chemically inert and physically stable behaviors. On the other hand, because of its low thermal conductivity, researchers have focused on to enhance the thermal conductivity of paraffin by combining with other materials. Thermal properties of paraffin as a phase change material specifically related with paraffin actuators will be discussed in the next chapter in terms of theoretical basics and literature review.

The most important problem of paraffin actuators, which are used in a wide range of areas from automotive engine cooling systems to electronics and household appliances, is the paraffins poor thermal conductivity and therefore its poor thermal hysteresis behavior. In this thesis, the opportunity for thermal property improvement of paraffin as a phase change material in the industrial application area of paraffin actuators in terms of nanotechnological touch by nanofiber addition experimentally is evaluated.

Primarily the interaction between paraffin and nanofibers is assessed. Paraffin samples which have different number of carbons in their molecular chain with different melting points and electrospun polyvinyl alcohol nanofibers mat are investigated. Microscopic images revealed that liquid paraffin can be held on the surface on the nanofibers. Contact angle measurement results revealed that heptadecane has the highest and pentadecane has the lowest contact angle on PVA nanofibrous mat structures. As a conclusion, wettability of the nanofibers by liquid paraffin can be enhanced if the paraffin is used which has less number of the carbon atoms. Furthermore the examined

wettability of the electrospun nanofibers by paraffin, encouraged us working on development of a genuine method for facile production of paraffin-nanofiber hybrid system.

Accordingly a one-step preparation method of paraffin/polyacrylonitrile hybrid nanofibers via single needle (uniaxial) electrospinning system was invented. Solid paraffin with the melting point of 32ºC nonadecane ($C_{19}H_{40}$), 58ºC heptacosane ($C_{27}H_{56}$), 89ºC tetratetracontane ($C_{44}H_{90}$) and 114ºC hectane ($C_{100}H_{202}$) were employed for the preparation of the paraffin/polyacrylonitrile nanofibers. Formation of paraffin-nanofiber hybrid structure is verified with FTIR, DSC, TGA and SEM Analysis.

As-spun paraffin/polyacrylonitrile nanofibers with the molecular weight of were used for thermal hysteresis enhancement of paraffin actuators. Paraffin actuator sub-components are defined and its sample preparation is explained in terms of methods and materials. Paraffin compound of the paraffin actuators was prepared with a mixture of pure nonadecane paraffin. An eye kept on opening stroke behavior of the paraffin actuators while determining the paraffin-nanofiber weight ratio. Paraffin/ Polyacrylonitrile nanofiber mixtures prepared with the wt. % of 2.5, 5, 7.5 and 10. The hysteresis value was successfully enhanced as 1.7, 3.4, 11.9 and 15.3% sequentially for the samples produced with the above ratios. Hysteresis enhancement of the paraffin actuator is discussed in terms of percolation threshold and thermal conductivity contrast effect theoretically.

Alternatively metal oxide microparticles and nanoparticles found use to improve thermal properties of paraffin in the paraffin actuators applications. A meaningful comparison between nanofiber addition and metal oxide nanoparticle addition was brought to light to examine the benefits of our development. Thermal hysteresis enhancement of paraffin actuators with nanofiber addition is compared with that of metal oxide nanoparticle. Nonadecane paraffin is used as the thermal expansion compound. Besides pure paraffin compound, paraffin mixed with the wt. % of 10 electrospun polyacrylonitrile nanofiber, CuO, Fe_3O_4, ZnO, Al_2O_3 nanoparticles are

used as nanocomposites in paraffin actuator for thermal hysteresis enhancement. Literally interconnection between nanofibers lanes and mats built a thermal network in the composite structure. Those interconnecting hubs in nanoscale are appointed by SEM images. Despite lowest thermal conductivity value of the polymeric material, nanofiber addition showed through other metal oxide nanoparticle added samples, best hysteresis value improvement as 30.8 % respectively compared with pure paraffin.

Another comparison carried out to examine the long term thermal behavior enhancement of nanofiber addition and metal oxide nanoparticle addition to the paraffin actuators which is essential for the product life time determination. High temperature storage test is performed to investigate the dispersion thermal stability of the paraffin actuator samples. Due to considerably lower density of the nanofiber very close to that of paraffin, nanofiber addition showed the least precipitation in the paraffin matrix through other metal oxide nanoparticle added samples. Nanofiber added paraffin actuator sample revealed best dispersion thermal stability with a hysteresis performance loss of 2.2%. Computer tomographic images expressed the precipitation behavior of nanofiber and metal oxide particles which supported the thermal hysteresis performance change exactly same.

2. THEORETICAL BASICS and LITERATURE REVIEW

2.1. Electrospinning of Nanofibers

Nanofibers have fiber cross sectional diameter less than one micron, produced with different production methods. Properties of nanofibers are figured according to production process and used among a large application area from medical to aerospace technologies. Main nanofiber production methods can be listed as electrospinning, phase separation, drawing, self-assembly, electroblowing, template synthesis and centrifugal spinning. Through these methods of nanofiber production, electrospinning provides the most multipurpose process via the diversity of applied materials such as polymers, metallic and ceramic as well as composite structures produced directly or through post-spinning processes. (Teo and Ramakrishna, 2006)

Electrospinning technology depends on electrostatic spinning of polymer solution droplets in an electric field. In 1969 the mathematical model of electrospinning studied by Taylor and the conical shape of the fluid droplets which is called “Taylor cone”. (Taylor, 1969) Polymer solutions, which forms a Taylor cone under electrospinning process, are subjected to fabricate nanofibers in different diameters and size.

Many kind of synthetic or natural polymers as well hybrid structures are already electrospinned from solutions, sol-gel suspensions or melts. Nanofiber morphology is affected by process parameters of electrospinning are applied voltage, distance of collector to capillary and flow rate of polymer solution. Solution parameters are affecting the nanofiber morphology which can be listed as polymer concentration, solvent volatility and solvent conductivity. Table 2.1 ,cited by Sill and von Recum’s research,shows the relationship between these parameters and fiber formation. Nevertheless, the exact relationship must be considered individually for each polymer-solvent system. For the same polymer and electrospinning setup, it can be fabricated fibers with many different fiber formation depending on solution specifications. These are general frameworks useful for defining the optimum parameters for a individual system (Sill and von Recum, 2008)

Table 2.1. Morphology of fiber affected by ectrospinning parameters (Sill and von Recum, 2008)

Parameter	Effect on fiber morphology
Applied voltage ↑	Fiber diameter ↓ initially, then ↑ (not monotonic)
Flow rate ↑	Fiber diameter ↑ (beaded morphologies occur if the flow rate is too high)
Distance between capillary and collector ↑	Fiber diameter ↓ (beaded morphologies occur if the distance between the capillary and collector is too short)
Polymer concentration (viscosity) ↑	Fiber diameter ↑ (within optimal range)
Solution conductivity ↑	Fiber diameter ↓ (broad diameter distribution)
Solvent volatility ↑	Fibers exhibit microtexture (pores on their surfaces, which increase surface area)

Different types of Electrospinning process are developed for fabrication of specific fiber structures. These can be sorted as Solution Based Electrospinning, Gas-Jacket Electrospinning, Melt Electrospinning, , Needleless Electrospinning ,Bubble Electrospinning , Magneto Electrospinning ,Conjugate Electrospinning, Centrifugal Electrospinning , Co-axial Electrospinning.

2.1.1. Solution based electrospinning

At the basic electrospinning process, the polymer solution droplet in a plastic syringe is pressed into the syringe needle by hydraulic pressure, where the droplet is subjected a strong electric field. The strong electric field intensed on the droplet surface and formed a cone-like surface shape which is called as the Taylor cone (Taylor, 1969). As soon as the electrical field overtakes a limit value, the electrical forces exceed the polymers

droplets surface tension and a nanoscaled polymer solution jet flow begins. Electrically charged jet accelerates elongates and reduces the polymer diameter to under micron scales. Solidification occurs through evaporation of the solvent by strong ventilation. Nanofibers randomly lay on the collector surface and assemble a thin layered nonwoven structure. Applied voltage is as high as 20-100kV. Distance of needle tip and collector is between 10-25cm in the spinning set-up (Greiner and Wendorff, 2007). Solution based electrospining effected by interfacial viscosity of streaming solution within air, viscosity of polymer solution, electrostatic repulsion force acted on liquid solution, applied voltage, needle to collector distance, ambiant temperature as illustrated in Figure 2.1. (Pelipenko et al., 2013)

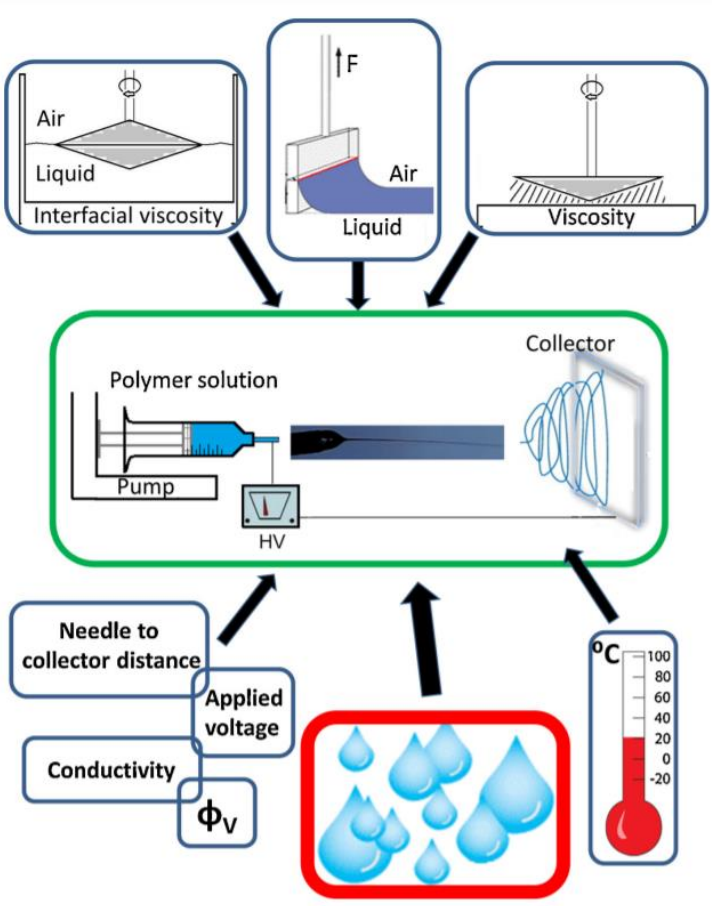

Figure 2.1. Electrospinning process **s**chematic representation , with parameters influences the electrospun product morphology. (modified from source: Pelipenko et al., 2013)

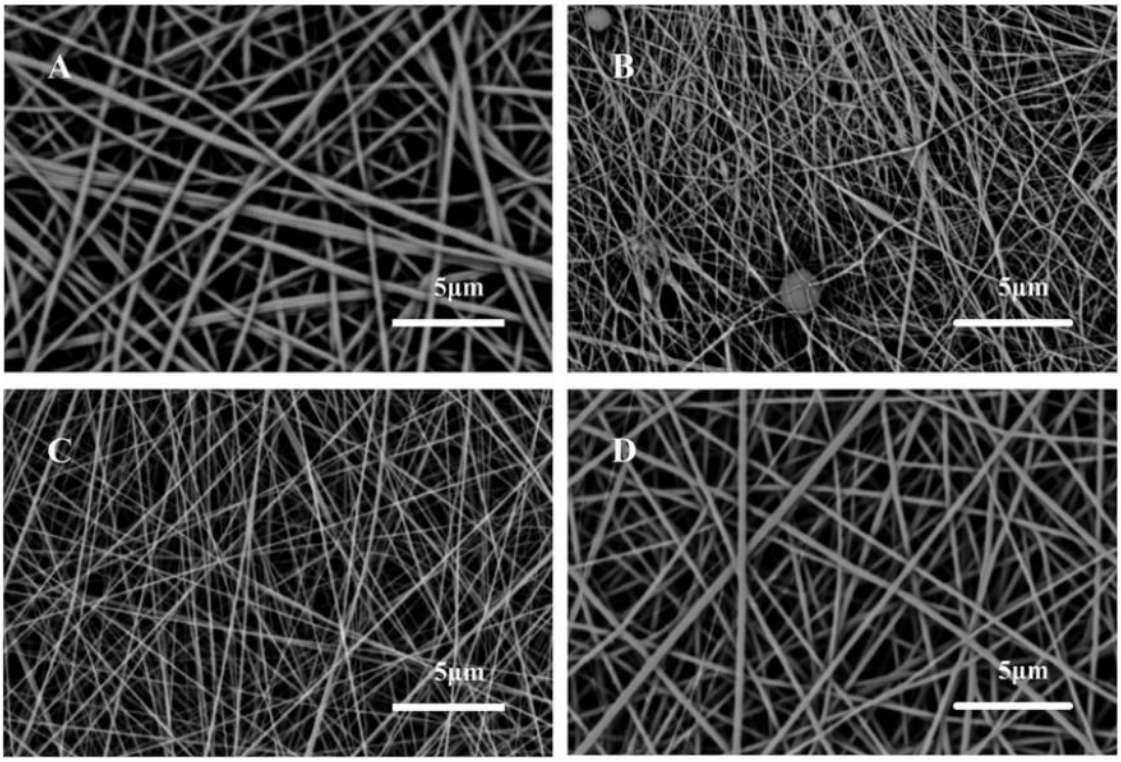

Figure 2.2. PAN nanofibers SEM images (A) and different concentration electrospun PAN–AA nanofibers of (B) 6 wt%, (C) 8 wt%, and (D) 10 wt%. (Yang et al., 2017)

Figure 2.2 demonstrates the nanofibers produced by solution based electrospining process with different solution concentrations , as well viscosity where obviosly dependence of the nanofiber diameter to the viscosity is visible. (Yang et al., 2017)

2.1.2. Melt electrospinning

Polymer melts can also be used for nanofiber production via electrospinning. The main advantage of the melt electrospinning is avoiding from solvent chemicals and using temperature to feed the liquid polymer to electrospinning zone. Viscoelastic behavior of molten polymer forms the Taylor cone on the end of spinneret at a specific voltage level and nanofiber spinning starts when the electrostatic loading exceeds the surface tension of polymer droplet. Even environmental and safety requirements commit non-chemical solvents usage, melt electrospinning is used for limited applications. Rheology of molten polymer which is directly affected by the small deviations of heat supply obstruct the continuous production of nanofiber with same quality. (Lyons et al., 2004)

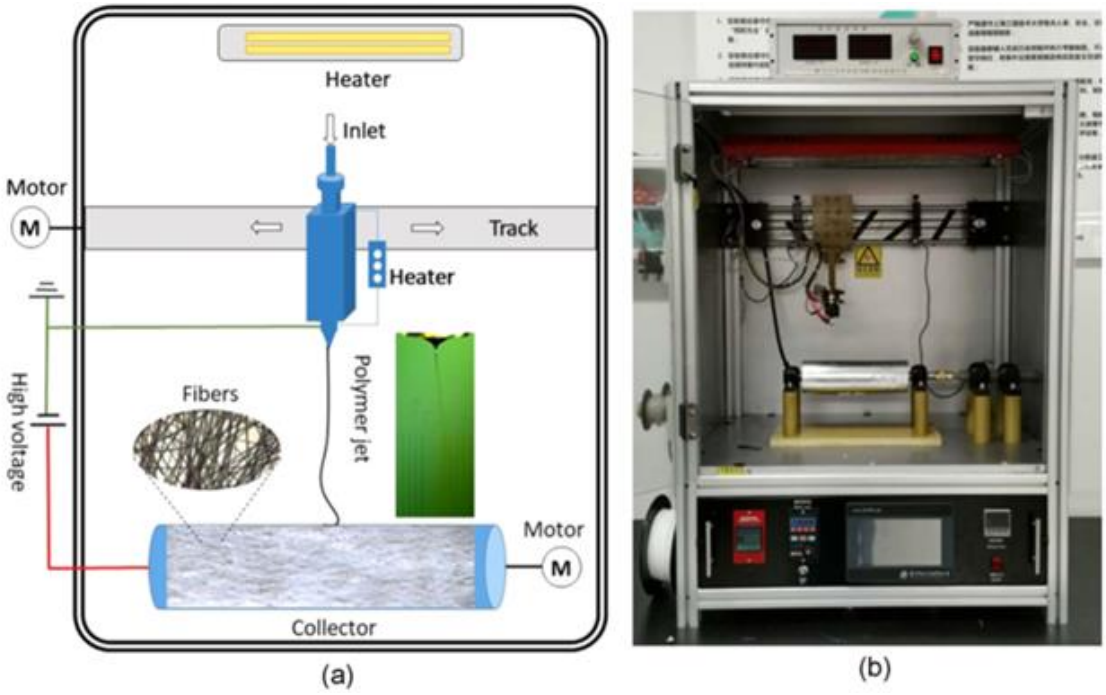

Figure 2.3. Melt Spinning- (a) Schematical Diagram and (b) picture of experimental device setup . (Mu et al., 2021)

Mu et al. investigated on factors acting on melt electrospinning process. Figure 2.3 shows the schematic diagram and the device picture of the mentioned investigation. Pellet-like Polypropylene was used as the polymer material. Temperature had an important effect on jet motion and Taylor cone. High voltage application caused to an electric field load on the droplet and a high speed jet formation occurred. Taylor cone size was smaller at that sample with at 220ºC than that of 300ºC. However more obvious whipping jet observed. It can be declared that different temperatures affected the viscosity and surface tension of molten polymer which influenced to the blowing of the jet and the Taylor cone's initial shape . This resulted changes in nanofiber diameter, structure and morphology.

In Mu's investigation temperature effects on fiber diameter is studied and various positions are used for observation of the fiber morphology. Temperature of nozzle heating has a magnificent effect on thefiber diameter and the orienetation of fiber.

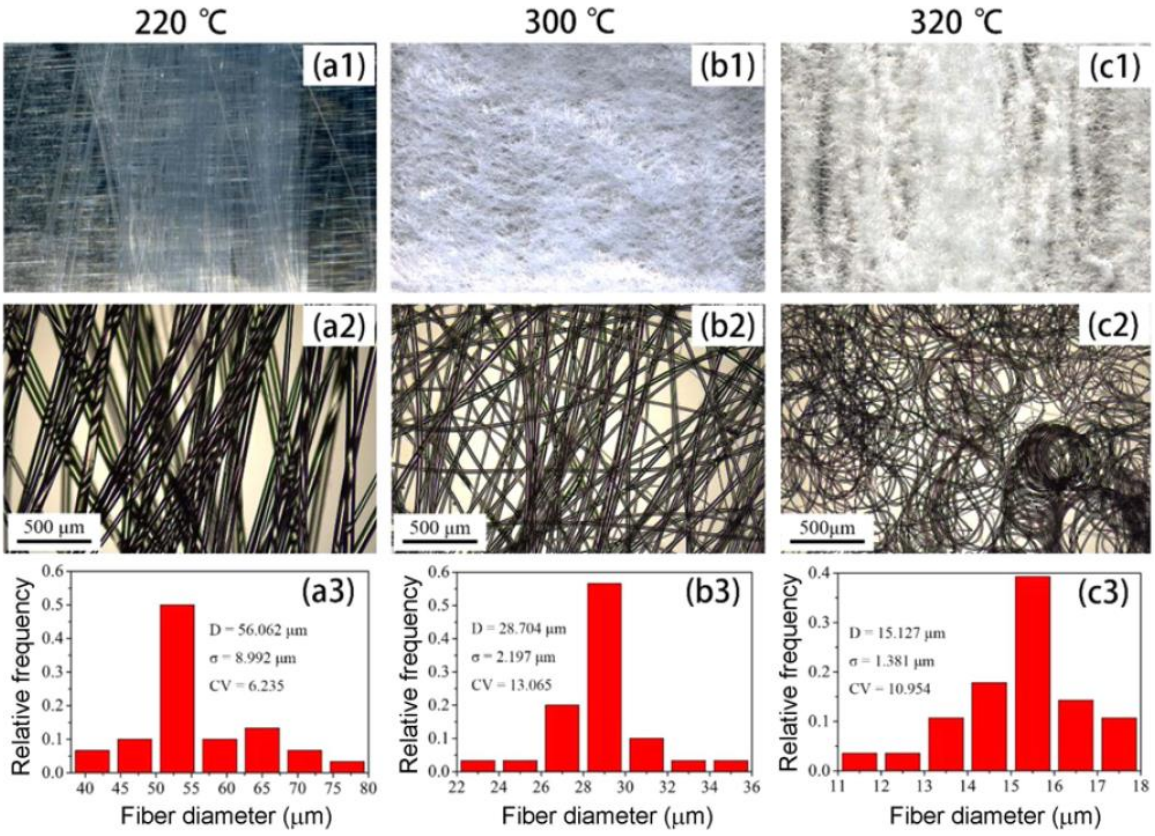

Figure 2.4. Fiber mats microscope images , with the temperatures of 220 ºC, 300 ºC, 320 ºC; (a1, c1) melt-electrospun microfiber mats images, (a2, c2) melt-electrospun fibers images, and (a3, c3) melt-electrospun microfibers diameters. (Mu et al., 2021)

Temperature increase changed the fiber shape enormosly. Parallelly oriented fibers are observed at 220 °C with uniformly distribution. At 300 °C, curly and wavy patterned fibers with alignment in horizontal and vertical directions revelaed as seen in Figure 2.4. Fiber crystallinity is affected directly from temperature where at 220ºC 42,59%, at 300ºC 41,71% and at 320ºC 36,60% crystallinity is measured. Mu concluded from the data that as the temperature increases, the fiber crystallinity degree decreases where it can be explained as the polypropylene's molecular chain of polypropylene is weakened at a an over temperature, decreasing the crystallinity. On the other hand mechanical properties of the fiber is dramatically affected by temperature change where breaking strength decreased from 13,87Mpa to 0,80MPa with the temperature increase from 220ºC to 320ºC. (Mu et al., 2021)

2.1.3. Gas-jacket electrospinning

Some polymer types are difficult to process in electrospinning by lack of insufficient forces based on electrical voltage. A special force source must support the electrospinning forces to boost the jet flow formation of polymer solution. An inert gas flow is used to execute a gas jacket around the spinneret tip.

Polyacrylic acid nanofibers were produced by the gas-jacket electrospinning technic by Aminyan and Bazgira. Figure 2.6 shows the diagram of the gas-assisted electrospinning of the research. They declared that gas-assisted method provides flawless and more regular fibers compared to the conventional electrospinning. In different ratios of NaOH 0, 15, 30 and 45% was used for the neutralization improving the spinnability and fiber properties. SEM micrographs revealed that increasing neutralization have an effect on swelling ratio with 30% neutralization. Increasing of feeding rate affected also swelling ratio as decreasing where optimal feeding rate was 20 μL/min. Increasing Polyacrylic acid concentration, decreased the ratio of swelling, with an optimal value of 9 wt% solution.

Figure 2.5. shows two nanofiber PLA electrspun nanofibers, left side conventional as-melt electrospun and right side gas assisted system applied where depending on the deformation through the hot gas stream, fibers with sub micron diameters can be produced with melt-electrospinning as seen in the figure. (Zhmayev et al,2010)

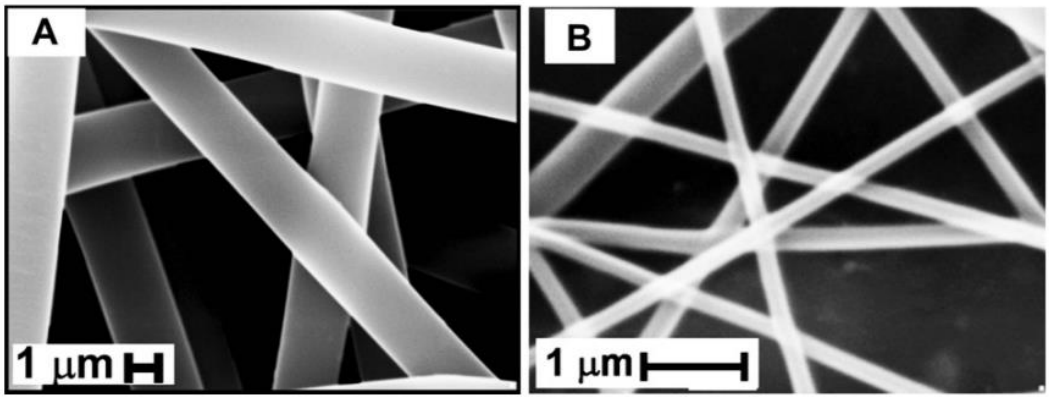

Figure 2.5. Melt-electrospun PLA fiber mats SEM Images: (A) gas-assisted system not used and (B) using gas-assisted system (Zhmayev et al,2010)

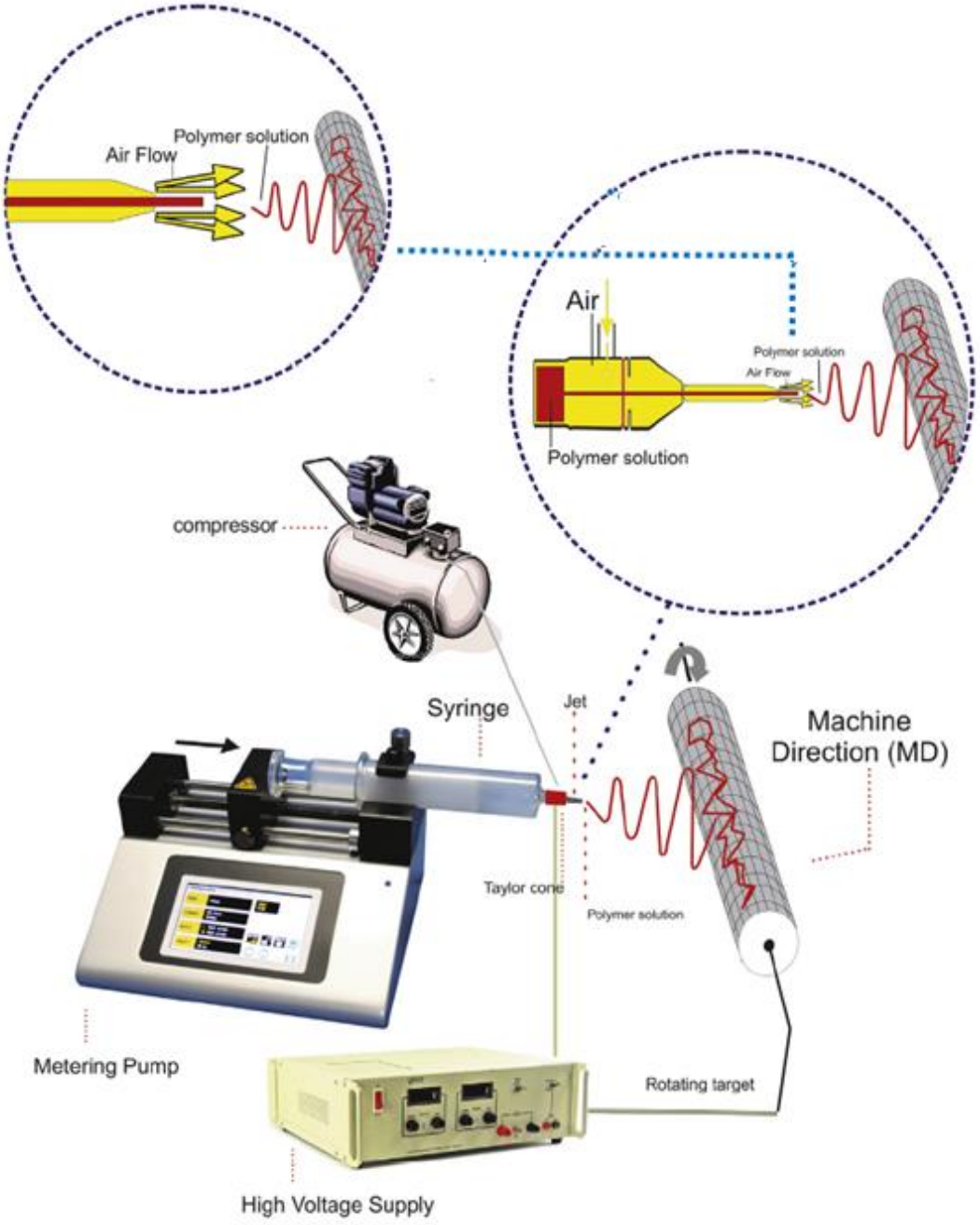

Figure 2.6. Gas-assisted electrospining system. (modified from source: Aminyana and Bazgira, 2019)

2.1.4. Bubble electrospinning

Bubble electrospinning uses an electric field charged to the polymer bubble surface, which quickly loosens on the bubble surface. As soon as the electric field exceeds the critical value needed to exceed the surface tension, the bubble ruptures and the broken bubble is pushed

upward to form a charged jet, which is then received as nanofibers on the metal receiver. (Zhao et al. 2015)

Figure 2.7 shows an example for a bubble electrospinning setup made by Liu and Friends, which includes DC high-voltage generator, flat metal plate grounded as collector, reservoir of solution, a gas tube, a gas pump, a metal thin electrode. (Liu et al. 2015)

Nanofiber are collected as randomly oriented non-woven form at Bubble-Electrospinning. This causes low molecular orientation as well as low mechanical properties. Low molecular orientation was caused by randomly oriented nanofibers. Shao and friends investigated on bubble electrospinning to modify it and placed a positively charged ring between parallel electrode collector and the bubble and for improving the nanofiber alignment degree. The results showed nanofiber diameter is decreased by the modification decreased, the diameter distribution and alignment of nanofiber is improved. (Shao et al. 2018)

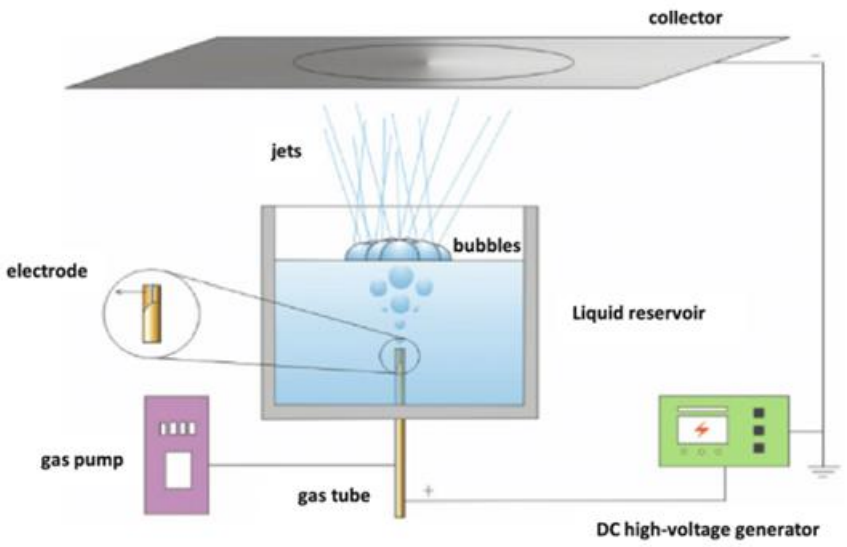

Figure 2.7. Bubble electrospinning setup (Liu et al. 2015)

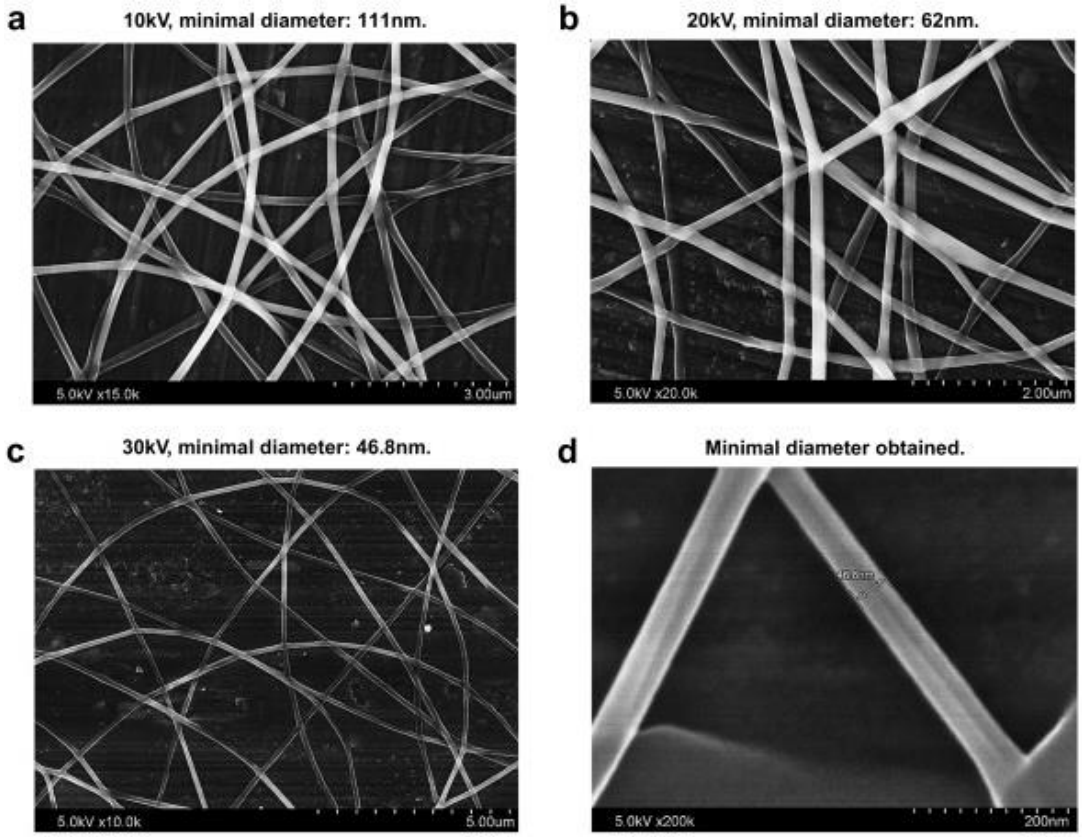

Figure 2.8. Distribution of fiber diameter size and SEM images of bubble-electrospun nanofibers. Applied voltages (a) 10 kV, (b) 20 kV, (c) 30 kV. (Yang et al. 2009)

Bubble-electrospun nanofibers produced by Yang et al. with three different voltages, from 8mm nozzel distance to the collector as shown in Figure 2.8, different nanofiber diameters generated at 10 kV, diameter minimum: 111 nm., 20 kV, diameter minimum: 62 nm. And, 30 kV, diameter minimum: 46.8 nm. (Yang et al. 2009)

2.1.5. Magneto electrospinning

Magneto Electrospinning of polymers based on magnetic nanoparticle embedded polymers. Aluminum foil is subjected to a magnetic field. The magnetic field is parallel to the electric field and perpendicular to collector in the system as shown in Figure 2.9. (Kartikowati et al., 2016) Magneto electrospinning has potential application areas like tissue-engineering scaffolds, magnetic filters, magnetic sensors, electromagnetic wave absorbers, microwave absorbers (Park et al., 2009), magnetic catalysts (Ghasemi et al.,

2015),, magnethic hyper thermia (Kim et al. 2013) and ferroelectric photovoltaic devices (Fei et al. 2015)

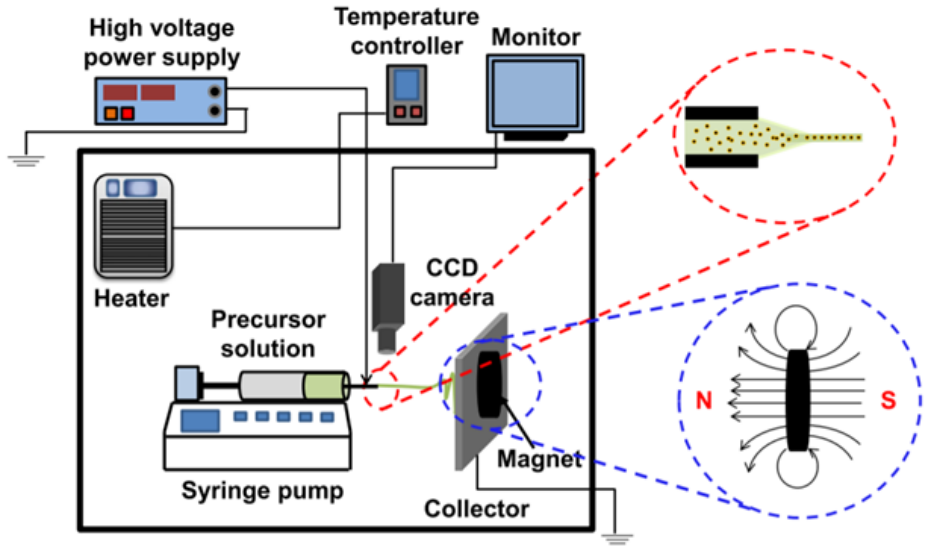

Figure 2.9. Magneto-electrospinning setup (Kartikowati et al., 2016)

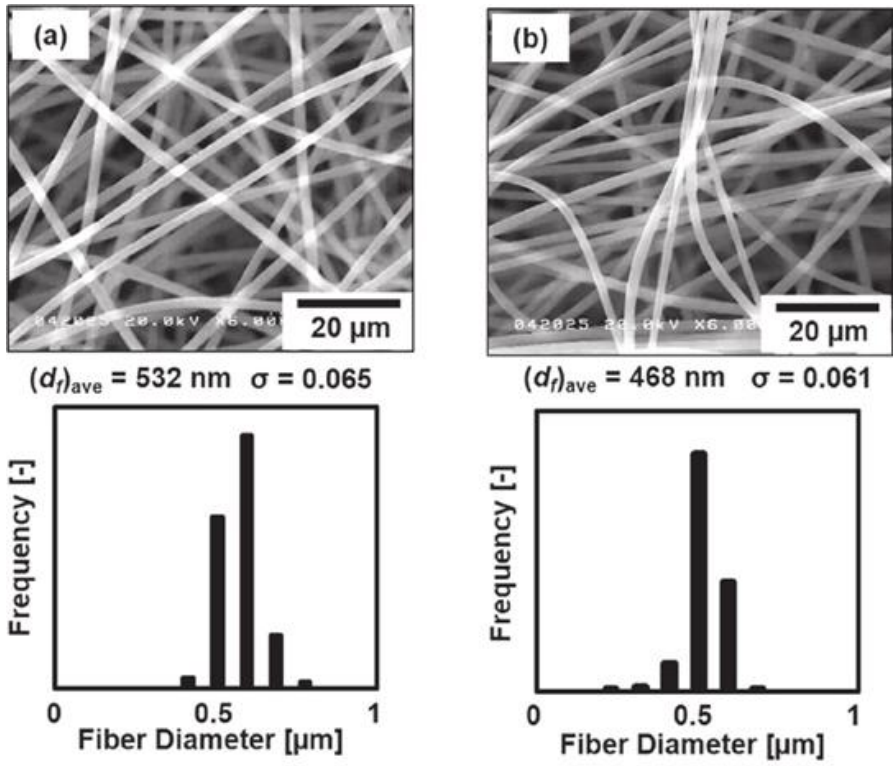

Figure 2.10. PVP nanofibers size distirbution and SEM images without magnetic field (a) and with magnetic field (b) (Kartikowati et al., 2016)

Figure 2.10 demonstrates the PVP nanofibers SEM images and diameter distribution of Kartikowati's study. Magnetic field applied nanofibers have lower diameter, revealing a distributiom with a lower standard deviation.

2.1.6. Conjugate electrospinning

At conjugated electrospinning two different solutions containing one oxidant and the other one reductant solution turns into nanofibers via two branch electrospinning method under a curing reaction mechanism. The opposite charges coupled these electrospinning jets. Active monomers are polymerized in the presence of free radicals produced in situ from a redox reaction that the jet containing oxidant met to the jet containing reductant. This process finalized as solidification of nanofibers from the conjugated jets. Figure 2.11 illustrates the electrospinning equipment and conjugated jet pictures from the experimental setup of Wang's study. (Wang et al. , 2019)

Fan et al. fabricated a polyaniline- polyacrylonitrile using the conjugate electrospinning based on microyarns simultaneously endowed with electrical conductivity .The hetero-structured microyarns had twisted structure and highly oriented fibers. The hetero-structured microyarns improved luminescent properties. (Fan et al., 2019)

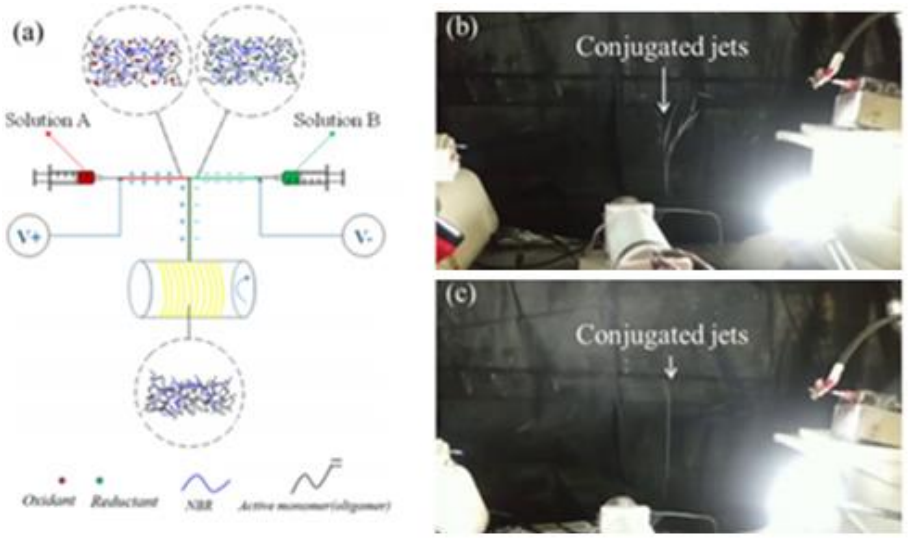

Figure 2.11. (a) Conjugate reaction e-spinning system and pictures (b, c) of conjugate electrospining process (modified from source: Wang et al. ,2019)

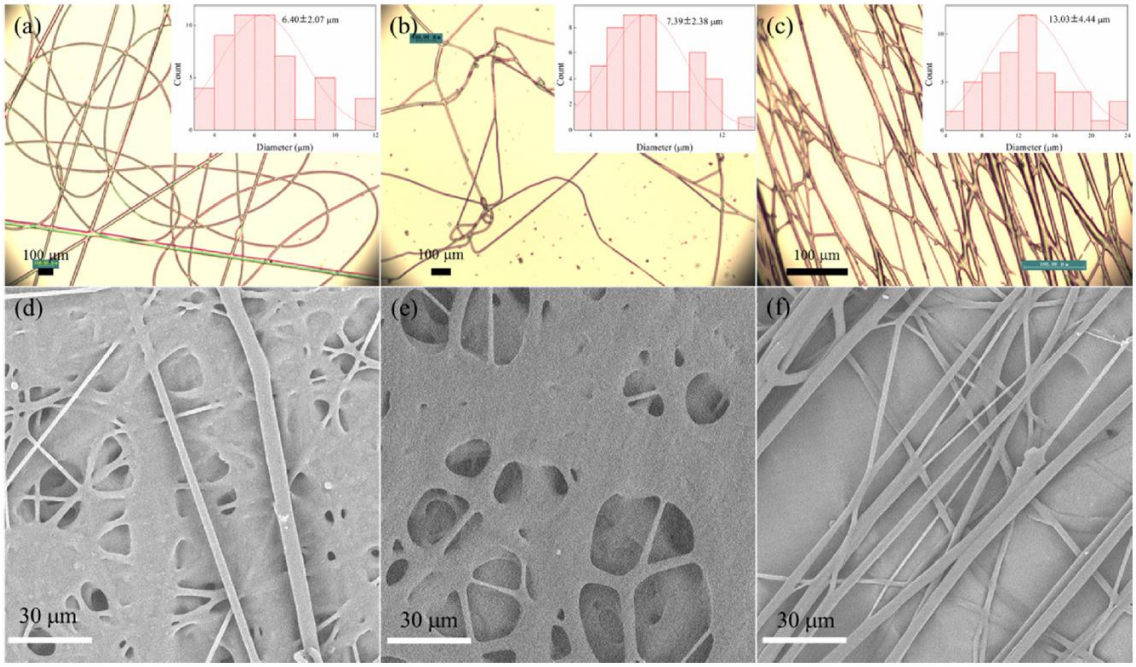

Figure 2.12 (a, b) Optical images of electrospun fibers of A and B single, as well as one (c) of A/B conjugated electrospun fibers soon after electrospinning. (d–f) SEM images of single A, B and conjugated A/B electrospun fibers 48 h after electrospinning process, respectively. (a),(b) and (c) Inset images are the diameter distributions of the as-spun fibers. (Wang et al. , 2019)

Figure 2.12 demonstrate the conjugated and non-conjugated nanofibers SEM imaes from Wang's study. (Wang et al. , 2019)

2.1.7. Co-axial electrospinning

Coaxial electrospinning consisting two capillaries which are coaxialy arranged . The composite droplet forms a composite Taylor cone is formed by composite droplet where the core polymer and shell polymer are pulled by Taylor cone. The shell polymer and core polymer are attracted to the Taylor cone of the composite droplet. The nanosized polymers are drawn by the electrospinning beam and collected on the fiber mat collector. (Reznik et al., 2006).

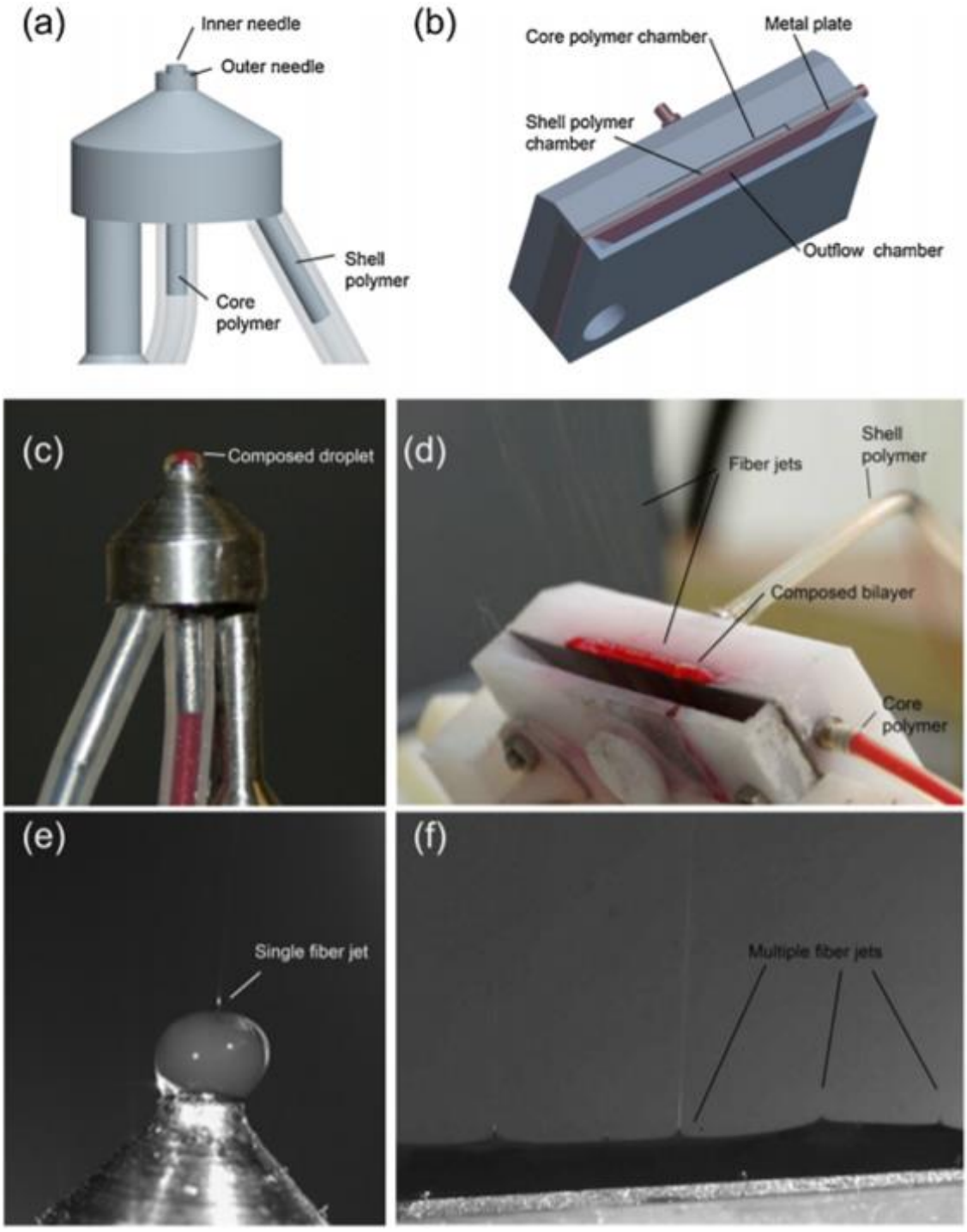

Figure 2.13. Coaxialy electrospinning: (a) coaxial spinneret with needle, (b) coaxial (weir) spinneret without needle, (c) polymeric droplet of coaxial needle spinneret , (d) polymeric bilayer of coaxial spinneret without needle, (e) polymer droplet of coaxial spinneret with needle , highspeed camera image, and (f) bilayer of coaxial spinneret without needle, high-speed camera image. (Vyslouzilova et al.,2017)

Vyslouzilova et al. investigated on the special spinneret for large amount coaxial nanofibers production. Figure 2.13 demonstrates its co-axial spineret equipment set-up. On the top of linear spinneret, bi-liquid layer is formed by the spinneret where formation of coaxial nanofibers enabled by electrospinning without needle. Production capacity of fibers increased by the fiber's core/shell morphology. (Vyslouzilova et al.,2017)

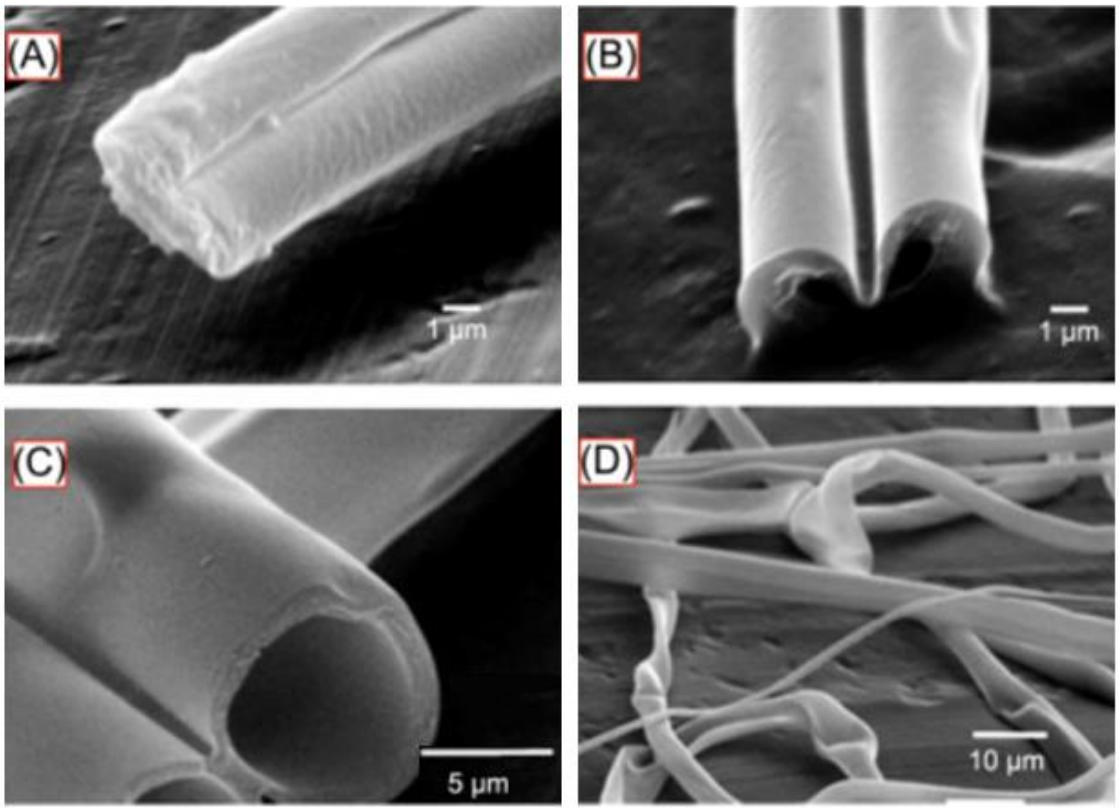

Figure 2.14. Coaxial electrospun, ID = 0.8/2.5 mm (core/sheath), SEM images of etched PMMA 20 wt% PMMA sheath solution with 1 mL/h feed rate, feed rates of mineral oil (A) 0.10 mL/h, (B) 0.40 mL/h, (C) 0.60 mL/h, and (D) 1,0 mL/h, (Chan and Kotaki, 2009)

Figure 2.14 depicts the relationship between morphologies of hollow fiber and feeding rates of core studied by Chan and Kotaki . The optimum feeding rate was 0.6 mL/h for production of structures with hollow form. Increase in feeding rate of core was changed morphology is gradually. (Chan and Kotaki, 2009)

2.1.8. Needleless electrospinning

Classical needle electrospinning has limited production capacity. Many investigations afforded to improve the productivity of electrospinning process. Needleless electrospinning technology was subject of for many research thus production with multiple jets meant to enhance the nanofiber production efficiency significantly.

Wei et al. investigated on needleless electrospinning with a system consist of a control pump of solution , spinneret made of metal dish, collector rotating system , a moving platform, spinneret base, power supply of DC high voltage. The insulating tube is connected with a hole to polymer solution in middle of spinneret. Feeding pump was set in center of the insulating tube which is used to transfer the solution to the spineret. As soon as a certain radian is reached by the solution, polyacrylonitrile solution is passed the metal dish. Figure 2.15 shows the new electrospinning device without needle for fabrication of nanofiber membranes . The device includes a temperature / humidity control system ,an unwinding system , a metal plate nozzle, rotating roller collector, a cross control system, and a high-voltage DC power supply. For industrialization, high quality nanofiber membranes can be produced with high efficiency. Surface morphology, pore diameter, filtration properties and stress-strain depending on main spinning parameters were investigated. A similar trend between filtration resistance and filtration efficiency revealed by results . Low resistance of filtration and high efficiency of filtration were 140 Pa and 94% , respectively. (Wei et al., 2021)

Mikes et al. used needleless electrospinning for facile production of lignin nanofibers. As the electric field source AC and DC and systems tested electrospinning without needle setup. Polymer dosing and fiber collection was complicated at DC needleless system where the AC electrospinning was more compatible technology in terms of for large-scale productions in future works. (Mikes et al., 2020)

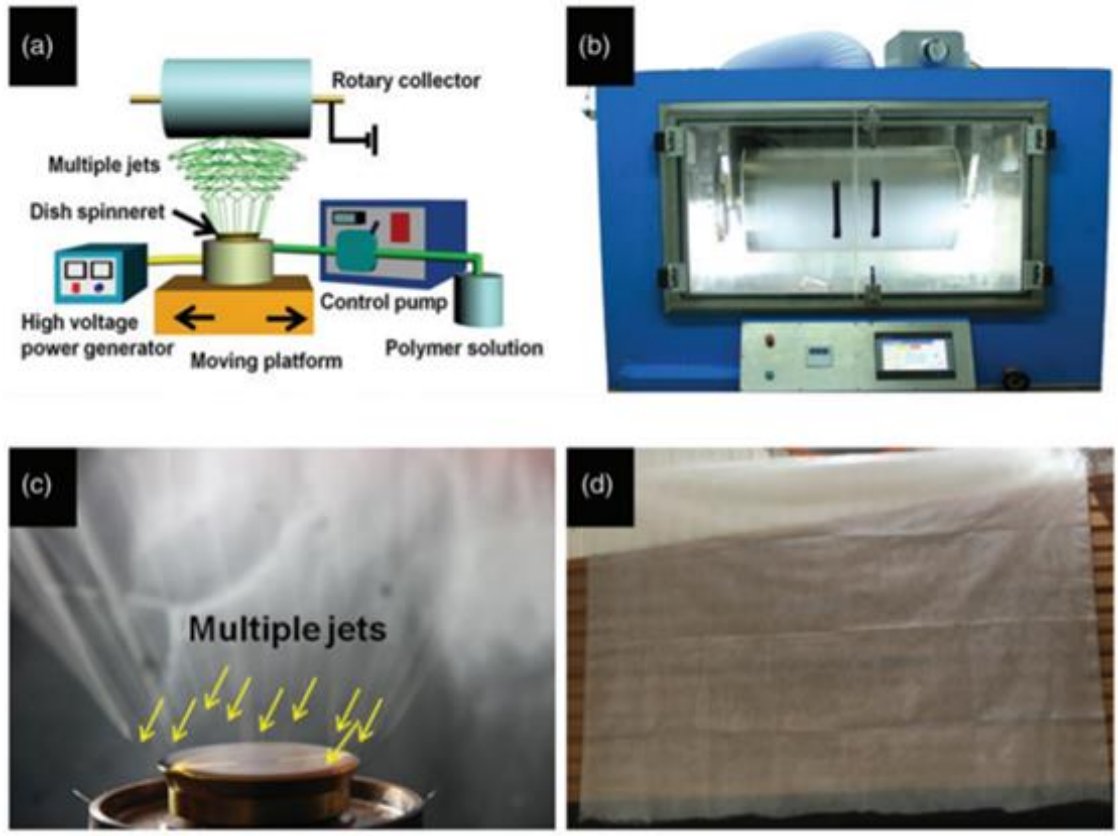

Figure 2.15. (a) and schematic map (b) setup of electrospinning without needle (c) multiple jets images and (d) membrane made of nanofiber. (modified from source: Wei et al., 2021)

Figure 2.16 shows visual results of electrospinning parameters; voltage and concentration effecting on the nanofiber morphology with the 15cm collecting distance at needleless electrospinning with multiple-jet. Applied voltages and solution concentrations are grouped in three different values for the nanofiber fabrication. Obviously that finer nanofibers could be fabricated with higher voltage and lower concetration value (65 kV, 10 wt %). Thicker nanofiber morphology observed, compared with higher solution concentrations of polymer and with lower the voltage supply. (Wei et al., 2021)

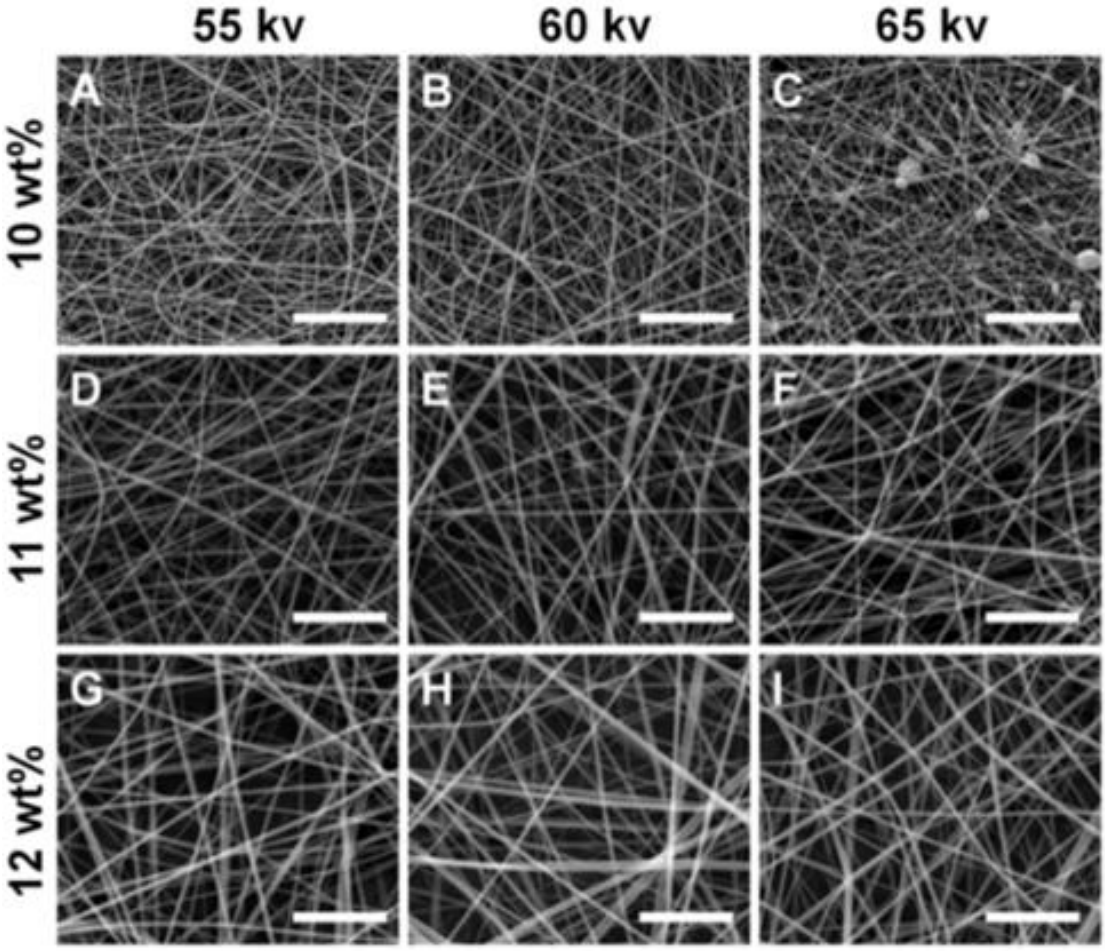

Figure 2.16. Different conditions of the spinning process used for nanofiber production. Scale bar : 5 μm (A) 10 wt %, 55 kV, (B) 10 wt % 60 kV, (C) 10 wt, 65 kV (D) 11 wt %, 55 kV (E) 11 wt %, 60 kV (F) 11 wt %, 65 kV (G) 12 wt %, 55 kV, (H) 12 wt %, 60 kV (I) 12 wt %. 65 kV. (Wei et al., 2021)

2.1.9. Centrifugal electrospinning

Centrifugal electrospinning comprises a collector and an electrospinning rotating spinneret which consist of compartments for solution; with two channels for hosting of media. Wang et al. presented a directional advance in multi- aligned fibers using multiple compartments and in engineering blended fibers where centrifugal and electrical forces issued for spinning process shown as in Figure 2.17. A combination of Polystyrene and Polyvinyl Pyrrolidone polymers was investigated where the system meant to be practicable to viscoelastic polymeric materials. (Wang et el., 2017)

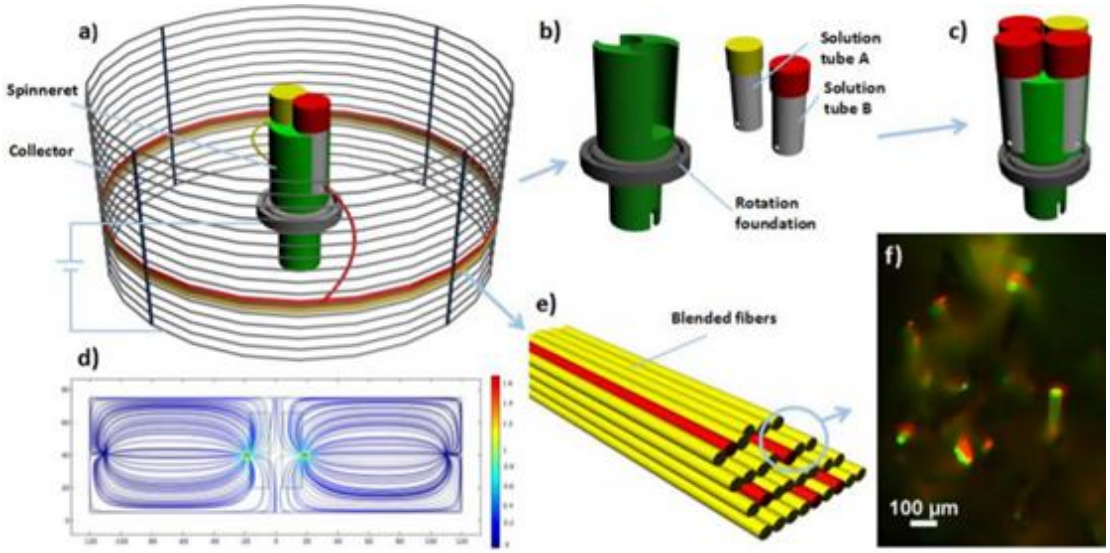

Figure 2.17. Centrifugal electrospinning system setup and fibers produced. (a) Centrifugal electrospinning system with combinatorial multi-compartment system-Schematic setup. (b) Two compartments detached spineret . (c) Four compartments hosted by spineret (d) Two individual jets - computational detail under an applied electric field. (e) Composite material illustration (f) Polyvinylpyrollidone blended system in fluorescent micrograph (Wang et el., 2017)

Hofmann and Kühne presented a productive method for PAN nanofiber nonwovens fabrication with centrifugal electrospinning where the parameter range for producing sub-micrometer sized nanofibers in a nonwoven membrane is established. (Hofmann and Kühne, 2021)

Rihova and friends studied on a cost effective centrifugal electrospinning method represented in Figure 2.18. where scanning electron microscopy images obtained from Polyvinylalcohol and Polyvinylpirollidone electrospun fibers with different polymeric concentrations. SEM images showed a smooth surface of fiber without visible defects, such as droplets, beads, cracks other imperfections upto 20 wt. %. On the other hand , Polyvinylpirollidone (10 wt. %) contained beads caused by low concentration. (Rihova et al., 2021)

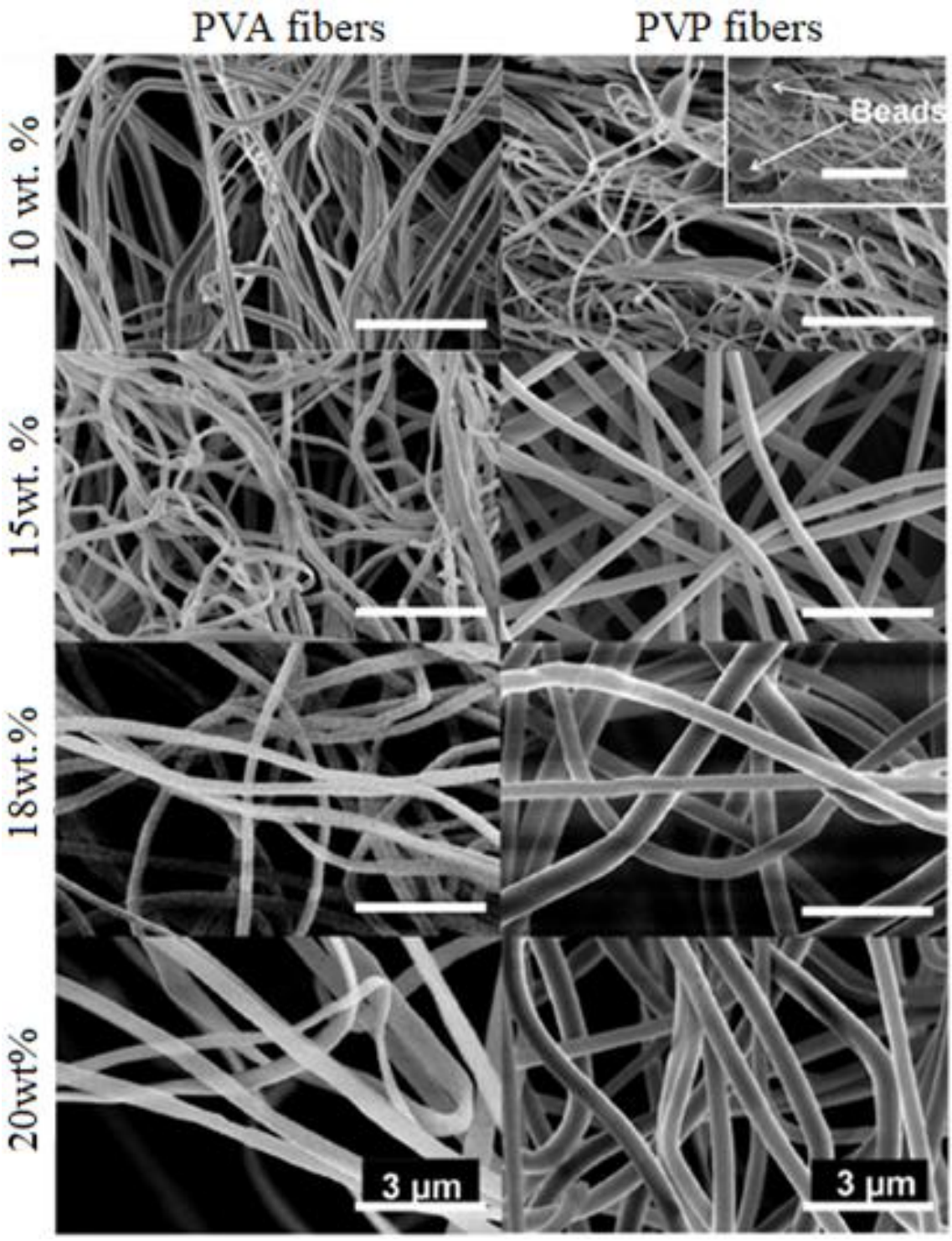

Figure 2.18. Electrospun fibers produced by the special 4SPIN® tool, SEM Images (scale bar: 3 µm) (Rihova et al., 2021)

2.2. Paraffins as Phase Change Materials

2.2.1. Phase change basics

Phase-change materials, defined by Fleicher as materials which shows a solid to liquid and liquid to solid phase transition at a temprature, better known as the melting-solifiying cycle, within a selected thermal applications operating range. When a material changes its phase from solid to liquid, it absorbs thermal energy from its environment while keeping a constant or nearly-constant temperature. The energy absorbed by the material increases the energy of composing molecules or composing atoms and increases their vibrational state. At the melting temperature, atomic bonds are loosen and the material turns from solid to liquid. Reversion of this process is solidifcation, in which the liquid material exposes energy to its environment and the molecules and atoms lose energy and forming into their solid phase. (Fleischer, 2015)

In the last few decades , energy storage materials, including paraffins, eutectic mixtures of organic and inorganic compounds, hydrated salts, fatty acids are subjected to many investigations .Researches on phase change materials are basically focused on thermal energy storage where various material types have been examined previously. Figure 2.20 shows range of melting enthalpy and melting temperature for the certain materials. (Cabeza et al., 2011)

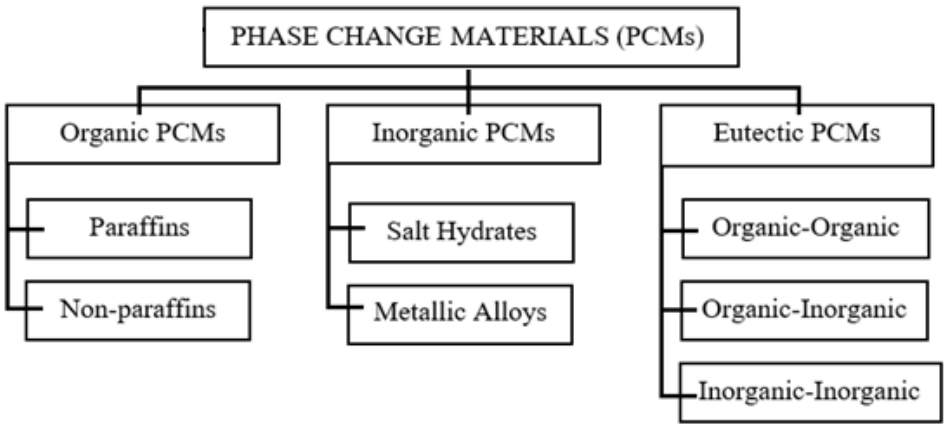

Figure 2.19. Scheme of phase-change material classification (Kapsalis and Karamanis,2016)

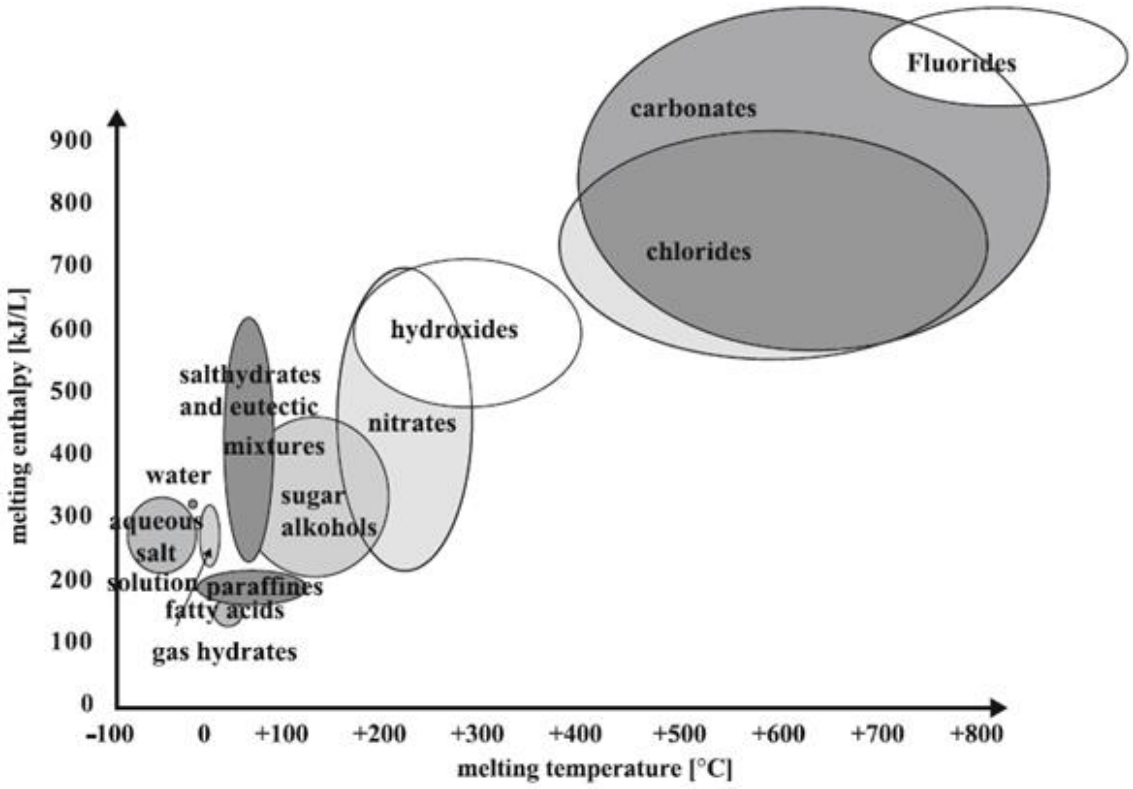

Figure 2.20. Material classes applicable as phase change material regarding to specific melting enthalpy and melting temperature range (Cabeza et al., 2011)

Classification of phase change materials can be noticed according to their content eutectic, inorganic and organic. Figure 2.19 demonstrates the classification of phase change materials. Inorganic materials have a larger temperature range and usually density over 1g/cm3 and have higher melting enthalpy organic phase change materials. Organic materials have mostly density smaller 1g/cm3 and lower melting enthalpy. Mixture of organic and inorganic phase change materials also investigated to cover the advantages of both classes. Organic phase change materials are consist of paraffins and non-paraffins. Energy storage materials can be categorized into two groups organic and inorganic according to their composition. Further two subcategories can be used as eutectic and mixed temperature ranges. (Kapsalis and Karamanis,2016)

2.2.2. Paraffins

Paraffins belong to organic phase change materials besides sugar alcohols and fatty acids. The most common used organic phase change materials are paraffins. Melting temperature of paraffins concludes between 6ºC and 108ºC. Paraffins have linear alkane molecular chains with the formula of C_nH_{2n+2} with the chemical structure shown in Figure 2.21. Classification of the paraffins according to physical states and the number of carbon atoms done by Gulfam R. et al. where pure alkanes for 1–4 numbers of carbons in a gas phase at room temperature, liquid paraffins for 5–17 carbons, solid waxes for more than 17 are designated. Solid paraffin waxes are consisting a mixture of saturated hydrocarbons of high branched, linear, cyclo and isoalkanes. (Gulfam et al. 2019)

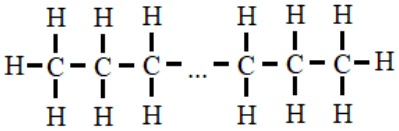

Figure 2.21. Paraffin- chemical structure (Boese et al.1999)

Packaging of n-alkanes demonstrates the crystal structure of paraffins in Figure 2.21 based on Boese and friends investigations. The investigation resulted that the molecular structures of the n-alkanes have a carbon skeleton with planar arrangement. The mean $C(H_2)$- $C(H_2)$ and $C(H_3)$- $C(H_2)$ distances of the investigated n-alkanes are both 1.521(1) Armstrong. The mean angles for $C(H_2)$-$C(H_2)$-$C(H_2)$ and $C(H_3)$-$C(H_2)$-C are 112.8(1) and 113.5(1), respectively.

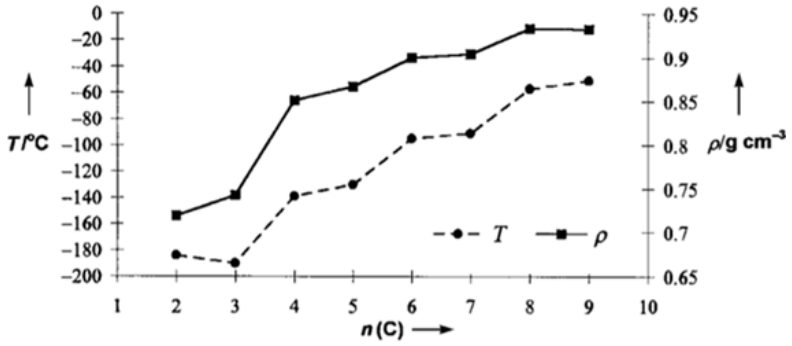

Figure 2.22. Trends in melting points [$T/^oC$] and densities [$\rho/g\ cm^{-3}$] of the n-alkanes C atoms [$n(C)$] number increase (Boese et al.1999)

These values represent the X-ray standard values of undistorted n-alkanes. n-Alkanes with even-numbered carbon atoms have ideal intermolecular contacts at both molecular chain ends. n-Alkanes with odd-numbered carbon atoms have ideal intermolecular contact at one molecular chain end, and at other end have longer distance. This leads to less dense packing of individual n-alkanes obtained at odd-numbered n-alkanes because of this phenomenon which leads to lower melting points than even-numbered n-alkanes, as shown in Figure 2.23. Relation between the melting points and carbon atom number is shown at Figure 2.22. (Boese et al.1999)

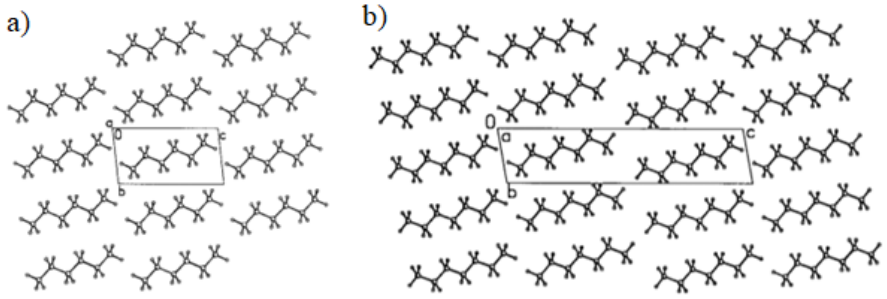

Figure 2.23. Packing of n-hexane (a) and of n-heptane (b) viwed along the a axis. (Mann et al. 2018)

Table 2.2 demonstrates the paraffins with different carbon atom numbers as a member of n-alkanes. Paraffins have low density, high phase change enthalpy with very stable melting and solidifying behavior. Boese's investigation declared that paraffins are very deaf to temperature changes with a thermal conductivity as low as 0,186 W/mK in solid state and 0,138 W/mK in liquid state as seen at Figure 2.24. Volumetric expansion of paraffin waxes from solid to liquid phase is as high as up to 15%. (Mann et al. 2018) This high volumetric expansion rate makes the paraffin ideal for paraffin actuators applications.

Paraffins are not soluble in water, do not react with common chemicals reagents. They are very compatible with metals. Paraffins have very few safety constraints. (Mehling and Cabeza, 2008) These properties provided to paraffin a wide application area in automotive engine cooling systems as paraffin actuators in thermostats with a very safe and high reliable lifetime experiences.

Table 2.2. Thermophysical properties of n-paraffins and commercial paraffinic phase change materials (Sharma and Tyagi 2009), (Khan et al. 2016)

Materials	Melting point (°C)	Latent heat (kJ/kg)	*Density (kg/m³)	**Thermal conductivity(W/mK)
n-Tetradecane	6	228-230	763	0.14
n-Pentadecane	10	205	770	0.2
n-Hexadecane	18	237	770	0.2
n-Heptadecane	22	213	760	0.145
n-Octadecane	28	245	865	0.148
n-Nonadecane	32	222	830	0.22
n-Eicosane	37	246		
n-Henicosane	40	200,213	778	
n-Docosane	44.5	249	880	0.2
n-Tricosane	47.5	232		
n-Tetracosane	52	255		
n-Pentacosane	54	238		
n-Hexacosane	56.5	256		
n-Heptacosane	59	236		
n-Octacosane	64.5	253		
n-Nonacosane	65	240		
n-Triacontane	66	251		
n-Hentriacontane	67	242		
n-Dotriacontane	69	170		
n-Triatriacontane	71	268	880	0.2
Paraffin C_{16}-C_{18}	20-22	152		
Paraffin C_{13}-C_{24}	22-24	189	900	0.21
RT 35 HC	35	240	880	0.2
Paraffin C_{16}-C_{28}	42-44	189	910	
Paraffin C_{20}-C_{33}	48-50	189	912	
Paraffin C_{22}-C_{45}	58-60	189	920	0.2
Paraffin C_{21}-C_{50}	66-68	189	930	
RT 70 HC	69-71	260	880	0.2
Paraffin natural wax 811	82-86	85		0.72 (solid)
Paraffin natural wax 106	101-108	80		0.65 (solid)
*At 20°C. , **Just above melting point (liquid phase).				

-Main physical criteria of phase change materials in use of paraffin actuators are the phase change temperature to assure the initial movement temperature of the paraffin actuator. This specific temperature is called as first opening temperature of the paraffin actuator and must have an accurate value with a very narrow tolerance such as ±0.5 ºC. Because of that in terms of paraffins, a highly purified paraffin molecules are required to provide the accurate phase change temperature. This significant issue will be discussed in next topic.

-High thermal conductivity is required for the high sensibility to environmental temperature change. Low thermal conductivity causes postponed reaction of paraffin actuator to the temperature fluctuation of cooling circuits especially in terms of short time acceleration of engines. Thermal conductivity of paraffins will be interpreted under the topic thermal behavior of paraffins.

-Low thermal hysteresis is preferred to assure the equivalent / balanced actuator movement from solid to liquid and liquid to solid phase change determined as opening and closing of the actuator. Thermal hysteresis will be explained deeply under the topic thermal behavior of paraffins.

-Low subcooling is requested to maintain the same temperature for melting and solidifying of the paraffin compound. Subcooling of the phase change materials will be discussed under the topic thermal behavior of paraffins.
Following points can be concluded as the further selection requirements of phase change materials.

-High phase change volume expansion is required to achieve enough actuator stroke. For conventional applications an actuator stroke of 10mm is essential for fulfill the opening requirement of cooling circuits.

-High reproducibility of phase change is recommended for the actuation accuracy of whole lifetime. To validate the reproducibility up 100.000 cycles of cold/hot conditions is settled for modern engines.

-High environmental stability is required against high temperature, high pressure, chemical and physical factors. High temperature of engine environment up to 150ºC, aggressive coolants and high inner pressure of paraffin actuators up to 200bars must be compensated by the paraffin compound. Non-toxicity is required for employee safety requirements and environmental reasons. Payable price for required for economical serial production cost required. A balance with high quality paraffin with price-performance ratio

2.2.3. Thermal behavior of paraffins

2.2.3.1. Thermal conductivity of paraffins

Thermal conductivity of paraffin is so low that in many application it is used as thermal insulation material. (Torres-Rodriguez et al. 2020) Table2.2 shows the thermal conductivity values of paraffins with different carbon atom numbers C_{40} to C_{50} which varies from 0.14 to 0.20 W/mK. A practical calculation of thermal conductivity of paraffins is established by Freund et al. which is meant to be valid for macrocrystalline paraffin waxes having melting points in the 50 to 54 °C range, over the temperature range from —180°C to +30 °C, using the following empirical -equation:

$$\lambda = 0.005 \cdot (1\text{-}0.0016t)$$

where λ is thermal conductivity in J/m•°C•s, and t is temperature in °C. The above relationship is acceptable as an approach for microcrystalline waxes and for paraffins liquid at ambient temperature. The relationship between thermal conductivity and temperature implies that increasing the temperature of the paraffin will decrease the thermal conductivity it. Investigations of Velez et al. confirm this relation with experimental results for n-pentadecane, n-nonadecane, n-octadecane, n-heptadecane, n-eicosane and n-hexadecane. Thermal conductivity reduction of paraffins occurs after phase change from solid to liquid significantly. Near the melting point of the paraffin there is a big jump of thermal conductivity is conducted which can be observed at all paraffins with different carbon atom numbers.

A more specific equation for the thermal conduction of phase change materials established by Bony and Citherlet where the thermal conductivity difference between the solid states and liquid states of a material, the model allows two different values for the conduction coefficient; one for the liquid phase and one for the solid phase. λ_{solid} refers to the thermal conductivity below the enthalpy value H1at solid state before the phase change, and λ_{liquid} refers to the thermal conductivity above the enthalpy value H2 at liquid state after the phase change. $\lambda_{sol/liq}$ refers to the thermal conductivity between these two enthalpy values calculated by the following linear interpolation where, H^t is the value of enthalpy at temperature step t shown by Figure 2.24 depends on their study. (Bony and Citherlet, 2007)

$$\lambda_{sol/liq} = \lambda_{sol} + \frac{(\lambda_{sol} - \lambda_{liq})}{H2 - H1}(H^t - H1)$$

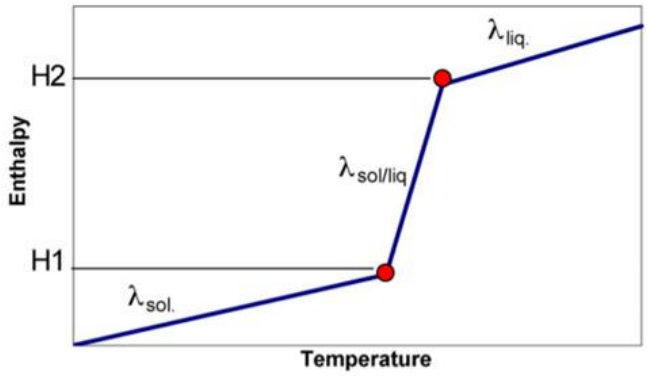

Figure 2.24. Thermal conductivity λ relative to enthalpy *H*. (Bony and Citherlet, 2007)

The temperature increase in solid state and liquid state has a smooth tangential line. At the temperature interval where the paraffin phase changed there is a steep tangential line in a very short period caused by the jump. This characteristic is repetitive revealed for investigated paraffin , n-eicosane, n-nonadecane, n-octadecane, n-heptadecane, n-hexadecane, n-pentadecane in different researchs studied by Velez, Holmen, Assael, Yaws, Wada, Bogatov, Rastorguev, Duan, Stryker, Nabil and Fang as seen in Figure 2.25. Figures are reproduced from works of Velez et al. 2015-I and 2015-II.

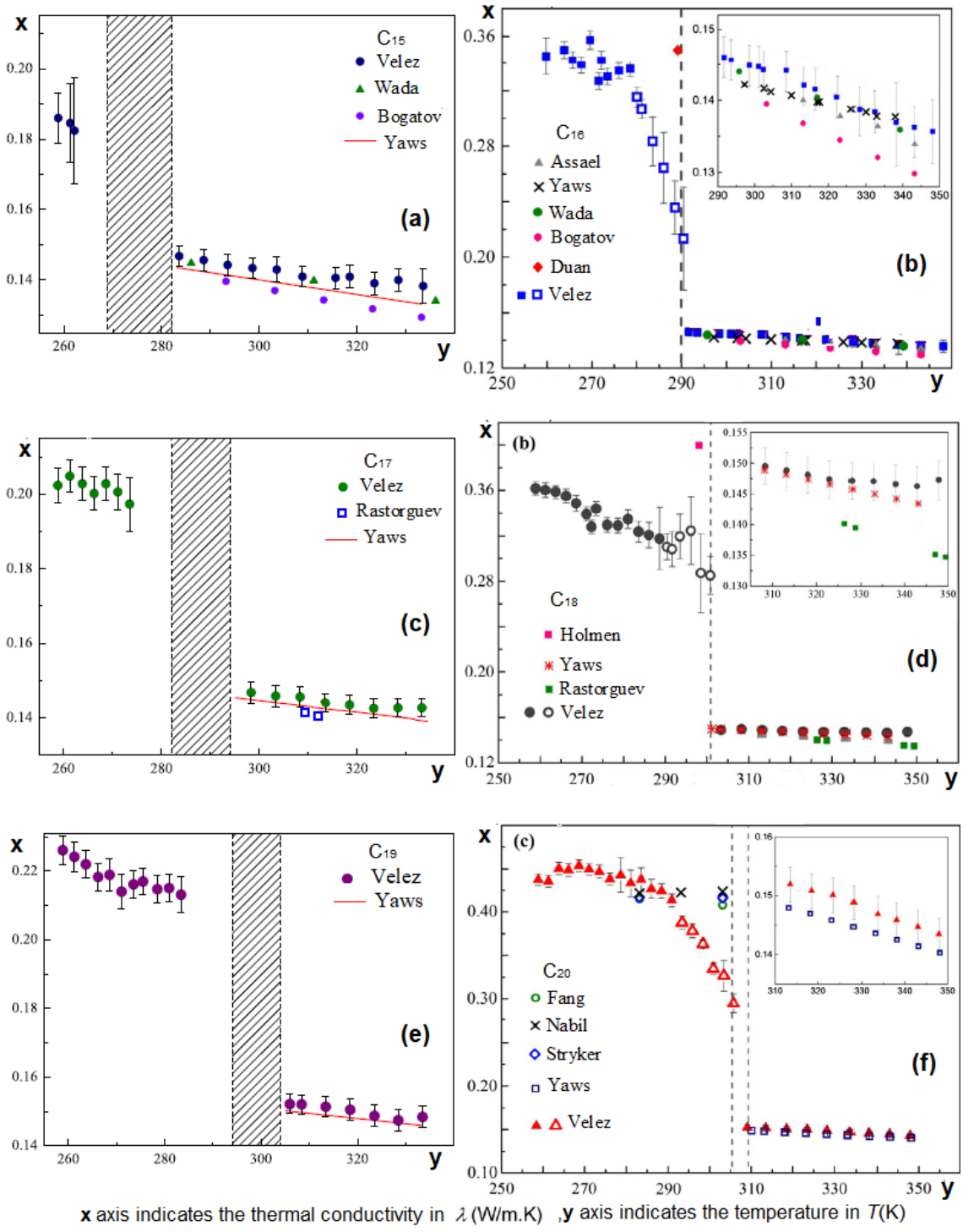

Figure 2.25. Thermal Conductivity measured for (a) C_{15} n-pentane, (b) C_{16} n-hexadecane , (c) C_{17} n-heptadecane, (d) C_{18} n-octadecane, (e) C_{19} n-nonadecane, (f) C_{20} n-eicosane in accordance with temperature, together with literature data as depicted. The patterned area correspond to the disordered solid state (between the two observed DSC peaks) (modified from source: Velez et al. 2015-I and 2015-II)

Another output of these investigations can be declared that the increase in carbon atom numbers of paraffin increases the thermal conductivity value respectively. Thermal Conductivity of odd-numbered paraffins presents a discontinuity at the solid-liquid phase transition. Thermal conductivity affects the response time of the paraffin actuators in terms of acceleration of the opening and closing stroke. Higher thermal conductivity of paraffin compound provides a faster volume expansion and it is converted to faster stroke of paraffin actuator. So that the higher sensitivity of paraffin actuator to environment temperature change can be granted.

2.2.3.2. Thermal hysteresis behavior of paraffins

Paraffin has a high thermal hysteresis value due to the thermal conductivity difference that of solid state and liquid state as well as during phase transition. Figures 2.25 shows the temperature dependend thermal conductivity measurements for given paraffin types. Hysteresis can be detected also in the enthalpy temperature curve with interruption of melting and cooling down of paraffin shown in Figure 2.26. (Andrassy, Z. and Szantho, Z., 2019) Thermal hysteresis of the paraffin can be observed at paraffin actuators in the curves of opening/closing stroke versus temperature while heating and cooling cycles. The closing curve does not match with the opening curve where always a temperate gap in-between exists.

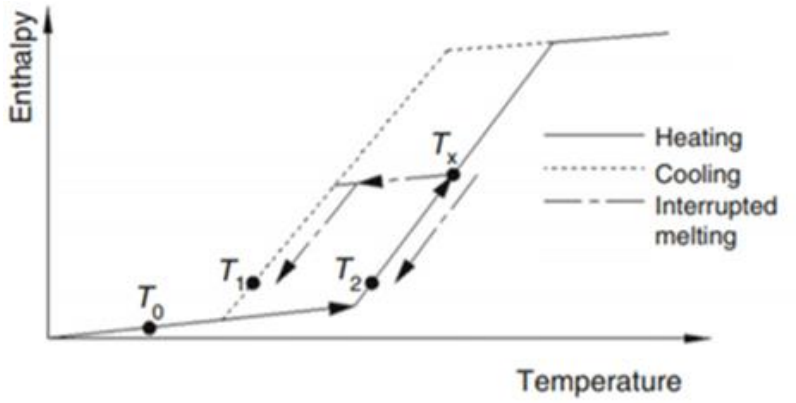

Figure 2.26. Phase change material behavior model while interrupted melting and cooling down of phase change material (Andrassy and Szantho, 2019)

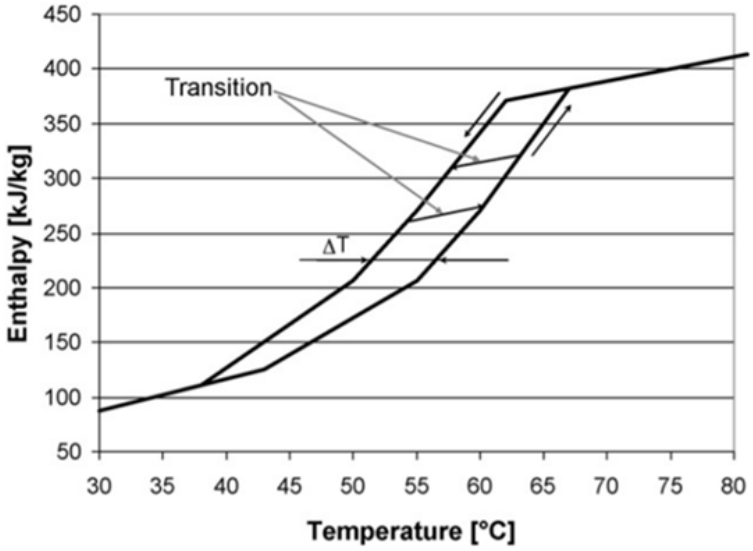

Figure 2.27. Hysteresis model (Chandrasekharan et al. 2013)

Thermal hysteresis behavior of phase change materials is modelled by Bony and Citherlet as Transition Model and by Chandrasekharan as Non-Transition Model in two different methods.

Transition model demonstrates the enthalpy curve shift in accordance with a differential temperature defined by a parameter. While a cooling or heating step in the phase change region, the slope of transition is equal to the solid phase one in the phase change bottom part. It is also same to the slope of the liquid phase in the phase change superior part. Enthalpy curve's discontinuity is avoided when the point of transition is close to the complete solid or liquid phase change as shown in Figure 2.28. (Bony and Citherlet, 2006)

At the transition model the phase change material shows hysteresis which initially is cooling in the phase change region, on the freezing curve where the transition specific heat is calculated as the average value of liquid and solid specific heats. Research of Chandrasekharan indicates the phase change materials which follow the same curve during melting and solidification in the same phase change region as shown in Figure 2.27. This non-transition approach covers the materials when it cools from a complete

liquid state. (Chandrasekharan et al. 2013) Thermal Hysteresis behavior of Paraffin actuator coincides with the non-transition model of Chandrasekharan.

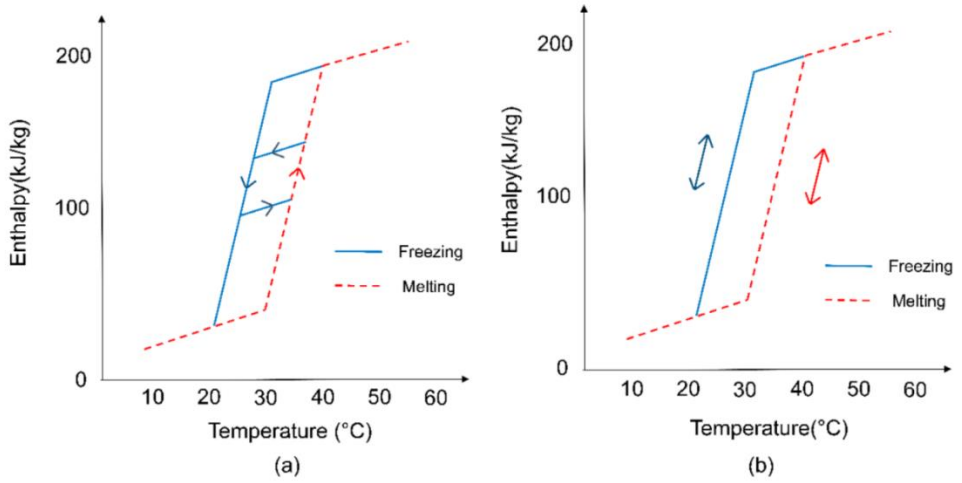

Figure 2.28 (a) Transition model (b) One curve model (Bony and Citherlet, 2006)

2.2.3.3. Subcooling behavior of paraffins

Subcooling of paraffin is a thermal phase change property which can negatively affect on closing function of paraffin actuator. If the liquid paraffin cooled down below melting temperature, the solidification is expected. If the solidification needs lower temperature than melting point, then this phase change phenomenon is called subcooling and this lower solidification temperature is called nucleation temperature. Sub-cooling's reason is, either growth rate of the nuclei or the nucleation rate (or both) is slow (Dincer and Rosen, 2002).

Subcooling effect of phase change materials can be seen at Figure 2.29 and a combination of subcooling and hysteresis at Figure 2.30 . (Bony and Citherlet, 2007)
At the temperature depended closing curve of the paraffin actuator can suffer from subcooling as shown in Figure 2.30.

Huang and friends investigated the subcooling of paraffins experimentally as paraffin-water emulsion. Pure paraffins showed small subcooling lower than 2K. Even though paraffins are having identical properties, the nucleation temperatures in the emulsion is

effected by paraffin type. Surfactants had insignificant impact on the melting temperatures of paraffins but surfactant type changes the subcooling and nucleation temperature. Nucleating agents can reduce the subcooling where the agent and fraction of agent had significant role both on the nucleation and melting temperature. Emulsions melting temperature decreases and temperature of nucleation increases with the increase of nucleation agent fraction. If the the sufficient additional seeds in the droplets of paraffins procured by nucleation agent support, the subcooling can be reduced.

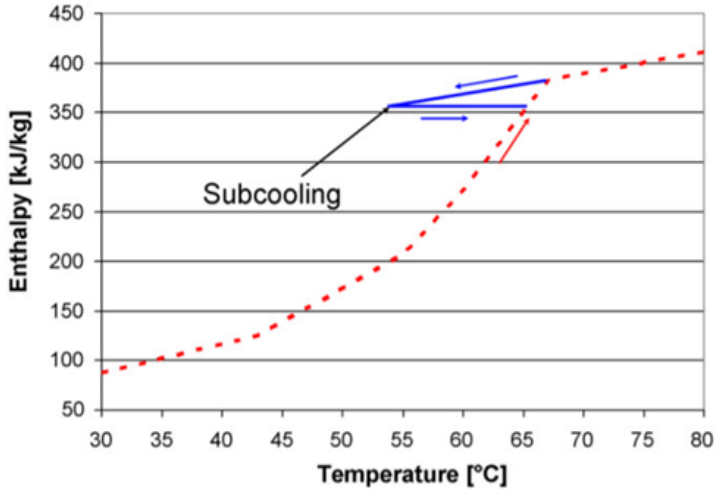

Figure 2.29. Subcooling model (Bony and Citherlet, 2007)

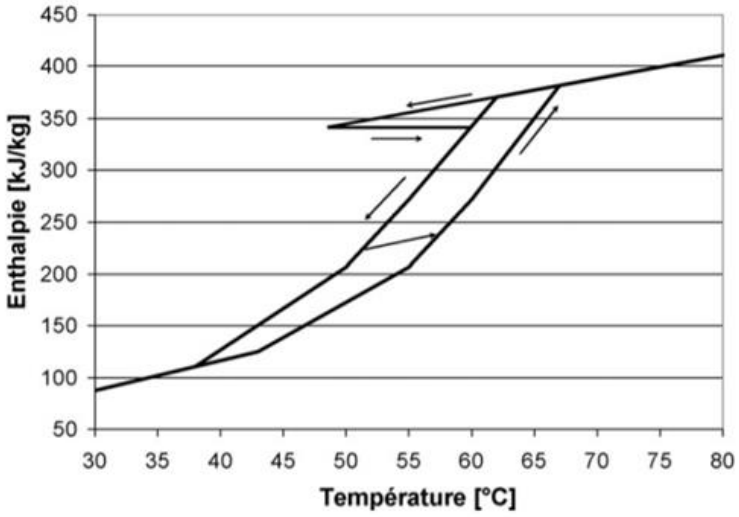

Figure 2.30. Combination of subcooling and hysteresis (Bony and Citherlet, 2007)

2.2.4. Thermal property enhancement of paraffins

Paraffins are widely used as thermal regulating materials because of its exclusive properties including diverse melting temperatures, chemically inert and stable behaviors.With outstanding heat capacity and thermal expansion properties paraffins have a large range of application area. However, it suffers from insufficient thermal behavior literally very low thermal conductivity. On the other hand, in accordance with its poor thermal conductivity, many research works have focused on enhancing the thermal conductivity of paraffin by combining it with other materials . (Kutlu et al. 2021), (Chaichan et al.,2015) , (Lin and Rao,2017), (Rathod and Banerjee, 2013)

Many different methods and materials are investigated to improve the thermal conductivity of paraffins. Enhancement methods can be classified according to medium type as using metallic and non-metallic medium, according to medium size and structures as using porous medium, meso to micro particles, nanoparticles and nanofibers.

Paraffins are thermally enhanced in following researches with metallic fillers and fins.An experimental setup was developed by Hussein et al. to investigate the influence of metallic strips and finned pipes on the enhancement of thermal conductivity of paraffin. The setup is functioning as heat transfer channels across the paraffin, where even paraffin turns to solid phase over pipes of heat exchange, heat transfer proceeds. Temperature homogeneity in the molten paraffin is improved by fins and metallic strips. Inrease of thermal energy release from the paraffin to the streaming water has measured 47% by finned pipes application, and 304% by copper strips application. Placing copper strips in solar water heaters using paraffin for heat storage substance functioning as a heat transfer network made of channels, thereby improving the heating capacity of the heater and the heat transfer rate across the paraffin. Thermal transfer mode has changed from natural convection to conduction by addition of copper strips at finned and unfinned pipes application , where thermal transfer from the paraffin to the colder water pipes strongly supported. It is cocluded that the possibilities of using metallic strips with

paraffins is higher than that of thermal fins depending on of its exclusive thermal transfer performance and its lower cost. (Hussein et al., 2017)

Li et al. investigated on open-cell metallic foam filled paraffin in terms of melting phase change heat transfer theoretically and experimentally. Seven foam samples with high porosity made of copper , and phase change material of paraffin used in the experiments. Distribution of temperature inside media is investigated where the effects of parameters like morphology, porosity, pore diameter studied. A heat transfer enhancement is revealed during melting. Thermal non-equilibrium, non-Darcy effect, and local natural convection is measured, and resulted in conformance with experimental results. The overall thermal resistance of the paraffin-foam composite was lower than that of pure paraffin. Porosity has influenced more than pore density to thermal conductivity. Decreasing pore density and decreasing porosity is required to improve the uniformity of thermal distribution. (Li et al. 2012)

Chaichan presented his attempt on enhancing thermal conductivity of paraffin by the addition of Al_2O_3, TiO2 and carbon nano tubes to make a phase change composite material of enhanced thermal conductivity and high latent heat. The nanocomposite materials showed improved properties than pure paraffin. Increase of thermal conductivity achieved by increasing mass fraction of nano-particle in the paraffin. With addition of 5% TiO_2 and Al_2O_3 , the enhancement of thermal conductivity was 40%, and 60% respectively. Charging period is decreased by nano-particle addition into paraffin at melting temperature. (Chaichan et al.,2015)

Khedkara et al. studied in effects of Fe_3O_4 nanoparticles addition into paraffin on the viscosity and thermal conductivity. % 0.01 to % 0.1 range of volume fraction of nanoparticles were investigated. Ultrasonic device is used for the intensive dispersion of Fe_3O_4 nanoparticles into paraffin. The Fe_3O_4 nanoparticles with 25 nm avarage diameter used. TA instruments rheometer is used for viscosity measurement and KD2Pro device based on transient hot-wire used for measurement of thermal conductivity. Increase of thermal conductivity is achieved by increase in volume fraction of particle. 20% enhancement is recorded with 0.1 volume fraction of Fe_3O_4

nanoparticle addition in paraffin at room temperature. The effects of shear rate and concentration and on the rheological properties and the thermal conductivity of nanofluids were studied. The nanofluid composition showed improvement in both viscosity and thermal conductivity, and the percent increase in thermal conductivity was much higher in comparison with viscosity . The paraffin - Fe_3O_4 nanofluid represented Newtonian property at high shear rates and non-Newtonian property in the low shear rate range. (Khedkara et al., 2013)

Another study on thermal property enhancement with metal oxide nanoparticles is made for paraffin as phase change material by Al_2O_3 nanoparticles emulsifiying in paraffin by using non-ionic type surfactant. 5 and 10 wt.% alumina nanopartical addition investigated experimentally. Dynamic viscosity and thermal conductivity for the paraffin-nanoparticle emulsion showed a nonlinear increase in comparison with pure paraffin depending on temperature. Thermal conductivity of the paraffin-nanoparticle emulsion results compared by various temperatures together with that of the pure paraffin. Thermal conductivity of the paraffin-nanoparticle emulsion was increased in accordance with mass fraction of the nanoparticles more than 6% and 2%y respectively, for the paraffin emulsion with 10 wt.% and 5 wt.% of nanoparticles at 30 °C temperature. Thermal conductivity improvement relatively at 60 °C increased over 17% with nanoparticle addition of 10 wt.%. (Ho and Gao, 2009)

Sahan and Paksoy synthesized ZnO nanopowder with hexagonal crystal structure with nano-tubular shape for the thermal property improvement of paraffin. In terms of thermal energy storage application, a paraffin-ZnO composite was prepared with 10% wt. Experimental investigations resulted with reduction of heat storage capacity where phase change property was stable. (Sahan and Paksoy, 2017)

In a comparative research the usage of phase change material and nanofluid for photovoltaic fluid collector system as coolant where ZnO and CuO nanoparticles addition is investigated experimentally. Thermal efficiency, energy, surface temperature and the comparison between two nanoparticle type is studied. In comparison with classicla method, the CuO nanoparticle implemented version achieved 15% higher

image of electric. The CuO nanoparticles addition increased the thermal image up to 8% for photovoltaic thermal and 12% for paraffin material without any consumption of energy. The electrical efficiency of the paraffin /CuO showed more intense effect than paraffin /ZnO by resulting 16% more efficiency. Surface temperature reduction to considerable level achived by nanoparticle addition, besides enhancement of the power efficiency. The overall thermal output of paraffin was raised by 46% in comparison with the photo voltaic system. It is concluded that of the photovoltaic thermal system's specific heat can be increased and the thermal losses ca be reduced momentarily by paraffin medium usage. It was revealed that paraffin –nanofluid medium is an suitable choise for enhancement of cooling performance in photovoltaic thermal systems without additional energy consuming supplementation . (Manigandan and Kumar, 2019)

Wang et al. investigated on CuO-paraffin nanocomposites regarding thermal conductivity enhancement and dispersion stability. CuO nanoparticles added to paraffin with mass fractions of 0.3, 0.6, 0.9 and 1.2%. Morphology of nanoparticle and stability of dispersion in CuO-paraffin nanocomposite phase change media were investigated by scanning electron microscopy and spectrophotometer . Results declared that increase in the thermal conductivity of the nanocomposite is measured by 24.4% in case of 1.2% CuO nanoparticles addition into the paraffin, as well as reduction in the phase change latent heat measured as 1.5%. (Wang et al. 2020)

Another investigation on thermal conductivity enhancement of the paraffin wax by copper oxide nanoparticles addition issued by Kumar et al. Samples of paraffin nanocomposite were synthesized by dispersing 2.0, 1.5, 1.0, 0.5, and 0 wt. % of CuO nanoparticles in paraffin wax. The CuO nanoparticles raised the paraffin's thermal conductivity in solid and liquid phase to 172.7%, 131.8, 95.5%, 50% and 8.89%, 7.785%, 6.11% and % 2.77% and respectively. Field emission scanning electron microscope is used for the observation of the surface morphology of the CuO nanoparticles-paraffin mixture of in the composite structure. Increase in CuO nanoparticles proportion in paraffin wax enhanced the thermal conductivity substantially. The experimental values are looking higher than the theoretical models;

still variation in thermal conductivity follows the same trend as by the theoretical model. Solid phase of paraffin was raised drastically, in comparison with liquid phase thermal conductivity. (Kumar et al. 2020)

A comparable research with ours is investigated by Owalabi et al.. Paraffin nanocomposites prepared with addition of Al, Cu, Fe and Zn nanoparticles into pure paraffin wax with weight ratio of 1.5, 1.0, and 0.5% to investigate the thermal energy storage behavior theoretically and experimentally. Thermal behavior of the nanocomposites were enhanced by increasing the weight ratio of nanoadditives regarding thermal energy storage properties. Zn and Cu nanoparticle addition of 1.5 wt.% improved the nanocomposite thermal conductivity by 61.5 and 20.6% respectively. A Reduction of specific heat is revealed where a proportional increase of thermal conductivity and thermal diffusity observed. The Hamilton-Crosser and Maxwell models expressed the nearest results to the experimental values. The improved paraffin nanocomposites showed better capability of thermal energy storage, especially for applications of solar thermal energy storage. Overall results of the research predicted that the thermal conductivity of the nanocomposite is enhanced in terms of 1.5 wt.% addition of Zn, Fe, Al and Cu nanoparticle addition, by 61.5, 52, 24.2, 20.6 %, respectively. (Owalabi et al., 2016)

Amin et al. reserached the effect of nanoparticle addition into paraffin to observe the change in the nanocomposite's latent heat. Paraffin was used as phase change material with $ZnO, TiO2, CuO$ and Fe_3O_4 nanoparticles are added. Paraffin and nanoparticle mixture prepared by sonification with the weight ratio of of 15, 10, and 5 wt%. Paraffin's melting point, thermal properties and latent heat were examined with Differential Scanning Calorimetry . Test results revealed that the paraffin nanocomposite's latent heat was increased by 20.17%, 7.5%, 78.89% and 20.67% for the addition of ZnO (5 wt%), TiO2 (15 wt%), CuO (10 wt%), and Fe_3O_4 (5 wt%), respectively. 10 wt% mass fraction of CuO nanoparticle-paraffin showed better result in terms of latent energy storage. On the other hand nanoparticles addition did not affected on the paraffins melting point distinctly. According to the investigation it can be revealed that paraffin –metaloxide nanoparticle nanocomposite is an based nano-phase

change material is a superior media in therms storage of thermal energy. (Amin et al., 2017)

2.2.5. Dispersion thermal stability of paraffin nanocomposites

The thermal analysis, rheology and dispersion behavior of nanomaterials in paraffin was experimentally evaluated in terms of ZnO nanoparticles by Suhaib et al. The ZnO nanoparticles are dispersed in liquid paraffin at different concentrations (0–1 wt%). Sedimentation and Dynamic Light Scattering (DLS) methods are used to determine the dispersion stability. The thermal conductivity of the stabilized nanofluid at concentrations and different temperatures are investigated and an enhancement till 18% is revealed for 0.5 wt% of ZnO paraffin nanofluid. (Ilyas et al., 2019)

Conductive nanoparticles implemented nanocomposites were aimed to be added into paraffin of phase change material for improvement of thermal transfer where the dispersion stability has an important effect on the long term thermal transfer behavior of the specific application. Although many researches involved on the thermal property improvement of paraffin with nanoparticle addition, there are not sufficient investigations on the long term effect on thermal behavior. Study of Saydam and Duan attempted to understand the precipitation behavior by researching the stability of nanoparticle enhanced nanocomposite under repeated thermal (solidification- melting) cycles. Base phase change paraffin is used for the mixture with nanoadditives of multi-walled carbon nanotubes, graphene nanoplatelets and Al_2O_3. Stability of various nanocomposite preparations was experimented applying continual thermal cycles implemented in a special thermal chamber. After a few thermal cycles, deposition/ coagulation of nanoparticles were registered irrespective dispersion process of the nanoparticle type and concentration. The highest thermal conductivity improvement was registered for 2%wt paraffin-multiwall carbon nanotubes wax by 13% at the temperature of 35 °C. A limited thermal conductivity improvement is also registered by nanoparticle addition of Al_2O_3. Nanoparticle precipitation is observed after common time for thermal equilibrium occured. Compared with pure paraffin, nanoparticle-paraffin nanocomposites showed negligible imrovement in terms of thermal transfer due

to the sedimentation and nanoparticle agglomeration, therefore it was not providing the required nanoparticle network within the measurement region. (Saydam and Duan, 2019)

2.2.6. Nanofiber - paraffin interaction

Leakage of paraffin causes a limited use for thermal applications such as heat storage, thermal regulating, and phase change material. In order to use paraffin with considering leakage, paraffins have been encapsulated into other materials for stable usage. Encapsulation of paraffin in cellulose nanofibers and the formation of stable thermal regulation nanocomposites were investigated by Li et al.. Paraffin was encapsulated by cellulose nanofiber through a pickering emulsion method, while simultaneously forming of composite material. The phase change material (PCM) composite showed a solid content of paraffin of more than 72 wt.%. (Li et al., 2017)

Iqbal and Sun reported development of microencapsulated paraffin - monofilament fibre using melt spinning method. Incorporation of 12% microcapsules was succesfully implemented into the monofilaments of polypropylene with the latent heat of 9.2 J/g. Mechanical properties and surface morphology of monofilament of the produced fibre is also studied. The developed statistical model for modulus of monofilament fibre, tenacity and latent heat was complying with the fibre properties of ampirical results. The investigation achived to build thermoregulating structure of paraffin microencapsulation with melt spun monofilament fiber.

Lu et al. used coaxial electrospinning method for a simple production process of paraffin loaded flexible nanofibers with structure of core-sheath. Polymethyl methacrylate sheath-layer encapsulated the paraffin core layer successfully. An increase in speed rate of core solution from 0.1 mL/h to 0.5 raised the fiber core diameter from 395 nm to 848 nm. 58.25 J/g of latent heat and −56.49 J/g solidifying enthalpy are registered by the core-sheath nanofiber films. On the other hand a limited change in latent heat was revealed after 200 thermal cycles, which shows that it is useful for the

paraffin-loaded core-sheath structure to improve the thermal stability properties and defeat the leakage issue the thermal regulation application.

Another investigation applied coaxial electrospinning method using ethanol as solvent for the production of nanofibers with paraffin as core and hydrophobic shell by Sun et al.. Effects of Core and shell fluid's flow rate and ethanol - polyvinyl butyral concentration on the polyvinyl butyral-paraffin nanofibers morphology were studied. The thermo-regulating capability was demonstrated by observing the Inner and surface temperatures of fiber covered model houses was observed to determine the ability of thermal regulation. Increase in shell flow rate and concentration of polyvinyl butyral improved the core-shell polyvinyl butyral-paraffin nanofibers morphology which enables enhanced encapsulation. Higher core flow rate with constant shell flow rate resulted better encapsulation of paraffin in polyvinyl butyral nanofibers. Production parameters of 0.60 ml/ h core flow rate and 3.0 ml/h shell flow rate with 20 % (w/v) concentration of polyvinyl butyral reached to the up to 46.4 % encapsulation ratio of the polyvinyl butyral-paraffin nanofibers. The enthalpy of crystallization and enthalpy of melting of these polyvinyl butyral-paraffin nanofibers were 106.5 J/g and 105.9 J/g , respectively. The paraffin-polyvinyl butyral nanostructure shows a good thermal regulation property in solar irradiation, optimizing the temperature of 28ºC. The fabricated paraffin-polyvinyl butyral nanofibers resulted successful repeatability and stability in the thermal regulation capability.

Mengjin et al. studied on thermally regulating fibers focused on paraffin and polyvinyl alcohol which was produced via wet-composites spinning. In the produced fiber, paraffin was supporting phase change material for energy storage and polyvinyl alcohol was matrix polymer. Fiber's thermal properties, thermal stabilities, mechanical properties, fiber morphology and the thermal properties of the fibers were investigated. The results revealed that the thermoregulatory fiber has satisfiying stability 30 % or less paraffin content. The best fiber properties of strength was 2.6 cN/dtex, elongation at break was 19.9%. (Mengjin et al., 2008)

2.2.7. Separation and Purification of Paraffins

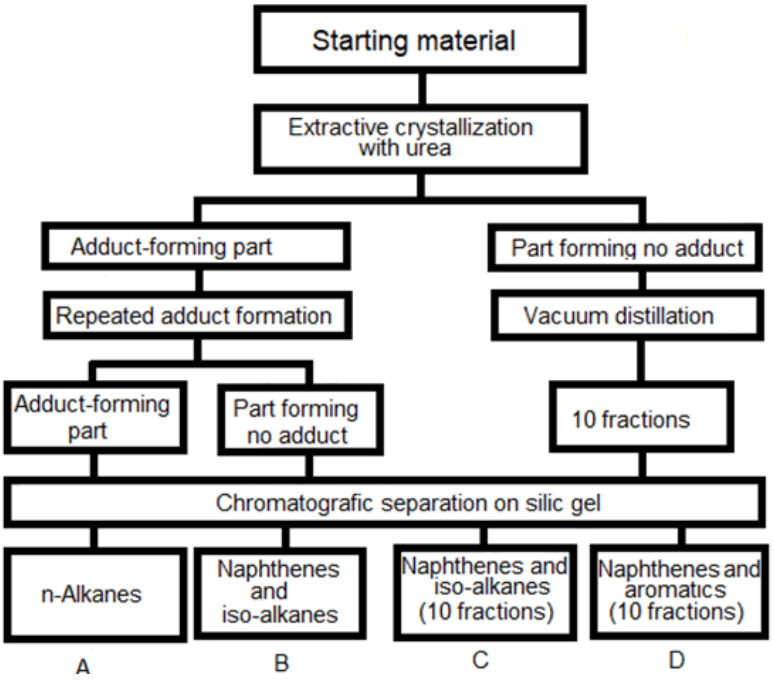

Figure 2.31. Diagram of seperation of slack wax. (Freund et al., 1982)

Separation of the paraffin wax from other n-alkanes and purification according to melting point is processed by petroleum industrial technologies. Slab wax is paraffin wax produced by cooling, pressing and sweating from low-viscosity distillates. Slack wax is intermediate product of cooling and pressing without sweating or refining. Scale wax is the product obtained by just sweating. Products obtained from slack waxes subjected to further purification are recognized by the attribute “purified”. Diagram of separation of slack wax show the steps for the separation of slack wax. The result of this separation steps for the group B is presented in Figure 2.31 where the hydrocarbon composition and distribution by carbon number is declared, by Freund an friends. (Freund et al., 1982)

It is revealed from Figure 2.32 that after this classical separation metheod there are still diversed kind of paraffins in the composition and further separation / purification is necessary for an accurate melting point of the paraffin with less deviation. (Freund et al., 1982)

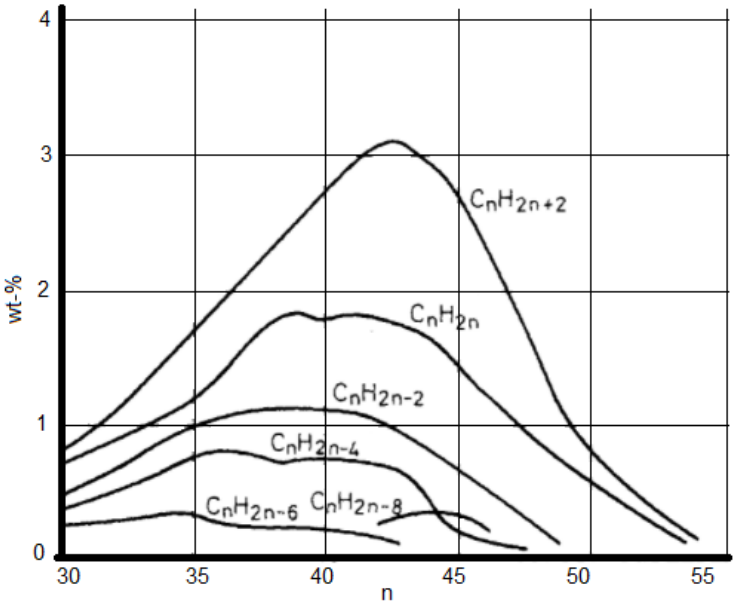

Figure 2.32. Hydrocarbon composition of fraction B obtained from slack wax from neutral oil (Freund et al., 1982)

Purification of the 29 types of Paraffin by distillation studied by Forziati et al. where refractive index measurement, purification results, density, boiling point and boiling point's pressure coefficient at 1 atm and, particularly point of freezing, including calculated impurity amount reported. Number of distilling columns and distillation time is recorded as process parameters.

Gang et al. studied on driving force vacuum sweating for forced paraffin separation process. The result showed that vacuum pressure for forced separation is applicable with an optimal pressure of 80 kPa. Also the final temperature affected on the product yield, where the driving force is raised by final temperature increase while sweating enhace the productivity and shortened the fabrication time. The analyse results of X-ray differaction, , gas chromatography, fourier transform infrared spectroscopy, differential scanning calorimetry revealed that distribution range of the carbon atom number in the products are narrowed due to increase in temperature of forced separation and n-paraffin content is drastically increased. (Gang et al. 2019)

Zolotarev and Nigmatullin developed a method where slack wax is processed with a aluminum chloride complex for enhancement of the purity by improving the efficiency of deoiling. Deoiling supported the slack wax purification, where the oil content is decreased by 15-20% relatively. (Zolotarev and Nigmatullin, 1997)

A filter medium with nanofiber coating is used for crude wax purification by Missau et al. The study focused on the elimination of inorganic contents in the crude wax composition. Forcespinning equipment is used for Nylon-6 nanofibers /nano structure surfaced filter media production. A comparison made between the filter media with nanofiber-coating and with the one without treatment in terms of filtering performance. The filter cake's specific resistance, resitance of filter medium and volume of the filtrate defined, keeping pressure, temperature, filtering time and constant at 2.5 bar, 170°C, 1h, respectively. The excellent filtering performance performed by the filter with nanofiber coating, better inorganic material retention and promoting greater wax filtrate volume and with values of 99,6% and 5,39x 10^{-5} m^3 and respectively. (Missau et al., 2018)

2.2.4. Polyacrylonitrile/ paraffin and phase change material investigations

Paraffin – polyacrylonitrile studies investigated mainly in terms of taking the advantage of phase change properties of paraffin and use it for thermal applications in nano and micro scales. More investigations worked on diversed non-paraffin phase change materials and polyacrylonitrile fibers.

Polyacrylonitrile together with the vinylidene chloride polymere and the paraffin n-octadecane investigated by Zhang and friends. Wet spinning process is used to produce 40 wt % paraffin containing fibers in microscales. The fiber morphology, structure and thermal properties were investigated by using scanning elec tron microscopy, fourier transform infrared , wide -angle X - ray diffraction, dynamic mechanical analysis and differential scanning calorimetry. Thermoregulation properties of heat evolving and heat absorbing temperatures of the fibers are increased by increasing of paraffin content. The crystallization enthalpy and melting enthalpy was increased by increasing the paraffin

content. On the other hand increasing the paraffin amount in fiber content, decreased the modulus of the fiber modulus. (Zhang et al., 2006)

Wan and friends investigated coaxial electro-spinning technology to produce a wearable phase change material - polyacrylonitrile core-sheath nanofiber. Polyacrylonitrile was considered as the the sheath material to use the advantage of fibers as comfort for skin of human body, and paraffin and isopropyl palmitate for thermal management behaviour. The electrospinning parameters adjusted for encapsulating a phase change material by a polyacrylonitrile shell, resulting a uniform sheath–core structure. SEM images showed the successful formation of the hollow nanofibers and phase change material encapsulation with a narrow fiber diameter deviation of the nanofibers shown as in Figure 2.33. The study proved the fabricatin of Polyacrylonitrile/Paraffin sheath - core nano-fibers with uniform thermal behavior. (Wan et al., 2016)

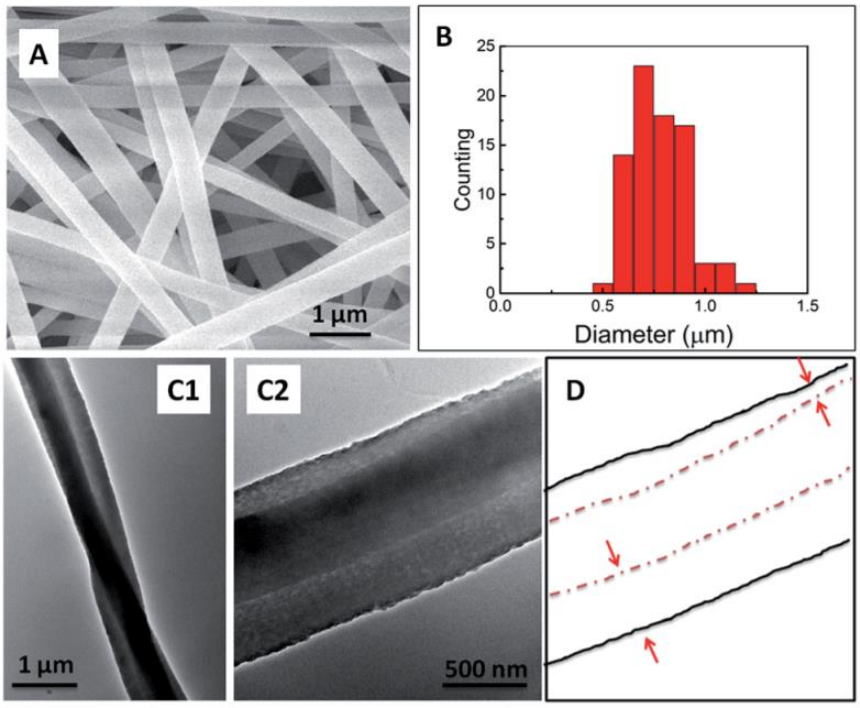

Figure 2.33. PAN/IPP fiber morphology with 2 mL /h PAN flow rate. (A) SEM nanofiber images, (B) distribution of fiber diameter, (C) HR-TEM nanofiber images, (D) sheath–core structure sketch. uniform sheath thickness depicted by arrows. (Wan et al., 2016)

Che and friends improved a simple centrifugal spinning method to replace electrospinning, using phase changing material polyethylene glycol and supporting polymer polyacrylonitrile with conducting nano-SiC filler. The phase change process did not affect on the fiber shapes. DSC results showed that 69.91 J/g latent heat of phase-change and 51.31 °C melting temperature achieved with 4.0 wt% nano-SiC containing nanofibers. A 79% improvement on fiber's thermal conductivity achived with SiC addition shoen in Figure 2.34. The thermal conductive enhancement was attributed to effective thermal transfer provided by nano-SiC. After 200 times thermal cycles, Phase change fibers latent heat values of the were still in acceptable range. On the other hand capacity of latent heat and fiber morphology affected negatively with the increase of nano-SiC in the fiber structure. Shape stability of the structure improved via nano-SiC incorporation in the phase change-nanofiber. (Che et al., 2020)

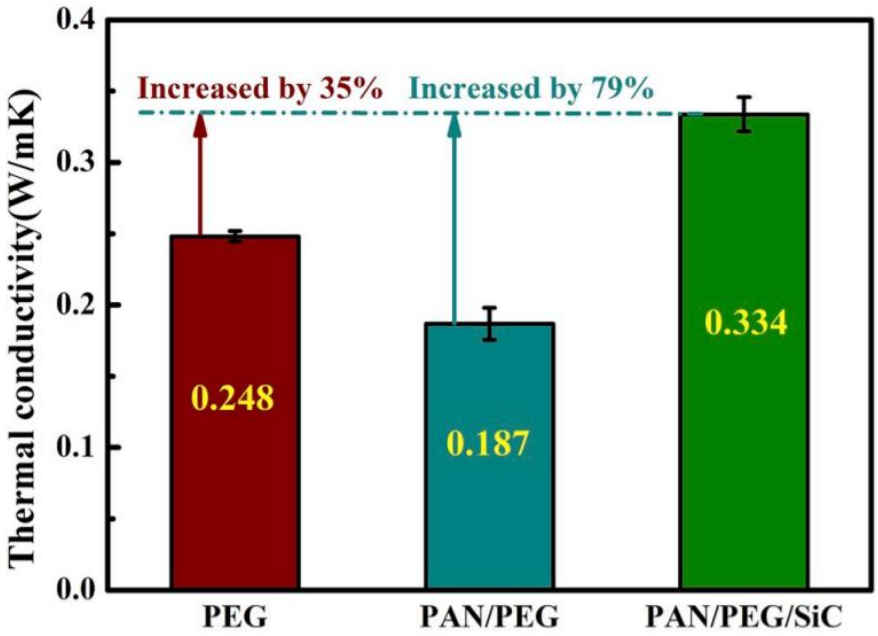

Figure 2.34. Thermal conductivity values at 25 °C, of PAN/ PEG/SiC, PAN/PEG, pure PEG phase change materials (Che et al., 2020)

Application of phase change materials in systems for latent heat storage is one of the most effective technology depending on conversion of energy with minimum loss. Single electrospinning process is used for composite phase change fiber fabrication made of polyacrylonitrile with the phase chage materials lauric acid and methyl

palmitate of fatty acid eutectics. Copper nanoparticles combined for enhanecment of the phase change material. Fabricated composite fiber's structure and morphology observed by SEM. Moreover the thermal performance is also investigated. The three-dimensional fiber structure supported the liquid fatty in terms of stability. Thermal conductivity is enhanced more than 115.2% with nanoparticle addition where 85.07 J/g of latent heat measured. Thermal conductivity values listed in the Table 2.3. Thermal reliability of the fiber-phase change characteristic was tested with multiple thermal cycles. Thermal cycles with long-time periods did not affect on phase change properties and confirmed the excellent thermal reliability. (Xie et al., 2020)

Table 2.3. Methyl palmitate -Lauric acid/ PAN composite fibers and PAN fiber thermal conductivity values with/without Cu Nanoparticles addition (modified from source: Xie et al., 2020)

Samples	PAN	Methyl palmitate -Lauric acid/ PAN	Methyl palmitate -Lauric acid/ PAN (100/100) 1wt% Copper Nanoparticles	Methyl palmitate-Lauric acid/ PAN (100/100) 1.5 wt% Copper Nanoparticles
Thermal Conductivity (w/m.K)	0.10557	0.11067	0.18252	0.23810

An innovative investigation made by Kea and Weia on to fabricate fiber membrane based phase change material with higher form stability. Three different phase change materials with melting temperature in the range of 20–33 °C capric-myristic acid binary eutectic , capric- palmitic-stearic acid ternary eutectic and butyl stearate are investigated for physical adsorption into the nanofibrous membranes. Polyacrylonitrile nanofibers filled with silver nanoparticles is produced with electrospinning as nanofibrous membranes. Thermogravimetric analysis, differential scanning calorimeter, scanning electron microscopy, measurement of solidifcation and melting times used for thermal properties characterization and fiber morphology detection. Below 100 °C operation

temperature, nanofibrous membranes made of polyacrylonitrile/sliver nanoparticles composite are showed good thermal stability. Uniformly dispersion of solid-liquid phase change materials in the nanofiber –membrane structure is showed Figure 2.35. Thermal conductivity values are improved distinctively according to results of thermal performance chracterization depending on excellent thermal conductive silver nanoparticle addition. (Ke and Wei, 2019

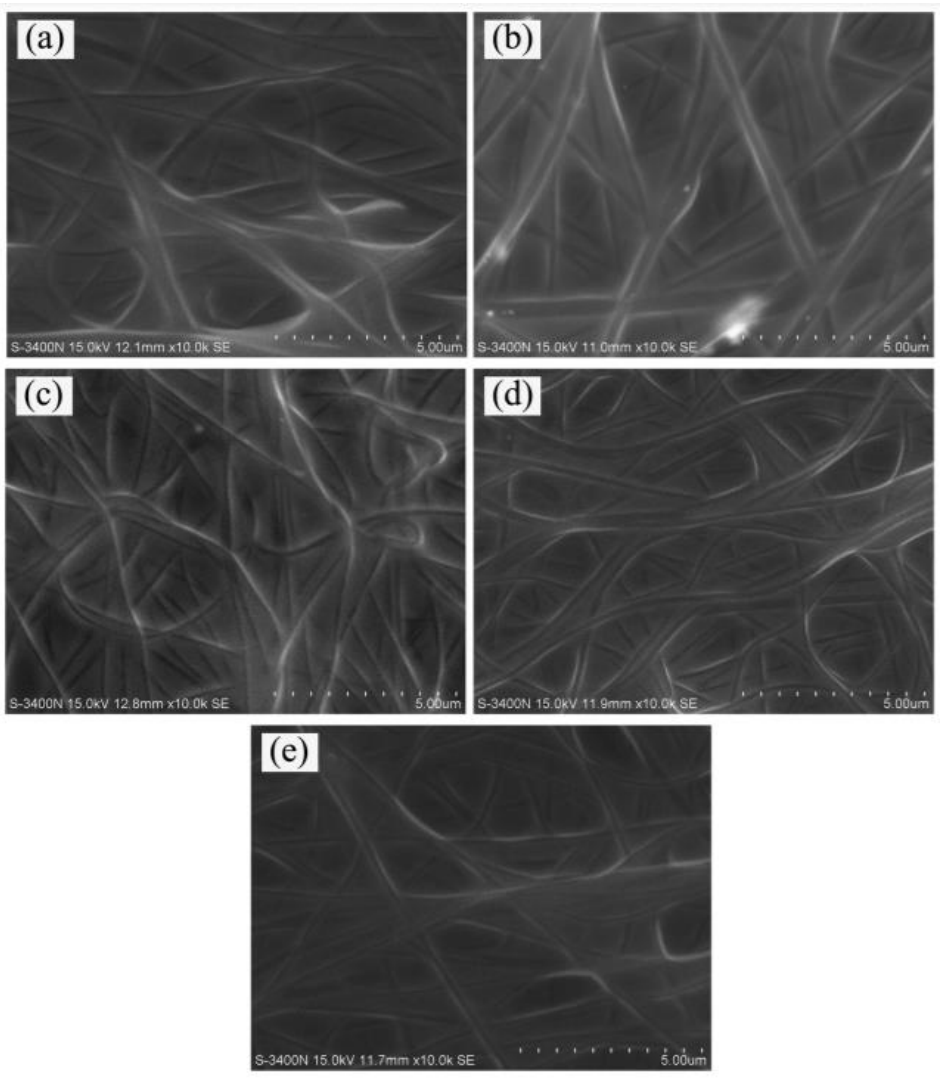

Figure 2.35. Representative SEM images of fibrous membranes-phase change composite (a) butyl stearate /PAN, (b) butyl stearate /PAN/Silver-NPs5, (c) butyl stearate /PAN/Silver-NPs10, (d) capric acid-myristic acid /PAN/Silver-NPs10, and (e) capric acid- palmitic acid- stearic acid PAN/ Silver-NPs10. (Ke and Wei, 2019)

3. MATERIALS and METHODS

3.1. Paraffin/PAN Hybrid Nanofibers for Paraffin Actuators

3.1.1. Chemicals and equipments

Polyacrylonitrile (PAN, Mw of 150.000) and N,N-dimetilformamide were supplied from Sigma Aldrich and used without any purification. The paraffins (P) were purchased from the International Group, Inc (Toronto, ON, Canada). New Era (NE-300) micropump was used as a solution feeding equipment. Gamma High Voltage Research D-ES 30PN/M692 power supply was employed as a voltage source for electrospinning process. Plastic medical syringe with needle gauge number 21 was used, and the needle of syringe was cut to set 1.5 cm before the usage.

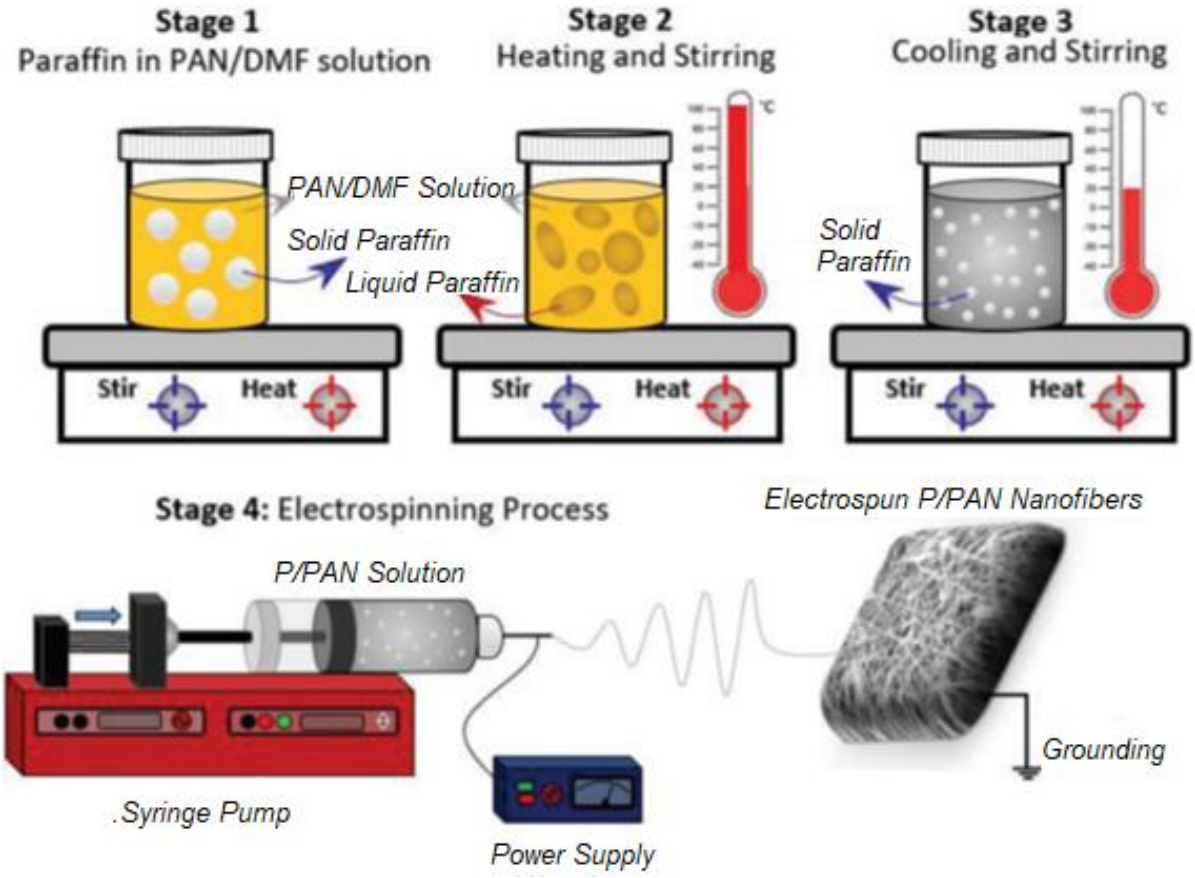

Figure 3.1. Schematic illustration of the one step preparation P/PAN solutions and nanofiber production via electrospinning process.

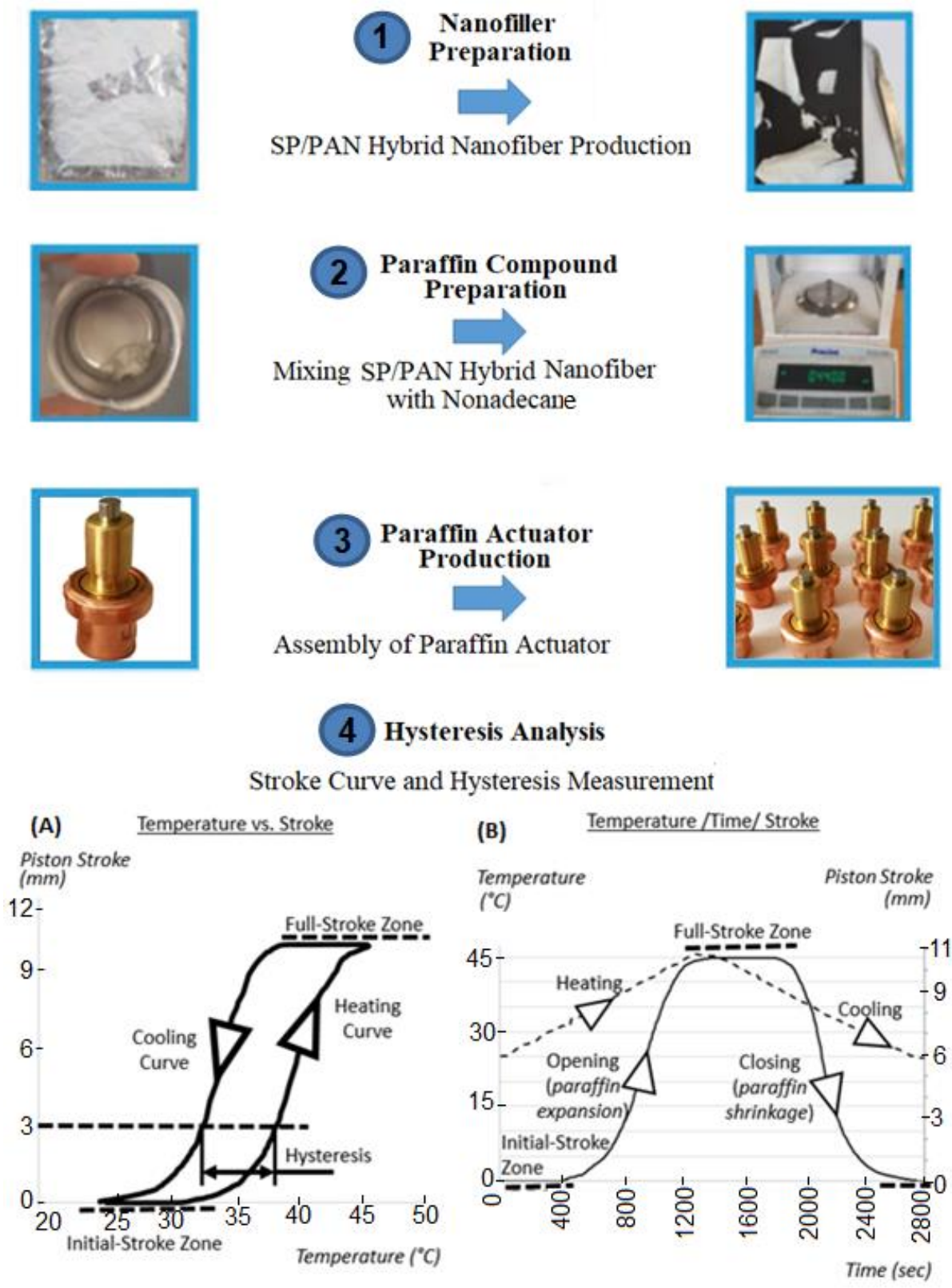

Figure 3.2. Steps of sample preparation from as spun nanofibers, testing and analysis

Table 3.1. Paraffin actuator samples: P/PAN hybrid nanofiber composition

Samples	N-Eicosane weight (mg)	P/PAN hybrid nanofiber weight (mg)	N-Eicosane rate by weight (%)	P/PAN hybrid nanofiber rate by weight (%)
S1	440	0	100	0
S2	429	11	97,5	2,5
S3	418	22	95	5
S4	407	37	92,5	7,50
S5	396	44	90	10

3.1.2. Preparation of solutions and electrospinning of P/PAN hybrid nanofibers

Firstly, 8 wt.% of PAN in DMF was dissolved by magnetic stirring at an ambient condition in a glass vial. Preparation of PAN nanofiber by using electrospinning method has been investigated by several groups (Gu et al., 2005), (Zhang et al., 2014). In this study, 6ml of the prepared solutions were filled into the separate vials. The defined weight of solid paraffins were added into each vial. Two different sample groups were prepared. In the first group, the same amount of paraffins was added into the same amount of PAN/DMF solutions, and weight of paraffin and PAN were the same in the final solution. The labels of the selected paraffin types were P1, P2, P3 and P4 for the samples which had melting points of 32, 58, 89 and 114ºC. Paraffin/polyacrylonitrile hybrid nanofibers were labeled as P/PAN (Ex: if P3 was used in P/PAN nanofibers, it was labeled as P3/PAN). In the second group, P3 was selected and different amount of paraffins were added into the same amount of PAN/DMF solutions. P/PAN weight ratios were adjusted as 15/100, 30/100 and 100/100 in the PAN/DMF solutions, and the samples are symbolized as P3/PAN-1, P3/PAN-2 and P3/PAN-3. All the vials were capped strongly. Then the vials were put on a magnetic stirrer and stirred by simultaneous heating. Each stage of the solution preparation was schematically shown in Figure 3.1. When the paraffins in the solutions were transformed to liquid state (stage 2), the solution was stirred harshly (at 500 rpm) to break liquid paraffin apart into small particles and the heater was turned off and stirring was continued until the temperature of the solutions reached to the ambient condition. When the temperature came to the ambient condition, small paraffin particles were obtained in the solution (stage 3). The

prepared final solution was filled in the plastic syringes (21-gauge, needle length was 1, 5 cm) and electrospinning was performed and demonstrated as stage 4 in Figure 3.1. Electrospinning was carried out with 1ml/h feeding rate and 17.5 kV applied voltage, and keeping the collector to tip of the needle distance as 15 cm. In order to eliminate clogging of the needle and unwanted spraying of the solution, tip of the needle was cleaned up with 5 minutes intervals. The solution was ejected from the needle to the grounded collector, and finally P/PAN hybrid nanofibers were obtained on the collector in the mat form. DMF in the solution was evaporated during the nanofiber formation between tip of the needle and the collector.

Characterizations of P/PAN hybrid nanofiber Morphological investigation of as-spun pure PAN and paraffin loaded P/PAN hybrid nanofibers was conducted with a ZEISS EVO 40 scanning electron microscopy (SEM). The samples were conductive coated with gold-palladium (60/40) about 30 seconds for better imaging by using a Baltec sputter coater. Fiber diameter was measured by pixel processing based free, open source program, ImageJ program (The National Institutes of Health, USA). 100 nanofibers were measured in the SEM images. Fiber diameter distribution chart built as fiber diameter vs frequency in MS Excel. FTIR spectra was acquired with a FTIR spectrometer (Bruker Optics Tensor37, Ettlingen, Germany) equipped with ATR detector. The measurements were carried out between 4000 and 400 cm^{-1} wavelength with 4 cm^{-1} resolution.

DSC tests were carried out with Differential Scanning Calorimetry Analyzer (TA Instruments/Discovery DSC251, New Castle, USA) using 10C/min of heating rate from 0 to 400 ˚C. TGA tests were conducted with a simultaneous thermogravimetric analyzer (Hitachi Hi-Tech STA7200, Tokyo, Japan) with 75ml/min nitrogen flow and 10ºC/min of heating rate from 30 to 600 ºC. Sample preparation of paraffin actuator Paraffin compounds were prepared from pure N-Eicosane (Melting point 32ºC, P1) and N-Eicosane mixed with P1/PAN hybrid nanofiber 2.5%, 5%, 7.5%,10% by weight and named as S2, S3, S4 and S5. Table 3.1. shows detailed information for each prepared sample. A stepwise visual demonstration of sample preparation and hysteresis testing of the paraffin actuator are shown in Figure 3.2.

3.1.2. Working principle of paraffin actuator

A paraffin actuator consists of a sealed stainless steel capsule (4), stainless steel cover (2), stainless steel piston (1), elastomeric diaphragm sealing (3) and paraffin compound (5) as shown Figure 3(a). The paraffin compound is sealed inside the capsule which avoids the leakage of the paraffin to the outside of the capsule during melting/expansion. When the temperature of the medium outside the capsule rises and exceeds the melting point of the paraffin compound of the actuator, the paraffin compound expands and presses against the diaphragm sealing. The movement is transferred to the piston. The cover part guides the movement of the piston into the vertical direction and keeps the diaphragm sealing in upright position. Counter spring pushes the piston back inside the diaphragm sealing if the medium temperature decreases down under the melting point where the paraffin compound shrinks. Volume change of the paraffin compound is converted to displacement of the piston where the opening stroke of the paraffin actuator is recorded by displacement sensor in millimeter. Principle of the thermal hysteresis has been explained in following topic.

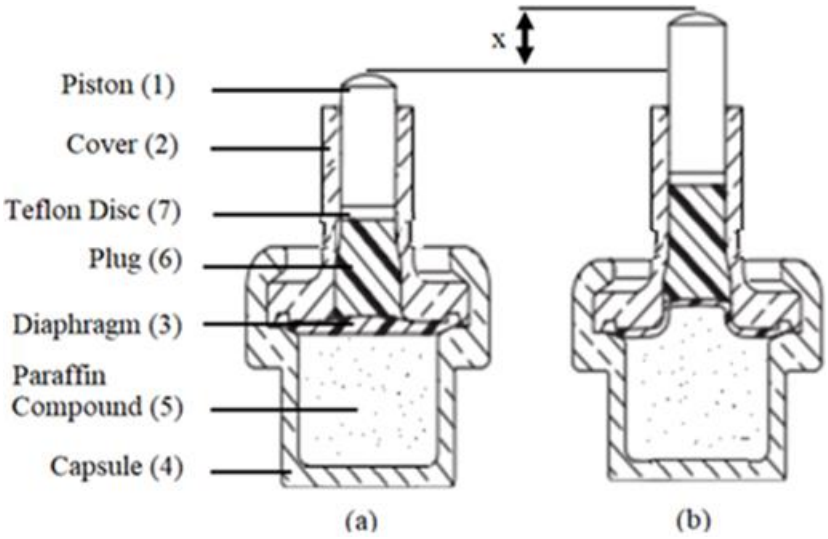

Figure 3.3. Paraffin actuator subcomponents (a) closed paraffin actuator: before heating/displacement of piston, (b) opened paraffin actuator heated - molten expanded paraffin.

3.1.3. Thermal hysteresis of paraffin actuators in terms of volume expansion

Volume expansion of paraffin is upto 15% during phase change from solid phase to liquid phase (Chen et al., 2008). However, temperature depended volume change speed of the paraffin compound lacks of hysteresis. Volume shrinkage speed of solidification is remarkable lower than volume expansion speed of melting at a Paraffin actuator. This thermal hysteresis phenomenon can be observed on piston displacement curve versus heating and cooling of the paraffin actuator in a cooling circuit. External factors, which affect on the expansion performance/thermal hysteresis of the paraffin content, depend on counter force of the spring in the thermostat, heating - cooling speed of the test bath, thermal conductivity of coolant media, circulation speed of the coolant media. Thermal hysteresis is the ΔT of heating-cooling cycle based on temperature-stroke curve at 3mm stroke. Initial stroke zone is the temperature range where the piston is subjected to movement from the rest by means of paraffin expansion via phase change from solid to liquid. After the initial stroke zone, the paraffin actuator performs a relative high opening course until it reachs to full-stroke zone. Full stroke zone is the temperature range where the paraffin expansion ends.

3.1.4. Testing setup for thermal hysteresis

Testing setup consists of paraffin actuator, compression spring, displacement sensor, heated/circulated coolant bath, analog digital converter, electrical resistance heater, K-type thermocouple, circulation pump, temperature programmer, computer/data logger and fixing apparatus for the fixation of the paraffin actuator in the coolant bath. In testing setup, the paraffin actuator is fixed in an apparatus and only the vertical movement of the piston is allowed. A spring having a spring constant (k) of 7N/mm is working against the piston with the initial force of 70N to confine the piston movement during paraffin melting phase change and compressing it in to capsule during solidification. Circulated coolant media is flowing around the capsule for securing the dynamic temperature transfer from coolant to paraffin actuator simulating the coolant flow in the car cooling system. Temperature programmer gives the input for the heating and cooling temperature speed to operate the electrical resistance heater. K-Type thermocouple and displacement sensor record the temperature value and piston stroke

simultaneously where the computer collects these data in a text file for later data processing.

Common specifications for hysteresis require 1ºC/min heating up speed and 1ºC/min cooling down speed for the paraffin actuator where the thermal bath temperature starts with 5ºC before the first movement of the piston and heated until 15ºC hereafter. The bath is cooled down with a speed of 1ºC/min until the starting temperature (5ºC before initial stroke of the piston). At the testing setup, all the affecting external factors are kept (spring force, heating-cooling speed, coolant media, circulation speed) constant and just the alterations of the paraffin compound in the paraffin actuator samples are investigated.

Testing setup is programmed to record into a text file the data of the opening stroke value of the paraffin actuator against temperature change and time interval during the heating and cooling process. A combined Time/ Temperature/Opening curve is plotted from the recorded data into a Microsoft Excel file. Excel Scatter Chart is used to create the hysteresis curve where the opening stroke of the paraffin actuator is depicted according to heating and cooling cycle independent of time interval.

3.2. Thermal Hysteresis Enhancement and Dispersion Thermal Stability

3.2.1. Chemicals and equipments

Polyacrylonitrile and N,N-dimetilformamide, paraffin Nonadecane (P) were supplied identically as detailed in Chapter 3.1.1. CuO with particle size 38nm, Fe_3O_4 with particle size 18.0-28.0nm, Al_2O_3 with particle size 18.0nm and ZnO with particle size 30.0-50.0 nm metal oxide nanoparticles were purchased from Nanografi Nanotechnology AS (Cankaya/Ankara TURKEY).

Table 3.2 shows the properties of metal oxide nanoparticles declared by the manufacturer. Same electrospinning equipments and process parameters are used with that of explained in Chapter 3.1.1.

Table 3.2. Properties of metal oxide nanoparticles declared by the manufacturer.

Nanoparticle	CuO	Fe_3O_4	ZnO	Al_2O_3
Purity (%)	99.99	98.45	99.5	99.5
Color	black	dark brown	milky white	white
Average Particle Size (nm)	38.0	18.0 - 28.0	30.0 - 50.0	18.0
Specific Surface Area (m^2/g)	>20	>55	70	140
True Density (g/cm^3)	6.5	5.1	5.5	3.9

3.2.2. Electrospinning of PAN nanofibers

Firstly, 8 wt.% of PAN in DMF was dissolved by magnetic stirring at an ambient condition in a glass vial. Preparation of PAN nanofiber by using electrospinning method has been investigated by several groups (Gu et al. 2005, Zhang et al. 2014). In this study, 6ml of the prepared solutions were filled into the vial. Then the vial was put on a magnetic stirrer and stirred. The solution was stirred harshly (at 500 rpm). The prepared final solution was filled in the plastic syringes (21-gauge, needle length of 1,5cm).

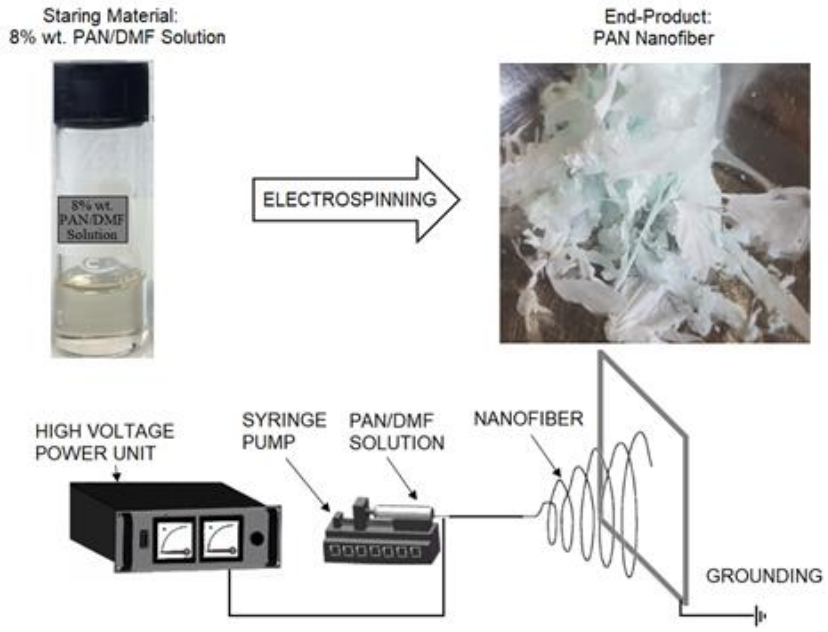

Figure 3.4. Electrospining of PAN Nanofiber

The Electrospining was complianced with the process described in capital 3.1.2, here just the polymer solution was prepared without any addition of paraffin. The process is shown in Figure 3.4.

3.2.3. Characterizations of paraffin nanocomposite

Morphological investigations, fiber diameter detection and EDS Analysis were carried out with same methods explained in Chapter 3.1.2.

3.2.4 Paraffin nanocomposite samples preparation

Paraffin nanocomposite samples were prepared with Nonadecane paraffin (Melting point 32ºC), paraffin /CuO nanoparticles, paraffin /Fe_3O_4 nanoparticles, paraffin /Al_2O_3 nanoparticles, paraffin /ZnO nanoparticles, paraffin /PAN nanofiber wt.10% and named as N1, N2, N3, N4 and N5.

For each metal oxide nanocomposite sample, 1.8g Nonadecane paraffin is heated to 100ºC and 0.2g nanoparticle added to liquid paraffin in one portion. The mixture is harshly stirred with a 13.000 rpm high speed mixer until the nanocomposite is solidified down to 25ºC.

Table 3.3 shows detailed information for each prepared sample. Nonadecane /PAN nanofiber nanocomposite is prepared with addition of 0.2g nanofiber into 1.8g Nonadecane at 100ºC. Nanofiber/paraffin mixture is smoothly kneaded until solidified and cooled down to 25ºC.

All samples are prepared in a separate stainless steel pot. The visual property of the mixtures are also observed where all the paraffin-metal oxide mixtures have shiny color and paraffin-PAN nanofiber has matte color.

Table 3.3. Paraffin nanocomposite samples

Sampl. Name	*Picture of the Nanocomposite*	*Nano-composite*	*Color*	*Mixing Type*	*Weight*
N1		*CuO / Paraffin*	*Shiny black-ish*	*harshly stirred via 13000rpm high speed mixer until solidified*	*0.2g CuO Nanoparticle/ 1.8g Nonadecane*
N2	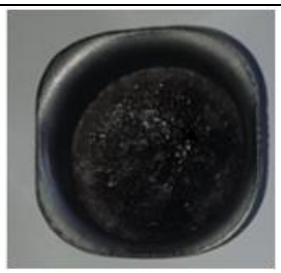	Fe_3O_4 / *Paraffin*	*Shiny brown -ish*	*harshly stirred via 13000rpm high speed mixer until solidified*	*0.2g* Fe_3O_4 *Nanoparticle/ 1.8g Nhonadecane*
N3		*ZnO / Paraffin*	*Shiny milky white*	*harshly stirred via 13000rpm high speed mixer until solidified*	*0.2g ZnO Nanoparticle/ 1.8g Nonadecane*
N4		Al_2O_3 / *Paraffin*	*Shiny white*	*harshly stirred via 13000rpm high speed mixer until solidified*	*0.2g* Al_2O_3 *Nanoparticle/ 1.8g Nonadecane*
N5	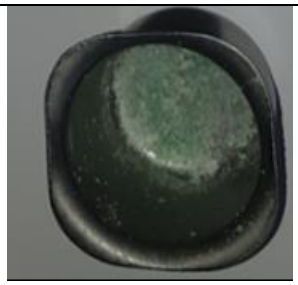	*PAN /Paraffin*	*Matte white to hell grey*	*Smothly kneaded with tweezers until solidified*	*0.2g PAN Nanofiber / 1.8g Nonadecane*

3.2.5. Dispersion thermal stability test (DTST) and sample preparation

Samples are prepared from paraffin nanocomposites N1, N2, N3 N4, N5 and pure nonadecane and named for 45ºC storage as L1, L2, L3, L4, L5 and L6, for 100 ºC storage as H1, H2, H3, H4, H5 and H6 respectively shown in Figure 3.6.. Table 3.4 shows sample and test information for each test. BD U-100 0.5ml Insulin syringe without plunger is used as test container of thermal stability test where one can see the precipitation through the transparent plastic wall visually. Demonstration of sample preparation and thermal stability testing paraffin nanocomposites are shown in Figure 3.5.

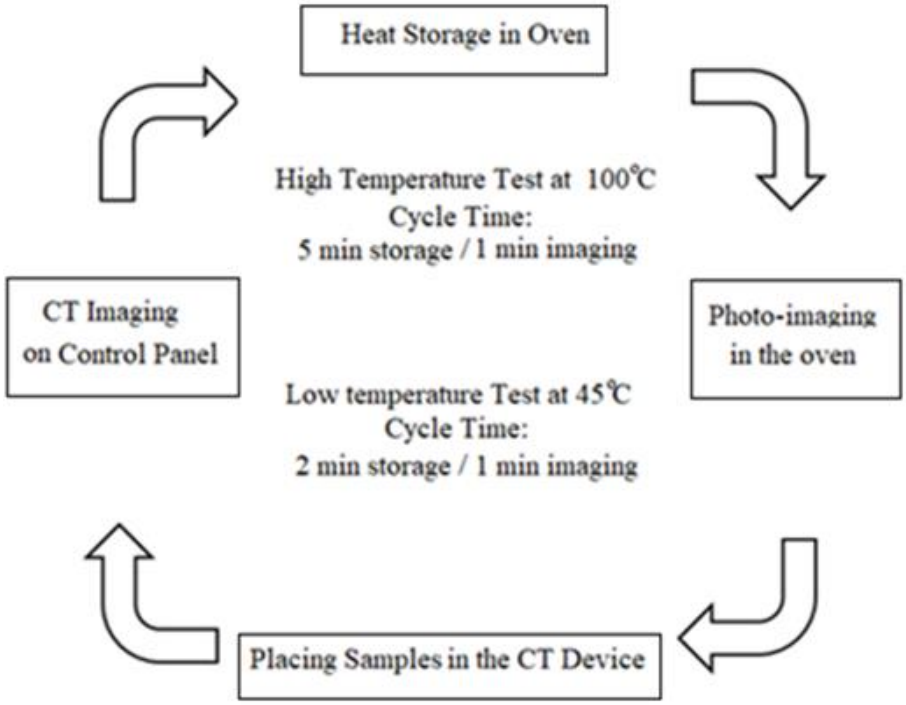

Figure 3.5. Dispersion thermal stability test setup

Dispersion thermal stability tests are performed by storing the samples at certain temperature in Nukleon NST120 Oven. The sample contents prepared for tests are listed in Table 3.4. In Figure 3.5 shown test samples are fixed in a special jig and put into the oven for a given time at certain temperature. High temperature test is done to observe the fully precipitation of nanoparticles at 100ºC which is well above the melting point.

The duration of high temperature storage where the fully precipitation occurred, is used as basic time information for the second level test of hysteresis for paraffin actuators.

Table 3.4. Properties of DTST Samples

Content	Sample Name	Nanocomposite in use	Sample Weight
CuO	L1 and H1	N1	0.570g
Fe_3O_4	L2 and H2	N2	0.550g
ZnO	L3 and H3	N3	0.550g
Al_2O_3	L4 and H4	N4	0.545g
PAN	L5 and H5	N5	0.540g
Nonadecane	L6 and H6	pure paraffin	0.520g

Low temperature dispersion thermal stability test is performed at 45ºC which corresponds the top temperature of hysteresis cycle and indicating the dispersion morphology of nanocomposite during heating up of the paraffin actuator. The samples stored in the oven are subjected to periodical inspection at Computer Tomography (CT) YXLON Y.MU2000-D for storage at 100ºC after every 5 minutes and for storage at 45ºC after every 2 minutes. Both storage tests were completed after 20 minutes. The density of nanocomposite changes as the paraffin melts and the nanoadditives precipitates. The darkness distribution of the CT-imaging determines the density homogeneity and precipitation of the nanoparticles in nanocomposites respectively. Test periods of dispersion thermal stability test are listed in Table 3.5.

Table 3.5 DTST Periods

Test Name	100ºC Storage	45ºC Storage
Samples tested	H1, H2, H3, H4,H5,H6	L1, L2, L3, L4, L5, L6
Test Duration	20min	20 min
Inspection Period	5min	2 min

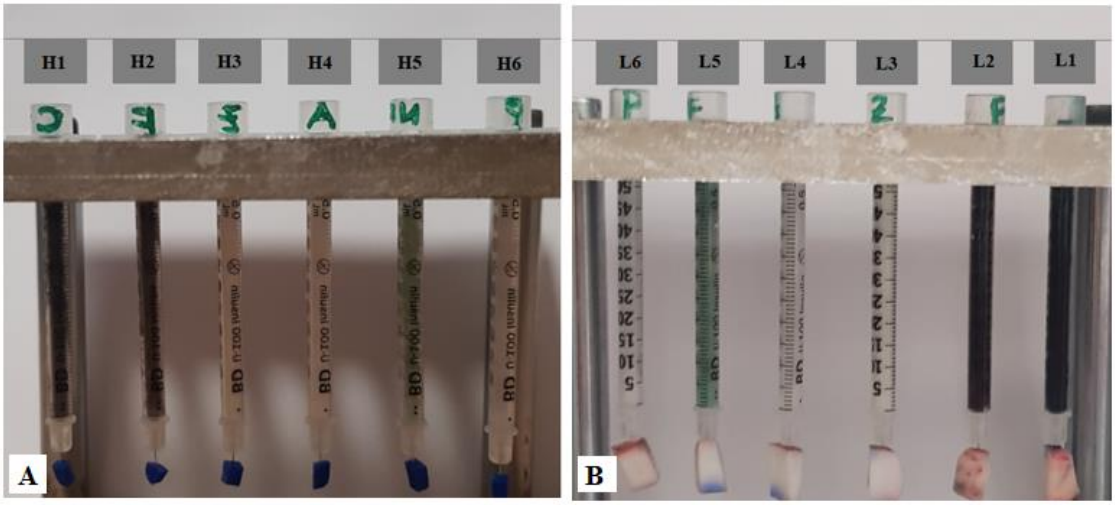

Figure 3.6. A) High temperature DTST samples H1: CuO-Paraffin, H2: Fe_3O_4-Paraffin, H3: ZnO-Paraffin, H4:Al_2O_3-paraffin, H5: PAN-paraffin, H6: pure paraffin, B) Low temperature DTST samples L1: CuO-Paraffin, L2: Fe_3O_4-Paraffin, L3: ZnO-Paraffin, L4: Al_2O_3-paraffin, L5: PAN-paraffin, L6: pure paraffin

3.2.6. Thermal hysteresis test and paraffin actuator sample preparation

A stepwise visual demonstration of sample preparation, hysteresis testing and working principle of paraffin actuator are explained in detail at our previous research (Kutlu et al. 2021). A paraffin actuator consists of a sealed stainless steel capsule, stainless steel cover, stainless steel piston and elastomeric diaphragm sealing and paraffin compound. The paraffin compound sealed inside the capsule which avoids the leakage of the paraffin to the outside of the capsule during melting/expansion. When the temperature of the medium outside the capsule rises and exceeds the melting point of the paraffin compound of the actuator, the paraffin compound expands and presses against the diaphragm sealing. The movement is transferred to the piston. The cover part guides the movement of the piston into the vertical direction and keeps the diaphragm sealing in upright position. Counter spring pushes the piston back inside the diaphragm sealing if the medium temperature decreases down under the melting point where the paraffin compound shrinks. Volume change of the paraffin compound is converted to displacement of the piston where the opening stroke of the paraffin actuator is recorded by displacement sensor in millimeter. Testing setup for thermal hysteresis is a replication that of previous work. (Kutlu et al. 2021).

Hysteresis test was performed with 1ºC/min heating up speed and 1ºC/min cooling down speed from 25ºC to 45ºC coolant bath temperature. At the testing setup, all the affecting external factors are kept constant and just the alterations of the paraffin nanocomposite in the paraffin actuator samples are investigated.

At recent investigation, two levels hysteresis test is performed and sample annotation regarding the test is listed in Table 3.6. At first test level, hysteresis of all paraffin actuator samples P1, P2, P3, P4, P5 and P6 are depicted with paraffin actuators made of as mixed and solidified nanocomposite where no precipitation is occured. After first level test, all the paraffin actuator samples were stored in an oven at 100ºC. The duration of this high temperature storage was determined by the high temperature dispersion thermal stability test results in which almost all the metal oxide nanoparticles deposited to the bottom. Thereafter a second level test was performed with these paraffin actuator samples to ascertain the precipitation effect on thermal hysteresis, conceivably to verify the avail of nanofiber-paraffin nanocomposite which scarcely precipitates.

Table 3.6. Properties of Paraffin Actuator Samples

Content	Sample Name	Nanocomposite in use	Sample Weight
CuO	P1	N1	0.470g
Fe_3O_4	P2	N2	0.460g
ZnO	P3	N3	0.460g
Al_2O_3	P4	N4	0.455g
PAN	P5	N5	0.450g
Nonadecane	P6	pure paraffin	0.440g

3.3 Effect of the Number of Carbon in Paraffin on Interaction with Nanofibers

Conventional electrospinning method was applied to produce nanofibers (Huang et al., 2003), (Lackowski et al., 2013), (Liu et al., 2019). 7,5% of PVA was dissolved in distilled water at THINKY ARE-250 Planetary Mixer by 200rpm speed and 20 minutes

at the ambient condition. The dissolved solution was filled in a plastic syringe which has a metal hollow needle (0.5 mm inner diameter). The syringe was put in front of a grounded collector that covered with aluminum foil. The distance between the tip of the needle and the collector was adjusted to 15 cm. PVA nanofibrous mat structure on the aluminum foil by applying 15 kV voltage to the metal needle and feeding the solution with 1 ml/hrs to the existence of the needle. Liquid paraffin was interacted with the nanofibers by electrospraying them on the nanofibrous mat structures.Morphological analysis of the PVA fibers and PVA/paraffin systems were performed with optical microscopy Zeiss Axio Vert.A1, thermal analysis was conducted with a differential scanning calorimeter TA/Discovery DSC250, and wettability was investigated by Attension Theta contact angle measurement device.

Liquid paraffin is accumulated /deposited on nonwoven nanofiber structure as a composite layer via electrospraying. Microscopic analysis of PVA/paraffin system, and interaction of paraffin with PVA nanofiber mat surface was investigated by performing contact angle measurement. Following three different types of paraffin pentadecane, hexadecane, and heptadecane were used for wettability study.

4. RESULTS and DISCUSSION

4.1 Paraffin/PAN Hybrid Nanofibers for Thermal Hysteresis Enhancement

Morphological observation of P/PAN nanofibers due to paraffin type and amount morphlogy analysis of as-spun paraffin loaded P/PAN nanofibers were carried out via electron microscopy imaging due to the both paraffin content (Figure 4.1) and type of the paraffin (Figure 4.2) at P/PAN nanofibers. As seen from Figure 4.1 (A1, A2, a), pure PAN nanofibers exhibited a random distribution in the mat, higly uniform nanofibers were obtained, just a few negligable bead defect structure was observed. Since some paraffin particles were stayed in the solution in suspension form, these particles mostly in sphere forms were directly ejected on the nanofibers and were seen on the nanofibers mat surface at low magnification SEM images as seen in Figure 4.1 (B1) to (D1). The mentioned spherical particles were not observed at low magnification SEM image of pure PAN nanofibers in Figure 4.1 (A1). On the other hand, also bead-on-a-string morphology defect structure was observed by the addition of paraffin in P/PAN nanofiber as seen from the inset Figures in Figure 4.1 (B1) to (D1). The amount of bead-on-astring morphology defect structure in the nanofiber mats increased by increasing paraffin ratio in electrospinning solution (inset Figures in Figure 4.1 (B1) to (D1). Even though the electrospinning process was applied at the ambient condition and the paraffins in the solutions were in solid state, Figure 4.1 (C3) revealed that some paraffin particles were melted during the electrosinning and solidified when they reached on the nanofiber surface, and these molted paraffin bonded the fibers by solidification. During the electrospinning process, some sparks can be seen because of high voltage electricity. These sparks may had melted some paraffin. Another reason for the formation of this structure may be that some parrafin particles melt during the sputter coating (during the SEM sample preperation) and then bonded to the fibers after solidification. Nanofiber diameters were measured from selected 100 nanofibers in SEM images and diameter distribution chart graphics were given in Figure 4.1 (A3) to (D3) with average nanofiber diameters. As seen from the graphs, most of the pure PAN fibers have the diameters ranging between 300-500 nm. The diameter tendency shifted to lower values with the addition of paraffin, and nanofibers had the diameter range

between 150 and 300, 150 and 300, 100 and 250nm for samples P3/PAN-1, P3/PAN-2 and P3/PAN-3 respectively. Average nanofiber diameter in PAN nanofibers mat was measured as 376 nm. Average nanofiber diameter decreased with the addition of paraffin into PAN nanofibers, and the counted average fiber diameters were 220, 241 and 214nm for samples P3/PAN-1, P3/PAN-2 and P3/PAN-3 respectively.

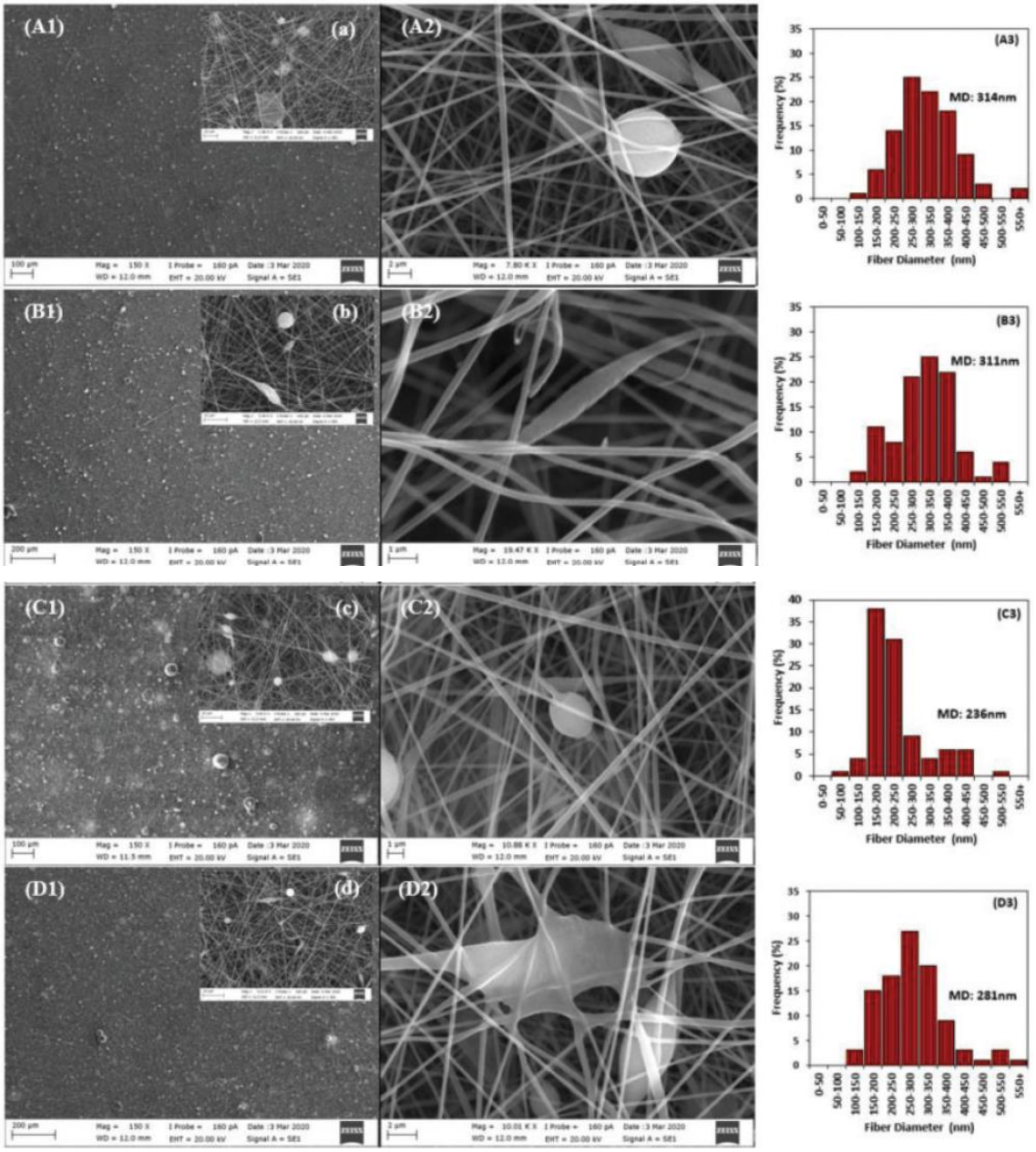

Figure 4.1. SEM images of P/PAN hybrid nanofibers (depending on paraffin type): (a) P1/PAN, (b) P2/PAN, (c) P3/PAN and (d) P4/PAN.

SEM images of P/PAN nanofibers due to paraffin types were shown in Figure 4.1. Nanofiber diameter distribution chart graphics with the average nanofiber diameters of different paraffin type P/PAN nanofibers were demonstrated in Figure 4.1 (A3) to (D3). As seen from the graphs, the fiber diameter distributions were various depending on paraffin type. Sphere type particles were observed on the surface of nanofibrous mat at all the sample types as seen from the low magnification SEM images in Figure 4.1 (A1) to (D1). Some little beaded defect structures were also seen in all types of paraffin additions. Nanofibers have the diameter range mostly between 250-400, 250-400, 150-300 and 200-350nm for samples P1/PAN, P2/PAN, P3/PAN and P4/PAN respectively. Average nanofiber diameter in PAN nanofibers mat was measured as 376 nm. Average nanofiber diameter decreased with the addition of paraffin into PAN nanofibers, and the counted average fiber diameters were 314, 311, 236 and 381 nm for samples P1/PAN, P2/PAN, P3/PAN and P4/PAN respectively.

Chemical analysis of pure PAN and P/PAN nanofibers due to paraffin type and amount was conducted via FTIR analysis to investigate if there was any chemical change in the nanofibers. Firstly, the chemical structure of the pure paraffins used in the study were observed as seen in Figure 4.2 (a). The same amount of these paraffins were added in the same concentration of PAN/DMF solution.

Effect of the amount of paraffin in P/PAN nanofiber mats were analysed and the results were shown in Figure 4.2 (b). Nanofibers were produced by electrospinning and chemical analysis of P/PAN nanofibers depending on paraffin types were demostrated in Figure 4.2 (c). As seen from Figure 4.2 (a), the prominent paraffin peaks detected around 715–719 cm^{-1} were attributed to inplane vibration of CH_2 groups (Zhang et al., 2019), (Haghighat et al.,2018). The peaks between 729 and 731 cm^{-1} could be attributed to rocking absorbtion band of lineer aliphatic structure of paraffin (Varshney et al., 2012) . The peak between 1452 and 1462 cm^{-1} corresponds to scissoring mode of CH_2 groups [35], 1469–1471 cm^{-1} assigned to C–H bending vibration (Zhang et al., 2019) and 2912–2914 cm^{-1} corresponds to CH_2 asymmetric stretching (Chaber et al.,2017). The peak 2947 cm^{-1} is related to C–H stretching vibrations of CH_3 groups (Nie et al.,2015) , and the peak at 2955 cm^{-1} assigned to asymmetric stretching of CH_3 groups

(Chaber et al.,2017) . Additionally, the symmetric carbon-hydrogen bending absorption of the CH_3 groups are detected at 1371 cm^{-1} for P1 and 1377 cm^{-1} for P2 and P3 samples (Varshney et al., 2012).

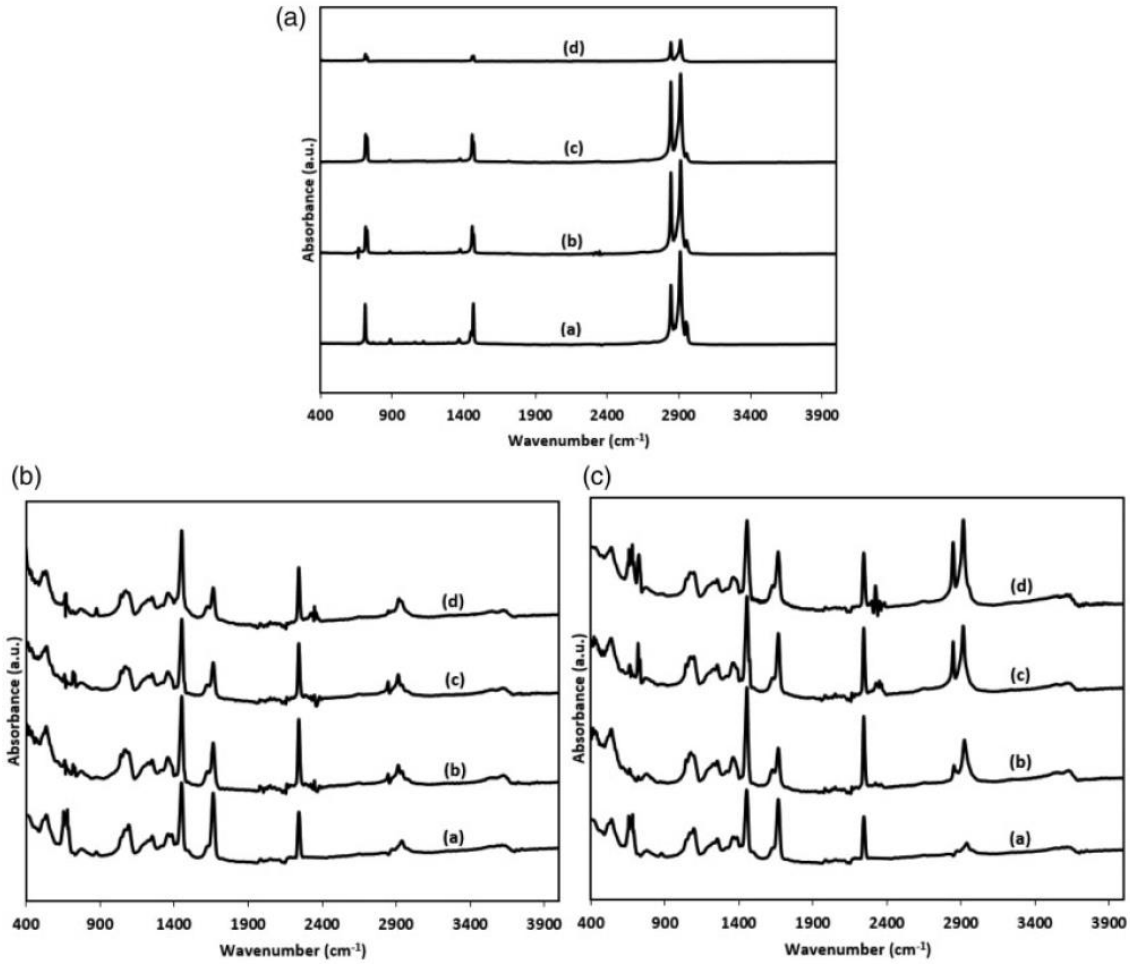

Figure 4.2. FTIR spectra of (a) pure paraffins (a) P1, (b) P2, (c) P3 and (d) P4; (b) P/PAN nanofibers with different paraffin concentration (a) just PAN, (b) P3/PAN-1, (c) P3/PAN-2 and (d) P3/ PAN-3; and (c) P/PAN nanofibers with different paraffin types (a) just PAN, (b) P1/PAN, (c) P2/ PAN, (d) P3/PAN and (e) P4/PAN.

FTIR spectrum of pure PAN nanofibers were demostrated in Figures 4.2(b) and (c) as inset plots indicated by “a”. Prominent peaks for pure PAN nanofibers were detected at 1359, 1450, 1664, 2243 and 2939 cm^{-1}. C-H wagging of methyl groups was detected at 1359 cm^{-1} (Badii et al., 2016) and bending vibrations of methylene groups were observed at 1450 cm^{-1} (Ji et al.,2009). The peak at 1664 cm^{-1} could be related to trapped residual non evaporeted DMF solvent (Tighilt et al., 2007). Stretching vibration of C-N

nitrile functional group was observed at 2243 cm^{-1} (Chen et al., 2008), (Varshney et al., 2012) . C-H stretching vibration was seen at 2939 cm^{-1} (Cetin and Camurlu, 2018). As seen from Figure 4.2.(c), when the FTIR spectra was inspected by the addition of different melting point paraffins to PAN nanofibers, the peak intensities at 2847 and 2912–2614 cm^{-1} were significanly increased with all types of paraffin additions to PAN nanofibers revealing the existence of parrafins in the structure. Intensities of these peaks were not proportionally changed by changing paraffin contents in P/PAN nanofibers (Figure 4.2(b)). This implied that either the paraffin content didn't increase proportionally in P/PAN nanofibers or the distribution of the paraffin in the nanofibers or mat were not homogeneous. Even though the paraffin content was increased proportionally in the electrospinning solution, since the final paraffin suspensions were not homegeniously distributed in the solution and there should have been some paraffin precipitation in the plastic syring during the electrospinning procces. The intensities of paraffin peals were not in a proportional orders due to their rate in P/PAN nanofibers. These positions of the corresponding peaks coming from PAN molecules in P/PAN nanofibers as in Figure 4.2(b) didn't change significanltly comparing PAN nanofibers. This revealed that there was not a chemical interaction between PAN and paraffin molecules both at solution and nanofiber preperation processes. So, the phase transition property of paraffin could be very applicable for the cyclic usage.

Differential scannig caloriemeter measurements were carried out to observe melting points (Tm) and entalpies of the pure paraffins (Figure 4.3(a)) and paraffin loaded P/PAN nanofibers (Figure 4.3(b) and (c)). As seen from Figure 4.3(a), single melting peaks (Tm) were detected at 38.5, 89.9 and 114.7ºC for the samples P1, P3 and P4. Sample P2 demonstrated two distinct melting peaks located at 58.6 and 69.5ºC. They revealed that this sample could have contained two different crystalline structures. Since these two peaks are coalesced, both peaks were considered for the entalpy determination of the sample. Producing P/PAN nanofibers with different concentration of the same type of paraffin didn't change the melting point of

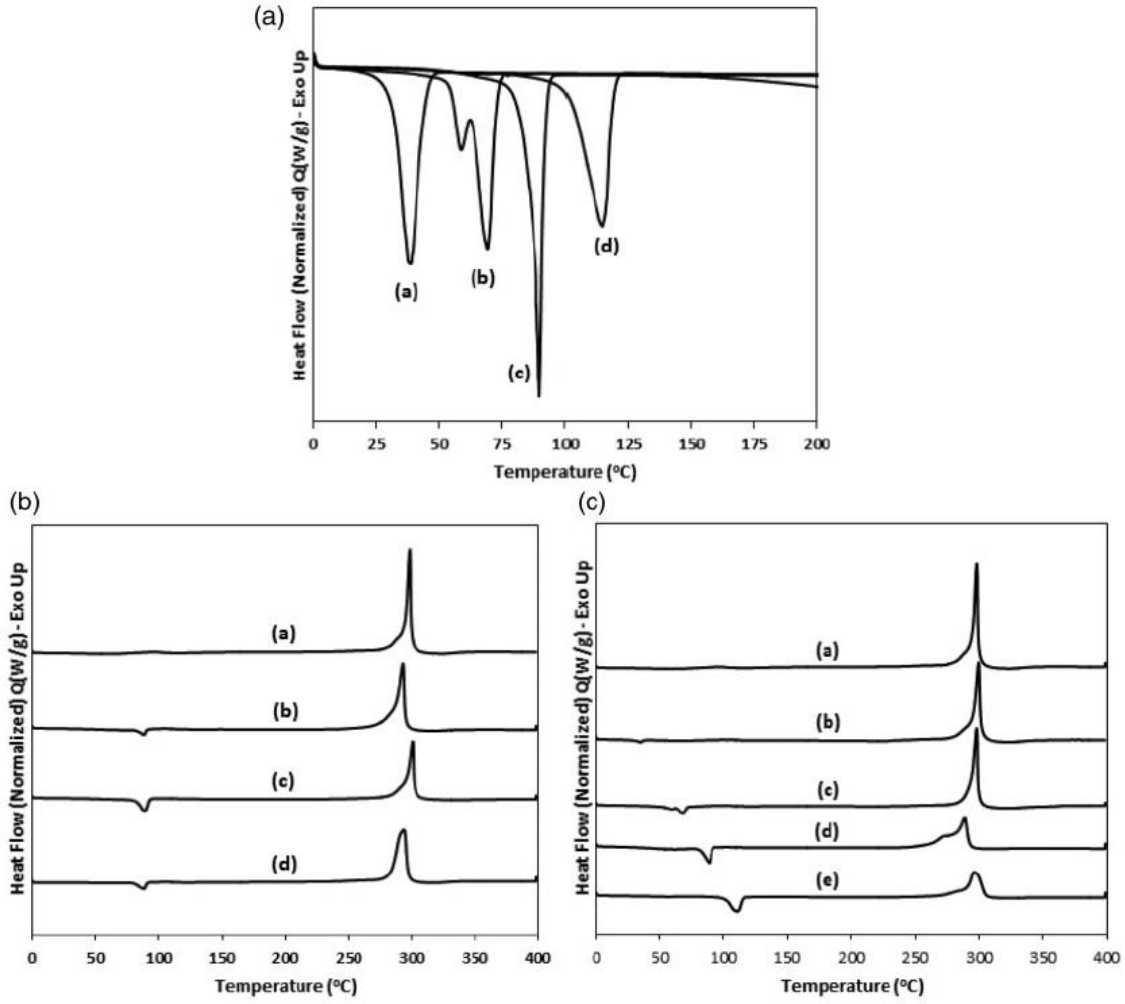

Figure 4.3. DSC of neat paraffins and P/PAN nanofibers: (a) pure paraffins (a) P1, (b) P2, (c) P3 and (d) P4; (b) P/PAN nanofibers with different paraffin concentration (a) just PAN, (b) P3/PAN-1, (c) P3/PAN-2 and (d) P3/PAN-3; and (c) P/PAN nanofibers with different paraffin types (a) just PAN, (b) P1/PAN, (c) P2/PAN, (d) P3/PAN and (e) P4/PAN.

Producing P/PAN nanofibers with different concentration of the same type of paraffin didn't change the melting point of paraffin part in the nanofibers distinctively as demonstrated in Figure 4.3(b). The positions of melting points of paraffins were shifted when they were loaded with different paraffin types and produced in the form of P/PAN nanofibers. The detected paraffin melting points in P/PAN nanofibers were 34.5, 88.3 and 110.7ºC for P1/PAN, P3/PAN and P4/PAN samples respectively (Figure 4.3(c)). Melting points were shifted to 59.8 and 88.3ºC for P2/PAN and P3/PAN sample as shown in Figure 4.3(c). As seen, melting points of paraffins decreased for P1, P3 and P4

samples when the paraffin was loaded to PAN nanofibers as in P1/PAN, P3/PAN and P4/PAN. Even though the first detected melting point of P2/PAN increased to 59.8ºC, the second detected melting point decreased to 67.8ºC. As seen from Figure 4.3(b) and (c), a strong exotermic peak was detected at 298.1ºC for pure PAN nanofiber. This peak is related to complex chemical reaction (dehydrogenation, cyclization, and cross-linking) (Zhu et al., 2003) taking place at PAN molecules in the nanofibers. The position of this peaks didn't increase or decrease consistently with either paraffin type or with the amount of paraffin in P/PAN nanofibers (Figure 4.3(b)). But the intensity of the peak decreased with increasing melting point of added paraffin (Figure 4.3(c)). The reduction of the peak could be related to the stronger interaction of paraffin and PAN molecules compared to pure PAN nanofibers (Ji et al., 2008).

Melting enthalpy (DHm) of the pure parrafins obtained from the DSC plots were 231.1, 219.7, 242.0 and 233.9 J/g for P1, P2, P3 and P4 samples respectively as demonstrated in Figure 4.3(a). The results showed that melting enthalpy did not change consistently due to increase of melting point of the paraffins (Figure 4.3(b). When the same amount of weight but different type of the paraffins were included in P/PAN nanofibers, melting enthalpy increased with increasing melting point of the paraffin as in Figure 4.3(c). The measured enthalpies of paraffin parts in P/PAN nanofibers were 9.6, 51.9, 64.2 and 101.5 J/g for P1/PAN, P2/PAN, P3/PAN and P4/PAN samples respectively as in Figure 4.3(c). But melting enthalpy differences were not consistent at P/PAN nanofibers when changing the amount of paraffin addition in the electrospinning solution (Figure 4.3(b). Melting enthalpy of pure PAN nanofibers was measured as 298.1 J/g. The melting entalpy of PAN nanofibers did not change consistently with the addition of paraffin type and rate.

TGA measurements at the temperature range between 30 and 600ºC in nitrogen atmosphere were conducted in order to observe the thermal stabilities and weight losses of pure paraffin, PAN and P/PAN nanofibers. The results of TGA measurement were presented in Figure 4.4. As shown in Figure 4.4(a), only one step weight loss was observed for all paraffin types and the weight loss was related to volatilization of paraffin (Memon et al., 2015). TGA results of pure PAN and P/PAN nanofibers were

given in Figure 4.4(b) for different paraffin concentrations and in Figure 4.4(c) for different paraffin types. First weight loss mainly began around 100ºC and made a plateau at around 134ºC corresponding to water loss from the nanofibers. Since mostly PAN part held water molecules, the release of water was higher at pure PAN nanofibers comparing to P/PAN nanofibers as seen at inset in Figure 4.4(b) and (c). Release of excess DMF from the fibers started at the beginning of the test. Weight loss mostly took place between 295 and 471ºC. The weight loss at PAN nanofibers could be related to chemical reactions taking place in PAN molecules and removal of volatilities

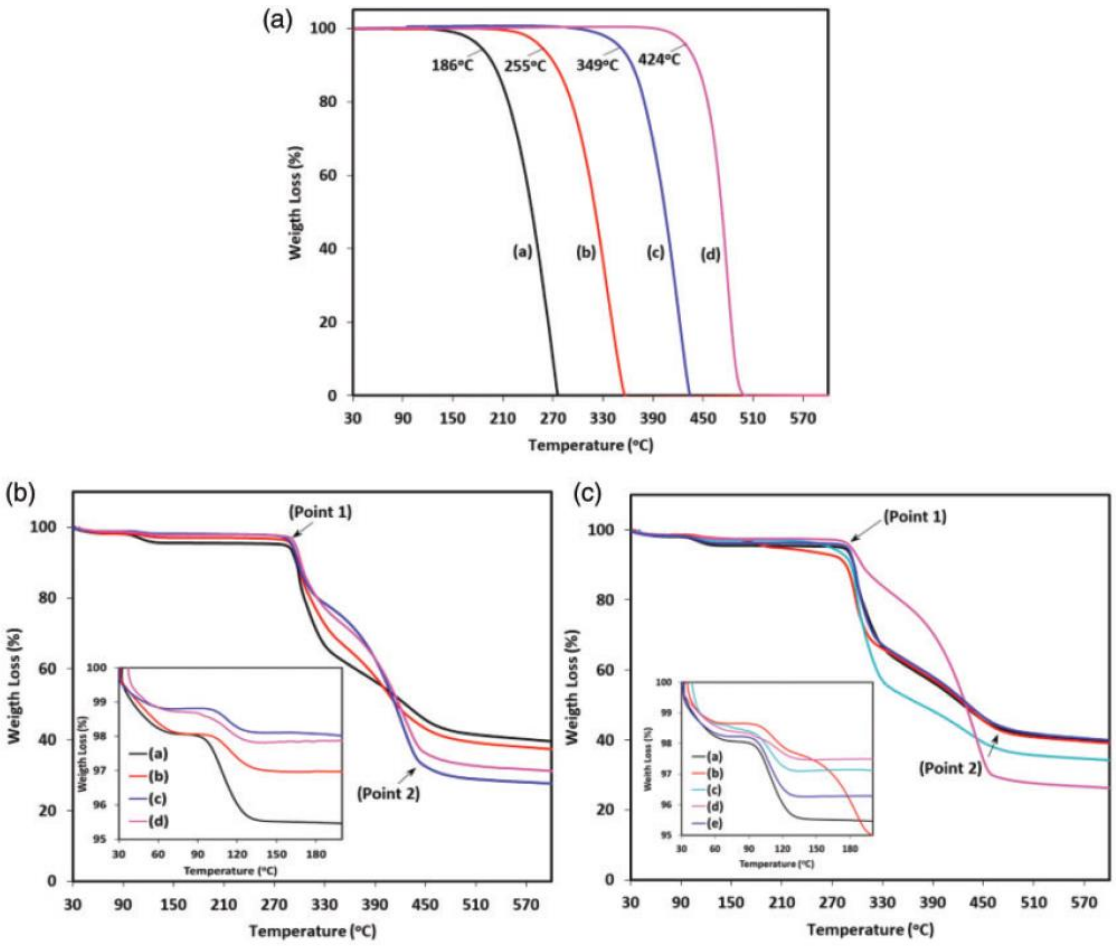

Figure 4.4. Thermogravimetric analysis (TGA plots) of (a) pure paraffins (a) P1, (b) P2, (c) P3 and (d) P4; (b) P/PAN nanofibers with different paraffin concentration (a) just PAN, (b) P3/PAN-1, (c) P3/PAN-2 and (d) P3/PAN-3; and (c) P/PAN nanofibers with different paraffin types (a) just PAN, (b) P1/PAN, (c) P2/PAN, (d) P3/PAN and (e) P4/PAN.

from the system. Similar weight loss plot has been reported in the literature by conducting TGA examination of PAN nanofiber in the nitrogen environment (Onwudiwe et al., 2015), (Wu et al., 2012).

As seen from TGA plots in Figure 4.4(b), weight losses mostly started earlier at P/PAN nanofibers especially when low melting point paraffins were loaded. This could be related to the evaporation of paraffins before the starting degradation temperature of PAN. The residual percentage of pure PAN nanofibers after TGA measurements at 600ºC was 39.2 wt.%. Except the sample P4/PAN, the residuals of P/PAN nanofibers decreased comparing to pure PAN nanofiber sample. The residuals of the different type of paraffin loaded P/PAN samples after TGA measurements under nitrogen atmosphere were 38.7, 33.9, 26 and 39.5% respectively for P1/PAN, P2/PAN, P3/PAN and P4/PAN nanofiber samples.

In this work, it was aimed to produce a paraffin-PAN hybrid nanocomposite which is compatible for simply mixing in paraffin compound of paraffin actuator by its nano-sized impregnated/encapsulated paraffin portion. Moreover, the PAN nanofiber portion of the nanocomposite is meant to carry the thermal properties of PAN-nanofibers as a thermal network into paraffin actuator. The investigation started with P3 paraffin in different mixing proportions with PAN polymer. The goal was to ensure the best suitable mixing range of PAN and paraffin molecules. It was found experimentally that the best applicable proportion for mixing and electrospinning process was 50% PAN polymer and 50% paraffin for the hybrid nanofiber synthesis. Especially higher paraffin proportions were found to cause difficulties during electropinning. Further hybrid nanofibers with paraffins of different melting points were produced to confirm the compliance of this simple process for a wide range of paraffin types. Among these paraffin types, DSC results showed that P1/PAN hybrid nanofiber had literally lowest melting enthalpy in comparison with pure paraffin. This throughput indicated that the thermal behaviour of the P1/PAN nanocomposite inclined to thermal properties of PAN portion rather than paraffin portion of hybrid structure. In terms of melting enthalpy of DSC results the other samples (P2/PAN P3/PAN and P4/PAN) incline**s** to thermal properties of paraffin portion of nanocomposite.

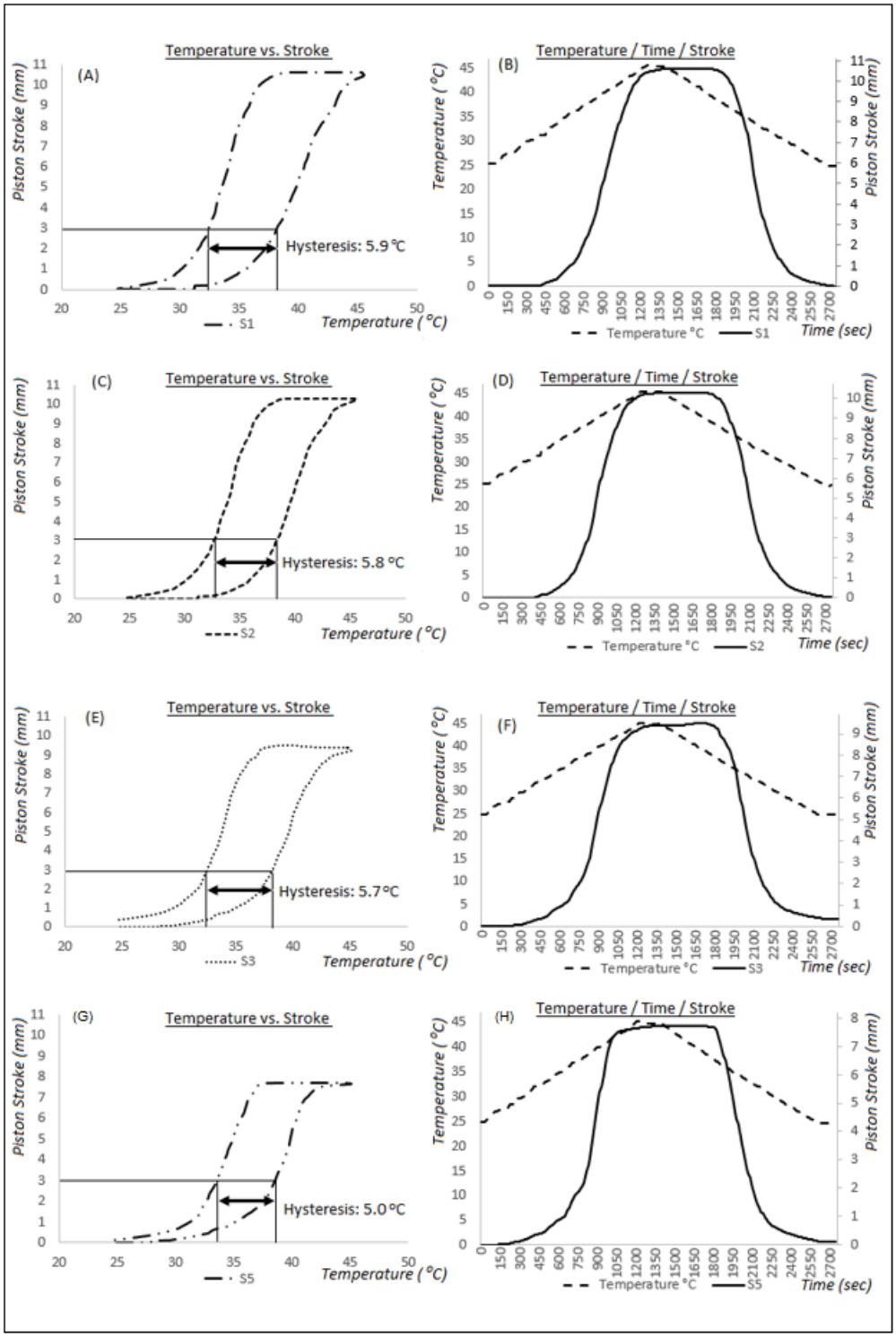

Figure 4.5. Temperature/Time/Stroke Curves and time independent Temperature/Stroke Curves for the samples a) and b) for S1, c) and d) for S2, e) and f) for S3, g) and h) for S4, i) and j) for S5.

Under this circumstances, we have incorporated P1/PAN hybrid nanofiber in paraffin actuator application whose melting temperature is truly suitable for thermal management of e-vehicle batteries cooling systems.

Hysteresis of the paraffin actuator was affected by adding nanofiller into paraffin compound as indicated in Figures 4.5 and 4.6. Hysteresis results according to samples were listed in the Table 4.1 . Increase of the nanofiber amount in the paraffin compound improved the hysteresis in a direct proportional way. Figure 4.7(a) depicts the trend of hysteresis change according to nanofiber addition amount. The highest improvement of hysteresis was recorded at S5 with the 10% of P1/PAN hybrid nanofiber ratio by weight. Hysteresis enhancement up to 15.3% was achieved. In Figure 4.5 from A to J depicted temperature/stroke curves and temperature/stroke/time curves for all samples S1, S2, S3, S4 and S5 separately.

In the paraffin actuator, addition of 2.5 and 5% nanofillers improved the hysteresis moderately up to 3.4% while the addition of 7.5 and 10% nanofillers indicated a jump up to 15,3% hysteresis improvement compared with pure paraffin. This jump demonstrated the thermal percolation threshold effect of the nanofibers in paraffin actuator.

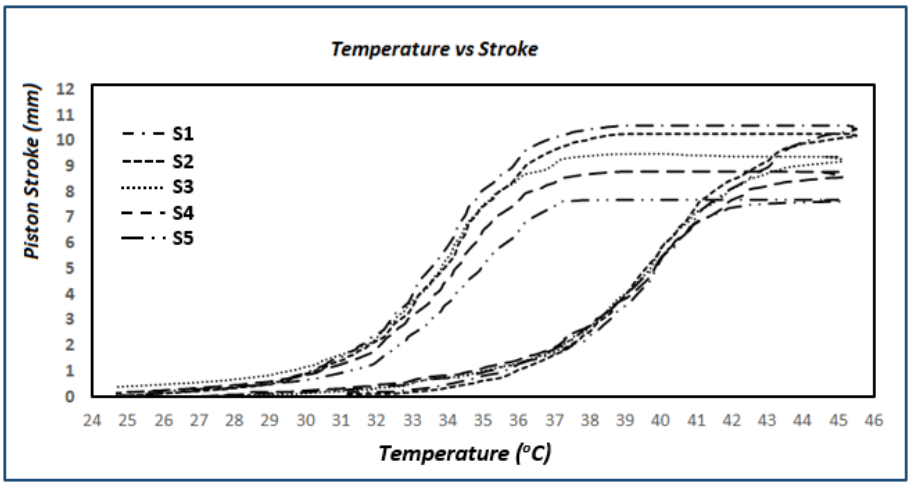

Figure 4.6. Temperature vs Stroke curves of the samples S1, S2, S3, S4, and S5 on the same graph for the comparison.

A substantial nanofiber network with highly inter fiber connections formed especially at the samples of S4 and S5 with nanofiber content of 7.5 and 10%. This feature complied with the findings of the investigation of Tian and Yang on Phonon Transport and Thermal Conductivity Percolation in Nanocomposites and can be explained as follows (Tian and Yang 2008). At the paraffin actuators S2 and S3 with low volumetric concentration of high thermal conductivity constituent, percolation network could not be formed and the thermal conductivity of the composites was effectively controlled by the low thermal conductivity constituents (hereby paraffin proportion) and phonon-interface scattering. When the volumetric concentration of high thermal conductivity constituents (hereby nanofiber proportion) is higher than the percolation threshold as seen at paraffin actuators S4 and S5, geometrically percolate channels for phonon transport is formed (Tian and Yang 2008). This structure allowed the paraffin actuator to achieve the hysteresis enhancement jump at sample S3 by 3.4%, at sample S5 by 11.9%.

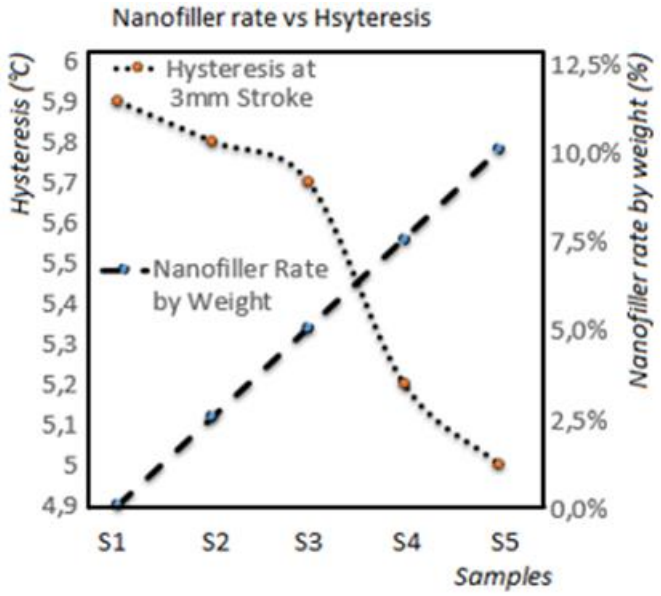

Figure 4.7. Change in Hysteresis according to nanofiller rate by weight of 5 paraffin actuator samples

In Figure 4.7, it can be seen that the opening curves of the 5 samples are very close to each other during the paraffin phase change from solid to liquid at heating cycle. Thermal conductivity of solid paraffin is higher than thermal conductivity of liquid

paraffin. This trend proved the thesis of Mamunya et al that short of high thermal conductivity contrast ratio was postulated to be the main reason for the lack of the thermal conductivity percolation in composite materials (Mamunya et al., 2002). The contrary closing curve of the 5 samples were dissociating from each other during cooling cycle where the liquid paraffin changed to solid phase. Thermal conductivity of n- Eicosane k solid is slightly over 0.350W/m K and k liquid is close to 0.150W/m K. Literally, thermal conductivity contrast between nanofiller and n-Eicosane increased 2.33 times because of the thermal conductivity loss during phase change

Table 4.1. Paraffin actuator hysteresis test results due to nanofiller content

Samples	N-Eicosane rate by weight (%)	PI/PAN hybrid nanofiber rate by weight (%)	Full-stroke at 45°C (mm)	Cooling temperature at 3 mm stroke (°C)	Heating temperature at 3 mm stroke (°C)	Hysteresis at 3 mm stroke (°C)	Hysteresis enhancement (%)
S1	100	0	10.59	32.3	38.2	5.9	0
S2	97.5	2.5	10.26	32.6	38.4	5.8	1.7
S3	95	5	9.49	32.5	38.2	5.7	3.4
S4	92.5	7.50	8.78	32.9	38.1	5.2	11.9
S5	90	10	7.70	32.5	38.5	5.0	15.3

The total paraffin compound filling capacity of the paraffin actuator capsule was 440 mg. The paraffin content of the paraffin compound was reduced and nanofiller was added gradually with following nanofiller/paraffin (mg/mg) amounts of 0/440, 11/429, 22/418, 37/403 and 44/396. Thus the expandable phase change material was replaced with nanofiller, and so the full stroke amount decreased accordingly.

Figure 4.8 depicts a relative change of full stroke amount parallel to sample preparation of paraffin compound. Nanofiller addition had a positive effect on thermal performance of the paraffin actuator but a stroke loss up to %27 was observed with 10% nanofiller addition. Full stroke amount of each sample at 45ºC are listed at Table 4.1. The capsule

inner volume of the paraffin actuator should be increased in accordance with the nanofiller addition if the stroke loss needs to be eliminated for a specific application area.

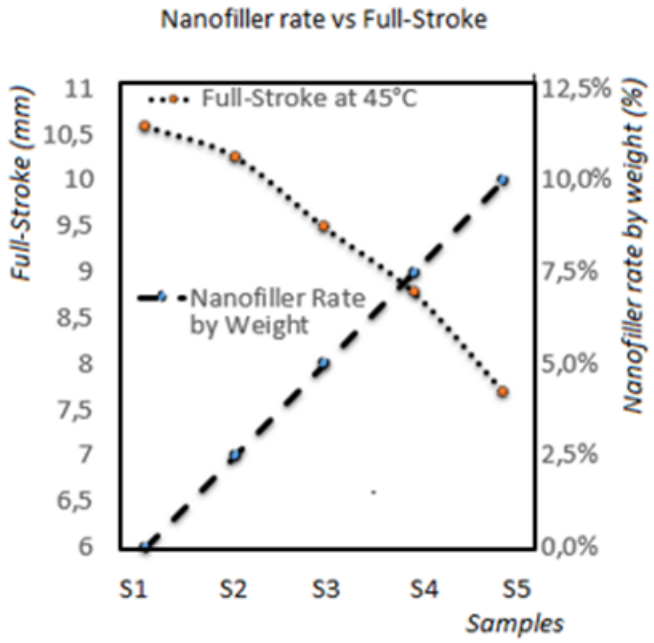

Figure 4.8. Change in full stroke at 45 C nanofiller rate by weight for 5 paraffin actuator samples.

4.2. Thermal Hysteresis Enhancement and Dispersion Thermal Stability

4.2.1. Morphological observation of PAN nanofibers

Morphology analysis of as-spun PAN nanofibers was carried out via electron microscopy imaging. PAN nanofibers are randomly distributed and fairly uniform nanofibers were obtained. Some negligible bead defect structure was observed at low magnification SEM images, as can be seen in Figure 4.9. More than 100 nanofibers were measured for diameters. Computed diameter distribution is presented in Figure 4.10. Minimum nanofiber diameter was 205nm and maximum nanofiber diameter was 544nm where mainly nanofiber diameters scattered between 320 and 440 nm and the average nanofiber diameter was calculated as 376nm.

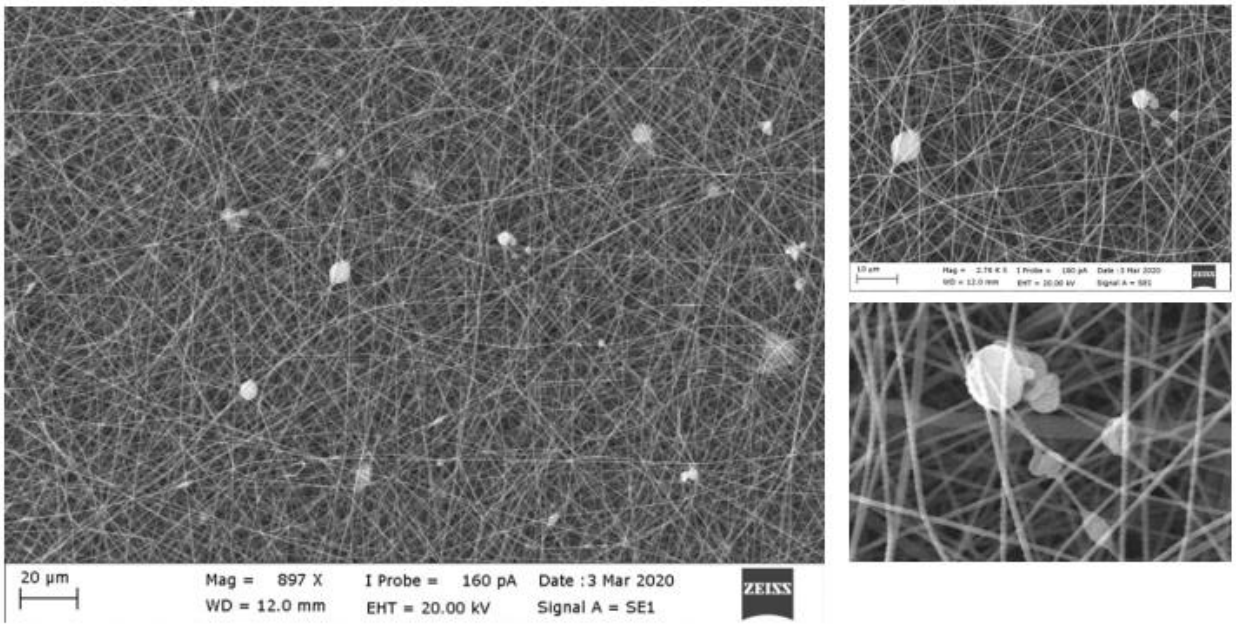

Figure 4.9. SEM Images of Electrospun PAN Nanofiber

Tightly interconnecting nanofibers are pretender for the thermal conduction path as thermal property enhancer of paraffin actuator in nanoscale. In Figure 4.11, the shown SEM image exhibits the interconnection hubs of the nanofibers where on a 12 micrometer square area 7 pieces' nanofiber cuts have 12 hubs. Computed total length of these cuts measured as 21.80 micronmeter. The volume of these nanofiber cuts is calculated with average nanofiber diameter of 376 nanometers as 2.419 cubic micrometers and as well as with density of 1.18g/cc, 2.85E-12g weight .

Diameter Bins (nm)	Frequency
240-	1
240-280	2
280-320	11
320-360	28
360-400	29
400-440	16
440-480	9
480-520	3
520+	1

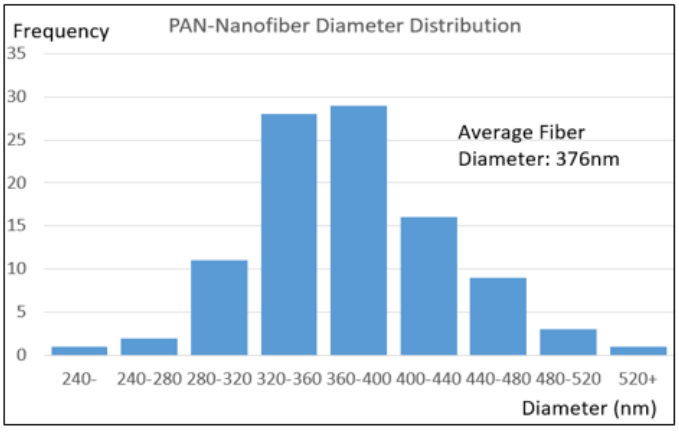

Figure 4.10. Diameter distribution of PAN Nanofibers

This tiny amount of 2.85E-12 g nanofiber revealed 12hubs, furthermore 0.45g PAN-Nanofiber which we have used for paraffin actuator sample P5, estimated, has 1.58E+11 interconnecting hubs. These extraordinary amount of hubs are expected to pass the thermal energy through nanocomposite structure and serves as a conductive network to enhance the thermal behavior of paraffin.

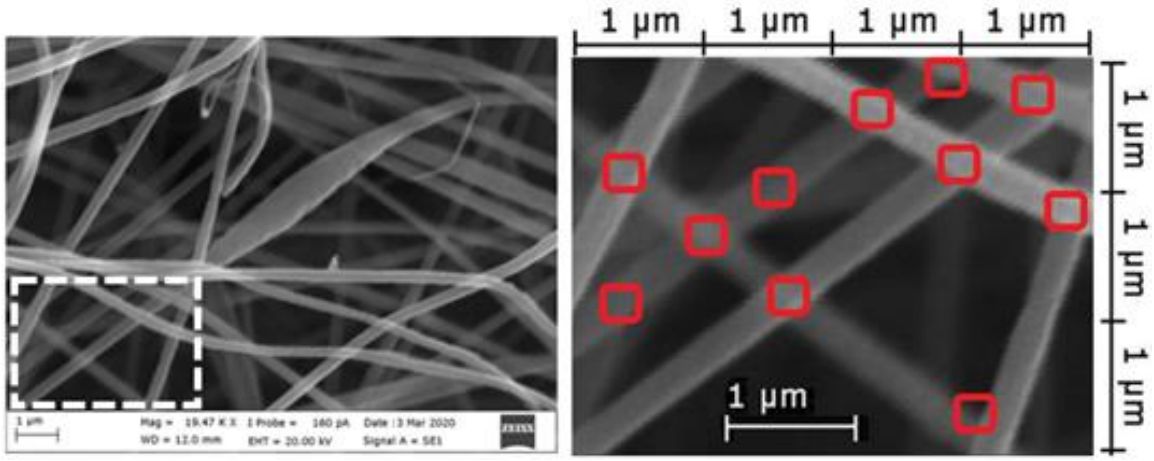

Figure 4.11. SEM Images of Electrospun PAN Nanofiber-interconnecting hubs

4.2.2. Paraffin-nanocomposite SEM and EDS results

In Figure 4.12-A, SEM images of Al_2O_3-Paraffin nanocomposite show that the nanoparticles have spherical shape which are agglomerated and coated/encapsulated with paraffin (Figure 4.12-B). Right bottom side of Figure 4.12-C exhibits that there are still pure paraffin blocks which are not homogeneously mixed with nanoparticles. These pure paraffin block structures do not reflect the thermal conductive features of Al_2O_3 nanoparticles and diminish the overall thermal behavior enhancement. A better mixing method should be developed to minimize the pure paraffin blocks amount in the nanocomposite.

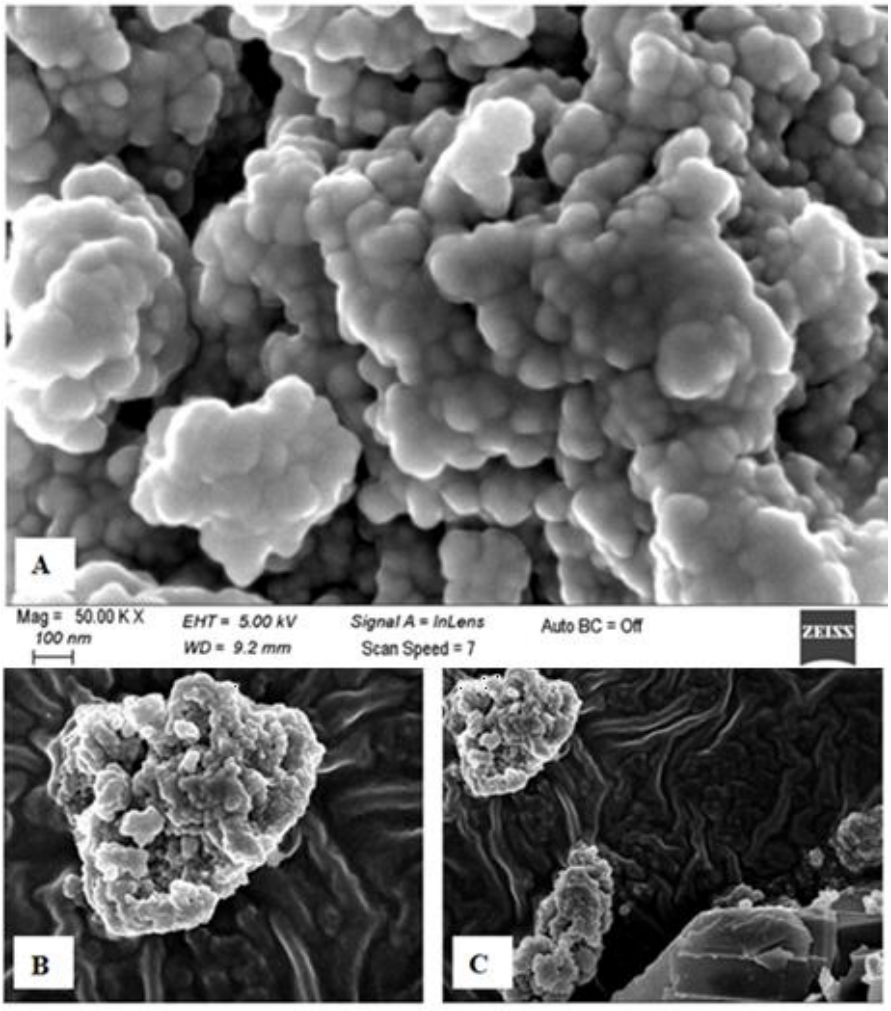

Figure 4.12. SEM images of Al_2O_3-Nonadecane nanocomposite

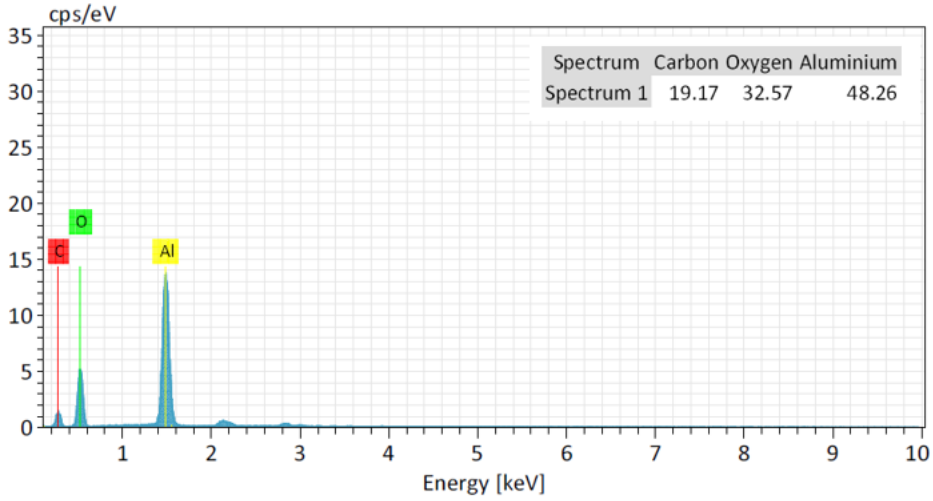

Figure 4.13. EDS image of Al_2O_3-Nonadecane nanocomposite

Presence of aluminum atoms in the composition of sample at the atomic level is confirmed by EDS analysis. Figure 4.13 shows the peaks of atoms in accordance with precence in the nanostructure characterized via energy dispersive X-ray spectroscopy analysis.

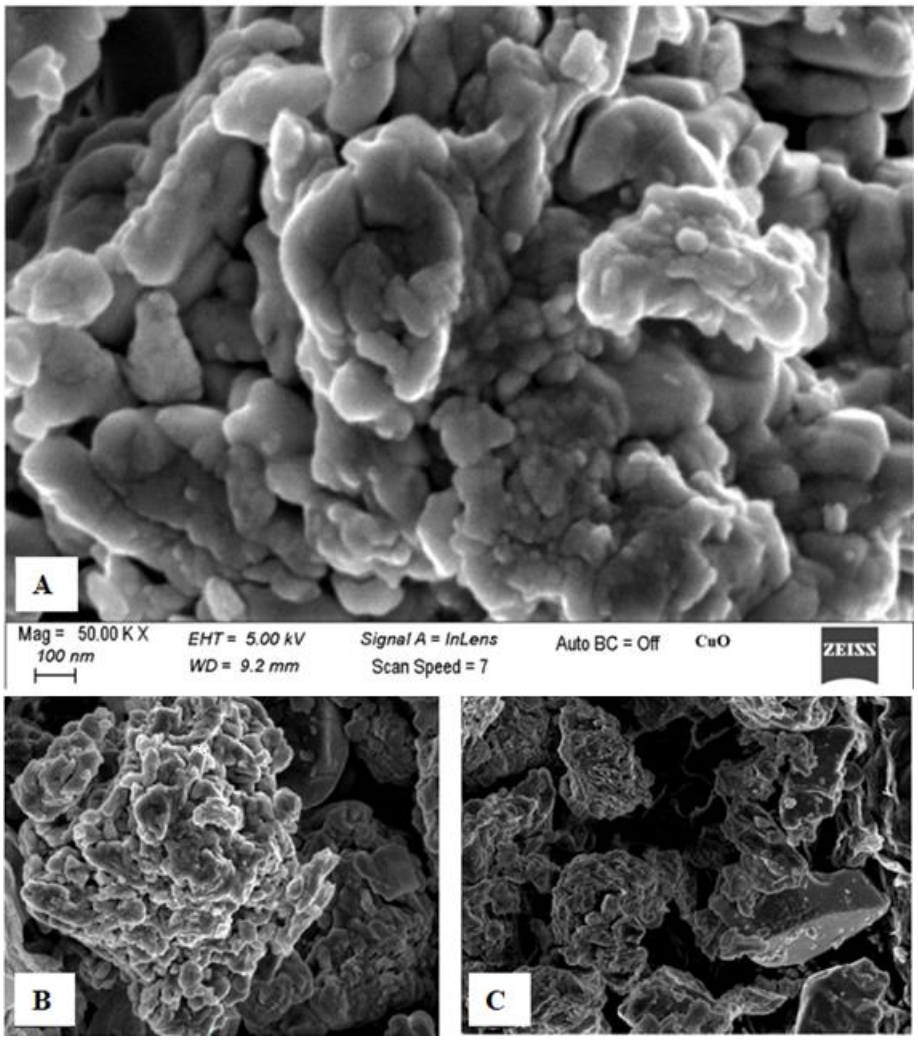

Figure 4.14. SEM images of CuO-Nonadecane nanocomposite

In Figure 4.14-A, SEM images of CuO-Paraffin nanocomposite show that the nanoparticles have non-spherical shape which are agglomerated and coated with paraffin (Figure4.14-B). Right bottom side of Figure 4.14-C exhibits that there are still pure paraffin blocks, seen as Al_2O_3-paraffin nanocomposite which are not homogeneously mixed with nanoparticles. These pure paraffin block structures do not reflect the thermal conductive features of CuO nanoparticles and diminish the overall

thermal behavior enhancement. A better mixing method should be developed to minimize the pure paraffin blocks amount in the nanocomposite.

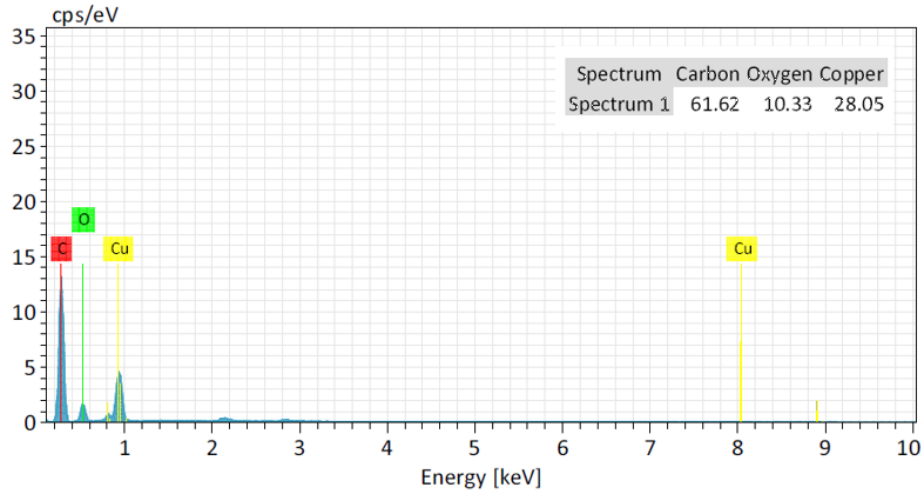

Figure 4.15. EDS image of CuO-Nonadecane nanocomposite

Presence of copper atoms in the composition of sample at the atomic level is confirmed by EDS analysis. Figure 4.15 shows the peaks of atoms in accordance with precence in the nanostructure characterized via energy dispersive X-ray spectroscopy analysis.

SEM images of Fe_3O_4-paraffin nanocomposite in Figure 4.16-A show that the nanoparticles have semi-spherical shape which are agglomerated and coated with paraffin (Figure 4.16-B). Fe_3O_4 nanoparticles have smaller size in comparison with Al_2O_3 and CuO nanoparticles according to SEM images.

Presence of iron atoms in the composition of sample at the atomic level is confirmed by EDS analysis. Figure 4.17 shows the peaks of atoms in accordance with precence in the nanostructure characterized via energy dispersive X-ray spectroscopy analysis.

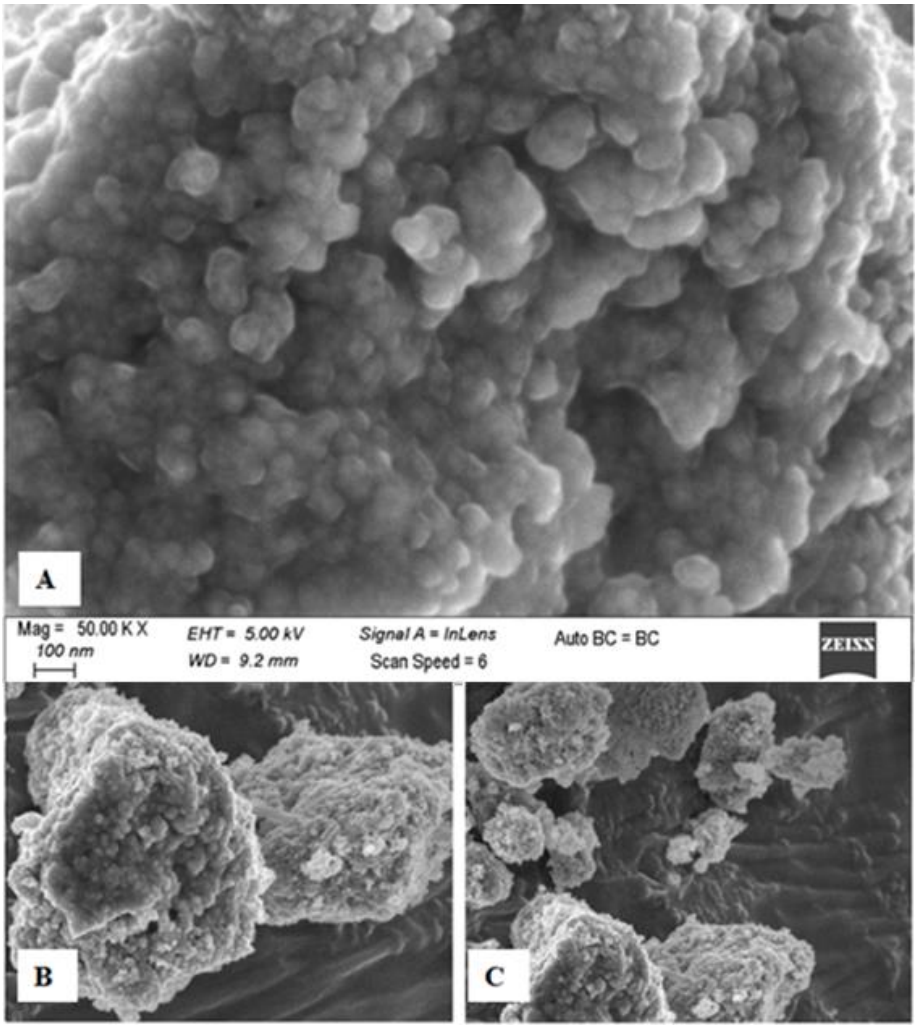

Figure 4.16. SEM images of Fe_3O_4-Nonadecane nanocomposite

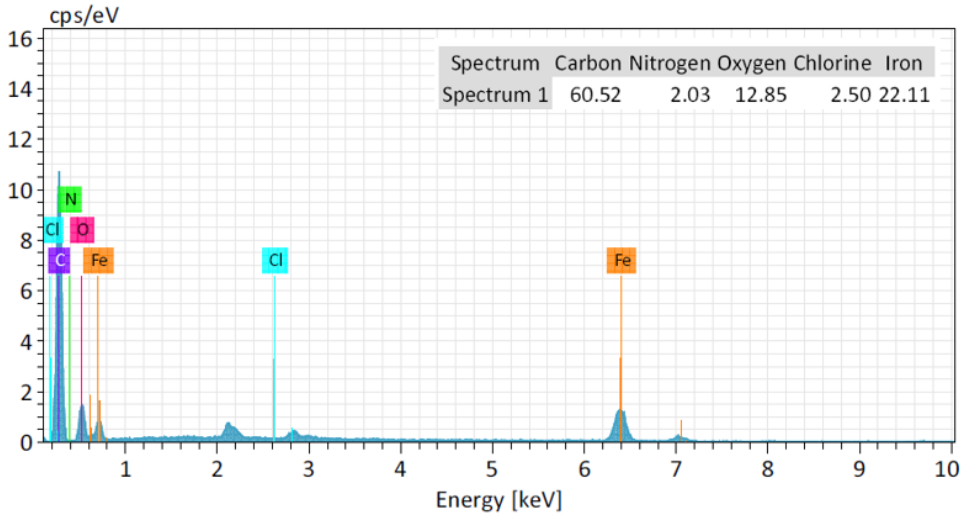

Figure 4.17. EDS image of Fe_3O_4-Nonadecane nanocomposite

SEM images of ZnO-Paraffin nanocomposite in Figure 4.18-A show that the nanoparticles have hexagonal short-rod shape. The agglomeration is very limited incomparable with Al_2O_3, CuO and Fe_3O_4 nanoparticle and coated with paraffin (Figure 4.18-B). Right bottom side of Figure13-C exhibits that there are still pure paraffin blocks, seen as Al_2O_3 and CuO-paraffin nanocomposite which are not homogeneously mixed with nanoparticles. These pure paraffin block structures do not reflect the thermal conductive features of ZnO nanoparticles and diminish the overall thermal behavior enhancement. A better mixing method should be developed to minimize the pure paraffin blocks amount in the nanocomposite.

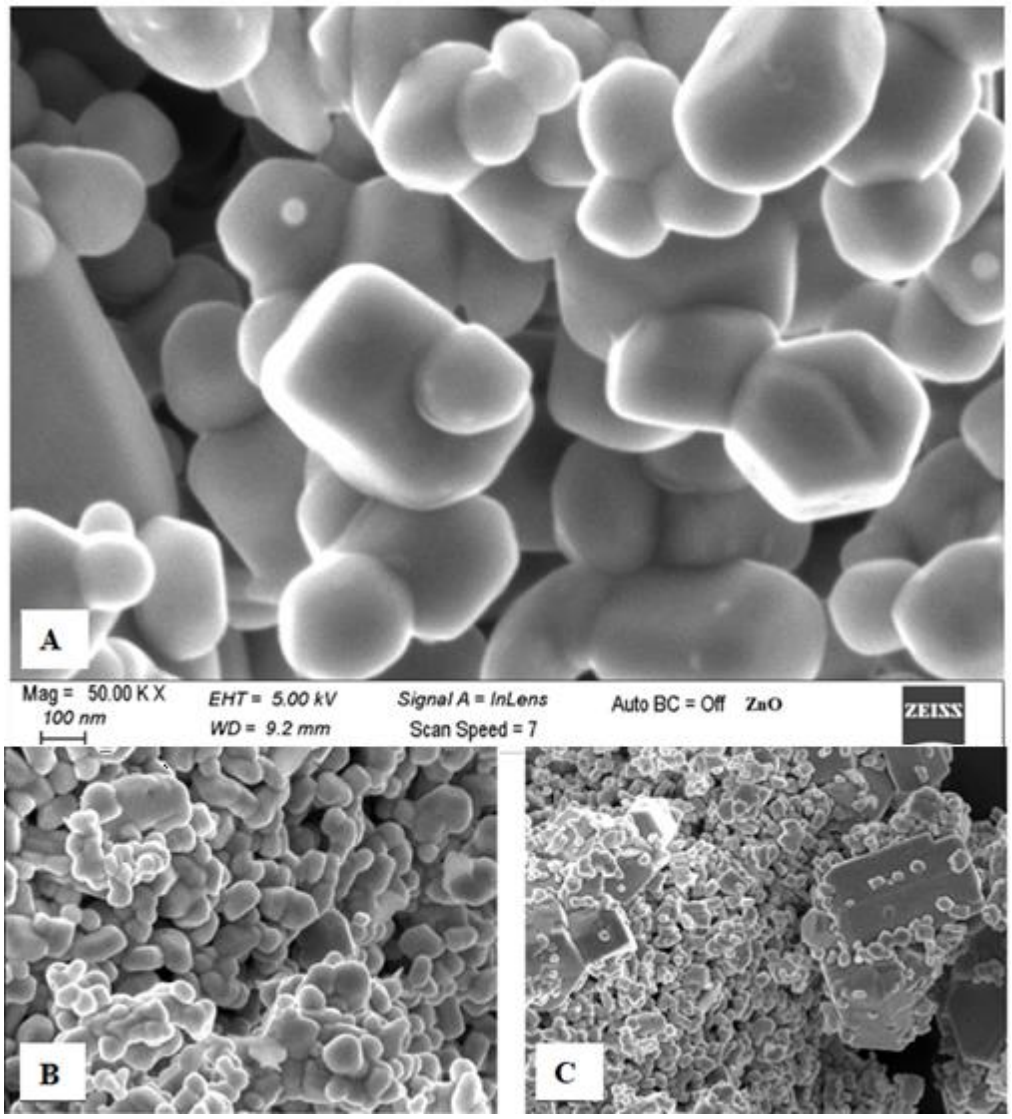

Figure 4.18. SEM images of ZnO-Nonadecane nanocomposite

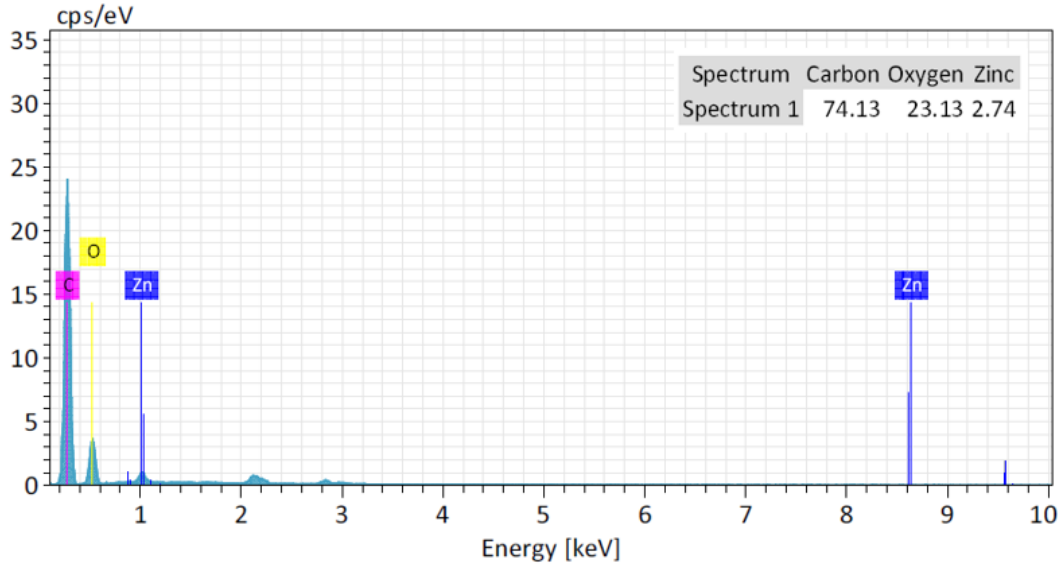

Figure 4.19. EDS image of ZnO-Nonadecane nanocomposite

Presence of zink atoms in the composition of sample at the atomic level is confirmed by EDS analysis. Figure 4.19 shows the peaks of atoms in accordance with precence in the nanostructure characterized via energy dispersive X-ray spectroscopy analysis.

SEM images of PAN Nanofiber-Paraffin nanocomposite in Figure 4.20-A show that the nanofibers are coated/encapsulated with paraffin (Figure 4.20-B). Interconnected network structure of pure PAN nanofibers is still existing after mixing with paraffin. Figure 4.20-C exhibits that the paraffin amount, which is not directly coating individual nanofibers, is encasing nanofiber bundles and forming fiber reinforced laminate-like structure. Thin paraffin laminate-like layers supported with nanofibers are meant to sense the temperature change more efficiently than the pure paraffin blocks found in metal oxide-paraffin nanocomposites. That could be the reason of better thermal hysteresis enhancement of PAN nanofiber-paraffin nanocomposite.

The EDS analyse results confirm that the PAN-nanofibers-paraffin nanocomposite has no external high conductive metalic content, and hysteresis enhancement is achieved just with PAN nanofibers. Figure 4.21 shows the peaks of atoms in accordance with precence in the nanostructure characterized via energy dispersive X-ray spectroscopy analysis.

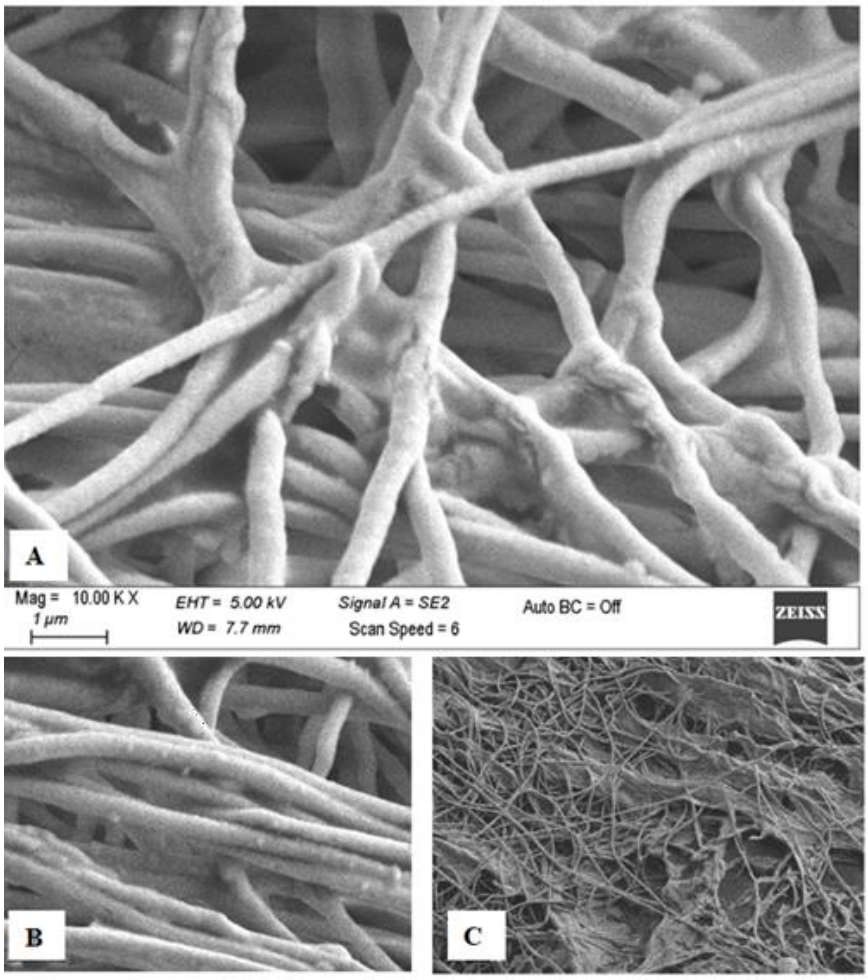

Figure 4.20. SEM images of PAN Nanofiber-Nonadecane nanocomposite

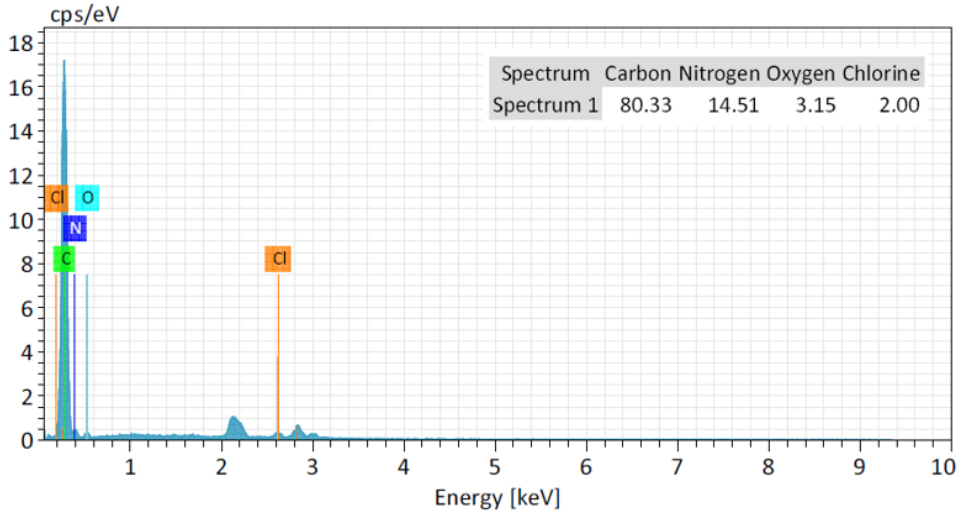

Figure 4.21. EDS image of PAN Nanofiber-Nonadecane nanocomposite

4.2.3. Thermal properties of pure nonadecane DSC and TGA results

DSC measurement showed in Figure 4.22 experimental melting and solidification curve obtained from pure nonadecane sample. The onset X temperature 31.01ºC corresponds the start of phase transition. The peak temperature of 36.14ºC corresponds the maximum energy absorption during melting. Solidification phase transition starts at onset X temperature of 30.07ºC and maximum energy release occurs at peak temperature of 30.50ºC during solidification.

Normalized enthalpy of melting is measured as 232.22 J/g and that of solidification 235.34 J/g. Enthalpy values are very close to results of Zhang's investigation. (Zhang et al, 2009). DSC analysis revealed that the solidification phase transition has a delay of 0.94ºC with respect to melting phase transition and also solidification peak temperature has a delay of 5.64ºC with respect to melting peak temperature. This delay of solidification with respect to melting points out the thermal hysteresis delay of paraffin actuator during heating and cooling thermal cycles.

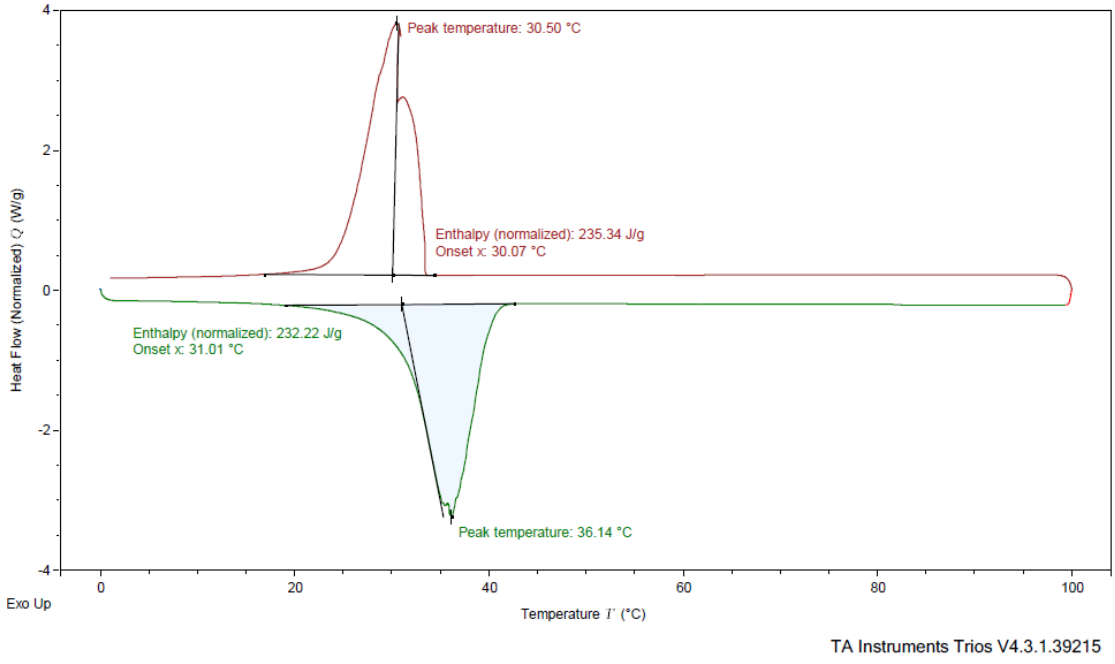

Figure 4.22. DSC curve of pure nonadecane

The TGA thermograms of pure nonadecane is shown in Figure 4.23. Pure n-nonadecane begins to degrade at approximately 145ºC and it completely loses its weight at 275ºC. The TGA thermogram of nonadecane exhibits a one step and sharp process without any remaining residuals. This reveals the purity of the nonadecane sample composed of a short linear alkane molecules $C_{19}H_{40}$.The sharp weight loss of nonadecane without residual is in agreement with the investigation of Timurah et.al. (K. Timuah et al, 2015)

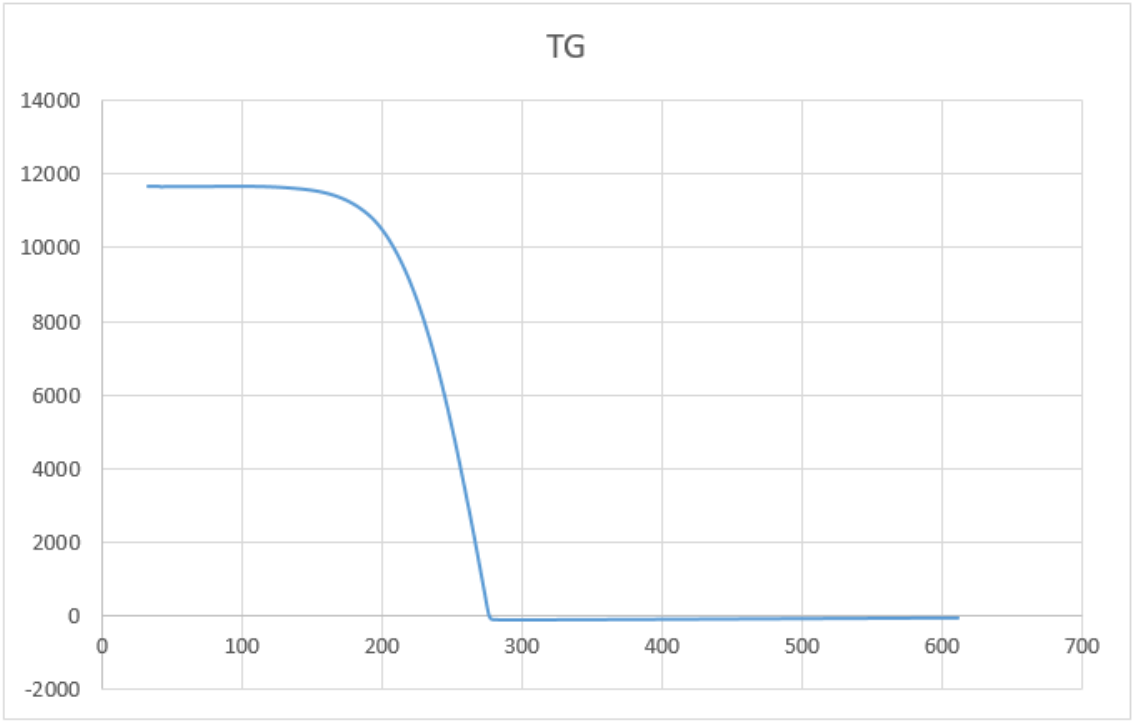

Figure 4.23. TGA curve of pure nonadecane

4.2.4. Dispersion thermal stability test results

High temperature dispersion thermal stability test is performed to determine the precipitation behavior of paraffin-nanocomposites at 100ºC which is about 70ºC higher than melting point of nonadecane. Figure 4.24 shows the photo-images and the CT - images at the same time laps. While CT-images are presenting the inner density homogeneity, photo-images are presenting the transparency/saturation of the nanocomposites from outside.

Samples of high temperature test, are seen at Figure 4.24-A2 CT-images, exhibiting light dots assigning very low density caused by air gaps and dark dots assigning very dense structure caused by agglomeration of nanoparticles, especially H1 and H3 including dark dots and H4 and H5 white dots. Sample H2 has light and dark dots dispersed relatively small sized and more homogenous.

Figure19-B1shows that nonadecane at 100ºC in 5 minutes changes its phase from solid to liquid, where the sample H6 transforms to transparent status. Although paraffin is in liquid phase, an obvious precipitation is seen only at sample H2. Samples H1 and H3 indicates a particular precipitation at bottom of the container. Figure 4.24-B2 exhibits that the light and dark dots at samples H1, H2 and H3 disappear from start of the test to 5^{th} minute. This denotes that the precipitation of the nanoparticles sweeps down the non-uniformities like agglomerated structures and air gaps. Samples H4, H5, H6 demonstrate no trace of precipitation at the bottom of the container. On the other hand, in these three samples, light dots indicating air gaps conjoined together and become larger and more visible. This reveals that the air gaps do not diffuse in paraffin during expansion and phase change of paraffin from solid to liquid. Instead, it pushes the air gaps to each other and generates larger bubbles. Storage from 5^{th} minute to 10^{th} minute dark area, indicating precipitation at samples H1, H2 and H3, becomes longer. From 10^{th} to 20^{th} minute, a clear transparency comes in view where the floating nanoparticles sunk down, as seen in Figure19-C1 to D1 and E1. At sample H2, this transparency improvement can be seen apparently. As a proof of it, Figure 4.24 C2 to D2 and E2 the bottom of container becomes more and more dense with the compacting of precipitated nanoparticles on each other. In the meantime, again at samples H4, H5 and H6 no trace of precipitation is revealed, neither at CT-Imaging, nor at Photo-Imaging.

According to high temperature dispersion thermal stability test result, it is concluded to perform the second level hysteresis test after a 20 minutes' storage of paraffin actuators at 100ºC.

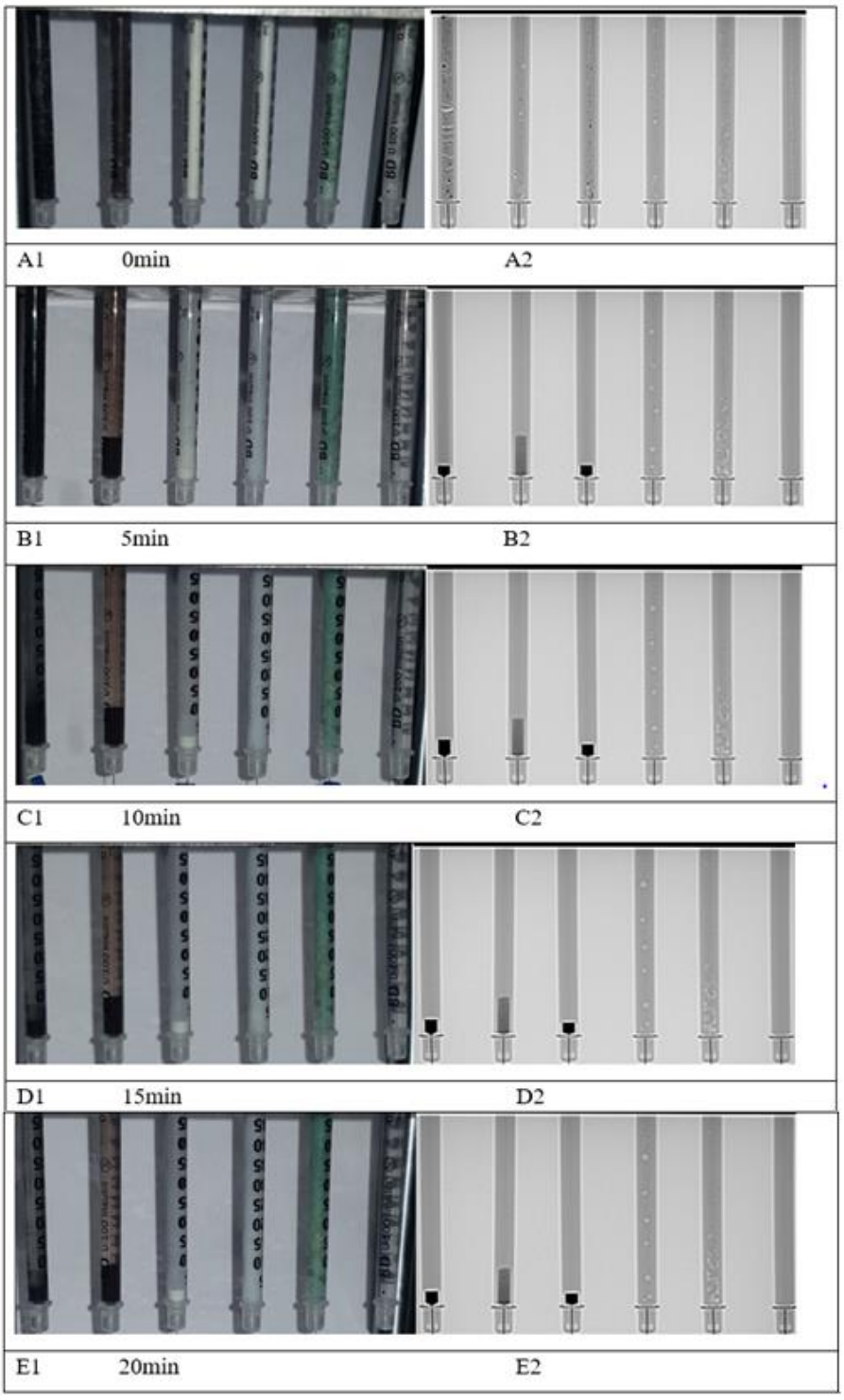

Figure 4.24. Dispersion Thermal Stability Test at 100ºC, photo-images and CT-images, A1 and A2 at test begin, B1 and B2 at 5th min, C1 and C2 at 10th min, D1 and D2 15th min, E1 and E2 at 20th min

Results of low temperature thermal stability tests are shown in Figure 4.25. This test at 45ºC provides an observation for smooth precipitation of nanoparticles. Top temperature of this test coincides with the top temperature of thermal hysteresis measurement which can supply an idea about the dispersion morphology of nanocomposite in paraffin actuator subjected to thermal hysteresis measurement during phase change.

Figure 4.25-A2 to D2 exhibits no precipitation at the first 6 minutes of storage in the nanocomposite structure which means the paraffin is still in solid phase. After 8th minute a very small amount of precipitation is seen at the bottom of the sample L3. Figure 4.25-E2 shows the precipitation of the nanoparticles at samples L1, L2 and L3 which means the nanocomposites start phase change from solid to liquid. Precipitation amount is increasing gradually from 10th minute to 20th minute at samples L1, L2 and L3 produced with CuO, Fe_3O_4 and ZnO nanoparticles.

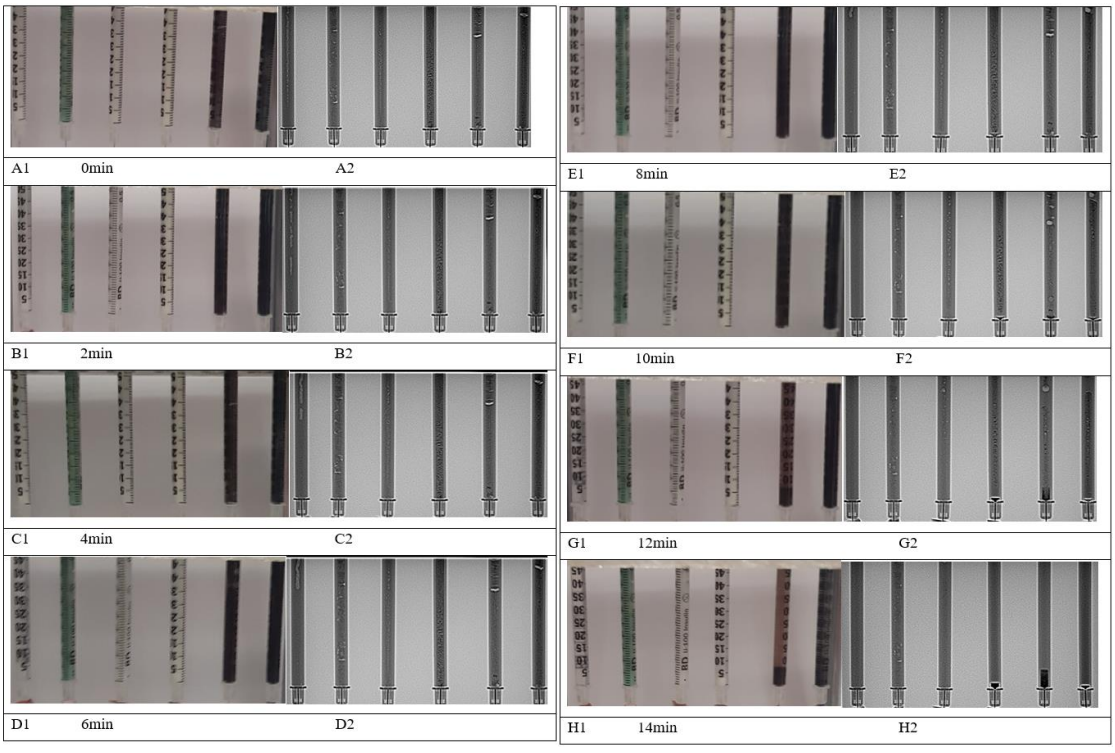

Figure 4.25. Dispersion Thermal Stability Test at 45ºC, photo-images and CT-images , A1 and A2 at test begin,B1 and B2 at 2nd min, C1 and C2 at 4th min, D1 and D2 at 6th min, E1 and E2 at 8th min, F1 and F2 at 10th min, G1 and G2 at 12th min, H1 and H2 at 14th min, I1 and I2 at 16th min, J1 and J2 at 18th min, K1 and K2 at 20th min

4.2.5. Thermal hysteresis test results

The higher thermal hysteresis value means a longer time spent for valve closing of thermostat due to time delay of paraffin actuator. For this reason, lower thermal hysteresis value is expected from paraffin actuator providing higher control performance for thermal management systems.

First level hysteresis test was performed with paraffin actuators where no precipitation in the paraffin nanocomposites occurred. High temperature dispersion thermal stability test revealed that at 100ºC 20-minute storage is enough for the almost precipitation of the metal oxide–paraffin nanocomposites. Therefore, the second level hysteresis test was performed after 20-minute storage of paraffin actuator in an oven at 100ºC.

Hysteresis curves of paraffin actuators are shown in Figure 4.26 to Figure 4.31, measured before the storage at 100ºC and labeled as hysteresis curve-pre and measured after storage at 100ºC and labeled as curve-post. An overlapped hysteresis curve between 2 to 4mm lift is particularly depicted to analyse the hysteresis diminution.

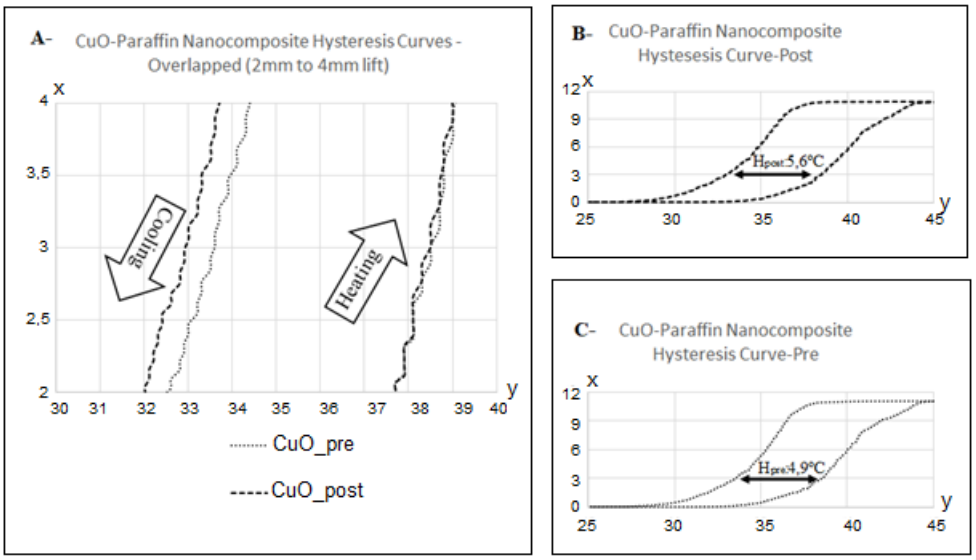

Figure 4.26. TH of P1 with CuO-Paraffin Nanocomposite, A-2mm to 4mm lift overlapped curves, B-Hysteresis after 100ºC Storage C-Hysteresis before 100ºC Storage

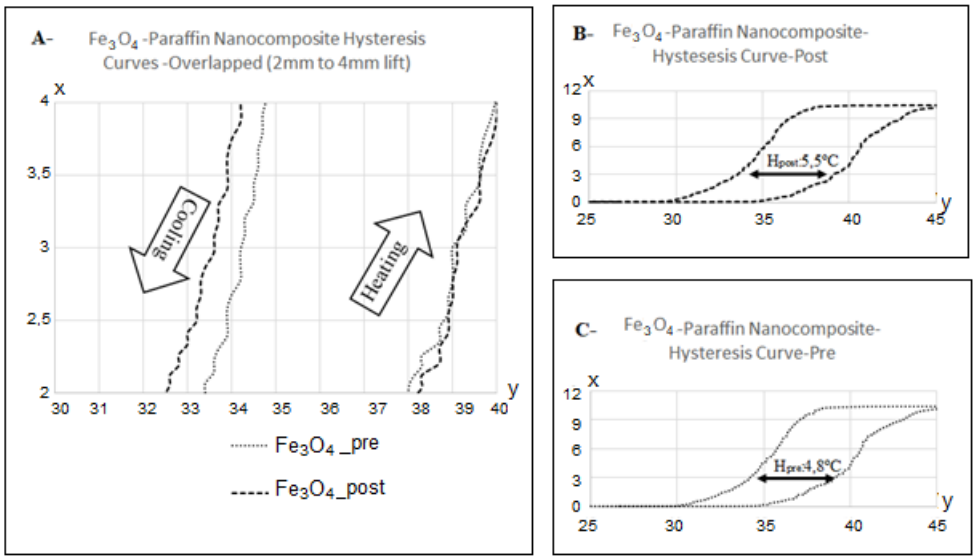

Figure 4.27. TH of P2 with Fe_3O_4-paraffin nanocomposite, A-2mm to 4mm lift overlapped curves, B-Hysteresis after 100ºC Storage C-Hysteresis before 100ºC Storage

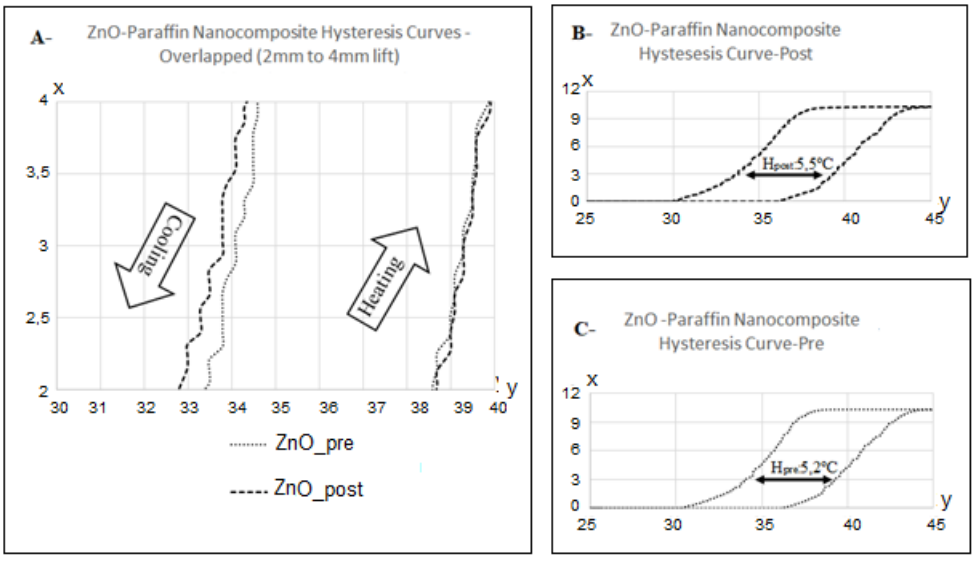

Figure 4.28. TH of P3 with ZnO-Paraffin Nanocomposite, A-2mm to 4mm lift overlapped curves, B-Hysteresis after 100ºC Storage C-Hysteresis before 100ºC Storage

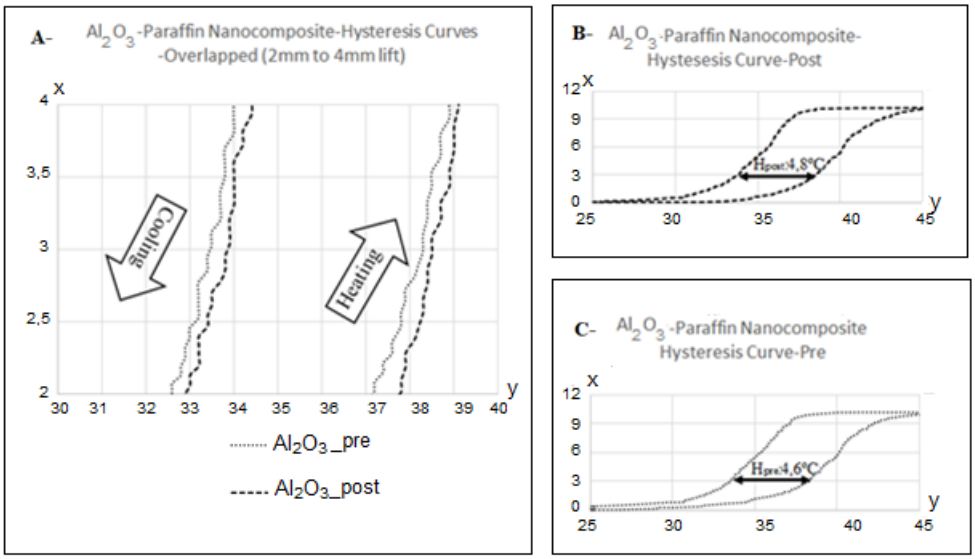

Figure 4.29. TH of P4 with Al_2O_3-paraffin nanocomposite, A-2mm to 4mm lift overlapped curves, B-Hysteresis after 100ºC Storage C-Hysteresis before 100ºC Storage

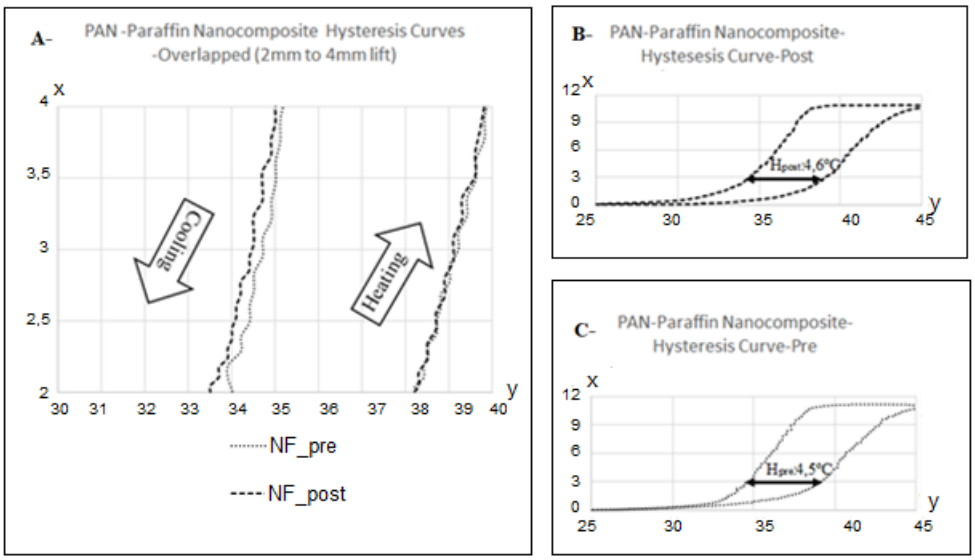

Figure 4.30. TH of P5 with PAN nanofiber-paraffin nanocomposite, A-2mm to 4mm lift overla.pped curves, B-Hysteresis after 100ºC Storage C-Hysteresis before 100ºC Storage

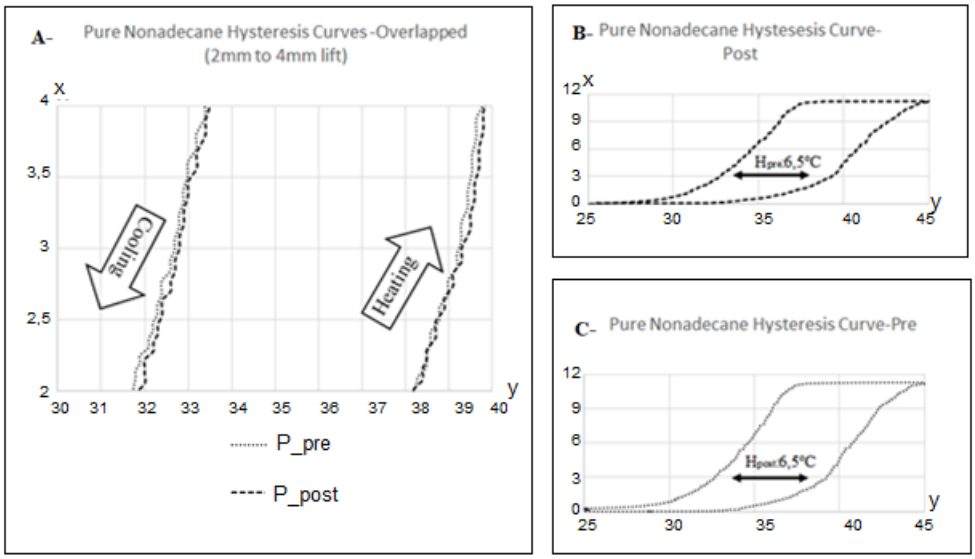

Figure 4.31. TH of P6 Paraffin Actuator with Pure Paraffin, A-2mm to 4mm lift overlapped curves, B-Hysteresis after 100ºC Storage C-Hysteresis before 100ºC Storage.

Figure 4.26A , Figure 4.27A and Figure 4.28A depict the overlapped hysteresis curves of first level and second level measurements for samples P1, P2 and P3. Curves are in agreement for both measurement levels at heating period where a hysteresis diminution occurs at cooling period. Figure 4.29A depicts a shifted curve at heating and cooling period where a limited hysteresis diminution is registered. Figure 4.30A reveals a very limited hysteresis diminution at cooling period where at heating period the curves of first and second level measurement are very close to each other. Figure 4.31A indicates no noteworthy change at hysteresis curves from first level to second level hysteresis measurement as expected sample P6 produced with pure paraffin.

Sample P5 revealed barely hysteresis diminution 2.2% as expected where the nanofiber density is close to paraffin density. Interconnected PAN nanofiber structure stands in the liquid paraffin like a nano scaled skeleton. This very low change at thermal hysteresis complies with dispersion thermal stability results of H5 and L5 samples.

Sample P4 has shown less hysteresis diminution than the other metal oxide samples, from first level to second level hysteresis measurements, which coincides with results of

high and low temperature dispersion thermal stability test of samples H4 and L4 where no precipitation was detected. This can be effect of the high surface area of Al_2O_3 nanoparticles with 140 m^2/g higher specific surface area and lower density in comparison with other investigated metal oxide nanoparticle additives.

Table 4.2. Results of first level hysteresis measurement before 100ºC storage and second level hysteresis measurement after 100ºC storage.

Sample Name	Sample Status	Temperature of 3mm lift while 1ºC/min heating up	Temperature of 3mm lift while 1ºC/min cooling down	Thermal Hysteresis at 3mm Lift	Change at Thermal Hysteresis
P1	First level TH, Pre 100ºC storage	38.50ºC	33.60ºC	4.90ºC	0.7 ºC
	Second level TH, Post 100ºC storage	38.50ºC	32.90ºC	5.60ºC	
P2	First level TH, Pre 100ºC storage	39.00ºC	34.20ºC	4.80ºC	0.7 ºC
	Second level TH, Post 100ºC storage	39.10ºC	33.60ºC	5.50ºC	
P3	First level TH, Pre 100ºC storage	39.30ºC	34.10ºC	5.20ºC	0.3 ºC
	Second level TH, Post 100ºC storage	39.30ºC	33.80ºC	5.50ºC	
P4	First level TH, Pre 100ºC storage	38.50ºC	33.90ºC	4.60ºC	0.2 ºC
	Second level TH, Post 100ºC storage	38.30ºC	33.50ºC	4.80ºC	
P5	First level TH, Pre 100ºC storage	39.20ºC	34.70ºC	4.50ºC	0.1 ºC
	Second level TH, Post 100ºC storage	39.10ºC	34.50ºC	4.60ºC	
P6	First level TH, Pre 100ºC storage	39.20ºC	32.70ºC	6.50ºC	0.0 ºC
	Second level TH, Post 100ºC storage	39.30ºC	32.80ºC	6.50ºC	

Table 4.2 demonstrates the hysteresis enhancement of paraffin actuators using paraffin-nanocomposite structure. All the samples P1, P2, P3, P4 and P5 produced with nanostructure addition has a significant hysteresis improvement at first level measurement in comparison with P6 produced with pure paraffin, with following values

24.6, 26.2, 20.0, 29.2, 30.8 % respectively. Nevertheless, after high temperature storage, samples P1, P2 and P3 lose their enhancement substantially via precipitation of nanoparticles and come down an enhancement of 13.8, 15.4 and 15.4% respectively, in comparison with sample P6. Samples P4 and P5 maintain their hysteresis essentially of 26.2 and 29.2% respectively, in comparison with sample P6.

5. CONCLUSION

5.1. Effect of the Number of Carbon in Paraffin on Interaction Nanofibers

The interaction of liquid paraffin with PVA nanofiber surfaces was investigated by using electrospun PVA nanofibrous mat and liquid paraffins with different amount of carbon in their structures. Microscopic images revealed that liquid paraffin could be held on the surface on the PVA nanofibers. Contact angle measurement results revealed that heptadecane has the highest and pentadecane has the lowest contact angle on PVA nanofibrous mat structures. As a conclusion, wettability of the PVA nanofibers by liquid paraffin can be enhanced if the paraffin is used which has less number of carbon atoms.

5.2. Paraffin/PAN Hybrid Nanofibers for Thermal Hysteresis Enhancement

Paraffins with different melting temperatures were successfully loaded to PAN nanofiber via electrospinning process at the ambient temperature. A simple preparation procedure was followed by mixing paraffin in PAN/DMF solution at over melting temperature of paraffin via magnetic stirring. After paraffin was melted in the solution, the mixture was slowly cooled down to the ambient temperature with continuous stirring. Homogeneous colloidal molten paraffin particles transformed to homogenious suspension just by cooling the system down under melting temperature according to paraffin type. Paraffins with melting temperatures of 32, 58, 89 and 114ºC were included in PAN nanofibers.

The addition of paraffin reduced the PAN nanofiber diameter from 376nm (neat PAN) to as low as 214nm under the same electrospinning parameters. Enthalpies of the paraffin portion in P/PAN nanofibers increased from 9.6 to 101.5 J/g respectively by increasing melting point of the loaded paraffin. FTIR results demonstrating the positions of the corresponding peaks of PAN molecules in P/PAN nanofibers didn’t change significantly compared to neat PAN nanofibers. These revealed that since there was not a chemical interaction between PAN and paraffin molecules both at solution

and nanofiber preperation processes, the phase transition property of paraffin could be very applicable for the cyclic usage of P/PAN nanofibers in thermal regulation applications. P/PAN hybrid nanofibers were successfully applied in paraffin actuator which is adequate for e-vehicle battery cooling systems.

Paraffin compound of the paraffin actuator was prepared with a mixture of pure paraffin and P/PAN nanofiber with weight ratios of 2.5, 5, 7.5 and 10%. Hysteresis value at 3mm stroke was improved at 1.7, 3.4, 11.9 and 15.3% levels respectively. The effect of thermal percolation was observed between the samples with 5.0 and 7.5% nanofiber additions. Effect of thermal conductivity contrast on the nanocomposite structure was observed between solid and liquid paraffins by the thermal response performance of the paraffin actuator, which showed difference during heating and cooling periods due to weight ratio of hybrid nanofibers in paraffin compound.

5.3. Thermal Hysteresis Enhancement and Dispersion Thermal Stability

A uniform PAN-Nanofiber structure was produced via electrospinning. Nonadecane paraffin with melting point of 32 ^{o}C is thermally characterized as a phase change material. Nanocomposite materials prepared via addition of CuO, Fe_3O_4, ZnO, Al_2O_3 nanoparticles and PAN nanofibers into nonadecane wt. % of 10 for the thermal behavior enhancement. Metal oxide- and nanofiber-paraffin nanocomposites are characterized by SEM and EDS analysis.

Besides pure paraffin compound, the produced nanocomposites are used as thermal expansion material in paraffin actuator. CuO, Fe_3O_4, ZnO, Al_2O_3 nanoparticles and nanofiber addition have successfully improved the thermal hysteresis value by 24.6, 26.2, 20.0, 29.2 and 30.8% for the samples respectively compared with pure paraffin at first level hysteresis test.

Although PAN-nanofiber has considerably lower thermal conductivity compared with investigated metal oxide nanoparticles, it revealed better thermal hysteresis enhancement in terms of paraffin actuator application due to the thermal conductive

network in nanocomposites. This thermal conductive structure built-up by interconnected fiber network is demonstrated with SEM images. Nanofiber reinforced paraffin actuator exhibited 30.8% before precipitation and 29.2% after precipitation. First and second level hysteresis test has proved that PAN-nanofiber based paraffin nanocomposite achieved best thermal behavior enhancement in terms of thermal hysteresis.

Effect of thermal dispersion stability on hysteresis performance of the nanocomposites is also investigated to ensure the long term consistent hysteresis performances advantages in paraffin actuator. PAN nanofiber added paraffin compound revealed a minor precipitation effect on hysteresis performance with a loss of 2.2%.
Thermal dispersion stability of the nanocomposites is comprehended via computer tomographic (CT) investigation in two different temperatures. The excessive precipitation of CuO-, Fe_3O_4- and ZnO-paraffin nanocomposite observed within 5 minutes at 100 ^oC where a gradually precipitation within 20 minutes at 45 ^oC is exposed. Precipitation of PAN nanofiber and Al_2O_3-paraffin nanocomposite was not visually detectable via CT-image and photo-image throughputs. Effect of thermal dispersion stability on hysteresis performance of the nanocomposites is also investigated to ensure the long term consistent hysteresis performance advantages in paraffin actuator. PAN nanofiber added paraffin compound revealed a minor precipitation effect on hysteresis performance.

Second level hysteresis test results were compliant with dispersion thermal stability test results where the highest hysteresis diminution occurred at samples of CuO-paraffin, Fe_3O_4-paraffin and ZnO-paraffin nanocomposites which are subjected to strong precipitation. Second level hysteresis test is performed after heat storage of paraffin actuators at 100ºC and following hysteresis diminution is revealed as 14.3, 14.6, 5.8, 4.3, 2.2 % respectively.

REFERENCES

Aminyan, R. and Bazgira, S. (2019). Fabrication and characterization of nanofibrous polyacrylic acid superabsorbent using gas-assisted electrospinning technique. *Reactive and Func.Polymers, 141*(45), 133–144. doi:10.1016/j.reactfunctpolym.2019.05.012

Amin, M., Afriyanti, F., Putra, N. (2018). Thermal properties of paraffin based nano-phase change material as thermal energy storage . *2nd international Tropical Renewable Energy Conference, IOP Conference Series: Earth and Environ. Science 105*(1), 012-028. DOI:10.1088/1755-1315/105/1/012028

Andrassy, Z. and Szantho, Z. (2019). Thermal behaviour of materials in interrupted phase change. *Journal of Thermal Analysis and Calorimetry*, *138*(6), 3915–3924. doi: 10.1007/s10973-019-08541-w

Assael, M. J., Charitidou, E., Karagiannidis, L. (1991). The thermal conductivity of n hexadecane, ethanol, n-decane and butanol mixtures. *International Journal of Thermophysics, 12*(3), 491–500. doi:10.1007/BF00502364

Aykut, Y. (2013). Electrospun MgO-loaded carbon nanofibers: Enhanced field electron emission from the fibers in vacuum. *Journal of Physics and Chemistry of Solids*, *74*(2), 328–337, DOI:10.1016/j.jpcs.2012.10.008328–337.

Aykut, Y., Pourdeyhimi, B., and Khan, S. A. (2013). Effects of surfactants on the microstructures of electrospun polyacrylonitrile nanofibers and their carbonized analogs. *Journal of Applied Polymer Science*, *130*(5), 3726–3735. doi:10.1002/APP.39637

Badii, K., Church, J.S., Golkarnarenji, G., Naebe, M., and Khayyam, H. (2016). Chemical structure based prediction of PAN and oxidized PAN fiber density through a non-linear mathematical model. *Polymer Degradation and Stability*, *131*, 53–61. doi:10.1016/J.POLYMDEGRADSTAB.2016.06.019

Boese, R., Weiss, H. C. and Bläser, D. (1999). The Melting Point Alternation in the Short-Chain n-Alkanes: Single-Crystal X-Ray Analyses of Propane at 30 K and of n-Butane to n-Nonane at 90K. *Angewandte Chemie International Edition, 38*(7), 988-992 doi:10.1002/(SICI)1521-3773(19990401)38:7<988::AID-ANIE988>3.0.CO;2-0

Bogatov, G. F., Rastorguev, Y.L., Grigorev, B. A. (1969). Thermal conductivity of normal hydrocarbons at high pressures and temperatures.*Chemical Technology of Fuels and Oil*, *5*(9), 651–653. doi:10.1007/BF00729686

Bony, J., Citherlet, S., (2007). Numerical model and experimental validation of heat storage with phase change materials. *Energy and Buildings*, *39*(10), 1065–1072. DOI:10.1016/J.ENBUILD.2006.10.017

Cabeza, L. F., Castell, A., Barreneche, C., de Gracia, A., Fernández, A. I., (2011). Materials used as PCM in thermal energy storage in buildings: A review. *Renewable and Sustainable Energy Reviews*, *15*(3), 1675–1695. DOI:10.1016/J.RSER.2010.11.018

Cetin, M. Z. and Camurlu, P., (2018). An amperometric glucose biosensor based on PEDOT nanofibers. *RSC Advances*, *8*(35), 19724–19731. DOI:10.1039/C8RA01385C

Chaber, R., Łach, K., Depciuch, J. (2017). Fourier transform infrared (FTIR) spectroscopy of paraffin and deparafinnized bone tissue samples as a diagnostic tool for ewing sarcoma of bones. *Infrared Physics and Technology*, *85*, 364–371. DOI:10.1016/J.INFRARED.2017.07.017

Chaichan, M. T., Kamel, S.H. and Al-Ajeely A. N. M. (2015). Thermal conductivity enhancement by using nano-material in phase change material for latent heat thermal energy storage systems. *Saussurea*, *5*(6), 48–55. Erişim Adresi: https://www.researchgate.net/publication/280923213_Thermal_Conductivity_Enhancement_by_using_Nanomaterial_in_Phase_Change_Material_for_Latent_Heat_Thermal _Energy_Storage_Systems

Chan, K. H. K., Kotaki, M., (2009). Fabrication and morphology control of poly(methyl methacrylate) hollow structures via coaxial electrospinning. *J. Appl. Polym. Sci. 111*(1), 408–416. DOI:10.1002/APP.28994

Che, G., Shi, T., Zhang, X., Cheng, F., Wu, X., Leng, G., Liu, Y., Fang, M., Min, X., Huang, Z., (2020). Polyacrylonitrile/polyethylene glycol phase-change material fibres prepared with hybrid polymer blends and nano-SiC fillers via centrifugal spinning, *Polymer*, *186*, 122012. DOI:10.1016/j.polymer.2019.122012

Chen, B. Y., Liu, Y., Zhang, X. H., & Sun, C. C. (2008, October). Study on influence factors of thermal hysteresis in paraffin actuator. In *2008 International conference on intelligent computation technology and automation (ICICTA) 1*, 1145-1148. doi: 10.1109/ICICTA.2008.272.

Duan, Q., Tan, F. L., Leong, K. C. (2002). A numerical study of solidification of n-hexadecane based on the enthalpy formulation. *J Mater Process Technol*, *120*(1), 249–58. DOI:10.1016/S0924-0136(01)01188-8

Elgafy, A., and Lafdi, K. (2005). Effect of carbon nanofiber additives on thermal behavior of phase change materials. *Carbon*, *43*(15), 3067–3074. DOI:10.1016/J.CARBON.2005.06.042

Fang, X., Fan L. W., Ding, Q., Wang, X., Yao, X. L., Hou, J. F. (2013). Increased thermal conductivity of eicosane-based composite phase change materials in the presence of graphene nanoplatelets. *Energy Fuel*, *27*(7), 4041–7. DOI:10.1021/EF400702A

Forziati, A. F., Glasgow, A. R., Willingham, C. B., Rossini, F. D. (1946), Purification and properties of 29 Paraffin, 4 Alkylcyclopentane, 10 Alkylcyclohexane, and 8 Alkyl Benzene Hydrocarbons, *Journal of Research of the National Bureau of Standards, 36,* 129-136. DOI:10.6028/JRES.036.005

Freund, M., Csikos, R., Keszthelyi, S., Mozes, G. Y. (1982). Paraffin Products-Properties, Technologies, Applications, Book, *Developments in petroleum science, 14*, 3-335, DOI:10.1016/s0376-7361(08)x7008-6

Fei, L., Hu, Y., Li, X., Song, R., Sun, L., Huang, H., Gu, H., Chan, H. L., and Wang, Y. (2015). Electrospun bismuth ferrite nanofibers for potential applications in ferroelectric photovoltaic devices, *Applied Material Interfaces*, *7*(6), 3665–70. DOI:10.1021/acsami.5b00069

Fan, L., Ma, Q., Tian, J., Li, D., Xi, X., Dong, X., Yu, W., Wang, J. and Liu, G. (2019). Conjugate Electrospinning Construction of Microyarns with Synchronous Color-Tuned Photoluminescence and Tunable Electrical Conductivity, *Journal of Electronic Materials*, *48*(3), 1511-1521. DOI:10.1007/s11664-018-06914-9

Fleischer, A. S., Chintakrinda, K., Weinstein, R. D., & Bessel, C. A. (2008). Transient thermal management using phase change materials with embedded graphite nanofibers for systems with high power requirements. *11th Intersociety Conference on Thermal and Thermomechanical Phenomena in Electronic Systems*, 561-566. DOI:10.1109/ITHERM.2008.4544317

Fleischer, A. S., (2015). Thermal Energy Storage Using Phase Change Materials-Fundamentals and Applications, Springer Briefs in Thermal Engineering and Applied Science, 1-5. (eBook, ISBN 978-3-319-20922-7) DOI:10.1007/978-3-319-20922-7.

Gang, B., Qinzhen, F., Jianfeng, S., Lihua, C. and Xi-Ming, S. (2019). A novel forced separation method for the preparation of paraffin with excellent phase changes, *RSC Adv*,*9*(52), 30453-30460. DOI: 10.1039/c9ra04722k

Ghasemi, E., Ziyadi, H., Afshar, A. M. and Sillanpä, M. (2015). Iron oxide nanofibers: a new magnetic catalyst for azo dyes degradation in aqueous solution. *Chemical Engineering Journal*, *264*,146–51. DOI:10.1016/J.CEJ.2014.11.021

Greiner, A., Wendorff, H. J. (2007). Electrospinning: A Fascinating Method for the Preparation of Ultrathin Fibers, *Angewandte Chemie*, *Int. Ed.*, *46*(30), 5670 – 5703. DOI:10.1002/ANIE.200604646

.

Gu, S. Y., Ren, J., and Vancso, G. J. (2005). Process optimization and empirical modeling for electrospun polyacrylonitrile (PAN) nanofiber precursor of carbon nanofibers. *European Polymer Journal*, *41*(11), 2559–2568. DOI:10.1016/J.EURPOLYMJ.2005.05.008

Gulfam, R., Zhang, P., Meng, Z. (2019). Advanced thermal systems driven by paraffin-based phase change materials—A review. *Applied Energy, 238,* 582-611. DOI:10.1016/J.APENERGY.2019.01.114

Holmen, R., Lamvik, M., Melhus, O. (2002). Measurements of the thermal conductivities of solid and liquid unbranched alkanes in the C16-to-C19 range during phase transition. *International Journal of Thermophysics, 23*(1), 27–39. DOI:10.1023/A:1013988507251

Hoffmann, A., Kuehne, A. (2021). High Throughput Centrifugal Electrospinning of Polyacrylonitrile Nanofibers for Carbon Fiber. *Nonwovens Polymers*, *13*(8), 1313. DOI: 10.3390/polym13081313

Hu, Y., Guo, R., Heiselberg, P. K., Johra, H. (2020). Modeling PCM Phase Change Temperature and Hysteresis, in Ventilation Cooling and Heating Applications, *Energies 13*(23), 6455. DOI: 10.3390/en13236455

Hussein, A., Abd-Elhady, M., El-Sheikh, M., Elmetwally, H. (2017). Improving Heat Transfer Through Paraffin Wax, by Using Fins and Metallic Strips , *Arabian Journal for Science and Engineering, 43,* 4433-4441. DOI: 10.1007/s13369-017-2923-2

Haghighat, F., Ravandi, S. A. H., Esfahany, M. N. (2018). A comprehensive study on optimizing and thermoregulating properties of core–shell fibrous structures through coaxial electrospinning. *Journal of Material Science*, *53*(6), 4665–4682. DOI:10.1007/s10853-017-1856-1

Ho, C. J., Gao, J. Y. (2009). Preparation and thermophysical properties of nanoparticle-in-paraffin emulsion as phase change material, *International Communications in Heat and Mass Transfer*, *36*(5), 467-470. DOI: 10.1016/j.icheatmasstransfer.2009.01.015.

Huang, Z. M., Zhang, Y. Z., Kotaki, M., Ramakrishna, S. (2003). A review on polymer nanofibers by electrospinning and their applications in nanocomposites. *Composite Science and Technology*, *63*(15), 2223-2253. DOI: 10.1016/S0266-3538(03)00178-7

Huang, L., Günther, E., Doetsch, C., Mehling, H. (2010). Subcooling in PCM emulsions—Part 1: Experimental, *Thermochimica Acta* , *509*(1-2), 93–99.DOI: 10.1016/j.tca.2010.06.006

Ilyas, S. U., Narahari, M., Tan, J., Theng, Y., Pendyala, R. (2019). Experimental evaluation of dispersion behavior, rheology and thermal analysis of functionalized zinc oxide-paraffin oil nanofluids, *Journal of Molecular Liquids*, *294*(1), 111613. DOI:10.1016/j.molliq.2019.111613

Iqbal, K., D. Sun, D. (2014). Development of thermo-regulating polypropylene fibre containing microencapsulated phase change materials. *Renewable Energy*, *71,* 473-479. DOI: 10.1016/j.renene.2014.05.063

Ji, L., Medford, A. J., and Zhang, X. (2009). Electrospun polyacrylonitrile/zinc chloride composite nanofibers and their response to hydrogen sulfide. *Polymer, 50*(2), 605–612. DOI: 10.1016/j.polymer.2008.11.016

Ji, L., Saquing, C., Khan, S.A. (2008). Preparation and characterization of silica nanoparticulate-polyacrylonitrile composite and porous nanofibers. *Nanotechnology, 19*(8), 085605. DOI:10.1088/0957-4484/19/8/085605

Jiling, Z. (2014). Battery thermal management systems of electric vehicles. Master of Science Thesis, Chalmers, University of Technology, Göteborg, Sweden, 2014.

Kapsalis, V.; Karamanis, D. (2016). Solar thermal energy storage and heat pumps with phase change materials. *Applied Themral Engineering, 99,* 1212–1224. DOI:10.1016/j.applthermaleng.2016.01.071

Kartikowati, C.W., Asep Suhendi, A., Zulhijah, R., Ogi, T., Iwaki, T., and Okuyama, K. (2016). Preparation and evaluation of magnetic nanocomposite fibers containing α″-Fe16N2 and α-Fe nanoparticles in polyvinylpyrrolidone via magnetoelectrospinning. *Nanotechnology, 27*(2), 025601. doi: 10.1088/0957-4484/27/2/025601

Ke, H. and Wei, Q., (2019). Determining influences of silver nanoparticles on morphology and thermal properties of electrospun polyacrylonitrile-based form-stable phase change composite fibrous membranes loading fatty acid ester/eutectics, *Thermochimica Acta 671,* 10–16. DOI: 10.1016/j.tca.2018.11.002

Khan, Z., Khan, Z., Ghafoor, A. (2016). A review of performance enhancement of PCM based latent heat storage system within the context of materials, thermal stability and compatibility. *Energy Conversion and Management, 115,* 132-158 . DOI: 10.1016/j.enconman.2016.02.045

Khedkara, R.S., Kiran, S., Sonawanea, S. S., Kailas, W., Suresh, S., Rohit, U. (2013). Thermo physical characterization of paraffin based Fe_3O_4 nanofluids, *Procedia Engineering, 51,* 342-346. DOI:10.1016/j.proeng.2013.01.047

Kim, Y.J., Ebara, M., and Aoyagi, T. (2013). A smart hyperthermia nanofiber with switchable drug release for inducing cancer apoptosis. *Adv. Funct. Mater*., *23*(46), 5753–61. DOI: 10.1002/adfm.201300746

Kumar, P. M., Anandkumar, R., Sudarvizhi, D., Mylsamy, K., Nithish, M. (2020). Experimental and Theoretical Investigations on Thermal Conductivity of the Paraffin Wax using CuO Nanoparticles, *Materials Today: Proceedings*, *22*(4), 1987-1993. DOI: 10.1016/j.matpr.2020.03.164

Kutlu, A., Eren, R., Aykut, Y. (2021). Paraffin/polyacrylonitrile hybrid nanofibers for thermal hysteresis enhancement of paraffin actuators, *Journal of Industrial Textiles*, DOI: 10.1177/1528083721988964

Lackowski, M., Krupa, A., Jaworek, A. (2013). Nanofabric nonwoven mat for filtration smoke and nanoparticles. *Polish Journal of Chemical Technology 15*(2), 48-52. DOI: 10.2478/pjct-2013-0023

Li, S.F., Chen, J.P., and Wu, W.T. (2007). Electrospun polyacrylonitrile nanofibrous membranes or lipase immobilization. *Jornal of Molecular Catalysis: B Enzymatic*, *47*(3), 117–124. DOI:10.1016/j.molcatb.2007.04.010

Li, W.Q., Qu, Z.G., He, Y.L., Tao, W.Q. (2012). Experimental and numerical studies on melting phase change heat transfer in open-cell metallic foams filled with paraffin, *Applied Thermal Engineering, 37,* 1-9. DOI: 10.1016/j.applthermaleng.2011.11.001

Li, Y., Yu, S., Chen, P. (2017). Cellulose nanofibers enable paraffin encapsulation and the formation of stable thermal regulation nanocomposites. *Nano Energy*, *34*:541–548. DOI:10.1016/j.nanoen.2017.03.010

Lin, C. and Rao, Z. (2017). Thermal conductivity enhancement of paraffin by adding boron nitride nanostructures: a molecular dynamics study. *Applied Thermal Engineering, 110,* 1411–1419. DOI: 10.1016/j.applthermaleng.2016.09.065

Lin, S.C., and Al-Kayiem, H.H. (2016). Evaluation of copper nanoparticles – paraffin wax compositions for solar thermal energy storage. *Solar Energy, 132,* 267–278. DOI: 10.1016/j.solener.2016.03.004

Liu, S., White, K.L., Reneker, D.H. (2019). Electrospinning Polymer Nanofibers With Controlled Diameters. *IEEE Transaction on Industry Applications , 55(5),* 5239-5243. DOI: 10.1109/TIA.2019.2920811

Liu, Y., Dong, L., Fan, J., Wang, R., Yu, J.Y. (2011). Effect of applied voltage on diameter and morphology of ultrafine fibers in bubble electrospinning. *Journal of Applied Polymer Science, 120*(1), 592–598 DOI:10.1002/app.33203

Lu, Y., Xiao, X., Zhan, Y., Huan, C., Qi, S., Cheng, H., and Xu, G. (2018)b, Core-Sheath Paraffin-Wax-Loaded Nanofibers by Electrospinning for Heat Storage , *ACS Applied Material Interfaces (2018), 10*(15), 12759−12767. DOI: 10.1021/acsami.8b02057

Lu, Y., Xiao, X., Fu, J. (2019). Novel smart textile with phase change materials encapsulated core-sheath structure fabricated by coaxial electrospinning. *Chemical Engineering Journal*, *555,* 532–539. DOI: 10.1016/j.cej.2018.08.189

Lu, Y., Xiao, X., Liu, Y. (2020). Achieving multifunctional smart textile with long afterglow and thermo-regulation via coaxial electrospinning. *Journal of Alloys Compounds, 812,* 152144. DOI:10.1016/j.jallcom.2019.152144

Lyons, J., Li, C., Ko, F. (2004). Melt-electrospinning part I: processing parameters and geometric properties, *Polymer,45*(22),7597–7603. DOI:10.1016/j.polymer.2004.08.071

Mamunya, Y.P., Davydenko, V.V., Pissis, P., (2002). Electrical and thermal conductivity of polymers filled with metal powders. *European Polymer Journal, 38*(9), 1887–1897. DOI:10.1016/S0014-3057(02)00064-2

Manigandan, S., Kumar, V.,(2019). Comparative study to use nanofluid ZnO and CuO with phase change material in photovoltaic thermal system, *International Journal of Energy Research, 43*(1-2), 1882–1891. DOI:10.1002/er.4442

Mann, A., Bürgel, C., Groche, P., (2018). A modeling strategy for predicting the properties of paraffin wax actuators, *Actuators, 7*(4), 81. DOI: 10.3390/act7040081

Mehling, H., Cabeza, F.L.,(2008). Heat and cold storage with PCM: An up to date introduction into basics and applications, Springer Verlag, ISBN: 978-3-540-68556-2, DOI:10.1007/978-3-540-68557-9

Mengjin, J., Xiaoqing, S., Jianjun, X., Guangdou, Y., (2008), Preparation of a new thermal regulating fiber based on PVA and paraffin. *Solar Energy Materials & Solar Cells, 92*, 1657–1660. DOI:10.1016/j.solmat.2008.07.018

Memon, S.A., Liao, W., Yang S. (2015). Development of composite PCMs by incorporation of paraffin into various building materials. *Materials, 8*(2), 499–518. DOI:10.3390/ma8020499

Mikes, P., Baker, D.A., Uhlin, A., Lukáš, D., Kuželová-Košťáková, E., Vidrich, A., Valtera, J., Kopřivová, B., Asatiani, N., Salmén, L., Tomani, P.,(2020). The Mass Production of Lignin Fibres by Means of Needleless Electrospinning. *Journal of Polymers and the Environment, 29*(7), 2164-2173. DOI:10.1007/s10924-020-02029-7

Missau, J., Rocha, J.G., Dotto, G.L., Bertuol, D.A., Ceron, P.L., Tanabe, E.H., (2018), Purification of crude wax using a filter medium modified with a nanofiber coating, *Chemical Engineering Research and Design, 136*, 734–743. DOI:10.1016/j.cherd.2018.06.031

Mu, X., Zheng, Y., Li, X., Xin, B., Lin, L. (2021). Effects of Temperature on Melt Electrospinning: Experiment and Simulation Study, *Fibers and Polymers, 22*(4), 964-971. DOI:10.1007/s12221-021-0465-4

Nabil, M., Khodadadi, J.M. (2013). Experimental determination of temperature dependent thermal conductivity of solid eicosane-based nanostructure enhanced phase change materials. *International Journal of Heat and Mass Transfer, 67*, 301–10. DOI: 10.1016/j.ijheatmasstransfer.2013.08.010

Nazoktabar, M., Arshtabar, K. and Mohammadkhani, H. (2020). Investigating the effect of coolant's heat transfer type on thermostat placement. *Journal of Thermal Analalitics and Calorimetry, 139*, 2519–2526. DOI: 10.1007/s10973-019-08805-5

Nie, C., Tong, X., Wu, S. (2015). Paraffin confined in carbon nanotubes as nanoencapsulated phase change materials: experimental and molecular dynamics studies. *RSC Advances, 5*(113), 92812–92817. DOI:10.1039/C5RA17152K

Onwudiwe, D.C., Strydom, C.A., Vala, R.M.K., (2015). Preparation and structural properties of electrospun PAN nanofibers reinforced with ZnS nanoparticles. *Synthesis and Reactivity in Inorganic Metal-Organic and Nano-Metal Chemistry, 45*(8), 1251–1259. DOI:10.1080/15533174.2013.862696

Owolabi ,A. L., Al-Kayiem, H. H., Baheta, A.T. (2016). Nanoadditives induced enhancement of the thermal properties of paraffin-based nanocomposites for thermal energy storage, *Solar Energy, 135*(11), 644-653. DOI:10.1016/j.solener.2016.06.008

Park, K.Y., Han, J.H., Lee, S.B., Kim, J.B., Yi, J.W. and Lee, S.K. (2009). Fabrication and electromagnetic characteristics of microwave absorbers containing carbon nanofibers and NiFe particles. *Compos. Sci. Technol., 69,* 1271–1278. DOI:10.1016/J.COMPSCITECH.2009.02.033

Pelipenko J., Kristl, J., Jankovi, B., Baumgartner, S., Kocbek, P., (2013). The impact of relative humidity during electrospinning on the morphology and mechanical properties of nanofibers, *International Journal of Pharmaceutics, 456*(1), 125– 134. DOI: 10.1016/j.ijpharm.2013.07.078

Rathod, M.K., and Banerjee J. (2013). Thermal stability of phase change materials used in latent heat energy storage systems: a review. *Renewable and Sustainable Energy Reviews, 18,* 246–258. DOI: 10.1016/j.rser.2012.10.022

Rastorguev, Y.L., Bogatov, G. F. (1972). Thermal conductivity of n-heptadecane and noctadecane at high pressures and temperatures. *Chem Technol Fuels Oil, 8*(4), 176–9. 10.1007/bf00730290

Rihova, M., Ince, A.E., Veronika Cicmancova, V., Hromadko, L., Castkova, K., Pavlinak, D., Vojtova, L., Macak, J.M., (2021). Water-born 3D nanofiber mats using cost-effective centrifugal spinning: comparison with electrospinning process: A complex study, *J Appl Polym Sci. , 138*(5), 49975. DOI:10.1002/app.49975

Saydam, V., Duan, X., (2019). Dispersing different nanoparticles in paraffin wax as enhanced phase change materials A study on the stability issue, *Journal of Thermal Analysis and Calorimetry, 135*(1), 1135–1144. DOI:10.1007/s10973-018-7484-4

Shao, Z., Song, Y., and Lan X.U.L. (2018). Formation Mechanism of Highly aligned Nanofibers by a Modified Bubble Electrospinning, *Thermal Science, 22(00),* 140-140. DOI:10.2298/TSCI160803140S

Sharma, A. and Tyagi, V. (2009). Review on thermal energy storage with phase change materials and applications. *Renewable and Sustainable Energy Reviews, 13*(2), 318-345. 10.1016/j.rser.2007.10.005

Sill, T. J., von Recum, H. A., (2008). Electrospinning: applications in drug delivery and tissue engineering. *Biomaterials, 29*(13), 1989–2006. DOI: 10.1016/j.biomaterials.2008.01.011

Stryker, P. C., Sparrow, E. M. 1990. Application of a spherical thermal conductivity cell to solid n-eicosane paraffin. *Int J Heat Mass Transf*er, *3*(9), 1781–93. DOI: 10.1016/0017-9310(90)90212-D

Sun, S. X., Xie, R., Wang, X. X., Wen, G. Q., Liu, Z., Wang, W., Ju, X. J., Chu, L. Y. (2015). Fabrication of nanofibers with phase-change core and hydrophobic shell, via coaxial electrospinning using nontoxic solvent, *Journal of Material Science, 50,* 5729–5738. DOI: 10.1007/s10853-015-9118-6

Şahan, N., Paksoy, H. (2017). Investigating thermal properties of using nano-tubular ZnO powder in paraffin as phase change material composite for thermal energy storage, *Composites Engineering, 126,* 88-9. DOI:10.1016/j.compositesb.2017.06.006

Taylor, S. G. (1969), Electrically driven jets, P*roceedings of the Royal Society of London Series A Mathematical and Physical Science*, *313*(1515), 453-475. DOI: 10.1098/rspa.1969.0205

Teo, W.E., Ramakrishna, S. 2006. A review on electrospinning design and nanofibre assemblies. *Nanotechnology, 17*(14), 89-106. DOI:10.1088/0957-4484/17/14/R01

Tian, W., and Yang, R. (2008). Phonon transport and thermal conductivity percolation in random nanoparticle composites. *CMES-Computer Modeling in Engineering and Sciences, 4*(2-3), 123–141. DOI: 10.3970/cmes.2008.024.123
Tighilt, F. Z., Gabouze, N., Sam, S. (2007). Morphology and specific interaction of PMMA coating with the surface of porous silicon. *Surface Science* , *601*(18), 4217–4221. DOI:10.1016/j.susc.2007.04.082

Torres-Rodríguez, A., Morillón-Gálvez, D., Aldama-Ávalos, D., Hernández-Gómez, V.H., García-Kerdan, I. (2020). Thermal performance evaluation of a passive building wall with CO2-filled transparent thermal insulation and paraffin-based phase change material. *Solar Energy*, *205*(1-3), 1-11. DOI:10.1016/j.solener.2020.04.090

Xie, N., Niu, J., Gao, X., Fang, Y., Zhang, Z., (2020). Fabrication and characterization of electrospun fatty acid form-stable phase change materials in the presence of copper nanoparticles, *International Journal of Energy Researchs*, *44*(11), 8567-8577. DOI:10.1002/er.5543

Wada, Y., Nagasaka, Y., Nagashima, A. 1985. Measurements and correlation of the thermal conductivity of liquid n-paraffin hydrocarbons and their binary and ternary mixtures. *International Journal of Thermophysics, 6*(3), 251-265. DOI: 10.1007/BF00522147

Wan, Y., Zhou, P., Liu, Y., Chena, H., (2016). Novel wearable polyacrylonitrile/phase-change material sheath/core nano-fibers fabricated by coaxial electro-spinning, *Royal Society of Chemistry Advances*, *6*(25), 21204–21209. DOI:10.1039/C6RA00281A

Wang, J., Li, Y., Wang, Y., Yang, L., Kong, X., Sundén, B. (2020). Experimental investigation of heat transfer performance of a heat pipe combined with thermal energy storage materials of CuO-paraffin nanocomposites, *Solar Energy*, *211*, 928-937. DOI: 10.1016/j.solener.2020.10.033

Wang, L., Ahmad, Z., Huange, J., Lia, J.S., Changa, M.W. (2017). Multi-compartment centrifugal electrospinning based composite fibers, *Chemical Engineering Journal* , *330*, 541-549. DOI:10.1016/j.cej.2017.07.179

Wang, Z. H., He, H. W., Liu, G. S., Yan, X., Ning, X., Long Y. Z. (2019), A newly reaction curing mechanism in conjugate electrospinning, *Process Materials Letters, 254*, 5–8. DOI:10.1016/j.matlet.2019.07.010

Warzoha, R. J., Weigand, R. M., and Fleischer, A. S. (2015). Temperature-dependent thermal properties of a paraffin phase change material embedded with herringbone style graphite nanofibers. *Applied Energy*, *137*, 716–725. DOI:10.1016/j.apenergy.2014.03.091

Wei, L., Yu, H., Sun, R., Liu, C., Chen, M., Liu, H., Xiong, J., Qin, X., (2021), Experimental investigation of process parameters for the filtration property of nanofiber membrane fabricated by needleless electrospinning apparatus, *Industrial Textiles*, *50*(9), 1528–1541. DOI:10.1177/1528083720901357

Wu, M., Wang, Q., Li, K. (2012). Optimization of stabilization conditions for electrospun polyacrylonitrile nanofibers. *Polymer Degradation Stability*, *97*(8), 1511–1519. DOI:10.1016/j.polymdegradstab.2012.05.001

Varshney, D., Ahmadi, M., Guinel, M.J.F. (2012). Single-step route to diamond-nanotube composite. *Nanoscale Research Letters*, *7*(1), 535. DOI:10.1186/1556-276X-7-535

Velez, C., Zárate, J.M.O., Khayet, M. (2015)a , Thermal properties of n-pentadecane, n-heptadecane and n-nonadecane in the solid/liquid phase change region,*International Journal of Thermal Sciences*, *94*, 139-146. DOI:10.1016/j.ijthermalsci.2015.03.001

Velez, C., J.M. Ortiz de Zárate, J.M., Khayet, M. (2015)b, Temperature-dependent thermal properties of solid/liquid phase change even-numbered n-alkanes: n-Hexadecane, n-octadecane and n-eicosane,*Applied Energy, 143*, 383–394. DOI:10.1016/j.apenergy.2015.01.054

Vysloužilová, L., Buzgo, M., Pokorný, P., Chvojka, J., Míčková,A., Rampichová, M., Kula, J., Pejchar, K., Bílek, M., Lukáš, D., Amler, E. (2017). Needleless coaxial electrospinning: A novel approach to mass production of coaxial nanofibers.

International Journal of Pharmaceutics, *516*(1-2), 293-300. DOI: 10.1016/j.ijpharm.2016.11.034

Yang, R., He, J., Lan, Xu, L., Yu, J., (2009). Bubble-electrospinning for fabricating nanofibers, *Polymer*, *50*(24): 5846-5850. DOI: 10.1016/j.polymer.2009.10.021

Yang, Y., Li, X., Shen, L., Wang, X., Hsiao, B., (2017). A durable thin-film nanofibrous composite nanofiltration membrane prepared by interfacial polymerization on a double-layer nanofibrous scaffold. *RSC Advances*, *7*(29), 18001-18013. DOI:10.1039/C7RA00621G

Zhao, J.H., Xu, L. and Liu, Q., Effect of Ethanol Post-Treatment on the Bubble-Electrospun Poly(Vinyl Alcohol), *Thermal Science*, *19*, 1353-1356. DOI:10.2298/TSCI1504353Z

Zhang, L., Aboagye, A., Kelkar, A. (2014). A review: carbon nanofibers from electrospun polyacrylonitrile and their applications. *Journal of Material Science*, *49*(2), 463–480. DOI:10.1007/s10853-013-7705-y

Zhang, X. X., Wang, X. C., Tao, X. M., Yick, K. L. 2006, Structures and Properties of Wet Spun Thermo-Regulated Polyacryolitrile-Vinyldene Chloride Fibers, *Textile Research Journal*, *76*(5) 351-359. DOI: 10.1177/0040517506061959

Zhang, K., Zhou, Q., and Ye, H. M. (2019). Optimizing the preparation of semi-crystalline paraffin/poly(urea-formaldehyde) microcapsules for thermal energy storage. *Applied Science*, *9*(3), 599-602. DOI:10.3390/app9030599

Zhmayev, E., Cho, D., Joo, Y.L., (2010). Nanofibers from gas-assisted polymer melt electrospinning, *Polymer*, *51*(18), 4140-4144. DOI:10.1016/j.polymer.2010.06.058

Zhu, D., Koganemaru, A., Xu, C. (2003). Oxidative stabilization of PAN/VGCF composite. *Journal of Applied Polymer Science*, *87*(13), 2063–2073. DOI:10.1002/app.11415

Zolotorev, P. A., Nigmatuilin, R.G. 1997, Purifiying and deoiling of slack wax for the manufacture of paraffin waxes. *Chemistry and Technology of Fuels and Oils*, *33*(6), 329-331. DOI:10.1007/BF02770078

APPENDIX

APPX 1 Paraffin Actuator Sample S1, Time/Temperature/Stroke Records

t (s)	T(°C)	S(mm)	t(s)	T(°C)	S(mm)	t(s)	T(°C)	S(mm)	t(s)	T(°C)	S(mm)	t(s)	T(°C)	S(mm)	t(s)	T(°C)	S(mm)
0	25,2	0	460	32,5	0,18	920	40	5,4	1380	45,3	10,58	1840	38	10,45	2300	30,7	1,38
10	25,2	0	470	32,6	0,2	930	40,2	5,67	1390	45,3	10,58	1850	37,9	10,41	2310	30,6	1,28
20	25,2	-0,01	480	32,7	0,22	940	40,4	5,86	1400	45,3	10,58	1860	37,7	10,37	2320	30,5	1,19
30	25,2	-0,01	490	32,8	0,24	950	40,5	6,11	1410	45,1	10,58	1870	37,5	10,32	2330	30,3	1,11
40	25,2	-0,01	500	32,9	0,25	960	40,7	6,37	1420	45,1	10,59	1880	37,4	10,26	2340	30,2	1,02
50	25,3	-0,01	510	33	0,27	970	40,8	6,59	1430	44,8	10,59	1890	37,2	10,2	2350	30	0,95
60	25,4	-0,01	520	33,2	0,29	980	40,9	6,78	1440	44,7	10,59	1900	37	10,11	2360	29,9	0,87
70	25,7	-0,01	530	33,4	0,32	990	41	7,03	1450	44,5	10,59	1910	36,8	10,02	2370	29,7	0,8
80	25,9	-0,01	540	33,6	0,36	1000	41,1	7,23	1460	44,4	10,59	1920	36,6	9,91	2380	29,6	0,74
90	26,2	-0,01	550	33,8	0,41	1010	41,3	7,47	1470	44,2	10,59	1930	36,4	9,77	2390	29,5	0,67
100	26,4	-0,01	560	34	0,47	1020	41,5	7,66	1480	44,1	10,59	1940	36,2	9,62	2400	29,3	0,62
110	26,7	-0,01	570	34,2	0,53	1030	41,7	7,86	1490	43,9	10,59	1950	36,1	9,455	2410	29,2	0,57
120	27	-0,01	580	34,4	0,59	1040	41,9	8,06	1500	43,7	10,59	1960	36	9,287	2420	29,1	0,53
130	27,1	-0,01	590	34,6	0,66	1050	42,2	8,27	1510	43,6	10,59	1970	35,9	9,103	2430	29	0,49
140	27,3	-0,01	600	34,8	0,72	1060	42,4	8,47	1520	43,4	10,59	1980	35,8	8,927	2440	28,8	0,46
150	27,4	-0,01	610	34,9	0,78	1070	42,6	8,64	1530	43,3	10,59	1990	35,6	8,746	2450	28,6	0,43
160	27,4	-0,01	620	35,1	0,83	1080	42,8	8,82	1540	43	10,59	2000	35,4	8,546	2460	28,4	0,4
170	27,5	-0,01	630	35,3	0,88	1090	43	8,94	1550	42,9	10,59	2010	35,3	8,362	2470	28,2	0,38
180	27,6	-0,01	640	35,5	0,93	1100	43,1	9,07	1560	42,8	10,59	2020	35,1	8,172	2480	28,1	0,35
190	27,6	-0,01	650	35,6	1	1110	43,2	9,25	1570	42,6	10,59	2030	34,9	7,949	2490	27,9	0,33
200	27,6	-0,01	660	35,7	1,06	1120	43,3	9,37	1580	42,4	10,59	2040	34,8	7,688	2500	27,8	0,31
210	27,8	-0,01	670	35,8	1,11	1130	43,4	9,52	1590	42,2	10,59	2050	34,6	7,414	2510	27,6	0,29
220	28	-0,01	680	35,9	1,18	1140	43,5	9,61	1600	42	10,59	2060	34,5	7,078	2520	27,4	0,28
230	28,2	-0,01	690	36	1,27	1150	43,7	9,78	1610	41,9	10,59	2070	34,3	6,69	2530	27,3	0,26
240	28,5	-0,01	700	36,2	1,36	1160	43,9	9,88	1620	41,7	10,59	2080	34,2	6,3	2540	27,1	0,24
250	28,8	-0,01	710	36,4	1,49	1170	44	9,97	1630	41,7	10,59	2090	34	5,86	2550	27	0,22
260	29,1	-0,01	720	36,6	1,6	1180	44,3	10,04	1640	41,3	10,59	2100	33,8	5,48	2560	26,8	0,21
270	29,3	-0,01	730	36,8	1,73	1190	44,5	10,16	1650	41,3	10,59	2110	33,6	5,13	2570	26,7	0,19
280	29,6	0	740	37	1,85	1200	44,7	10,23	1660	41,3	10,59	2120	33,4	4,81	2580	26,5	0,18
290	29,8	0	750	37,2	1,99	1210	44,9	10,28	1670	41,3	10,59	2130	33,2	4,51	2590	26,4	0,16
300	29,9	0	760	37,4	2,13	1220	45,1	10,31	1680	40,7	10,59	2140	33,1	4,22	2600	26,2	0,15
310	30	0	770	37,5	2,27	1230	45,2	10,35	1690	40,5	10,59	2150	33	3,94	2610	26,1	0,13
320	30	0	780	37,7	2,44	1240	45,4	10,38	1700	40,4	10,59	2160	32,9	3,68	2620	25,9	0,12
330	30,1	0	790	37,8	2,58	1250	45,4	10,41	1710	40,2	10,59	2170	32,7	3,43	2630	25,8	0,11
340	30,1	0	800	38	2,74	1260	45,5	10,43	1720	40	10,59	2180	32,5	3,2	2640	25,7	0,09
350	30,2	0	810	38,1	2,89	1270	45,5	10,45	1730	39,8	10,59	2190	32,4	2,99	2650	25,5	0,08
360	30,3	0	820	38,2	3,05	1280	45,5	10,47	1740	39,7	10,59	2200	32,3	2,79	2660	25,4	0,07
370	30,5	0	830	38,4	3,22	1290	45,4	10,48	1750	39,5	10,59	2210	32,2	2,6	2670	25,2	0,06
380	30,9	0	840	38,6	3,39	1300	45,4	10,49	1760	39,3	10,58	2220	32	2,42	2680	25,1	0,05
390	31	0,01	850	38,7	3,57	1310	45,4	10,51	1770	39,2	10,58	2230	31,8	2,26	2690	24,9	0,03
400	31,2	0,02	860	38,9	3,81	1320	45,4	10,52	1780	39	10,58	2240	31,7	2,11	2700	24,8	0,02
410	31,2	0,04	870	39,1	4,09	1330	45,4	10,53	1790	38,8	10,57	2250	31,5	1,96	2710	24,7	0,01
420	31,2	0,07	880	39,3	4,34	1340	45,4	10,55	1800	38,7	10,55	2260	31,4	1,83	2720	24,7	0
430	31,2	0,1	890	39,5	4,63	1350	45,4	10,56	1810	38,5	10,53	2270	31,2	1,71	2730	24,7	0
440	31,2	0,13	900	39,7	4,87	1360	45,3	10,57	1820	38,4	10,51	2280	31,1	1,59	2740	24,7	0,01
450	31,2	0,16	910	39,9	5,19	1370	45,3	10,57	1830	38,2	10,48	2290	30,9	1,48	2750	24,8	0,01

APPX 2 Paraffin Actuator Sample S2, Time/Temperature/Stroke Records

t (s)	T(°C)	S(mm)	t(s)	T(°C)	S(mm)	t(s)	T(°C)	S(mm)	t(s)	T(°C)	S(mm)	t(s)	T(°C)	S(mm)	t(s)	T(°C)	S(mm)
0	25,2	0	460	32,5	0,14	920	40	5,81	1380	45,3	10,26	1840	38	10,06	2300	30,7	1,3
10	25,2	-0,01	470	32,6	0,16	930	40,2	6,1	1390	45,3	10,26	1850	37,9	10,01	2310	30,6	1,21
20	25,2	-0,01	480	32,7	0,17	940	40,4	6,36	1400	45,3	10,26	1860	37,7	9,96	2320	30,5	1,14
30	25,2	-0,01	490	32,8	0,18	950	40,5	6,6	1410	45,1	10,26	1870	37,5	9,91	2330	30,3	1,06
40	25,2	-0,02	500	32,9	0,19	960	40,7	6,84	1420	45,1	10,26	1880	37,4	9,83	2340	30,2	0,99
50	25,3	-0,02	510	33	0,21	970	40,8	7,06	1430	44,8	10,26	1890	37,2	9,75	2350	30	0,92
60	25,4	-0,02	520	33,2	0,23	980	40,9	7,25	1440	44,7	10,26	1900	37	9,63	2360	29,9	0,85
70	25,7	-0,02	530	33,4	0,26	990	41	7,44	1450	44,5	10,26	1910	36,8	9,51	2370	29,7	0,79
80	25,9	-0,02	540	33,6	0,29	1000	41,1	7,63	1460	44,4	10,26	1920	36,6	9,36	2380	29,6	0,73
90	26,2	-0,02	550	33,8	0,32	1010	41,3	7,82	1470	44,2	10,26	1930	36,4	9,21	2390	29,5	0,68
100	26,4	-0,02	560	34	0,38	1020	41,5	8,04	1480	44,1	10,26	1940	36,2	9,02	2400	29,3	0,63
110	26,7	-0,02	570	34,2	0,43	1030	41,7	8,23	1490	43,9	10,26	1950	36,1	8,84	2410	29,2	0,58
120	27	-0,02	580	34,4	0,48	1040	41,9	8,41	1500	43,7	10,26	1960	36	8,68	2420	29,1	0,55
130	27,1	-0,02	590	34,6	0,52	1050	42,2	8,58	1510	43,6	10,26	1970	35,9	8,51	2430	29	0,51
140	27,3	-0,02	600	34,8	0,57	1060	42,4	8,75	1520	43,4	10,26	1980	35,8	8,34	2440	28,8	0,48
150	27,4	-0,02	610	34,9	0,62	1070	42,6	8,9	1530	43,3	10,26	1990	35,6	8,14	2450	28,6	0,45
160	27,4	-0,02	620	35,1	0,68	1080	42,8	9,06	1540	43	10,26	2000	35,4	7,96	2460	28,4	0,42
170	27,5	-0,02	630	35,3	0,71	1090	43	9,19	1550	42,9	10,26	2010	35,3	7,76	2470	28,2	0,4
180	27,6	-0,02	640	35,5	0,77	1100	43,1	9,32	1560	42,8	10,26	2020	35,1	7,55	2480	28,1	0,37
190	27,6	-0,02	650	35,6	0,81	1110	43,2	9,45	1570	42,6	10,26	2030	34,9	7,32	2490	27,9	0,35
200	27,6	-0,02	660	35,7	0,87	1120	43,3	9,55	1580	42,4	10,26	2040	34,8	7,07	2500	27,8	0,33
210	27,8	-0,02	670	35,8	0,94	1130	43,4	9,62	1590	42,2	10,26	2050	34,6	6,79	2510	27,6	0,32
220	28	-0,02	680	35,9	1	1140	43,5	9,69	1600	42	10,26	2060	34,5	6,37	2520	27,4	0,3
230	28,2	-0,01	690	36	1,08	1150	43,7	9,76	1610	41,9	10,26	2070	34,3	5,94	2530	27,3	0,28
240	28,5	-0,01	700	36,2	1,17	1160	43,9	9,83	1620	41,7	10,26	2080	34,2	5,55	2540	27,1	0,26
250	28,8	-0,01	710	36,4	1,29	1170	44	9,89	1630	41,7	10,26	2090	34	5,18	2550	27	0,25
260	29,1	-0,01	720	36,6	1,4	1180	44,3	9,93	1640	41,3	10,26	2100	33,8	4,86	2560	26,8	0,23
270	29,3	-0,01	730	36,8	1,52	1190	44,5	9,97	1650	41,3	10,26	2110	33,6	4,58	2570	26,7	0,22
280	29,6	-0,01	740	37	1,66	1200	44,7	10,02	1660	41,3	10,26	2120	33,4	4,3	2580	26,5	0,2
290	29,8	-0,01	750	37,2	1,78	1210	44,9	10,06	1670	41,3	10,26	2130	33,2	4,01	2590	26,4	0,19
300	29,9	-0,01	760	37,4	1,92	1220	45,1	10,11	1680	40,7	10,26	2140	33,1	3,75	2600	26,2	0,18
310	30	-0,01	770	37,5	2,08	1230	45,2	10,13	1690	40,5	10,26	2150	33	3,51	2610	26,1	0,16
320	30	-0,01	780	37,7	2,23	1240	45,4	10,15	1700	40,4	10,26	2160	32,9	3,28	2620	25,9	0,15
330	30,1	-0,01	790	37,8	2,39	1250	45,4	10,17	1710	40,2	10,26	2170	32,7	3,07	2630	25,8	0,14
340	30,1	-0,01	800	38	2,56	1260	45,5	10,18	1720	40	10,26	2180	32,5	2,87	2640	25,7	0,12
350	30,2	-0,01	810	38,1	2,71	1270	45,5	10,2	1730	39,8	10,26	2190	32,4	2,68	2650	25,5	0,11
360	30,3	-0,01	820	38,2	2,9	1280	45,5	10,21	1740	39,7	10,26	2200	32,3	2,51	2660	25,4	0,1
370	30,5	-0,01	830	38,4	3,09	1290	45,4	10,21	1750	39,5	10,26	2210	32,2	2,35	2670	25,2	0,09
380	30,9	-0,01	840	38,6	3,3	1300	45,4	10,22	1760	39,3	10,26	2220	32	2,2	2680	25,1	0,08
390	31	0	850	38,7	3,56	1310	45,4	10,23	1770	39,2	10,26	2230	31,8	2,06	2690	24,9	0,07
400	31,2	0,01	860	38,9	3,84	1320	45,4	10,24	1780	39	10,25	2240	31,7	1,93	2700	24,8	0,06
410	31,2	0,02	870	39,1	4,15	1330	45,4	10,25	1790	38,8	10,24	2250	31,5	1,81	2710	24,7	0,05
420	31,2	0,05	880	39,3	4,56	1340	45,4	10,25	1800	38,7	10,23	2260	31,4	1,69	2720	24,7	0,04
430	31,2	0,08	890	39,5	4,9	1350	45,4	10,26	1810	38,5	10,2	2270	31,2	1,59	2730	24,7	0,04
440	31,2	0,1	900	39,7	5,22	1360	45,3	10,26	1820	38,4	10,17	2280	31,1	1,49	2740	24,7	0,03
450	31,2	0,13	910	39,9	5,53	1370	45,3	10,26	1830	38,2	10,12	2290	30,9	1,39	2750	24,8	0,03

APPX 3 Paraffin Actuator Sample S3, Time/Temperature/Stroke Records

t (s)	T(°C)	S(mm)	t(s)	T(°C)	S(mm)	t(s)	T(°C)	S(mm)	t(s)	T(°C)	S(mm)	t(s)	T(°C)	S(mm)	t(s)	T(°C)	S(mm)
0	24,9	0,00	460	32,3	0,36	920	40	5,75	1380	44,9	9,37	1840	36,8	8,89	2300	29,4	0,96
10	24,9	0,00	470	32,4	0,38	930	40,1	5,98	1390	44,8	9,37	1850	36,6	8,81	2310	29,2	0,92
20	24,9	0,00	480	32,6	0,40	940	40,3	6,20	1400	44,6	9,37	1860	36,4	8,76	2320	29,1	0,87
30	24,9	0,00	490	32,8	0,43	950	40,4	6,42	1410	44,4	9,37	1870	36,2	8,70	2330	29	0,84
40	25,1	0,00	500	32,9	0,47	960	40,6	6,64	1420	44,2	9,37	1880	36,1	8,63	2340	28,8	0,80
50	25,3	0,00	510	33	0,52	970	40,8	6,86	1430	44	9,37	1890	36	8,51	2350	28,6	0,77
60	25,6	0,00	520	33,1	0,58	980	40,9	7,09	1440	43,9	9,37	1900	35,9	8,38	2360	28,5	0,75
70	26	0,00	530	33,3	0,63	990	41,1	7,30	1450	43,7	9,37	1910	35,7	8,22	2370	28,3	0,72
80	26,2	0,00	540	33,5	0,69	1000	41,4	7,50	1460	43,5	9,37	1920	35,5	8,06	2380	28,2	0,70
90	26,5	0,00	550	33,8	0,73	1010	41,6	7,70	1470	43,3	9,37	1930	35,3	7,88	2390	28	0,68
100	26,7	0,00	560	34,3	0,78	1020	41,8	7,88	1480	43,2	9,38	1940	35,2	7,69	2400	27,9	0,66
110	26,9	0,00	570	34,4	0,82	1030	41,9	8,04	1490	43	9,38	1950	35	7,50	2410	27,8	0,64
120	27	0,00	580	34,5	0,85	1040	42,1	8,19	1500	42,8	9,38	1960	34,9	7,28	2420	27,6	0,62
130	27,1	0,00	590	34,6	0,88	1050	42,3	8,31	1510	42,6	9,38	1970	34,7	7,00	2430	27,5	0,61
140	27,2	0,00	600	34,7	0,90	1060	42,4	8,41	1520	42,4	9,38	1980	34,5	6,67	2440	27,3	0,59
150	27,3	0,00	610	34,8	0,92	1070	42,5	8,51	1530	42,2	9,38	1990	34,4	6,31	2450	27,1	0,58
160	27,3	0,00	620	34,9	0,95	1080	42,7	8,58	1540	42,1	9,38	2000	34,2	5,96	2460	27	0,56
170	27,4	0,00	630	35	0,99	1090	42,9	8,67	1550	41,8	9,39	2010	34,1	5,59	2470	26,8	0,55
180	27,4	0,00	640	35,1	1,04	1100	43	8,73	1560	41,7	9,40	2020	33,9	5,25	2480	26,7	0,53
190	27,6	0,01	650	35,3	1,10	1110	43,1	8,79	1570	41,5	9,42	2030	33,8	4,94	2490	26,5	0,52
200	27,7	0,01	660	35,5	1,17	1120	43,3	8,84	1580	41,3	9,42	2040	33,6	4,64	2500	26,3	0,50
210	27,7	0,01	670	35,8	1,24	1130	43,4	8,89	1590	41,1	9,43	2050	33,5	4,36	2510	26,2	0,49
220	28,2	0,02	680	36	1,32	1140	43,5	8,94	1600	40,9	9,43	2060	33,3	4,09	2520	26	0,48
230	28,4	0,02	690	36,2	1,42	1150	43,7	8,99	1610	40,7	9,44	2070	33,1	3,83	2530	25,9	0,47
240	28,4	0,03	700	36,5	1,53	1160	44	9,04	1620	40,6	9,45	2080	32,9	3,59	2540	25,7	0,45
250	28,4	0,04	710	36,7	1,64	1170	44,2	9,07	1630	40,5	9,46	2090	32,8	3,36	2550	25,6	0,44
260	28,4	0,05	720	36,9	1,72	1180	44,5	9,10	1640	40,3	9,48	2100	32,6	3,16	2560	25,4	0,43
270	28,4	0,06	730	37,1	1,82	1190	44,6	9,13	1650	40,1	9,49	2110	32,5	2,96	2570	25,3	0,42
280	29,5	0,07	740	37,2	1,92	1200	44,9	9,16	1660	39,9	9,49	2120	32,3	2,78	2580	25,1	0,41
290	29,6	0,08	750	37,3	2,03	1210	45,1	9,19	1670	39,7	9,49	2130	32,2	2,60	2590	24,9	0,40
300	29,6	0,08	760	37,3	2,12	1220	45,1	9,23	1680	39,6	9,49	2140	32,1	2,44	2600	24,8	0,39
310	29,7	0,09	770	37,5	2,21	1230	45,1	9,26	1690	39,4	9,49	2150	32	2,30	2610	24,7	0,38
320	29,8	0,10	780	37,5	2,31	1240	45,1	9,28	1700	39,2	9,48	2160	31,9	2,16	2620	24,6	0,37
330	29,9	0,12	790	37,7	2,44	1250	45	9,30	1710	39,1	9,48	2170	31,7	2,02	2630	24,5	0,37
340	30,1	0,14	800	37,9	2,59	1260	44,9	9,32	1720	38,9	9,48	2180	31,5	1,90	2640	24,5	0,36
350	30,3	0,16	810	38	2,75	1270	44,8	9,34	1730	38,7	9,48	2190	31,3	1,79	2650	24,6	0,36
360	30,5	0,18	820	38,2	2,94	1280	44,8	9,35	1740	38,5	9,47	2200	31,1	1,68	2660	24,8	0,36
370	31	0,21	830	38,4	3,21	1290	44,7	9,36	1750	38,4	9,45	2210	30,9	1,59	2670	25	0,35
380	31,1	0,23	840	38,6	3,54	1300	44,6	9,37	1760	38,2	9,43	2220	30,7	1,50	2680	25,2	0,35
390	31,3	0,26	850	38,8	3,83	1310	44,6	9,37	1770	38	9,41	2230	30,5	1,41	2690	25,4	0,35
400	31,5	0,27	860	39,1	4,11	1320	44,7	9,37	1780	37,8	9,39	2240	30,4	1,33	2700	25,4	0,35
410	31,9	0,29	870	39,3	4,42	1330	44,7	9,37	1790	37,6	9,36	2250	30,3	1,26	2710	25,5	0,35
420	31,9	0,31	880	39,5	4,69	1340	44,7	9,37	1800	37,4	9,32	2260	30,1	1,19	2720	25,4	0,35
430	32	0,32	890	39,7	4,99	1350	44,7	9,37	1810	37,2	9,28	2270	29,9	1,13	2730	25,3	0,35
440	32	0,34	900	39,8	5,26	1360	44,7	9,37	1820	37,1	9,20	2280	29,8	1,07	2740	25,2	0,35
450	32,1	0,35	910	39,9	5,51	1370	45	9,37	1830	37	9,08	2290	29,6	1,01	2750	25,1	0,34

APPX 4 Paraffin Actuator Sample S4, Time/Temperature/Stroke Records

t (s)	T(°C)	S(mm)	t(s)	T(°C)	S(mm)	t(s)	T(°C)	S(mm)	t(s)	T(°C)	S(mm)	t(s)	T(°C)	S(mm)	t(s)	T(°C)	S(mm)
0	24,9	0,00	460	32,3	0,49	920	40	5,41	1380	44,9	8,76	1840	36,8	8,25	2300	29,4	0,69
10	24,9	0,00	470	32,4	0,51	930	40,1	5,63	1390	44,8	8,76	1850	36,6	8,10	2310	29,2	0,65
20	24,9	0,00	480	32,6	0,53	940	40,3	5,85	1400	44,6	8,76	1860	36,4	8,03	2320	29,1	0,62
30	24,9	0,00	490	32,8	0,55	950	40,4	6,06	1410	44,4	8,76	1870	36,2	7,94	2330	29	0,59
40	25,1	0,00	500	32,9	0,58	960	40,6	6,27	1420	44,2	8,76	1880	36,1	7,79	2340	28,8	0,56
50	25,3	0,00	510	33	0,63	970	40,8	6,48	1430	44	8,77	1890	36	7,65	2350	28,6	0,54
60	25,6	0,00	520	33,1	0,67	980	40,9	6,68	1440	43,9	8,77	1900	35,9	7,49	2360	28,5	0,52
70	26	0,00	530	33,3	0,72	990	41,1	6,84	1450	43,7	8,77	1910	35,7	7,31	2370	28,3	0,49
80	26,2	0,00	540	33,5	0,77	1000	41,4	7,05	1460	43,5	8,77	1920	35,5	7,13	2380	28,2	0,47
90	26,5	0,01	550	33,8	0,82	1010	41,6	7,22	1470	43,3	8,77	1930	35,3	6,95	2390	28	0,45
100	26,7	0,01	560	34,3	0,86	1020	41,8	7,41	1480	43,2	8,77	1940	35,2	6,74	2400	27,9	0,44
110	26,9	0,01	570	34,4	0,91	1030	41,9	7,58	1490	43	8,77	1950	35	6,48	2410	27,8	0,42
120	27	0,01	580	34,5	0,94	1040	42,1	7,73	1500	42,8	8,77	1960	34,9	6,18	2420	27,6	0,40
130	27,1	0,02	590	34,6	0,97	1050	42,3	7,84	1510	42,6	8,77	1970	34,7	5,87	2430	27,5	0,39
140	27,2	0,02	600	34,7	1,00	1060	42,4	7,93	1520	42,4	8,77	1980	34,5	5,56	2440	27,3	0,37
150	27,3	0,02	610	34,8	1,03	1070	42,5	8,08	1530	42,2	8,77	1990	34,4	5,25	2450	27,1	0,36
160	27,3	0,02	620	34,9	1,06	1080	42,7	8,14	1540	42,1	8,77	2000	34,2	4,96	2460	27	0,34
170	27,4	0,03	630	35	1,11	1090	42,9	8,18	1550	41,8	8,77	2010	34,1	4,69	2470	26,8	0,32
180	27,4	0,03	640	35,1	1,16	1100	43	8,23	1560	41,7	8,78	2020	33,9	4,42	2480	26,7	0,31
190	27,6	0,04	650	35,3	1,22	1110	43,1	8,27	1570	41,5	8,78	2030	33,8	4,16	2490	26,5	0,29
200	27,7	0,05	660	35,5	1,28	1120	43,3	8,31	1580	41,3	8,78	2040	33,6	3,93	2500	26,3	0,28
210	27,7	0,07	670	35,8	1,36	1130	43,4	8,34	1590	41,1	8,78	2050	33,5	3,68	2510	26,2	0,27
220	28,2	0,08	680	36	1,44	1140	43,5	8,36	1600	40,9	8,78	2060	33,3	3,45	2520	26	0,25
230	28,4	0,10	690	36,2	1,56	1150	43,7	8,39	1610	40,7	8,78	2070	33,1	3,25	2530	25,9	0,24
240	28,4	0,12	700	36,5	1,65	1160	44	8,43	1620	40,6	8,78	2080	32,9	3,04	2540	25,7	0,23
250	28,4	0,14	710	36,7	1,75	1170	44,2	8,46	1630	40,5	8,78	2090	32,8	2,84	2550	25,6	0,22
260	28,4	0,16	720	36,9	1,85	1180	44,5	8,49	1640	40,3	8,78	2100	32,6	2,66	2560	25,4	0,20
270	28,4	0,17	730	37,1	1,99	1190	44,6	8,52	1650	40,1	8,78	2110	32,5	2,48	2570	25,3	0,19
280	29,5	0,18	740	37,2	2,10	1200	44,9	8,53	1660	39,9	8,78	2120	32,3	2,31	2580	25,1	0,18
290	29,6	0,19	750	37,3	2,19	1210	45,1	8,55	1670	39,7	8,78	2130	32,2	2,15	2590	24,9	0,17
300	29,6	0,20	760	37,3	2,27	1220	45,1	8,59	1680	39,6	8,78	2140	32,1	2,01	2600	24,8	0,16
310	29,7	0,21	770	37,5	2,36	1230	45,1	8,61	1690	39,4	8,78	2150	32	1,87	2610	24,7	0,15
320	29,8	0,21	780	37,5	2,45	1240	45,1	8,64	1700	39,2	8,78	2160	31,9	1,74	2620	24,6	0,14
330	29,9	0,23	790	37,7	2,57	1250	45	8,66	1710	39,1	8,77	2170	31,7	1,62	2630	24,5	0,13
340	30,1	0,24	800	37,9	2,68	1260	44,9	8,67	1720	38,9	8,77	2180	31,5	1,50	2640	24,5	0,12
350	30,3	0,26	810	38	2,81	1270	44,8	8,69	1730	38,7	8,76	2190	31,3	1,40	2650	24,6	0,12
360	30,5	0,29	820	38,2	3,01	1280	44,8	8,71	1740	38,5	8,75	2200	31,1	1,31	2660	24,8	0,12
370	31	0,31	830	38,4	3,20	1290	44,7	8,72	1750	38,4	8,73	2210	30,9	1,22	2670	25	0,12
380	31,1	0,34	840	38,6	3,45	1300	44,6	8,74	1760	38,2	8,71	2220	30,7	1,14	2680	25,2	0,12
390	31,3	0,36	850	38,8	3,68	1310	44,6	8,74	1770	38	8,68	2230	30,5	1,06	2690	25,4	0,12
400	31,5	0,39	860	39,1	3,90	1320	44,7	8,75	1780	37,8	8,65	2240	30,4	0,99	2700	25,4	0,12
410	31,9	0,41	870	39,3	4,15	1330	44,7	8,75	1790	37,6	8,61	2250	30,3	0,93	2710	25,5	0,12
420	31,9	0,43	880	39,5	4,40	1340	44,7	8,75	1800	37,4	8,57	2260	30,1	0,87	2720	25,4	0,12
430	32	0,44	890	39,7	4,67	1350	44,7	8,76	1810	37,2	8,51	2270	29,9	0,82	2730	25,3	0,12
440	32	0,46	900	39,8	4,92	1360	44,7	8,76	1820	37,1	8,43	2280	29,8	0,77	2740	25,2	0,11
450	32,1	0,47	910	39,9	5,19	1370	45	8,76	1830	37	8,33	2290	29,6	0,73	2750	25,1	0,11

APPX 5 Paraffin Actuator Sample S5, Time/Temperature/Stroke Records

t (s)	T(°C)	S(mm)	t(s)	T(°C)	S(mm)	t(s)	T(°C)	S(mm)	t(s)	T(°C)	S(mm)	t(s)	T(°C)	S(mm)	t(s)	T(°C)	S(mm)
0	24,9	0,00	460	32,3	0,40	920	40	5,38	1380	44,9	7,70	1840	36,8	7,31	2300	29,4	0,56
10	24,9	0,00	470	32,4	0,42	930	40,1	5,61	1390	44,8	7,70	1850	36,6	7,17	2310	29,2	0,54
20	24,9	0,00	480	32,6	0,44	940	40,3	5,79	1400	44,6	7,70	1860	36,4	7,02	2320	29,1	0,51
30	24,9	0,00	490	32,8	0,46	950	40,4	6,00	1410	44,4	7,70	1870	36,2	6,85	2330	29	0,49
40	25,1	0,00	500	32,9	0,50	960	40,6	6,31	1420	44,2	7,70	1880	36,1	6,67	2340	28,8	0,47
50	25,3	0,00	510	33	0,54	970	40,8	6,53	1430	44	7,71	1890	36	6,48	2350	28,6	0,46
60	25,6	0,00	520	33,1	0,58	980	40,9	6,74	1440	43,9	7,71	1900	35,9	6,29	2360	28,5	0,44
70	26	0,00	530	33,3	0,63	990	41,1	6,91	1450	43,7	7,71	1910	35,7	6,08	2370	28,3	0,42
80	26,2	0,00	540	33,5	0,68	1000	41,4	7,06	1460	43,5	7,71	1920	35,5	5,88	2380	28,2	0,40
90	26,5	0,00	550	33,8	0,72	1010	41,6	7,19	1470	43,3	7,71	1930	35,3	5,67	2390	28	0,39
100	26,7	0,00	560	34,3	0,76	1020	41,8	7,30	1480	43,2	7,71	1940	35,2	5,43	2400	27,9	0,37
110	26,9	0,01	570	34,4	0,79	1030	41,9	7,38	1490	43	7,71	1950	35	5,20	2410	27,8	0,36
120	27	0,01	580	34,5	0,82	1040	42,1	7,42	1500	42,8	7,71	1960	34,9	4,94	2420	27,6	0,35
130	27,1	0,01	590	34,6	0,85	1050	42,3	7,47	1510	42,6	7,71	1970	34,7	4,70	2430	27,5	0,33
140	27,2	0,01	600	34,7	0,87	1060	42,4	7,49	1520	42,4	7,71	1980	34,5	4,46	2440	27,3	0,32
150	27,3	0,01	610	34,8	0,89	1070	42,5	7,51	1530	42,2	7,71	1990	34,4	4,24	2450	27,1	0,31
160	27,3	0,01	620	34,9	0,92	1080	42,7	7,53	1540	42,1	7,71	2000	34,2	4,00	2460	27	0,29
170	27,4	0,01	630	35	0,96	1090	42,9	7,54	1550	41,8	7,71	2010	34,1	3,77	2470	26,8	0,28
180	27,4	0,02	640	35,1	1,00	1100	43	7,55	1560	41,7	7,71	2020	33,9	3,55	2480	26,7	0,27
190	27,6	0,02	650	35,3	1,05	1110	43,1	7,56	1570	41,5	7,71	2030	33,8	3,33	2490	26,5	0,26
200	27,7	0,03	660	35,5	1,15	1120	43,3	7,57	1580	41,3	7,70	2040	33,6	3,12	2500	26,3	0,25
210	27,7	0,04	670	35,8	1,23	1130	43,4	7,58	1590	41,1	7,70	2050	33,5	2,91	2510	26,2	0,23
220	28,2	0,05	680	36	1,30	1140	43,5	7,59	1600	40,9	7,70	2060	33,3	2,71	2520	26	0,22
230	28,4	0,06	690	36,2	1,39	1150	43,7	7,60	1610	40,7	7,70	2070	33,1	2,53	2530	25,9	0,21
240	28,4	0,08	700	36,5	1,48	1160	44	7,61	1620	40,6	7,70	2080	32,9	2,36	2540	25,7	0,20
250	28,4	0,09	710	36,7	1,57	1170	44,2	7,61	1630	40,5	7,70	2090	32,8	2,16	2550	25,6	0,19
260	28,4	0,10	720	36,9	1,65	1180	44,5	7,62	1640	40,3	7,70	2100	32,6	2,00	2560	25,4	0,18
270	28,4	0,11	730	37,1	1,73	1190	44,6	7,63	1650	40,1	7,70	2110	32,5	1,85	2570	25,3	0,17
280	29,5	0,12	740	37,2	1,81	1200	44,9	7,64	1660	39,9	7,70	2120	32,3	1,72	2580	25,1	0,16
290	29,6	0,13	750	37,3	1,87	1210	45,1	7,65	1670	39,7	7,70	2130	32,2	1,59	2590	24,9	0,15
300	29,6	0,13	760	37,3	1,93	1220	45,1	7,65	1680	39,6	7,70	2140	32,1	1,47	2600	24,8	0,14
310	29,7	0,14	770	37,5	1,99	1230	45,1	7,66	1690	39,4	7,70	2150	32	1,36	2610	24,7	0,14
320	29,8	0,15	780	37,5	2,05	1240	45,1	7,66	1700	39,2	7,70	2160	31,9	1,27	2620	24,6	0,13
330	29,9	0,16	790	37,7	2,12	1250	45	7,68	1710	39,1	7,70	2170	31,7	1,18	2630	24,5	0,12
340	30,1	0,18	800	37,9	2,20	1260	44,9	7,68	1720	38,9	7,70	2180	31,5	1,10	2640	24,5	0,12
350	30,3	0,20	810	38	2,40	1270	44,8	7,68	1730	38,7	7,70	2190	31,3	1,03	2650	24,6	0,11
360	30,5	0,22	820	38,2	2,58	1280	44,8	7,68	1740	38,5	7,70	2200	31,1	0,96	2660	24,8	0,11
370	31	0,25	830	38,4	2,83	1290	44,7	7,68	1750	38,4	7,70	2210	30,9	0,90	2670	25	0,11
380	31,1	0,27	840	38,6	3,07	1300	44,6	7,68	1760	38,2	7,69	2220	30,7	0,84	2680	25,2	0,11
390	31,3	0,29	850	38,8	3,38	1310	44,6	7,68	1770	38	7,69	2230	30,5	0,79	2690	25,4	0,11
400	31,5	0,31	860	39,1	3,66	1320	44,7	7,70	1780	37,8	7,69	2240	30,4	0,75	2700	25,4	0,11
410	31,9	0,33	870	39,3	3,97	1330	44,7	7,70	1790	37,6	7,67	2250	30,3	0,71	2710	25,5	0,11
420	31,9	0,35	880	39,5	4,26	1340	44,7	7,70	1800	37,4	7,65	2260	30,1	0,67	2720	25,4	0,11
430	32	0,36	890	39,7	4,54	1350	44,7	7,70	1810	37,2	7,64	2270	29,9	0,64	2730	25,3	0,11
440	32	0,37	900	39,8	4,84	1360	44,7	7,70	1820	37,1	7,60	2280	29,8	0,61	2740	25,2	0,11
450	32,1	0,39	910	39,9	5,12	1370	45	7,70	1830	37	7,45	2290	29,6	0,59	2750	25,1	0,11

APPX 6 Paraffin Actuator, P1- CuO, Time/Temperature/Stroke Records P1_pre

t (s)	T(°C)	S(mm)	t(s)	T(°C)	S(mm)	t(s)	T(°C)	S(mm)	t(s)	T(°C)	S(mm)	t(s)	T(°C)	S(mm)	t(s)	T(°C)	S(mm)
0	25	0,00	480	32,3	0,04	960	40,6	6,98	1440	43,2	10,89	1920	36	7,87	2400	29,4	0,33
10	25,1	0,00	490	32,3	0,05	970	40,7	7,24	1450	43,1	10,89	1930	35,8	7,51	2410	29,2	0,30
20	25,1	0,00	500	32,3	0,05	980	40,7	7,49	1460	42,9	10,89	1940	35,7	7,15	2420	29	0,27
30	25	0,00	510	32,3	0,06	990	40,9	7,73	1470	42,7	10,89	1950	35,6	6,80	2430	28,9	0,24
40	25	-0,01	520	33,1	0,07	1000	41	7,97	1480	42,6	10,89	1960	35,4	6,47	2440	28,8	0,22
50	25,1	-0,01	530	33,3	0,09	1010	41	8,20	1490	42,6	10,89	1970	35,2	6,17	2450	28,6	0,20
60	25,1	-0,01	540	33,4	0,10	1020	41,4	8,41	1500	42,3	10,89	1980	35	5,88	2460	28,5	0,18
70	25,4	-0,01	550	33,5	0,13	1030	41,7	8,62	1510	42,3	10,89	1990	34,9	5,61	2470	28,2	0,16
80	25,6	-0,01	560	33,7	0,17	1040	41,7	8,84	1520	42,3	10,89	2000	34,8	5,34	2480	28,2	0,14
90	26,3	-0,01	570	34	0,21	1050	41,9	9,13	1530	42,3	10,89	2010	34,8	5,07	2490	28	0,12
100	26,7	-0,01	580	34,4	0,26	1060	42,3	9,40	1540	42,3	10,89	2020	34,6	4,82	2500	27,9	0,11
110	26,6	-0,01	590	34,6	0,30	1070	42,5	9,64	1550	42,3	10,89	2030	34,5	4,59	2510	27,8	0,09
120	26,7	-0,01	600	34,6	0,34	1080	42,8	9,85	1560	42,3	10,89	2040	34,3	4,35	2520	27,6	0,08
130	26,7	-0,01	610	34,8	0,37	1090	43	10,03	1570	42,3	10,89	2050	34,2	4,12	2530	27,5	0,06
140	27	-0,01	620	34,9	0,41	1100	43,1	10,18	1580	41	10,89	2060	34	3,90	2540	27,4	0,05
150	27,1	-0,01	630	34,9	0,46	1110	43,2	10,30	1590	40,8	10,89	2070	33,9	3,71	2550	27,3	0,04
160	27,6	-0,01	640	35,3	0,51	1120	43,3	10,41	1600	40,7	10,89	2080	33,7	3,51	2560	27,1	0,02
170	27,6	-0,01	650	35,3	0,56	1130	43,4	10,55	1610	40,6	10,89	2090	33,6	3,32	2570	27	0,02
180	27,6	-0,01	660	35,3	0,62	1140	43,5	10,64	1620	40,4	10,89	2100	33,4	3,15	2580	26,9	0,01
190	27,6	-0,01	670	35,5	0,69	1150	43,6	10,71	1630	40,3	10,89	2110	33,3	2,98	2590	26,8	0,01
200	27,7	-0,01	680	35,6	0,76	1160	43,7	10,75	1640	40,1	10,89	2120	33,2	2,83	2600	26,6	0,01
210	27,7	-0,01	690	35,9	0,88	1170	43,8	10,77	1650	40	10,88	2130	33	2,68	2610	26,5	0,01
220	27,7	-0,01	700	36,1	1,02	1180	43,9	10,79	1660	39,8	10,88	2140	32,8	2,54	2620	26,3	0,01
230	28,3	0,00	710	36,4	1,14	1190	44,1	10,81	1670	39,7	10,88	2150	32,6	2,40	2630	26,2	0,00
240	28,3	-0,01	720	36,7	1,28	1200	44,4	10,82	1680	39,5	10,87	2160	32,5	2,28	2640	26	0,00
250	28,4	0,00	730	36,8	1,41	1210	44,6	10,84	1690	39,4	10,87	2170	32,4	2,16	2650	25,9	0,00
260	28,6	0,00	740	37	1,54	1220	44,9	10,86	1700	39,2	10,87	2180	32,3	2,03	2660	25,5	-0,03
270	28,9	0,00	750	37,2	1,66	1230	45,2	10,87	1710	39	10,86	2190	32,2	1,92	2670	25,4	-0,03
280	29,3	0,00	760	37,3	1,79	1240	45,4	10,89	1720	38,9	10,85	2200	32	1,80	2680	24,9	-0,03
290	29,6	0,00	770	37,4	1,90	1250	45,6	10,89	1730	38,7	10,84	2210	31,9	1,70	2690	24,8	-0,03
300	29,7	0,00	780	37,6	2,01	1260	45,6	10,89	1740	38,6	10,83	2220	31,7	1,60	2700	24,9	-0,03
310	29,9	0,00	790	37,8	2,11	1270	45,6	10,89	1750	38,4	10,80	2230	31,6	1,49	2710	24,8	-0,03
320	30	0,00	800	37,9	2,25	1280	45,6	10,89	1760	38,3	10,77	2240	31,4	1,39	2720	25	-0,03
330	30,2	0,00	810	38,1	2,39	1290	45,6	10,89	1770	38,2	10,72	2250	31,2	1,29	2730	25,2	-0,03
340	30,4	0,00	820	38,3	2,56	1300	45,2	10,89	1780	38	10,66	2260	31	1,20	2740	25,2	-0,03
350	30,4	0,00	830	38,5	2,77	1310	45,1	10,89	1790	37,9	10,59	2270	30,9	1,11	2750	25	-0,03
360	30,5	0,01	840	38,7	3,01	1320	45	10,89	1800	37,8	10,51	2280	30,9	1,02	2760	25	-0,03
370	30,7	0,01	850	38,9	3,30	1330	44,9	10,89	1810	37,4	10,41	2290	30,8	0,94	2770	25,2	-0,03
380	30,7	0,01	860	39,1	3,59	1340	44,8	10,89	1820	37,4	10,31	2300	30,7	0,86	2780	25,1	-0,03
390	30,8	0,01	870	39,1	3,88	1350	44,6	10,89	1830	37,2	10,19	2310	30,5	0,79	2790	25	-0,03
400	31	0,01	880	39,3	4,21	1360	44,5	10,89	1840	37,1	10,05	2320	30,3	0,72	2800	25	-0,03
410	31,2	0,02	890	39,6	4,58	1370	44,4	10,89	1850	37	9,89	2330	30,2	0,66	2810	25,2	-0,03
420	31,5	0,02	900	39,9	4,95	1380	44,2	10,89	1860	36,9	9,73	2340	30	0,60	2820	25,4	-0,03
430	31,8	0,02	910	40	5,34	1390	44	10,89	1870	36,7	9,49	2350	30	0,54	2830	25,1	-0,03
440	32	0,02	920	40,1	5,72	1400	43,9	10,89	1880	36,6	9,18	2360	29,8	0,49	2840	25	-0,03
450	32,2	0,02	930	40,2	6,07	1410	43,6	10,89	1890	36,4	8,86	2370	29,7	0,44	2850	25,1	-0,03
460	32,3	0,03	940	40,4	6,39	1420	43,5	10,89	1900	36,3	8,53	2380	29,6	0,40	2860	25,2	-0,03
470	32,3	0,03	950	40,5	6,70	1430	43,4	10,89	1910	36,1	8,19	2390	29,5	0,37	2870	25,1	-0,03

APPX 7 Paraffin Actuator ,P1-CuO, Time/Temperature/Stroke Records P1_Post

t (s)	T(°C)	S(mm)	t(s)	T(°C)	S(mm)	t(s)	T(°C)	S(mm)	t(s)	T(°C)	S(mm)	t(s)	T(°C)	S(mm)	t(s)	T(°C)	S(mm)
0	25	0,00	480	32,3	0,04	960	40,6	6,98	1440	43,2	10,89	1920	36	7,87	2400	29,4	0,33
10	25,1	0,00	490	32,3	0,05	970	40,7	7,24	1450	43,1	10,89	1930	35,8	7,51	2410	29,2	0,30
20	25,1	0,00	500	32,3	0,05	980	40,7	7,49	1460	42,9	10,89	1940	35,7	7,15	2420	29	0,27
30	25	0,00	510	32,3	0,06	990	40,9	7,73	1470	42,7	10,89	1950	35,6	6,80	2430	28,9	0,24
40	25	-0,01	520	33,1	0,07	1000	41	7,97	1480	42,6	10,89	1960	35,4	6,47	2440	28,8	0,22
50	25,1	-0,01	530	33,3	0,09	1010	41	8,20	1490	42,6	10,89	1970	35,2	6,17	2450	28,6	0,20
60	25,1	-0,01	540	33,4	0,10	1020	41,4	8,41	1500	42,3	10,89	1980	35	5,88	2460	28,5	0,18
70	25,4	-0,01	550	33,5	0,13	1030	41,7	8,62	1510	42,3	10,89	1990	34,9	5,61	2470	28,2	0,16
80	25,6	-0,01	560	33,7	0,17	1040	41,7	8,84	1520	42,3	10,89	2000	34,8	5,34	2480	28,2	0,14
90	26,3	-0,01	570	34	0,21	1050	41,9	9,13	1530	42,3	10,89	2010	34,8	5,07	2490	28	0,12
100	26,7	-0,01	580	34,4	0,26	1060	42,3	9,40	1540	42,3	10,89	2020	34,6	4,82	2500	27,9	0,11
110	26,6	-0,01	590	34,6	0,30	1070	42,5	9,64	1550	42,3	10,89	2030	34,5	4,59	2510	27,8	0,09
120	26,7	-0,01	600	34,6	0,34	1080	42,8	9,85	1560	42,3	10,89	2040	34,3	4,35	2520	27,6	0,08
130	26,7	-0,01	610	34,8	0,37	1090	43	10,03	1570	42,3	10,89	2050	34,2	4,12	2530	27,5	0,06
140	27	-0,01	620	34,9	0,41	1100	43,1	10,18	1580	41	10,89	2060	34	3,90	2540	27,4	0,05
150	27,1	-0,01	630	34,9	0,46	1110	43,2	10,30	1590	40,8	10,89	2070	33,9	3,71	2550	27,3	0,04
160	27,6	-0,01	640	35,3	0,51	1120	43,3	10,41	1600	40,7	10,89	2080	33,7	3,51	2560	27,1	0,02
170	27,6	-0,01	650	35,3	0,56	1130	43,4	10,55	1610	40,6	10,89	2090	33,6	3,32	2570	27	0,02
180	27,6	-0,01	660	35,3	0,62	1140	43,5	10,64	1620	40,4	10,89	2100	33,4	3,15	2580	26,9	0,01
190	27,6	-0,01	670	35,5	0,69	1150	43,6	10,71	1630	40,3	10,89	2110	33,3	2,98	2590	26,8	0,01
200	27,7	-0,01	680	35,6	0,76	1160	43,7	10,75	1640	40,1	10,89	2120	33,2	2,83	2600	26,6	0,01
210	27,7	-0,01	690	35,9	0,88	1170	43,8	10,77	1650	40	10,88	2130	33	2,68	2610	26,5	0,01
220	27,7	-0,01	700	36,1	1,02	1180	43,9	10,79	1660	39,8	10,88	2140	32,8	2,54	2620	26,3	0,01
230	28,3	0,00	710	36,4	1,14	1190	44,1	10,81	1670	39,7	10,88	2150	32,6	2,40	2630	26,2	0,00
240	28,3	-0,01	720	36,7	1,28	1200	44,4	10,82	1680	39,5	10,87	2160	32,5	2,28	2640	26	0,00
250	28,4	0,00	730	36,8	1,41	1210	44,6	10,84	1690	39,4	10,87	2170	32,4	2,16	2650	25,9	0,00
260	28,6	0,00	740	37	1,54	1220	44,9	10,86	1700	39,2	10,87	2180	32,3	2,03	2660	25,8	0,00
270	28,9	0,00	750	37,2	1,66	1230	45,2	10,87	1710	39	10,86	2190	32,2	1,92	2670	25,7	0,00
280	29,3	0,00	760	37,3	1,79	1240	45,4	10,89	1720	38,9	10,85	2200	32	1,80	2680	25,6	0,00
290	29,6	0,00	770	37,4	1,90	1250	45,6	10,89	1730	38,7	10,84	2210	31,9	1,70	2690	25,4	0,00
300	29,7	0,00	780	37,6	2,01	1260	45,6	10,89	1740	38,6	10,83	2220	31,7	1,60	2700	25,3	-0,01
310	29,9	0,00	790	37,8	2,11	1270	45,6	10,89	1750	38,4	10,80	2230	31,6	1,49	2710	25,2	-0,01
320	30	0,00	800	37,9	2,25	1280	45,6	10,89	1760	38,3	10,77	2240	31,4	1,39	2720	25,1	-0,01
330	30,2	0,00	810	38,1	2,39	1290	45,6	10,89	1770	38,2	10,72	2250	31,2	1,29	2730	24,9	-0,01
340	30,4	0,00	820	38,3	2,56	1300	45,2	10,89	1780	38	10,66	2260	31	1,20	2740	24,8	-0,01
350	30,4	0,00	830	38,5	2,77	1310	45,1	10,89	1790	37,9	10,59	2270	30,9	1,11	2750	24,7	-0,01
360	30,5	0,01	840	38,7	3,01	1320	45	10,89	1800	37,8	10,51	2280	30,9	1,02	2760	24,7	-0,01
370	30,7	0,01	850	38,9	3,30	1330	44,9	10,89	1810	37,4	10,41	2290	30,8	0,94	2770	24,8	-0,01
380	30,7	0,01	860	39,1	3,59	1340	44,8	10,89	1820	37,4	10,31	2300	30,7	0,86	2780	24,9	-0,01
390	30,8	0,01	870	39,1	3,88	1350	44,6	10,89	1830	37,2	10,19	2310	30,5	0,79	2790	25,1	-0,01
400	31	0,01	880	39,3	4,21	1360	44,5	10,89	1840	37,1	10,05	2320	30,3	0,72	2800	25,3	-0,01
410	31,2	0,02	890	39,6	4,58	1370	44,4	10,89	1850	37	9,89	2330	30,2	0,66	2810	25	-0,01
420	31,5	0,02	900	39,9	4,95	1380	44,2	10,89	1860	36,9	9,73	2340	30	0,60	2820	24,9	-0,01
430	31,8	0,02	910	40	5,34	1390	44	10,89	1870	36,7	9,49	2350	30	0,54	2830	25	-0,01
440	32	0,02	920	40,1	5,72	1400	43,9	10,89	1880	36,6	9,18	2360	29,8	0,49	2840	25,1	-0,01
450	32,2	0,02	930	40,2	6,07	1410	43,6	10,89	1890	36,4	8,86	2370	29,7	0,44	2850	25	-0,01
460	32,3	0,03	940	40,4	6,39	1420	43,5	10,89	1900	36,3	8,53	2380	29,6	0,40	2860	24,9	-0,01
470	32,3	0,03	950	40,5	6,70	1430	43,4	10,89	1910	36,1	8,19	2390	29,5	0,37	2870	24,9	-0,01

APPX 8 Paraffin Actuator, P2-Fe_3O_4, Time/Temperature/Stroke Records P2_pre

t (s)	T(°C)	S(mm)	t(s)	T(°C)	S(mm)	t(s)	T(°C)	S(mm)	t(s)	T(°C)	S(mm)	t(s)	T(°C)	S(mm)	t(s)	T(°C)	S(mm)
0	24,9	0,00	480	32,6	0,00	960	40,6	6,03	1440	42,8	10,36	1920	35,6	6,44	2400	29	0,00
10	25	0,00	490	32,8	0,00	970	40,7	6,36	1450	42,7	10,36	1930	35,4	6,09	2410	28,8	0,00
20	25,1	0,00	500	32,9	0,00	980	40,8	6,64	1460	42,6	10,36	1940	35,3	5,76	2420	28,8	0,00
30	25,2	0,00	510	33	0,00	990	41	6,94	1470	42,4	10,36	1950	35,2	5,43	2430	28,8	0,00
40	25,1	0,00	520	33,2	0,00	1000	41,2	7,22	1480	42,3	10,36	1960	35	5,14	2440	28,4	0,00
50	25,2	0,00	530	33,4	0,00	1010	41,4	7,51	1490	42,1	10,36	1970	34,9	4,84	2450	28,4	0,00
60	25,4	0,00	540	33,5	0,00	1020	41,6	7,74	1500	42	10,36	1980	34,7	4,56	2460	28,4	0,00
70	25,6	0,00	550	33,7	0,01	1030	41,8	7,99	1510	41,8	10,36	1990	34,6	4,30	2470	28	-0,01
80	25,9	0,00	560	34,1	0,01	1040	42	8,21	1520	41,6	10,36	2000	34,5	4,04	2480	27,9	-0,01
90	25,9	0,00	570	34,2	0,02	1050	42,2	8,39	1530	41,5	10,36	2010	34,4	3,80	2490	27,8	-0,01
100	26,1	0,00	580	34,5	0,03	1060	42,6	8,57	1540	41,3	10,36	2020	34,3	3,56	2500	27,6	-0,01
110	26,4	0,00	590	34,6	0,05	1070	42,8	8,72	1550	41,2	10,36	2030	34,1	3,32	2510	27,5	-0,01
120	26,8	0,00	600	34,8	0,06	1080	43	8,85	1560	41	10,36	2040	33,9	3,09	2520	27,4	-0,01
130	27,2	0,00	610	35	0,08	1090	43,1	8,98	1570	40,9	10,35	2050	33,7	2,88	2530	27,2	-0,01
140	27,3	0,00	620	35,1	0,11	1100	43,2	9,09	1580	40,7	10,35	2060	33,6	2,68	2540	27	-0,01
150	27,3	0,00	630	35,2	0,15	1110	43,3	9,20	1590	40,5	10,35	2070	33,5	2,49	2550	27	-0,01
160	27,7	0,00	640	35,3	0,19	1120	43,5	9,29	1600	40,4	10,34	2080	33,3	2,31	2560	26,8	-0,01
170	27,7	0,00	650	35,3	0,23	1130	43,6	9,41	1610	40,2	10,33	2090	33,2	2,15	2570	26,6	-0,01
180	27,7	0,00	660	35,5	0,29	1140	43,7	9,50	1620	40	10,33	2100	33	1,99	2580	26,5	-0,01
190	27,8	0,00	670	35,7	0,35	1150	43,8	9,58	1630	39,9	10,32	2110	32,9	1,86	2590	26,4	-0,01
200	27,8	0,00	680	35,8	0,42	1160	44	9,68	1640	39,7	10,31	2120	32,8	1,73	2600	26,3	-0,01
210	27,9	0,00	690	36	0,50	1170	44,2	9,76	1650	39,7	10,31	2130	32,6	1,62	2610	26,2	-0,01
220	28,1	0,00	700	36,2	0,59	1180	44,4	9,82	1660	39,7	10,30	2140	32,4	1,50	2620	26,1	-0,01
230	28,1	0,00	710	36,4	0,70	1190	44,5	9,90	1670	39,3	10,29	2150	32,3	1,39	2630	25,9	-0,01
240	28,3	0,00	720	36,6	0,80	1200	44,6	9,96	1680	39,3	10,28	2160	32,2	1,29	2640	25,8	-0,01
250	28,6	0,00	730	36,8	0,93	1210	44,8	10,02	1690	39	10,28	2170	32,1	1,19	2650	25,7	-0,01
260	29	0,00	740	37,1	1,04	1220	45	10,09	1700	38,8	10,27	2180	32	1,09	2660	25,5	-0,01
270	29	0,00	750	37,3	1,17	1230	45,1	10,14	1710	38,7	10,26	2190	31,8	1,00	2670	25,4	-0,01
280	29,3	0,00	760	37,4	1,30	1240	45,1	10,18	1720	38,6	10,25	2200	31,6	0,91	2680	25,4	-0,01
290	29,5	0,00	770	37,7	1,43	1250	45,1	10,24	1730	38,4	10,23	2210	31,4	0,82	2690	25,2	-0,01
300	29,6	0,00	780	37,7	1,55	1260	45,1	10,28	1740	38,2	10,21	2220	31,3	0,73	2700	25,1	-0,01
310	29,8	0,00	790	37,9	1,67	1270	45,1	10,30	1750	38,1	10,17	2230	31,2	0,66	2710	25,2	-0,01
320	30,1	0,00	800	37,9	1,78	1280	45	10,33	1760	37,9	10,11	2240	31,1	0,59	2720	25,3	-0,01
330	30,3	0,00	810	38,1	1,89	1290	44,9	10,34	1770	37,8	10,04	2250	31	0,52	2730	25,2	-0,01
340	30,5	0,00	820	38,1	2,04	1300	44,9	10,36	1780	37,6	9,93	2260	30,8	0,45	2740	25,1	-0,01
350	30,6	0,00	830	38,3	2,19	1310	44,9	10,36	1790	37,5	9,79	2270	30,7	0,39	2750	25,1	-0,01
360	30,7	0,00	840	38,5	2,35	1320	44,6	10,36	1800	37,3	9,65	2280	30,6	0,33	2760	25,7	-0,01
370	30,9	0,00	850	38,7	2,55	1330	44,6	10,36	1810	37,2	9,50	2290	30,4	0,27	2770	25,3	-0,01
380	31	0,00	860	38,8	2,77	1340	44,4	10,36	1820	37,1	9,35	2300	30,3	0,21	2780	25,1	-0,01
390	31,1	0,00	870	39	3,01	1350	44,4	10,36	1830	36,9	9,19	2310	30,1	0,16	2790	25,1	-0,01
400	31,1	0,00	880	39,2	3,30	1360	44,1	10,36	1840	36,7	9,02	2320	30	0,11	2800	25,4	-0,01
410	31,3	0,00	890	39,4	3,59	1370	44,1	10,36	1850	36,6	8,84	2330	29,9	0,07	2810	25,2	-0,01
420	31,5	0,00	900	39,6	3,93	1380	43,8	10,36	1860	36,5	8,58	2340	29,7	0,03	2820	25,1	-0,01
430	31,6	0,00	910	39,8	4,35	1390	43,7	10,36	1870	36,3	8,32	2350	29,6	0,01	2830	25,2	-0,01
440	31,9	0,00	920	40	4,74	1400	43,5	10,36	1880	36,2	8,03	2360	29,5	0,00	2840	25,3	-0,01
450	32,2	0,00	930	40,2	5,08	1410	43,4	10,36	1890	36	7,69	2370	29,3	0,00	2850	25,2	-0,01
460	32,3	0,00	940	40,3	5,41	1420	43,2	10,36	1900	35,9	7,25	2380	29,1	0,00	2860	25,1	-0,01
470	32,5	0,00	950	40,5	5,72	1430	43	10,36	1910	35,7	6,81	2390	29	0,00	2870	25,1	-0,01

APPX 9 Paraffin Actuator P2-Fe_3O_4, Time/Temperature/Stroke Records P2_post

t (s)	T(°C)	S(mm)	t(s)	T(°C)	S(mm)	t(s)	T(°C)	S(mm)	t(s)	T(°C)	S(mm)	t(s)	T(°C)	S(mm)	t(s)	T(°C)	S(mm)
0	25	0,00	480	32,3	0,02	960	40,6	5,94	1440	43,2	10,48	1920	36	7,76	2400	29,4	0,06
10	25,1	0,00	490	32,3	0,02	970	40,7	6,25	1450	43,1	10,48	1930	35,8	7,37	2410	29,2	0,05
20	25,1	0,00	500	32,3	0,03	980	40,7	6,53	1460	42,9	10,48	1940	35,7	6,98	2420	29	0,05
30	25	0,00	510	32,3	0,03	990	40,9	6,80	1470	42,7	10,48	1950	35,6	6,62	2430	28,9	0,05
40	25	0,00	520	33,1	0,03	1000	41	7,08	1480	42,6	10,48	1960	35,4	6,30	2440	28,8	0,05
50	25,1	0,00	530	33,3	0,03	1010	41,2	7,34	1490	42,6	10,48	1970	35,2	6,00	2450	28,6	0,05
60	25,1	0,00	540	33,4	0,03	1020	41,4	7,61	1500	42,3	10,48	1980	35,1	5,70	2460	28,5	0,05
70	25,4	0,00	550	33,5	0,03	1030	41,7	7,88	1510	42,3	10,48	1990	34,9	5,41	2470	28,2	0,05
80	25,6	0,00	560	33,7	0,03	1040	41,9	8,14	1520	42,3	10,48	2000	34,8	5,13	2480	28,2	0,04
90	26,3	0,00	570	34	0,05	1050	42,1	8,38	1530	42,3	10,48	2010	34,7	4,85	2490	28	0,04
100	26,7	0,00	580	34,4	0,06	1060	42,3	8,60	1540	42,3	10,48	2020	34,6	4,60	2500	27,9	0,04
110	26,6	0,00	590	34,6	0,08	1070	42,5	8,80	1550	42,3	10,47	2030	34,5	4,35	2510	27,8	0,04
120	26,7	0,00	600	34,6	0,10	1080	42,8	9,00	1560	42,3	10,47	2040	34,3	4,11	2520	27,6	0,04
130	26,7	0,00	610	34,8	0,12	1090	43	9,17	1570	42,3	10,47	2050	34,2	3,87	2530	27,5	0,04
140	27	0,00	620	34,9	0,15	1100	43,1	9,33	1580	41	10,47	2060	34	3,63	2540	27,4	0,04
150	27,1	0,00	630	34,9	0,18	1110	43,2	9,46	1590	40,8	10,47	2070	33,9	3,41	2550	27,3	0,03
160	27,6	0,00	640	35,3	0,23	1120	43,3	9,58	1600	40,7	10,47	2080	33,7	3,19	2560	27,1	0,03
170	27,6	0,00	650	35,3	0,27	1130	43,4	9,68	1610	40,6	10,46	2090	33,6	2,97	2570	27	0,03
180	27,6	0,00	660	35,3	0,31	1140	43,5	9,75	1620	40,4	10,46	2100	33,4	2,77	2580	26,9	0,03
190	27,6	0,00	670	35,5	0,37	1150	43,6	9,84	1630	40,3	10,46	2110	33,3	2,58	2590	26,8	0,03
200	27,7	0,00	680	35,6	0,42	1160	43,7	9,90	1640	40,1	10,45	2120	33,2	2,42	2600	26,6	0,03
210	27,7	0,00	690	35,9	0,51	1170	43,8	9,97	1650	40	10,44	2130	33	2,26	2610	26,5	0,03
220	27,7	0,00	700	36,1	0,61	1180	43,9	10,03	1660	39,8	10,44	2140	32,8	2,13	2620	26,3	0,03
230	28,3	0,00	710	36,4	0,71	1190	44,1	10,09	1670	39,7	10,43	2150	32,6	1,99	2630	26,2	0,03
240	28,3	0,00	720	36,7	0,81	1200	44,4	10,14	1680	39,5	10,42	2160	32,5	1,86	2640	26	0,03
250	28,4	0,00	730	36,8	0,93	1210	44,6	10,19	1690	39,4	10,41	2170	32,4	1,74	2650	25,9	0,03
260	28,6	0,00	740	37	1,04	1220	44,9	10,24	1700	39,2	10,41	2180	32,3	1,62	2660	25,8	0,03
270	28,9	0,00	750	37	1,16	1230	45,2	10,28	1710	39	10,40	2190	32,2	1,51	2670	25,7	0,03
280	29,3	0,00	760	37,4	1,27	1240	45,4	10,35	1720	38,9	10,39	2200	32	1,39	2680	25,6	0,03
290	29,6	0,00	770	37,4	1,38	1250	45,6	10,41	1730	38,7	10,38	2210	31,9	1,28	2690	25,4	0,03
300	29,7	0,00	780	37,4	1,48	1260	45,6	10,43	1740	38,6	10,37	2220	31,7	1,18	2700	25,3	0,03
310	29,9	0,00	790	37,6	1,58	1270	45,6	10,46	1750	38,4	10,35	2230	31,6	1,09	2710	25,2	0,03
320	30	0,00	800	37,6	1,69	1280	45,6	10,47	1760	38,3	10,31	2240	31,4	0,99	2720	25,1	0,03
330	30,2	0,00	810	37,8	1,82	1290	45,6	10,48	1770	38,2	10,27	2250	31,2	0,90	2730	24,9	0,03
340	30,4	0,00	820	38	1,96	1300	45,2	10,48	1780	38	10,21	2260	31	0,81	2740	24,8	0,03
350	30,4	0,00	830	38,3	2,12	1310	45,1	10,48	1790	37,9	10,12	2270	30,9	0,73	2750	24,7	0,03
360	30,5	0,00	840	38,7	2,32	1320	45	10,48	1800	37,9	10,03	2280	30,9	0,65	2760	24,7	0,03
370	30,7	0,00	850	38,9	2,55	1330	44,9	10,48	1810	37,6	9,91	2290	30,8	0,58	2770	24,8	0,03
380	30,7	0,00	860	39,1	2,78	1340	44,8	10,48	1820	37,4	9,79	2300	30,7	0,51	2780	24,9	0,03
390	30,8	0,00	870	39,1	3,03	1350	44,6	10,48	1830	37,3	9,66	2310	30,5	0,44	2790	25,1	0,03
400	31	0,00	880	39,3	3,32	1360	44,5	10,48	1840	37,1	9,52	2320	30,3	0,38	2800	25,3	0,03
410	31,2	0,00	890	39,6	3,61	1370	44,4	10,48	1850	37	9,38	2330	30,2	0,32	2810	25	0,03
420	31,5	0,00	900	39,9	3,91	1380	44,2	10,48	1860	36,9	9,23	2340	30	0,26	2820	24,9	0,03
430	31,8	0,01	910	40	4,26	1390	44	10,48	1870	36,7	9,07	2350	30	0,21	2830	25	0,03
440	32	0,01	920	40,1	4,62	1400	43,9	10,48	1880	36,6	8,89	2360	29,8	0,16	2840	25,1	0,03
450	32,2	0,01	930	40,2	4,99	1410	43,6	10,48	1890	36,4	8,65	2370	29,7	0,12	2850	25	0,03
460	32,3	0,01	940	40,4	5,33	1420	43,5	10,48	1900	36,3	8,40	2380	29,6	0,08	2860	24,9	0,03
470	32,3	0,02	950	40,5	5,64	1430	43,4	10,48	1910	36,1	8,11	2390	29,5	0,06	2870	24,9	0,03

APPX 10 Paraffin Actuator, P3-Al_2O_3, Time/Temperature/Stroke Records P3_pre

t (s)	T(°C)	S(mm)	t(s)	T(°C)	S(mm)	t(s)	T(°C)	S(mm)	t(s)	T(°C)	S(mm)	t(s)	T(°C)	S(mm)	t(s)	T(°C)	S(mm)
0	25	0,00	480	27,9	0,07	960	35,6	1,27	1440	43,6	9,59	1920	40,5	10,09	2400	33,7	2,69
10	25,2	0,00	490	27,9	0,08	970	36	1,34	1450	43,8	9,64	1930	40,4	10,08	2410	33,5	2,52
20	25,3	0,00	500	28,1	0,08	980	36	1,41	1460	44	9,67	1940	40,2	10,07	2420	33,4	2,38
30	25,4	0,00	510	28,1	0,09	990	36,2	1,48	1470	44,1	9,72	1950	40,1	10,05	2430	33,2	2,25
40	25,3	0,00	520	28,1	0,09	1000	36,4	1,54	1480	44,2	9,77	1960	40	10,04	2440	33,2	2,13
50	25,3	0,00	530	28,3	0,10	1010	36,5	1,60	1490	44,4	9,81	1970	39,8	10,02	2450	33	2,00
60	25,3	0,00	540	28,4	0,10	1020	36,6	1,67	1500	44,6	9,84	1980	39,6	10,00	2460	32,9	1,90
70	25,3	0,00	550	28,6	0,11	1030	36,7	1,73	1510	45,1	9,86	1990	39,5	9,98	2470	32,8	1,80
80	25,3	0,00	560	28,7	0,12	1040	36,8	1,85	1520	45,1	9,89	2000	39,3	9,96	2480	32,6	1,70
90	25,3	0,00	570	28,8	0,13	1050	37	1,96	1530	45,1	9,90	2010	39,2	9,94	2490	32,4	1,61
100	25,3	0,00	580	29,1	0,14	1060	37,1	2,08	1540	45,2	9,92	2020	39	9,92	2500	32,3	1,53
110	25,3	0,00	590	29,2	0,16	1070	37,3	2,21	1550	45,3	9,94	2030	38,9	9,89	2510	32,2	1,45
120	25,3	0,00	600	29,5	0,18	1080	37,6	2,35	1560	45,4	9,96	2040	38,8	9,85	2520	32	1,37
130	25,3	0,00	610	29,8	0,20	1090	37,8	2,55	1570	45,4	9,99	2050	38,8	9,82	2530	32	1,31
140	25,3	0,00	620	30	0,22	1100	38	2,72	1580	45,4	10,01	2060	38,8	9,78	2540	31,8	1,25
150	25,3	0,00	630	30,3	0,24	1110	38,2	2,90	1590	45,3	10,03	2070	38,4	9,73	2550	31,6	1,18
160	25,3	0,00	640	30,5	0,26	1120	38,4	3,10	1600	45,2	10,04	2080	38,4	9,66	2560	31,5	1,13
170	25,4	0,00	650	30,7	0,27	1130	38,5	3,32	1610	45,1	10,06	2090	38,4	9,58	2570	31,4	1,08
180	25,4	0,00	660	30,8	0,29	1140	38,7	3,53	1620	45	10,07	2100	37,9	9,48	2580	31,2	1,04
190	25,4	0,00	670	31	0,30	1150	38,9	3,79	1630	44,9	10,09	2110	37,7	9,36	2590	31,1	0,99
200	25,4	0,00	680	31,1	0,31	1160	39,1	4,02	1640	44,7	10,10	2120	37,6	9,18	2600	31,1	0,96
210	25,4	0,00	690	31,1	0,32	1170	39,2	4,29	1650	44,6	10,10	2130	37,4	8,94	2610	30,8	0,92
220	25,4	0,00	700	31,3	0,33	1180	39,3	4,54	1660	44,4	10,10	2140	37,3	8,69	2620	30,8	0,89
230	25,4	0,00	710	36,4	0,71	1190	39,5	4,80	1670	44,3	10,10	2150	37,2	8,45	2630	30,6	0,86
240	25,4	0,00	720	31,3	0,36	1200	39,6	5,10	1680	44,2	10,11	2160	37,1	8,22	2640	30,6	0,83
250	25,5	0,00	730	31,3	0,38	1210	39,7	5,37	1690	44,1	10,11	2170	36,9	8,00	2650	30,6	0,81
260	25,5	0,00	740	31,3	0,40	1220	39,9	5,69	1700	43,9	10,11	2180	36,7	7,73	2660	30,6	0,79
270	25,5	0,00	750	31,3	0,43	1230	39,9	6,00	1710	43,7	10,11	2190	36,6	7,49	2670	30,6	0,77
280	25,5	0,00	760	32,1	0,46	1240	40,2	6,31	1720	43,6	10,11	2200	36,4	7,26	2680	30,6	0,76
290	25,5	0,00	770	32,4	0,50	1250	40,5	6,64	1730	43,4	10,11	2210	36,3	7,01	2690	30,6	0,74
300	25,5	0,00	780	32,7	0,53	1260	40,7	6,95	1740	43,3	10,11	2220	36,2	6,70	2700	29,7	0,72
310	25,5	0,00	790	33	0,56	1270	40,9	7,21	1750	43,1	10,11	2230	36	6,44	2710	29,6	0,71
320	25,6	0,00	800	33,1	0,59	1280	40,9	7,49	1760	42,9	10,11	2240	35,9	6,17	2720	29,4	0,69
330	25,6	0,00	810	33,3	0,62	1290	41	7,72	1770	42,8	10,11	2250	35,8	5,92	2730	29,3	0,68
340	25,6	0,00	820	33,5	0,65	1300	41,3	7,93	1780	42,7	10,11	2260	35,8	5,66	2740	29,1	0,66
350	25,6	0,00	830	33,6	0,67	1310	41,4	8,13	1790	42,7	10,11	2270	35,5	5,40	2750	29	0,65
360	25,6	0,00	840	33,7	0,69	1320	41,5	8,34	1800	42,4	10,11	2280	35,4	5,15	2760	28,8	0,63
370	25,6	0,00	850	33,8	0,71	1330	41,6	8,52	1810	42,4	10,11	2290	35,1	4,91	2770	28,7	0,62
380	25,7	0,00	860	33,9	0,73	1340	41,8	8,70	1820	42	10,11	2300	35	4,66	2780	28,6	0,61
390	25,8	0,00	870	33,9	0,76	1350	42,1	8,85	1830	42	10,11	2310	34,9	4,44	2790	28,4	0,59
400	25,9	0,00	880	34,1	0,81	1360	42,4	8,98	1840	41,8	10,11	2320	34,7	4,22	2800	28,3	0,58
410	26	0,00	890	34,2	0,85	1370	42,6	9,12	1850	41,8	10,11	2330	34,5	4,00	2810	28,2	0,57
420	26,3	0,01	900	34,5	0,89	1380	42,7	9,21	1860	41,5	10,11	2340	34,5	3,80	2820	28	0,55
430	26,6	0,02	910	34,7	0,94	1390	42,9	9,30	1870	41,3	10,11	2350	34,4	3,60	2830	27,9	0,54
440	26,6	0,03	920	34,9	1,00	1400	43	9,36	1880	41,1	10,11	2360	34,2	3,40	2840	27,8	0,53
450	27,4	0,04	930	35,2	1,07	1410	43,2	9,44	1890	41	10,11	2370	34	3,20	2850	27,7	0,52
460	27,4	0,05	940	35,4	1,14	1420	43,3	9,50	1900	40,8	10,11	2380	33,9	3,03	2860	27,5	0,51
470	27,4	0,06	950	35,6	1,20	1430	43,5	9,55	1910	40,7	10,10	2390	33,8	2,85	2870	27,4	0,50

APPX 11 Paraffin Actuator, P3-Al_2O_3, Time/Temperature/Stroke Records P3_post

t (s)	T(°C)	S(mm)	t(s)	T(°C)	S(mm)	t(s)	T(°C)	S(mm)	t(s)	T(°C)	S(mm)	t(s)	T(°C)	S(mm)	t(s)	T(°C)	S(mm)
0	25	0	480	27,7	-0,03	960	35,3	0,7	1440	43,4	9,59	1920	40,2	10,14	2400	33,2	2,33
10	25,2	0	490	27,8	-0,03	970	35,6	0,78	1450	43,6	9,66	1930	40	10,14	2410	33,2	2,19
20	25,2	0	500	28	-0,03	980	35,9	0,86	1460	43,7	9,74	1940	39,8	10,13	2420	33	2,06
30	25,2	0	510	28,1	-0,03	990	36	0,95	1470	43,9	9,78	1950	39,7	10,13	2430	32,9	1,95
40	25,2	0	520	28,3	-0,03	1000	36,2	1,03	1480	44,1	9,88	1960	39,6	10,12	2440	32,8	1,83
50	25,2	0	530	28,4	-0,03	1010	36,3	1,12	1490	44,4	9,93	1970	39,5	10,12	2450	32,6	1,73
60	25,1	0	540	28,6	-0,03	1020	36,5	1,21	1500	44,6	9,99	1980	39,3	10,12	2460	32,4	1,63
70	24,9	0	550	28,7	-0,03	1030	36,8	1,32	1510	44,8	10,04	1990	39,1	10,11	2470	32,3	1,54
80	24,9	-0,01	560	28,8	-0,03	1040	36,8	1,43	1520	45,1	10,07	2000	38,9	10,1	2480	32,2	1,45
90	24,8	-0,01	570	28,8	-0,03	1050	37,1	1,55	1530	45,2	10,1	2010	38,8	10,1	2490	32	1,36
100	24,8	-0,01	580	29	-0,03	1060	37,2	1,67	1540	45,2	10,11	2020	38,7	10,09	2500	32	1,28
110	24,8	-0,01	590	29	-0,03	1070	37,4	1,82	1550	45,3	10,13	2030	38,5	9,96	2510	31,8	1,2
120	24,8	-0,02	600	29	-0,03	1080	37,6	1,95	1560	45,4	10,16	2040	38,3	9,93	2520	31,6	1,13
130	24,8	-0,02	610	29	-0,03	1090	37,8	2,09	1570	45,4	10,17	2050	38,1	9,9	2530	31,5	1,06
140	24,9	-0,02	620	29	-0,03	1100	37,9	2,29	1580	45,3	10,18	2060	38	9,86	2540	31,4	0,99
150	24,9	-0,02	630	29	-0,03	1110	38,2	2,47	1590	45,3	10,18	2070	37,9	9,81	2550	31,2	0,93
160	25	-0,02	640	30,2	-0,03	1120	38,3	2,66	1600	45,2	10,18	2080	37,7	9,75	2560	31,1	0,87
170	25	-0,02	650	30,4	-0,03	1130	38,4	2,87	1610	45,1	10,18	2090	37,6	9,67	2570	31,1	0,81
180	25,1	-0,02	660	30,6	-0,03	1140	38,5	3,09	1620	44,9	10,18	2100	37,4	9,58	2580	30,8	0,76
190	25	-0,02	670	30,8	-0,02	1150	38,7	3,33	1630	44,8	10,18	2110	37,3	9,46	2590	30,8	0,71
200	25,2	-0,02	680	31,1	-0,02	1160	38,9	3,55	1640	44,6	10,18	2120	37,2	9,29	2600	30,6	0,67
210	25,2	-0,02	690	31,2	-0,02	1170	39	3,85	1650	44,4	10,18	2130	37,1	9,06	2610	30,6	0,62
220	25,2	-0,02	700	31,5	-0,02	1180	39,1	4,13	1660	44,3	10,18	2140	36,9	8,83	2620	30,6	0,59
230	25,1	-0,02	710	31,5	-0,01	1190	39,3	4,45	1670	44,1	10,18	2150	36,7	8,53	2630	30,6	0,55
240	25,1	-0,02	720	31,6	-0,01	1200	39,5	4,79	1680	44,1	10,18	2160	36,6	8,3	2640	30,6	0,52
250	25	-0,02	730	31,7	-0,01	1210	39,8	5,14	1690	44,1	10,18	2170	36,4	7,99	2650	30,6	0,49
260	25	-0,02	740	31,8	0	1220	40	5,45	1700	44,1	10,18	2180	36,3	7,7	2660	30,6	0,46
270	25	-0,02	750	31,9	0	1230	40,1	5,8	1710	44,1	10,18	2190	36,2	7,32	2670	29,7	0,44
280	24,9	-0,02	760	31,9	0,01	1240	40,2	6,13	1720	44,1	10,18	2200	36	6,94	2680	29,6	0,41
290	24,8	-0,03	770	32,1	0,02	1250	40,3	6,43	1730	43,1	10,18	2210	35,9	6,59	2690	29,4	0,39
300	24,8	-0,03	780	32,3	0,03	1260	40,4	6,73	1740	43	10,18	2220	35,8	6,26	2700	29,3	0,37
310	24,8	-0,03	790	32,5	0,04	1270	40,6	7,01	1750	42,8	10,18	2230	35,7	5,97	2710	29,1	0,35
320	24,8	-0,03	800	32,8	0,05	1280	40,7	7,27	1760	42,6	10,18	2240	35,5	5,69	2720	29	0,34
330	24,8	-0,03	810	33	0,07	1290	41	7,52	1770	42,5	10,18	2250	35,4	5,4	2730	28,8	0,32
340	25	-0,03	820	33,2	0,1	1300	41,2	7,77	1780	42,4	10,18	2260	35,1	5,13	2740	28,7	0,3
350	24,9	-0,03	830	33,3	0,13	1310	41,3	7,97	1790	42,2	10,18	2270	35	4,88	2750	28,6	0,29
360	25,1	-0,03	840	33,6	0,17	1320	41,5	8,18	1800	42	10,18	2280	34,8	4,65	2760	28,4	0,27
370	25,2	-0,03	850	33,8	0,21	1330	41,8	8,37	1810	41,9	10,18	2290	34,6	4,39	2770	28,3	0,26
380	25,3	-0,03	860	34,1	0,25	1340	41,9	8,53	1820	41,7	10,17	2300	34,5	4,15	2780	28,2	0,24
390	25,7	-0,03	870	34,2	0,29	1350	42,1	8,66	1830	41,6	10,17	2310	34,4	3,93	2790	28	0,23
400	25,9	-0,03	880	34,4	0,33	1360	42,1	8,79	1840	41,4	10,17	2320	34,2	3,72	2800	27,9	0,22
410	26,3	-0,03	890	34,5	0,36	1370	42,4	8,93	1850	41,3	10,17	2330	34	3,51	2810	27,8	0,21
420	26,6	-0,03	900	34,6	0,4	1380	42,6	9,05	1860	41,1	10,16	2340	34	3,31	2820	27,7	0,2
430	26,6	-0,03	910	34,7	0,44	1390	42,6	9,15	1870	40,9	10,16	2350	33,8	3,12	2830	27,5	0,18
440	27	-0,03	920	34,8	0,48	1400	42,9	9,23	1880	40,8	10,16	2360	33,7	2,95	2840	27,4	0,17
450	27	-0,03	930	34,8	0,53	1410	43,1	9,35	1890	40,6	10,15	2370	33,7	2,78	2850	27,3	0,16
460	27,3	-0,03	940	34,8	0,57	1420	43,1	9,42	1900	40,6	10,15	2380	33,5	2,62	2860	27,2	0,15
470	27,5	-0,03	950	35,1	0,63	1430	43,1	9,5	1910	40,6	10,15	2390	33,4	2,47	2870	27	0,14

APPX 12 Paraffin Actuator, P4-ZnO, Time/Temperature/Stroke Records P4_pre

t (s)	T(°C)	S(mm)	t(s)	T(°C)	S(mm)	t(s)	T(°C)	S(mm)	t(s)	T(°C)	S(mm)	t(s)	T(°C)	S(mm)	t(s)	T(°C)	S(mm)
0	24,9	0	480	27,9	0	960	35,6	0	1440	43,5	10	1920	40,3	10,29	2400	33,5	2,05
10	24,9	0	490	27,9	0	970	35,8	0	1450	43,7	10,1	1930	40,1	10,29	2410	33,3	1,89
20	24,8	0	500	27,9	0	980	35,9	0	1460	44,1	10,17	1940	40	10,29	2420	33	1,75
30	24,8	0	510	28,2	0	990	36,2	0	1470	44,1	10,22	1950	39,9	10,29	2430	33	1,61
40	24,9	0	520	28,2	0	1000	36,2	0,02	1480	44,3	10,24	1960	39,7	10,29	2440	32,8	1,49
50	25,1	0	530	28,5	0	1010	36,3	0,09	1490	44,5	10,25	1970	39,6	10,28	2450	32,8	1,38
60	25,2	0	540	28,5	0	1020	36,5	0,17	1500	44,8	10,26	1980	39,3	10,28	2460	32,6	1,28
70	25,2	0	550	28,5	0	1030	36,7	0,27	1510	44,9	10,27	1990	39,3	10,28	2470	32,4	1,18
80	25,3	0	560	28,8	0	1040	36,8	0,36	1520	45	10,28	2000	39,1	10,28	2480	32,3	1,09
90	25,3	0	570	28,8	0	1050	37	0,47	1530	45,1	10,28	2010	38,9	10,27	2490	32,2	0,99
100	25,4	0	580	29,2	0	1060	37,2	0,6	1540	45,2	10,29	2020	38,8	10,27	2500	32	0,9
110	25,4	0	590	29,4	0	1070	37,4	0,74	1550	45,3	10,29	2030	38,7	10,25	2510	31,9	0,82
120	25,4	0	600	29,7	0	1080	37,6	0,89	1560	45,2	10,29	2040	38,4	10,23	2520	31,8	0,73
130	25,4	0	610	29,8	0	1090	37,8	1,04	1570	45,2	10,29	2050	38,3	10,2	2530	31,6	0,65
140	25,4	0	620	29,9	0	1100	38,1	1,19	1580	45,2	10,29	2060	38,2	10,15	2540	31,5	0,57
150	25,4	0	630	30,3	0	1110	38,2	1,35	1590	45	10,29	2070	38	10,1	2550	31,4	0,49
160	25,4	0	640	30,4	0	1120	38,4	1,5	1600	44,9	10,29	2080	38	10,03	2560	31,1	0,42
170	25,4	0	650	30,6	0	1130	38,5	1,69	1610	44,9	10,29	2090	37,8	9,95	2570	31,1	0,35
180	25,4	0	660	30,8	0	1140	38,6	1,86	1620	44,6	10,29	2100	37,6	9,84	2580	30,8	0,28
190	25,4	0	670	31	0	1150	38,6	2,04	1630	44,6	10,29	2110	37,6	9,69	2590	30,7	0,21
200	25,4	0	680	31	0	1160	38,7	2,26	1640	44,5	10,29	2120	37,4	9,55	2600	30,6	0,15
210	25,4	0	690	31,2	0	1170	39	2,51	1650	44,4	10,29	2130	37,2	9,4	2610	30,5	0,1
220	25,4	0	700	31,3	0	1180	39,1	2,8	1660	44,2	10,29	2140	37,1	9,21	2620	30,4	0,03
230	25,4	0	710	31,5	0	1190	39,3	3,12	1670	44	10,29	2150	37	8,98	2630	30,3	0
240	25,4	0	720	31,7	0	1200	39,5	3,45	1680	43,9	10,29	2160	36,7	8,65	2640	30,2	0
250	25,4	0	730	31,7	0	1210	39,6	3,82	1690	43,8	10,29	2170	36,7	8,26	2650	30	0
260	25,4	0	740	31,7	0	1220	39,9	4,21	1700	43,7	10,29	2180	36,5	7,85	2660	30	0
270	25,4	0	750	32,1	0	1230	40,1	4,61	1710	43,5	10,29	2190	36,3	7,47	2670	29,7	0
280	25,4	0	760	32,1	0	1240	40,3	5,02	1720	43,3	10,29	2200	36,2	7,11	2680	29,5	0
290	25,4	0	770	32,4	0	1250	40,6	5,41	1730	43,2	10,29	2210	36,1	6,77	2690	29,5	0
300	25,4	0	780	32,5	0	1260	40,7	5,77	1740	43	10,29	2220	35,9	6,45	2700	29,2	0
310	25,4	0	790	32,8	0	1270	40,9	6,09	1750	42,8	10,29	2230	35,8	6,12	2710	29,2	0
320	25,5	0	800	32,9	0	1280	41	6,38	1760	42,8	10,29	2240	35,6	5,81	2720	29	0
330	25,5	0	810	33,4	0	1290	41,2	6,67	1770	42,5	10,29	2250	35,5	5,52	2730	28,9	0
340	25,5	0	820	33,4	0	1300	41,4	6,95	1780	42,3	10,29	2260	35,4	5,24	2740	28,8	0
350	25,5	0	830	33,4	0	1310	41,5	7,21	1790	42,3	10,29	2270	35,2	4,96	2750	28,6	0
360	25,5	0	840	33,5	0	1320	41,7	7,44	1800	42,1	10,29	2280	35,1	4,69	2760	28,4	0
370	25,5	0	850	33,7	0	1330	41,9	7,71	1810	41,9	10,29	2290	35	4,42	2770	28,3	0
380	25,7	0	860	33,9	0	1340	42	7,92	1820	41,8	10,29	2300	34,7	4,17	2780	28,1	0
390	25,8	0	870	33,9	0	1350	42,1	8,17	1830	41,7	10,29	2310	34,6	3,91	2790	28	0
400	26	0	880	34,1	0	1360	42,2	8,4	1840	41,5	10,29	2320	34,5	3,67	2800	27,9	0
410	26,3	0	890	34,3	0	1370	42,3	8,62	1850	41,4	10,29	2330	34,5	3,43	2810	27,8	0
420	26,7	0	900	34,5	0	1380	42,4	8,85	1860	41,2	10,29	2340	34,3	3,2	2820	27,6	0
430	27	0	910	34,7	0	1390	42,6	9,08	1870	41	10,29	2350	34,1	2,98	2830	27,5	0
440	27,2	0	920	34,9	0	1400	42,8	9,29	1880	40,8	10,29	2360	33,9	2,77	2840	27,4	0
450	27,5	0	930	35,1	0	1410	43	9,56	1890	40,8	10,29	2370	33,8	2,59	2850	27,3	0
460	27,7	0	940	35,3	0	1420	43,2	9,74	1900	40,6	10,29	2380	33,8	2,39	2860	27,1	0
470	27,8	0	950	35,6	0	1430	43,4	9,87	1910	40,5	10,29	2390	33,5	2,21	2870	27	0

APPX 13 Paraffin Actuator, P4-ZnO, Time/Temperature/Stroke Records P4_post

t (s)	T(°C)	S(mm)	t(s)	T(°C)	S(mm)	t(s)	T(°C)	S(mm)	t(s)	T(°C)	S(mm)	t(s)	T(°C)	S(mm)	t(s)	T(°C)	S(mm)
0	25	0	480	27,8	0	960	35,5	0	1440	43,8	10,03	1920	40,6	10,26	2400	33,7	2,66
10	24,9	0	490	27,9	0	970	35,6	0	1450	43,8	10,1	1930	40,4	10,25	2410	33,6	2,48
20	24,9	0	500	28	0	980	35,7	0	1460	43,9	10,15	1940	40,2	10,25	2420	33,5	2,31
30	24,9	0	510	28,2	0	990	35,9	0	1470	43,9	10,2	1950	40,1	10,24	2430	33,3	2,15
40	25,2	0	520	28,2	0	1000	36,2	0,06	1480	44	10,23	1960	40	10,23	2440	33,2	1,99
50	25	0	530	28,4	0	1010	36,4	0,16	1490	44,3	10,24	1970	40	10,23	2450	33	1,85
60	24,9	0	540	28,5	0	1020	36,8	0,26	1500	44,5	10,25	1980	39,6	10,22	2460	32,9	1,7
70	25,1	0	550	28,7	0	1030	36,9	0,37	1510	44,5	10,26	1990	39,6	10,22	2470	32,8	1,58
80	25,1	0	560	28,7	0	1040	36,9	0,47	1520	44,6	10,27	2000	39,4	10,21	2480	32,6	1,46
90	25,2	0	570	29,1	0	1050	37	0,58	1530	44,9	10,28	2010	39,3	10,21	2490	32,5	1,35
100	25,3	0	580	29,1	0	1060	37,2	0,71	1540	45,1	10,28	2020	39,3	10,2	2500	32,4	1,24
110	25,3	0	590	29,1	0	1070	37,4	0,83	1550	45,2	10,3	2030	38,9	10,18	2510	32,4	1,14
120	25,3	0	600	29,2	0	1080	37,6	0,95	1560	45,3	10,3	2040	38,8	10,17	2520	32,1	1,04
130	25,3	0	610	29,3	0	1090	37,8	1,09	1570	45,3	10,3	2050	38,6	10,14	2530	32,1	0,95
140	25,4	0	620	29,6	0	1100	38	1,23	1580	45,3	10,3	2060	38,5	10,1	2540	32,1	0,86
150	25,4	0	630	30	0	1110	38,2	1,35	1590	45,2	10,3	2070	38,3	10,06	2550	31,7	0,77
160	25,4	0	640	30,2	0	1120	38,4	1,47	1600	45,2	10,3	2080	38,2	10	2560	31,6	0,69
170	25,4	0	650	30,7	0	1130	38,6	1,6	1610	45,1	10,3	2090	38	9,92	2570	31,5	0,61
180	25,4	0	660	30,8	0	1140	38,8	1,75	1620	45	10,3	2100	38	9,82	2580	31,4	0,53
190	25,4	0	670	31	0	1150	39	1,92	1630	44,9	10,3	2110	37,8	9,7	2590	31,2	0,45
200	25,4	0	680	31,2	0	1160	39	2,13	1640	44,7	10,3	2120	37,6	9,55	2600	31	0,38
210	25,4	0	690	31,3	0	1170	39,2	2,4	1650	44,5	10,3	2130	37,5	9,4	2610	30,8	0,31
220	25,4	0	700	31,3	0	1180	39,4	2,67	1660	44,4	10,3	2140	37,4	9,22	2620	30,7	0,24
230	25,4	0	710	31,5	0	1190	39,6	3,02	1670	44,3	10,3	2150	37,2	8,97	2630	30,7	0,17
240	25,5	0	720	31,5	0	1200	39,7	3,36	1680	44,2	10,3	2160	37,1	8,73	2640	30,5	0,11
250	25,5	0	730	31,6	0	1210	39,9	3,75	1690	44,1	10,3	2170	36,8	8,45	2650	30,3	0,05
260	25,5	0	740	31,6	0	1220	40,1	4,13	1700	43,8	10,3	2180	36,8	8,16	2660	30,2	0
270	25,5	0	750	31,8	0	1230	40,3	4,56	1710	43,7	10,3	2190	36,6	7,86	2670	30,1	0
280	25,5	0	760	32	0	1240	40,5	4,97	1720	43,5	10,3	2200	36,5	7,58	2680	30	0
290	25,5	0	770	32,2	0	1250	40,6	5,34	1730	43,3	10,3	2210	36,3	7,26	2690	29,8	0
300	25,5	0	780	32,8	0	1260	40,6	5,7	1740	43,3	10,3	2220	36,2	6,92	2700	29,6	0
310	25,5	0	790	32,8	0	1270	40,8	6,03	1750	43,1	10,3	2230	36,1	6,61	2710	29,5	0
320	25,5	0	800	32,9	0	1280	40,8	6,32	1760	43,1	10,3	2240	35,9	6,32	2720	29,5	0
330	25,5	0	810	32,9	0	1290	41	6,58	1770	43,1	10,3	2250	35,8	6,04	2730	29,3	0
340	25,5	0	820	33	0	1300	41	6,83	1780	42,7	10,3	2260	35,6	5,77	2740	29,2	0
350	25,6	0	830	33,3	0	1310	41,1	7,06	1790	42,5	10,3	2270	35,6	5,51	2750	29,1	0
360	25,6	0	840	33,5	0	1320	41,3	7,3	1800	42,3	10,29	2280	35,3	5,25	2760	29	0
370	25,6	0	850	33,8	0	1330	41,4	7,53	1810	42,2	10,29	2290	35,1	5	2770	28,8	0
380	25,6	0	860	34	0	1340	41,6	7,77	1820	42	10,29	2300	35	4,77	2780	28,6	0
390	25,8	0	870	34,2	0	1350	41,9	8,01	1830	41,9	10,29	2310	34,9	4,53	2790	28,5	0
400	25,9	0	880	34,4	0	1360	42	8,26	1840	41,7	10,28	2320	34,8	4,3	2800	28,3	0
410	26,1	0	890	34,6	0	1370	42,4	8,53	1850	41,6	10,28	2330	34,7	4,08	2810	28,2	0
420	26,3	0	900	34,6	0	1380	42,5	8,81	1860	41,4	10,28	2340	34,6	3,86	2820	28,1	0
430	26,4	0	910	34,7	0	1390	42,8	9,08	1870	41,3	10,28	2350	34,4	3,65	2830	28	0
440	26,9	0	920	35	0	1400	43,1	9,37	1880	41,1	10,27	2360	34,3	3,43	2840	27,9	0
450	26,9	0	930	35	0	1410	43,2	9,61	1890	41	10,27	2370	34,1	3,23	2850	27,7	0
460	27,3	0	940	35	0	1420	43,5	9,79	1900	40,8	10,26	2380	34	3,02	2860	27,6	0
470	27,4	0	950	35,3	0	1430	43,6	9,92	1910	40,7	10,26	2390	33,9	2,83	2870	27,5	0

APPX 14 Paraffin Actuator, P5-NF, Time/Temperature/Stroke Records P5_pre

t (s)	T(°C)	S(mm)	t(s)	T(°C)	S(mm)	t(s)	T(°C)	S(mm)	t(s)	T(°C)	S(mm)	t(s)	T(°C)	S(mm)	t(s)	T(°C)	S(mm)
0	24,9	0	480	32,6	0,43	960	40,5	5,6	1440	43,2	11,09	1920	36	5,69	2400	29,6	0,2
10	24,9	0	490	32,7	0,44	970	40,7	5,89	1450	43,2	11,09	1930	35,8	5,34	2410	29	0,19
20	25	0	500	32,9	0,46	980	40,9	6,19	1460	42,9	11,09	1940	35,7	5,01	2420	29	0,17
30	25,6	0	510	33,2	0,49	990	41,1	6,48	1470	42,7	11,09	1950	35,5	4,68	2430	28,8	0,16
40	25,6	0	520	33,3	0,51	1000	41,3	6,78	1480	42,7	11,1	1960	35,4	4,37	2440	28,7	0,15
50	25,8	0	530	33,6	0,53	1010	41,6	7,11	1490	42,4	11,1	1970	35,2	4,05	2450	28,5	0,14
60	25,4	0	540	33,6	0,55	1020	41,7	7,44	1500	42,4	11,1	1980	35,1	3,76	2460	28,4	0,13
70	25,3	0	550	33,7	0,58	1030	41,9	7,71	1510	42,3	11,1	1990	35	3,47	2470	28,2	0,12
80	25,4	0	560	33,9	0,6	1040	42,1	7,99	1520	42	11,1	2000	34,9	3,21	2480	28	0,11
90	25,7	0	570	34,1	0,63	1050	42,2	8,23	1530	42	11,1	2010	34,7	2,96	2490	27,9	0,1
100	26,1	0,01	580	34,3	0,67	1060	42,4	8,45	1540	41,6	11,1	2020	34,5	2,72	2500	27,8	0,09
110	26,6	0,02	590	34,5	0,71	1070	42,5	8,66	1550	41,6	11,1	2030	34,4	2,5	2510	27,6	0,08
120	27,2	0,03	600	35	0,75	1080	42,7	8,85	1560	41,3	11,1	2040	34,2	2,29	2520	27,5	0,07
130	27,3	0,03	610	35	0,79	1090	42,8	9,06	1570	41,3	11,09	2050	33,9	2,09	2530	27,3	0,06
140	27,4	0,04	620	35	0,82	1100	42,9	9,22	1580	41,2	11,09	2060	34	1,91	2540	27,2	0,05
150	27,4	0,05	630	35	0,85	1110	42,9	9,4	1590	41	11,09	2070	33,9	1,75	2550	27,1	0,04
160	27,4	0,05	640	35,3	0,89	1120	43,3	9,64	1600	41	11,08	2080	33,7	1,6	2560	27	0,03
170	27,4	0,05	650	35,3	0,93	1130	43,3	9,8	1610	41	11,07	2090	33,5	1,46	2570	26,8	0,02
180	27,4	0,06	660	35,3	0,97	1140	43,6	9,94	1620	41	11,06	2100	33,4	1,33	2580	26,7	0,01
190	27,4	0,06	670	35,8	1,01	1150	43,8	10,05	1630	41	11,05	2110	33,4	1,21	2590	26,6	0
200	27,9	0,07	680	36	1,07	1160	44	10,16	1640	40,1	11,04	2120	33,1	1,11	2600	26,5	0
210	28	0,07	690	36,2	1,12	1170	44,1	10,27	1650	40,1	11,02	2130	33	1,02	2610	26,2	-0,01
220	28,3	0,08	700	36,5	1,17	1180	44,3	10,35	1660	39,9	11	2140	33	0,94	2620	26,2	-0,02
230	28,4	0,09	710	36,6	1,22	1190	44,5	10,45	1670	39,6	10,98	2150	32,8	0,86	2630	26,1	-0,03
240	28,9	0,1	720	36,7	1,26	1200	44,6	10,53	1680	39,6	10,95	2160	32,6	0,79	2640	25,9	-0,04
250	29	0,11	730	36,8	1,31	1210	44,8	10,59	1690	39,3	10,93	2170	32,6	0,73	2650	25,8	-0,04
260	29,1	0,12	740	37	1,37	1220	45	10,65	1700	39,3	10,9	2180	32,4	0,67	2660	25,7	-0,05
270	29,1	0,13	750	37,1	1,43	1230	45,2	10,68	1710	39,2	10,86	2190	32,2	0,63	2670	25,5	-0,06
280	29,2	0,14	760	37,3	1,5	1240	45,3	10,76	1720	39	10,82	2200	32	0,59	2680	25,4	-0,07
290	29,4	0,15	770	37,5	1,58	1250	45,4	10,8	1730	38,8	10,77	2210	31,9	0,55	2690	25,2	-0,07
300	29,7	0,16	780	37,6	1,66	1260	45,4	10,84	1740	38,5	10,71	2220	31,7	0,52	2700	25,1	-0,08
310	30	0,17	790	37,9	1,75	1270	45,4	10,88	1750	38,5	10,63	2230	31,6	0,49	2710	25	-0,09
320	30	0,18	800	38	1,87	1280	45,4	10,91	1760	38,3	10,53	2240	31,4	0,46	2720	25,2	-0,09
330	30	0,19	810	38,2	1,98	1290	45,3	10,95	1770	38,3	10,39	2250	31,3	0,44	2730	24,9	-0,1
340	30,3	0,2	820	38,4	2,1	1300	45,2	10,97	1780	38,1	10,15	2260	31,1	0,42	2740	24,9	-0,1
350	30,6	0,22	830	38,5	2,26	1310	45,1	10,98	1790	38	9,89	2270	31	0,4	2750	25	-0,11
360	30,7	0,23	840	38,7	2,41	1320	45	11	1800	37,8	9,63	2280	30,9	0,38	2760	24,9	-0,11
370	30,8	0,24	850	38,8	2,6	1330	44,8	11,01	1810	37,6	9,35	2290	30,7	0,36	2770	24,7	-0,12
380	30,8	0,25	860	39	2,78	1340	44,6	11,02	1820	37,5	9,06	2300	30,6	0,34	2780	24,7	-0,12
390	31,1	0,27	870	39,2	3	1350	44,6	11,03	1830	37,3	8,75	2310	30,5	0,32	2790	24,6	-0,12
400	31,1	0,29	880	39,4	3,24	1360	44,4	11,04	1840	37,3	8,41	2320	30,3	0,31	2800	25,1	-0,12
410	31,1	0,3	890	39,6	3,49	1370	44,4	11,05	1850	37	8,08	2330	30,2	0,29	2810	25,1	-0,12
420	31,1	0,32	900	39,8	3,77	1380	44,4	11,06	1860	36,8	7,75	2340	30	0,28	2820	24,9	-0,12
430	31,1	0,35	910	39,9	4,07	1390	44,4	11,07	1870	36,8	7,4	2350	29,9	0,26	2830	24,9	-0,12
440	31,1	0,36	920	40,1	4,38	1400	43,8	11,08	1880	36,6	7,05	2360	29,8	0,25	2840	25	-0,12
450	32,3	0,38	930	40,2	4,71	1410	43,7	11,08	1890	36,4	6,71	2370	29,6	0,23	2850	25	-0,12
460	32,5	0,4	940	40,2	5,05	1420	43,5	11,08	1900	36,4	6,37	2380	29,6	0,22	2860	25,1	-0,12
470	32,5	0,41	950	40,3	5,33	1430	43,4	11,09	1910	36,2	6,03	2390	29,6	0,21	2870	25,2	-0,12

APPX 15 Paraffin Actuator, P5-NF, Time/Temperature/Stroke Records P5_post

t (s)	T(°C)	S(mm)	t(s)	T(°C)	S(mm)	t(s)	T(°C)	S(mm)	t(s)	T(°C)	S(mm)	t(s)	T(°C)	S(mm)	t(s)	T(°C)	S(mm)
0	24,9	0	480	33,3	0,27	960	41	7,24	1440	42,8	10,89	1920	35,8	5,17	2400	29,3	0,34
10	25,3	0	490	33,5	0,29	970	41,3	7,51	1450	42,7	10,89	1930	35,6	4,89	2410	29,1	0,33
20	25,4	0	500	33,6	0,3	980	41,4	7,77	1460	42,7	10,89	1940	35,5	4,63	2420	29	0,32
30	25,5	0	510	33,7	0,32	990	41,5	7,99	1470	42,4	10,89	1950	35,4	4,37	2430	28,8	0,3
40	25,5	0	520	33,8	0,33	1000	41,6	8,23	1480	42,4	10,89	1960	35,1	4,13	2440	28,7	0,29
50	25,6	0	530	33,9	0,35	1010	41,8	8,45	1490	42	10,89	1970	35	3,89	2450	28,6	0,28
60	25,8	0	540	33,9	0,37	1020	42,1	8,65	1500	42	10,89	1980	34,9	3,66	2460	28,4	0,27
70	25,9	0	550	34,1	0,4	1030	42,4	8,84	1510	41,8	10,89	1990	34,7	3,45	2470	28,3	0,26
80	26	0	560	34,2	0,43	1040	42,6	9,03	1520	41,8	10,89	2000	34,5	3,23	2480	28,2	0,25
90	26,3	0	570	34,5	0,47	1050	42,7	9,2	1530	41,5	10,89	2010	34,5	3,04	2490	28	0,24
100	26,6	0	580	34,7	0,51	1060	42,9	9,37	1540	41,3	10,89	2020	34,4	2,85	2500	27,9	0,23
110	26,6	0	590	34,9	0,55	1070	43	9,52	1550	41,1	10,89	2030	34,2	2,69	2510	27,8	0,22
120	27,4	0	600	35,2	0,6	1080	43,2	9,71	1560	41	10,89	2040	34,1	2,53	2520	27,7	0,21
130	27,4	0	610	35,4	0,65	1090	43,3	9,84	1570	40,8	10,89	2050	34	2,37	2530	27,5	0,2
140	27,4	0	620	35,6	0,7	1100	43,5	9,97	1580	40,7	10,88	2060	33,9	2,24	2540	27,4	0,19
150	27,9	0	630	35,8	0,75	1110	43,6	10,08	1590	40,5	10,88	2070	33,7	2,11	2550	27,3	0,18
160	27,9	0	640	36	0,8	1120	43,8	10,18	1600	40,4	10,88	2080	33,5	1,99	2560	27,2	0,17
170	28,1	0	650	36,1	0,85	1130	44	10,27	1610	40,2	10,88	2090	33,4	1,88	2570	27	0,16
180	28,1	0	660	36,2	0,89	1140	44,1	10,34	1620	40,1	10,88	2100	33,2	1,78	2580	26,9	0,15
190	28,1	0	670	36,4	0,94	1150	44,2	10,41	1630	40	10,88	2110	33,2	1,69	2590	26,9	0,15
200	28,3	0	680	36,5	0,99	1160	44,4	10,48	1640	39,8	10,88	2120	33	1,6	2600	26,7	0,14
210	28,4	0	690	36,6	1,04	1170	44,6	10,53	1650	39,6	10,87	2130	32,9	1,52	2610	26,5	0,13
220	28,6	0	700	36,7	1,09	1180	45,1	10,57	1660	39,5	10,86	2140	32,8	1,44	2620	26,4	0,12
230	28,7	0	710	36,8	1,15	1190	45,1	10,61	1670	39,3	10,84	2150	32,6	1,36	2630	26,3	0,11
240	28,8	0,01	720	37	1,23	1200	45,1	10,65	1680	39,2	10,82	2160	32,4	1,29	2640	26,2	0,11
250	29,1	0,01	730	37,1	1,32	1210	45,2	10,68	1690	39	10,79	2170	32,3	1,21	2650	26,1	0,1
260	29,2	0,01	740	37,3	1,41	1220	45,3	10,71	1700	38,9	10,75	2180	32,2	1,15	2660	25,9	0,09
270	29,5	0,01	750	37,6	1,54	1230	45,4	10,73	1710	38,8	10,71	2190	32	1,09	2670	25,9	0,09
280	29,8	0,02	760	37,8	1,67	1240	45,4	10,81	1720	38,6	10,66	2200	32	1,02	2680	25,7	0,08
290	30	0,03	770	38	1,81	1250	45,4	10,83	1730	38,4	10,59	2210	31,8	0,97	2690	25,6	0,07
300	30,3	0,03	780	38,1	1,96	1260	45,3	10,85	1740	38,2	10,5	2220	31,6	0,91	2700	25,4	0,06
310	30,5	0,04	790	38,3	2,14	1270	45,2	10,86	1750	38	10,4	2230	31,5	0,85	2710	25,3	0,06
320	30,7	0,04	800	38,5	2,34	1280	45,1	10,87	1760	38	10,25	2240	31,4	0,8	2720	25,1	0,05
330	30,8	0,05	810	38,7	2,56	1290	45	10,87	1770	37,9	10,04	2250	31,2	0,76	2730	25,1	0,04
340	31	0,06	820	38,9	2,8	1300	44,9	10,88	1780	37,7	9,83	2260	31,1	0,71	2740	24,9	0,04
350	31,1	0,06	830	39,1	3,08	1310	44,7	10,88	1790	37,6	9,56	2270	31,1	0,67	2750	24,8	0,03
360	31,1	0,06	840	39,2	3,36	1320	44,6	10,89	1800	37,4	9,25	2280	30,8	0,63	2760	24,8	0,03
370	31,3	0,07	850	39,3	3,68	1330	44,4	10,89	1810	37,3	8,89	2290	30,8	0,59	2770	24,7	0,02
380	31,3	0,07	860	39,5	3,98	1340	44,3	10,89	1820	37,2	8,49	2300	30,6	0,56	2780	24,9	0,02
390	31,3	0,08	870	39,6	4,3	1350	44,2	10,89	1830	37,1	8,08	2310	30,4	0,53	2790	24,9	0,02
400	31,3	0,1	880	39,7	4,62	1360	44,1	10,89	1840	36,9	7,71	2320	30,4	0,5	2800	24,8	0,01
410	31,3	0,11	890	39,9	4,96	1370	43,9	10,89	1850	36,7	7,36	2330	30,2	0,47	2810	24,9	0,01
420	31,3	0,13	900	39,9	5,3	1380	43,7	10,89	1860	36,6	7,02	2340	30	0,45	2820	24,9	0,01
430	32,1	0,15	910	40,2	5,66	1390	43,6	10,89	1870	36,4	6,69	2350	30	0,43	2830	25,1	0,01
440	32,4	0,17	920	40,3	6	1400	43,4	10,89	1880	36,3	6,37	2360	30	0,41	2840	25,1	0,01
450	32,7	0,2	930	40,5	6,34	1410	43,3	10,89	1890	36,2	6,05	2370	29,7	0,39	2850	25,1	0,01
460	33	0,23	940	40,7	6,65	1420	43,1	10,89	1900	36	5,75	2380	29,6	0,38	2860	25,2	0,01
470	33,1	0,25	950	40,9	6,95	1430	42,9	10,89	1910	35,9	5,45	2390	29,4	0,36	2870	25,2	0,01

APPX 16 Paraffin Actuator, P6-Pure Time/Temperature/Stroke Records P6_pre

t (s)	T(°C)	S(mm)	t(s)	T(°C)	S(mm)	t(s)	T(°C)	S(mm)	t(s)	T(°C)	S(mm)	t(s)	T(°C)	S(mm)	t(s)	T(°C)	S(mm)
0	24,9	0	480	32,4	0,04	960	40,4	5,51	1440	44,7	11,34	1920	36,9	10,41	2400	30,1	1,03
10	24,9	0	490	32,5	0,04	970	40,7	5,88	1450	44,7	11,34	1930	36,7	10,2	2410	30	0,95
20	24,9	0	500	32,5	0,05	980	40,9	6,25	1460	43,9	11,34	1940	36,5	9,89	2420	29,9	0,89
30	25	0	510	32,9	0,07	990	41,1	6,62	1470	43,8	11,34	1950	36,4	9,55	2430	29,7	0,83
40	25	0	520	33,2	0,09	1000	41,3	6,97	1480	43,6	11,34	1960	36,2	9,21	2440	29,5	0,79
50	25,1	0	530	33,2	0,12	1010	41,5	7,3	1490	43,4	11,34	1970	36,1	8,88	2450	29,4	0,75
60	25,8	0	540	33,5	0,16	1020	41,7	7,6	1500	43,3	11,34	1980	36	8,58	2460	29,3	0,7
70	26,2	0	550	34,1	0,21	1030	41,8	7,86	1510	43,1	11,34	1990	35,8	8,24	2470	29,1	0,67
80	26,2	0	560	34,1	0,25	1040	41,9	8,11	1520	43	11,34	2000	35,7	7,96	2480	29	0,64
90	26,2	0	570	34,2	0,29	1050	42	8,35	1530	42,8	11,34	2010	35,6	7,67	2490	28,8	0,61
100	26,4	0	580	34,4	0,33	1060	42,1	8,57	1540	42,6	11,34	2020	35,4	7,39	2500	28,7	0,59
110	26,6	0	590	34,4	0,36	1070	42,2	8,78	1550	42,5	11,34	2030	35,3	7,11	2510	28,6	0,57
120	26,6	0	600	34,5	0,4	1080	42,3	8,95	1560	42,3	11,34	2040	35,1	6,82	2520	28,5	0,55
130	27	0	610	34,8	0,44	1090	42,4	9,18	1570	42,2	11,34	2050	35	6,55	2530	28,3	0,51
140	27,2	0	620	34,8	0,48	1100	42,6	9,39	1580	42	11,33	2060	34,9	6,29	2540	28,2	0,48
150	27,2	0	630	34,9	0,52	1110	42,8	9,64	1590	41,9	11,33	2070	34,7	6,02	2550	28,1	0,46
160	27,4	0	640	35,1	0,56	1120	43,1	9,85	1600	41,7	11,33	2080	34,5	5,76	2560	28	0,45
170	27,4	0	650	35,3	0,61	1130	43,3	10,05	1610	41,5	11,33	2090	34,4	5,51	2570	27,8	0,43
180	27,4	0	660	35,5	0,66	1140	43,4	10,24	1620	41,4	11,33	2100	34,2	5,27	2580	27,7	0,42
190	27,8	0	670	35,6	0,72	1150	43,6	10,46	1630	41,2	11,33	2110	34,1	5,02	2590	27,5	0,41
200	27,9	0	680	35,8	0,77	1160	43,8	10,63	1640	41,1	11,33	2120	34	4,78	2600	27,4	0,4
210	28	0	690	35,9	0,83	1170	44	10,77	1650	40,9	11,33	2130	33,9	4,55	2610	27,3	0,39
220	28,1	0	700	36,1	0,9	1180	44,1	10,9	1660	40,9	11,33	2140	33,7	4,33	2620	27,1	0,38
230	28,5	0	710	36,3	0,97	1190	44,2	11,05	1670	40,6	11,32	2150	33,6	4,12	2630	27	0,37
240	29	0	720	36,5	1,05	1200	44,6	11,13	1680	40,6	11,32	2160	33,4	3,92	2640	26,9	0,36
250	28,8	0	730	36,7	1,14	1210	44,7	11,18	1690	40,6	11,32	2170	33,2	3,7	2650	26,8	0,36
260	28,9	0	740	36,9	1,23	1220	44,8	11,2	1700	40,1	11,31	2180	33	3,51	2660	26,7	0,35
270	29,1	0	750	37,1	1,31	1230	44,9	11,21	1710	40	11,31	2190	32,9	3,32	2670	26,6	0,34
280	29,2	0	760	37,2	1,4	1240	45	11,22	1720	39,8	11,31	2200	32,8	3,15	2680	26,4	0,34
290	29,5	0	770	37,4	1,49	1250	45,1	11,22	1730	39,7	11,3	2210	32,7	2,99	2690	26,2	0,33
300	29,5	0,01	780	37,5	1,6	1260	45,2	11,23	1740	39,5	11,3	2220	32,6	2,84	2700	26,1	0,32
310	29,9	0,01	790	37,6	1,7	1270	45,3	11,32	1750	39,4	11,29	2230	32,4	2,67	2710	26	0,32
320	30	0,01	800	37,7	1,81	1280	45,3	11,33	1760	39,2	11,29	2240	32,3	2,53	2720	25,9	0,31
330	30	0,01	810	37,9	1,93	1290	45,4	11,33	1770	39	11,28	2250	32,2	2,42	2730	25,8	0,31
340	30,3	0,01	820	38,1	2,09	1300	45,4	11,33	1780	38,9	11,28	2260	32,1	2,3	2740	25,7	0,3
350	30,3	0,01	830	38,3	2,25	1310	45,4	11,34	1790	38,7	11,28	2270	31,9	2,19	2750	25,5	0,3
360	30,7	0,01	840	38,4	2,41	1320	45,3	11,34	1800	38,6	11,27	2280	31,8	2,09	2760	25,4	0,29
370	30,7	0,01	850	38,6	2,58	1330	45,3	11,34	1810	38,5	11,26	2290	31,6	1,97	2770	25,3	0,29
380	31,1	0,01	860	38,8	2,77	1340	45,3	11,34	1820	38,3	11,26	2300	31,5	1,86	2780	25,2	0,28
390	31,2	0,01	870	39	2,96	1350	45,3	11,34	1830	38,2	11,25	2310	31,3	1,76	2790	25	0,28
400	31,2	0,01	880	39,2	3,17	1360	45,2	11,34	1840	38	11,23	2320	31,2	1,66	2800	24,9	0,28
410	31,6	0,01	890	39,4	3,4	1370	45,2	11,34	1850	37,9	11,2	2330	31,1	1,58	2810	24,8	0,27
420	31,6	0,01	900	39,6	3,65	1380	44,9	11,34	1860	37,7	11,15	2340	30,9	1,49	2820	24,7	0,26
430	31,6	0,02	910	39,7	3,91	1390	44,9	11,34	1870	37,5	11,09	2350	30,8	1,39	2830	24,8	0,25
440	31,6	0,02	920	39,9	4,18	1400	44,7	11,34	1880	37,4	11	2360	30,7	1,31	2840	24,8	0,23
450	31,6	0,02	930	40	4,48	1410	44,7	11,34	1890	37,3	10,89	2370	30,5	1,24	2850	24,7	0,22
460	32,3	0,03	940	40,1	4,8	1420	44,7	11,34	1900	37,1	10,75	2380	30,4	1,17	2860	25	0,21
470	32,4	0,03	950	40,2	5,15	1430	44,7	11,34	1910	37	10,61	2390	30,4	1,1	2870	24,9	0,2

APPX 17 Paraffin Actuator, P6-Pure Time/Temperature/Stroke Records P6_post

t (s)	T(°C)	S(mm)	t(s)	T(°C)	S(mm)	t(s)	T(°C)	S(mm)	t(s)	T(°C)	S(mm)	t(s)	T(°C)	S(mm)	t(s)	T(°C)	S(mm)
0	25,5	0	480	31,3	0	960	39,9	4,22	1440	43,9	11,23	1920	36,7	10	2400	30,2	0,81
10	25,5	0	490	31,3	0,01	970	40	4,56	1450	43,7	11,23	1930	36,6	9,72	2410	30	0,74
20	25,5	0	500	32,1	0,03	980	40,2	4,86	1460	43,6	11,23	1940	36,4	9,41	2420	30	0,67
30	25,5	0	510	32,4	0,06	990	40,3	5,19	1470	43,4	11,23	1950	36,3	9,1	2430	29,8	0,62
40	25,5	0	520	32,7	0,1	1000	40,5	5,51	1480	43,3	11,23	1960	36,2	8,77	2440	29,7	0,56
50	25,5	0	530	33	0,13	1010	40,7	5,84	1490	43,1	11,22	1970	36	8,45	2450	29,6	0,51
60	25,6	0	540	33,1	0,16	1020	40,9	6,17	1500	42,9	11,22	1980	35,9	8,14	2460	29,4	0,46
70	25,6	0	550	33,3	0,19	1030	41	6,49	1510	42,8	11,22	1990	35,8	7,85	2470	29,3	0,42
80	25,6	0	560	33,5	0,21	1040	41,3	6,82	1520	42,7	11,22	2000	35,6	7,59	2480	29,1	0,39
90	25,6	0	570	33,6	0,24	1050	41,4	7,14	1530	42,7	11,22	2010	35,5	7,35	2490	29	0,36
100	25,6	0	580	33,7	0,26	1060	41,5	7,43	1540	42,4	11,22	2020	35,4	7,09	2500	28,8	0,33
110	25,6	0	590	33,8	0,28	1070	41,6	7,73	1550	42,2	11,22	2030	35,1	6,85	2510	28,7	0,31
120	25,7	0	600	33,9	0,3	1080	41,8	8	1560	42	11,22	2040	35	6,59	2520	28,6	0,28
130	25,8	0	610	33,9	0,32	1090	42,1	8,28	1570	42	11,22	2050	34,9	6,35	2530	28,4	0,26
140	25,9	0	620	34,1	0,35	1100	42,2	8,53	1580	41,8	11,22	2060	34,7	6,09	2540	28,3	0,24
150	26	0	630	34,2	0,39	1110	42,5	8,78	1590	41,7	11,22	2070	34,5	5,87	2550	28,2	0,22
160	26,3	0	640	34,5	0,43	1120	42,7	9,07	1600	41,5	11,22	2080	34,5	5,6	2560	28	0,2
170	26,6	0	650	34,7	0,48	1130	42,9	9,3	1610	41,3	11,22	2090	34,4	5,36	2570	27,9	0,18
180	26,6	0	660	34,9	0,53	1140	43	9,54	1620	41,1	11,22	2100	34,2	5,12	2580	27,8	0,16
190	27,4	0	670	35,2	0,58	1150	43,2	9,79	1630	41	11,22	2110	34	4,89	2590	27,7	0,14
200	27,4	0	680	35,4	0,64	1160	43,3	9,97	1640	40,8	11,22	2120	33,9	4,65	2600	27,5	0,13
210	27,4	0	690	35,6	0,7	1170	43,5	10,15	1650	40,7	11,22	2130	33,8	4,42	2610	27,4	0,11
220	27,9	0	700	35,8	0,75	1180	43,6	10,33	1660	40,5	11,22	2140	33,7	4,2	2620	27,3	0,1
230	27,9	0	710	35,9	0,82	1190	43,8	10,48	1670	40,4	11,22	2150	33,5	4	2630	27,2	0,09
240	28,1	0	720	36	0,88	1200	44	10,62	1680	40,2	11,22	2160	33,4	3,8	2640	27	0,08
250	28,1	0	730	36,2	0,93	1210	44,1	10,74	1690	40,1	11,22	2170	33,2	3,57	2650	26,9	0,06
260	28,1	0	740	36,4	0,99	1220	44,2	10,87	1700	40	11,22	2180	33	3,38	2660	26,9	0,05
270	28,3	0	750	36,5	1,04	1230	44,4	10,98	1710	39,8	11,22	2190	32,9	3,17	2670	26,7	0,04
280	28,4	0	760	36,6	1,1	1240	44,6	11,06	1720	39,6	11,22	2200	32,8	3	2680	26,5	0,03
290	28,6	0	770	36,7	1,16	1250	45,1	11,15	1730	39,5	11,22	2210	32,7	2,85	2690	26,4	0,02
300	28,7	0	780	36,8	1,23	1260	45,1	11,18	1740	39,3	11,22	2220	32,6	2,7	2700	26,3	0,01
310	28,8	0	790	37	1,31	1270	45,1	11,19	1750	39,2	11,22	2230	32,4	2,54	2710	26,2	-0,01
320	29,1	0	800	37,1	1,41	1280	45,2	11,2	1760	39	11,22	2240	32,3	2,4	2720	26,1	-0,02
330	29,2	0	810	37,3	1,51	1290	45,3	11,22	1770	38,9	11,21	2250	32,2	2,28	2730	25,9	-0,03
340	29,5	0	820	37,6	1,62	1300	45,4	11,22	1780	38,8	11,21	2260	32	2,16	2740	25,9	-0,04
350	29,8	0	830	37,8	1,73	1310	45,4	11,23	1790	38,8	11,21	2270	32	2,05	2750	25,7	-0,05
360	30	0	840	38	1,85	1320	45,4	11,23	1800	38,8	11,19	2280	31,8	1,93	2760	25,6	-0,06
370	30,3	0	850	38,2	2,01	1330	45,3	11,23	1810	38,4	11,18	2290	31,6	1,82	2770	25,4	-0,07
380	30,5	0	860	38,4	2,15	1340	45,2	11,23	1820	38,4	11,15	2300	31,5	1,72	2780	25,3	-0,08
390	30,7	0	870	38,5	2,3	1350	45,1	11,23	1830	38,4	11,13	2310	31,4	1,62	2790	25,1	-0,09
400	30,8	0	880	38,7	2,49	1360	45	11,23	1840	37,9	11,09	2320	31,2	1,51	2800	25,1	-0,1
410	31	0	890	38,9	2,65	1370	44,9	11,23	1850	37,7	11,05	2330	31,1	1,41	2810	24,9	-0,11
420	31,1	0	900	39,1	2,82	1380	44,7	11,23	1860	37,6	10,99	2340	31,1	1,31	2820	24,8	-0,11
430	31,1	0	910	39,3	3	1390	44,6	11,23	1870	37,4	10,88	2350	30,8	1,22	2830	24,8	-0,12
440	31,3	0	920	39,5	3,24	1400	44,4	11,23	1880	37,3	10,76	2360	30,8	1,13	2840	24,7	-0,13
450	31,3	0	930	39,6	3,46	1410	44,3	11,23	1890	37,2	10,63	2370	30,8	1,04	2850	24,9	-0,13
460	31,3	0	940	39,7	3,7	1420	44,2	11,23	1900	37,1	10,45	2380	30,6	0,96	2860	24,9	-0,14
470	31,3	0	950	39,8	3,96	1430	44,1	11,23	1910	36,9	10,23	2390	30,4	0,89	2870	24,8	-0,14

RESUME

Name Surname : AHMET KUTLU

Place and Date of Birth : 17.12.1979

Foreign Languages : GERMAN, ENGLISH

Education Status

High School : S.SCIENCE HIGH SCHOOL, ANKARA

Bachelor's : ULUDAG UNIVERSITY, BURSA

Master's : UNIVERSITY OF REUTLINGEN, GERMANY

Work Experience :

-RESEARCH AND DEVELOPMENT ENGINEER FOR CONSTRUCTION AND STRESS ANALYSIS IN AIRBUS A380,A350,A400M AIRCRAFTS PROGRAMMS

-RESEARCH AND DEVELOPMENT PROJECT SUPERVISOR FOR THERMAL MANAGEMENT SYSTEMS OF (VW) EA211, EA288 CAR ENGINE PROGRAMMS AND (RENAULT) K9K, HR10, HR12 CAR ENGINE PROGRAMMS AT TIER1 DEVELOPMENT AND PRODUCT SUPPLIER.

Contact (e-mail) : benkutlu@yahoo.com

Publications :

-Kutlu, A., Eren, R., Aykut, Y., (2021)**.** Paraffin/polyacrylonitrile hybrid nanofibers for thermal hysteresis enhancement of paraffin actuators,*Journal of Industrial Textiles*, January 24 2021

-Kutlu, A., Eren, R., Aykut, Y., (2019). Effect of the Number of Carbon in Paraffin on Interaction with PVA Nanofiber Mat, *17th National 3rd International the Recent Progress Symposium on Textile Technology and Chemistry*, 20-22,November 2019